DESIGN OF A BORON NEUTRON CAPTURE ENHANCED FAST NEUTRON THERAPY ASSEMBLY

A Dissertation
Presented to
The Academic Faculty

by

Zhonglu Wang

In Partial Fulfillment
of the Requirements for the Degree
Doctor of Philosophy in Health Physics
in the G.W. Woodruff School of Mechanical Engineering

Georgia Institute of Technology
December 2006

DESIGN OF A BORON NEUTRON CAPTURE ENHANCED FAST NEUTRON THERAPY ASSEMBLY

Approved by:

Dr. Nolan E. Hertel, Advisor
School of Mechanical Engineering
Georgia Institute of Technology

Dr. C-K Chris Wang
School of Mechanical Engineering
Georgia Institute of Technology

Dr. Ratib Karam
School of Mechanical Engineering
Georgia Institute of Technology

Dr. Eva K. Lee
School of Industrial & Systems Engineering
Georgia Institute of Technology

Dr. Arlene J. Lennox
Fermilab Neutron Therapy Facility
Fermi National Accelerator Laboratory

Dr. Rebecca Howell
Department Oncology
Emory University

Date Approved: July 19, 2006

In the memory of my grandparents,
Junwen and Shi Wang

ACKNOWLEDGEMENTS

I wish to thank all those who have helped me with this work, both directly and indirectly. I am deeply grateful to my advisor Dr. Nolan E. Hertel for giving me the opportunity to work with him on so many interesting projects. He has been a great advisor and friend to me through the years. Without his guidance, support, patience and inspiration I would not have come through my graduate life this way. I would like to thank Dr. C-K Chris Wang for his assistance and advice.

I thank Dr. Arlene Lennox for her support, assistance and insights for this project. I am grateful to her for spending the weekend helping me with the experiments when she was supposed to be with her family.

I would like to thank Dr. Ratib Karam, Dr. Eva Lee and Dr. Rebecca Howell for serving on my reading committee and for providing advice on this research.

I have benefited from the work of Dr. Jeremy E. Sweezy. His work has provided me a sound basis for this research. He also provided me assistance on MCNP and MCNPX problems.

I also want to thank Dr. Tom Kroc, Dr. Erik Ramberg and Mr. Mark Austin for their help. Dr. Kroc helped me with foil activation and depth-dose distribution measurements. Dr. Ramberg prepared most of the materials for the experiment. He stayed until midnight to run the LINAC and also provided insightful suggestions for the experiment. Mr. Martin provided the drawings of the head phantom based on which I performed the MCNP simulation.

I have to say a big thank to Eric Burgett for helping me with my experiments. Without his help there would be quite a few data points missing. Thanks to Dwayne Blaylock for his help with the hot cell operation.

I would like to thank Dr. John Valentine for recruiting me into the Nuclear Radiological Engineering and Health Physics program and thank Dr. Rodney Ice for hiring me as a Graduate Research Assistant in the Radiological Safety Office (ORS). Thanks to Jeremiah Sauber and Nazia Zaker for their help while I was working in the ORS.

To Yufen, my wife, I am grateful for her support, encouragement and motivation through the endeavors in the last fifteen years. To Xiaoyu and Xiaolei, I am so lucky to have them as my sons.

To my parents, Tongzhen and Yuhua, my brothers, Zhongfu and Zhongzheng, my sisters, Zhongxiang and Zhongling, my aunt, Tonglian, I appreciate all the support and love that you have given me through every endeavor.

TABLE OF CONTENTS

LIST OF TABLES

Page

LIST OF FIGURES

LIST OF ABBREVIATIONS

AAPM	American Association of Physicists in Medicine
Be	Beryllium
BMRR	Brookhaven Medical Research Reactor
BNCT	Boron Neutron Capture therapy
BNCEFNT	Boron Neutron Capture Enhanced Fast Neutron Therapy
BNL	Brookhaven National Laboratory
BPA-F	Boron Phenylalanine-Fructose
BSH	Sodium borocaptate
CAB	Cellulose Acetate Butyrate
ENDF	Evaluated Nuclear Data File
FNT	Fast Neutron Therapy
GBM	Glioblastoma Multiforme
HPGe	High-Purity Germanium
ICRP	International Commission on Radiological Protection
ICRU	International Commission on Radiation Units and Measurements
Linac	Linear Accelerator
LET	Linear Energy Transfer
MCNP	Monte Carlo N-Particle Transport Code
MIT	Massachusetts Institute of Technology
MU	Monitor Units
NIST	National Institute of Standards and Technology
PDE	Percent Dose Enhancement
ppm	Parts per million

RBE	Relative Biological Effectiveness
STP	Standard Temperature-Pressure (0 ˚C and 1000 kPa)
TE	Tissue Equivalent
UW	University of Washington

SUMMARY

The use of boron neutron capture to boost tumor dose in fast neutron therapy has been investigated at several fast neutron therapy centers worldwide. This treatment is termed boron neutron capture enhanced fast neutron therapy (BNCEFNT). It is a combination of boron neutron capture therapy (BNCT) and fast neutron therapy (FNT). It is believed that BNCEFNT may be useful in the treatment of some radioresistant brain tumors, such as glioblastoma multiforme (GBM).

A boron neutron capture enhanced fast neutron therapy assembly has been designed for the Fermilab Neutron Therapy Facility (NTF). This assembly uses a tungsten filter and collimator near the patient's head, with a graphite reflector surrounding the head to significantly increase the dose due to boron neutron capture reactions. The assembly was designed using Monte Carlo radiation transport code MCNP version 5 for a standard 20x20 cm^2 treatment beam. The calculated boron dose enhancement at 5.7-cm depth in a water-filled head phantom in the assembly with a 5x5 cm^2 collimation was 21.9% per 100-ppm ^{10}B for a 5.0-cm tungsten filter and 29.8% for a 8.5-cm tungsten filter. The corresponding dose rate for the 5.0-cm and 8.5-cm thick filters were 0.221 and 0.127 Gy/min, respectively; about 48.5% and 27.9% of the dose rate of the standard 10x10 cm^2 fast neutron treatment beam.

To validate the design calculations, a simplified BNCEFNT assembly was built using four lead bricks to form a 5x5 cm^2 collimator. Five 1.0-cm thick 20x20 cm^2 tungsten plates were used to obtain different filter thicknesses and graphite bricks/blocks were used to form a reflector. Measurements of the dose enhancement of the simplified

assembly in a water-filled head phantom were performed using a pair of tissue-equivalent ion chambers. One of the ion chambers is loaded with 1000-ppm natural boron (184-ppm ^{10}B) to measure dose due to boron neutron capture. The measured dose enhancement at 5.0-cm depth in the head phantom for the 5.0-cm thick tungsten filter is (16.6 ± 1.8)%, which agrees well with the MCNP simulation of the simplified BNCEFNT assembly, (16.4± 0.5)%. The error in the calculated dose enhancement only considers the statistical uncertainties. The total dose rate measured at 5.0-cm depth using the non-borated ion chamber is (0.765 ± 0.076) Gy/MU, about 61% of the fast neutron standard dose rate (1.255Gy/MU) at 5.0-cm depth for the standard 10x10 cm^2 treatment beam.

The increased doses to other organs due to the use of the BNCEFNT assembly were calculated using MCNP5 and a MIRD phantom. The activities of the activation products produced in the BNCEFNT assembly after neutron beam delivery were computed. The photon ambient dose rate due to the radioactive activation products was also estimated.

CHAPTER 1

INTRODUCTION

Of the estimated 17,000 primary brain tumors diagnosed in the United States each year, approximately 60% are gliomas [1]. Glioblastoma multiforme (GBM), a primary, grade IV brain tumor, is by far the most common and most malignant of the glial tumors. This type of tumor is very difficult to remove completely by surgery due to its finger-like extensions that infiltrate the surrounding normal brain tissue. Patients diagnosed with GBM normally die within three months without treatment, and the mean survival time of the treated GBM patients is about one year.

GBM is radioresistant and the trials of photon therapy and fast neutron therapy have failed to provide a cure. However, the use of postoperative radiotherapy has shown to increase the median survival rate [2]. Studies reported by Catterall et al. has shown that the anti-tumor effects for patients receiving fast neutron therapy are greater than for patients receiving megavoltage x-ray photon therapy [3].

Interest in the use of boron neutron capture therapy (BNCT) to treat giloblastoma started in the early 1950s. A ^{10}B containing drug would be administered to the GBM patient and the ^{10}B would be preferentially accumulated in the tumor volume. Then the tumor is irradiated with a thermal or epithermal neutron beam from a nuclear reactor or other neutron source. Boron-10 has a large thermal neutron capture cross section, and the highly ionizing alpha particle and lithium ion emitted from the reaction releases 2.34 MeV/interaction. Subsequently, the high linear energy transfer (LET) alpha particle and lithium ion give a large localized dose to the tumor cells. Despite the high tumor doses, the success of BNCT for GBM patients is quite limited, and it is still at the trial stage today.

Waterman proposed the combination of boron neutron capture therapy and fast neutron therapy in 1978 [4], often called boron neutron capture enhanced fast neutron therapy (BNCEFNT), or neutron capture augment FNT. This therapy takes the advantage of fast neutron therapy (better penetration) and the dose enhancement at the tumor volume from BNCT. Studies have been focused on the improvement of physical dose enhancement for the BNCEFNT. No patients have ever been treated with BNCEFNT.

1.1 Objective

The objective of this work was to design a reflected BNCEFNT assembly around the patient's head with the goal of providing a greater than 15% dose enhancement for a 100-ppm ^{10}B concentration. As a constraint on the BNCEFNT assembly, the total dose rate delivered to the patient should not decrease substantially. The design should not require any change in the structure of the standard treatment beam assembly.

The absorbed dose to other organs of the patient using the BNCEFNT assembly should be evaluated.

1.2 Organization

A brief review of boron neutron capture therapy (BNCT), fast neutron therapy (FNT) and boron neutron capture enhanced fast neutron therapy(BNCEFNT) is given in Chapter 2. The methods to measure fast neutron therapy dose and boron neutron capture dose are presented in Chapter 3. The calibration of the paired ion chambers used in this work, with an emphasis on the thermal neutron calibration, are also reported in Chapter 3. The measurements of spectral fluence rate of the Fermilab NTF neutron beam are presented in Chapter 4. In Chapter 5, the design of the BNCEFNT assembly using MCNP5 code is described and the calculated boron dose enhancements and total dose rate for various settings are given. The measurements and simulation of dose enhancement and total dose rate in a water-filled head phantom using a simplified BNCEFNT are also reported in

Chapter 5. The calculation of dose to other organs of the patient using the BNCEFNT assembly for treatment is reported in Chapter 6. The activities of the most common activation products in the filter and collimator of the BNCEFNT assembly and dose rate due to these activities are reported in Chapter 7. Conclusions and recommendations for future investigations are presented in Chapter 8.

Measurements and MCNPX calculations of the Fermilab NTF neutron spectral fluence rate are tabulated in Appendix A as are the responses of the foil activations ^{28}Al, ^{27}Mg, ^{24}Na, ^{62}Cu and ^{66}Cu used to construct the spectrum. The measurements and calculations of dose enhancement and total dose rate are tabulated in Appendix B. The raw data from the BNCEFNT design validation are given in Appendix C. Selected MCNPX and MCNP5 input files are listed in Appendix D.

CHAPTER 2

BACKGROUND

2.1 Boron Neutron Capture Therapy

The advantage of ^{10}B in neutron capture therapy over other isotopes is its large reaction cross section, 3839 barns for 0.0253 eV neutrons, its high natural abundance 19.8%, and its high-LET reaction products. ^{10}B is also available enriched to greater than 90%. The boron neutron capture reaction for BNCT is shown in Figure 1 . The lithium ion and alpha particle lose their energy over distances less than 10 μm, which is less than the diameter of a cell nucleus. The 1.47-MeV alpha particle has a stopping power of 150 MeV/mm and the 0.84-MeV lithium ion has a stopping power of 52 MeV/mm.

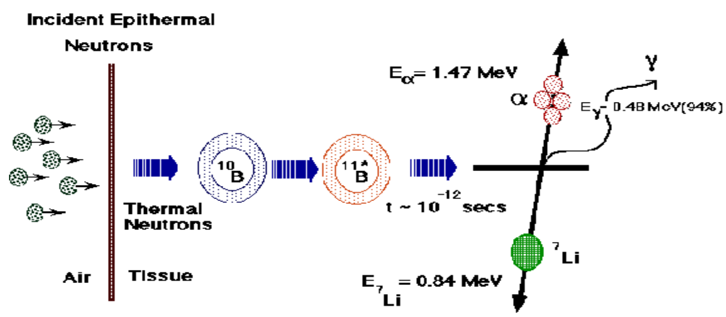

Figure 1: Demonstration of boron neutron capture reaction in tissue

William Sweet was the first to apply boron neutron capture therapy (BNCT) to the treatment of brain tumors. Sweet found that the blood-brain barrier prevented “first generation” borated compound from reaching normal tissue [5] and thus boron would be preferentially accumulated in the tumor volume where the blood-brain barrier was broken.

In the United States, the first clinical trial of boron neutron capture therapy (BNCT) for patients with GBM was initiated at Brookhaven National Laboratory’s Graphite Research Reactor (BGRR) in 1951 [6]. From 1959 to 1961 a series of patients with intracranial tumors received BNCT at the Brookhaven Medical Research Reactor (BMRR). Another group of patients with malignant gliomas was treated at a reactor at the Massachusetts Institute of Technology (MIT) during 1959~1961. Results from these trials were disappointing and all clinical trials in the US were stopped. The disappointing results were attributed to the inadequate penetration of thermal neutron beams and poor localization of boron in tumor.

In the 1980's, improvements in neutron beams and boron compounds allowed reconsideration of BNCT. Clinical trials re-started in 1994 in the United States. The treatments were given with a closed skull using epithermal beams. Both boron phenylalanine-fructose (BPA-F) and sodium borocaptate ($Na_2B_{12}H_{11}SH$: BSH) boron compounds were used in these trials. The primary objective of the protocols was to evaluate the safety of BPA-F mediated BNCT in patients with GBM. As a second objective, the palliation of GBM by BPA-F mediated BNCT was assessed. Between September 1994 and June 1999, 54 patients were treated with BPA-F based BNCT at the BMRR. Of the 28 patients treated under protocol 4 (the most recent data available) at Brookhaven National Laboratory, 11 received single field therapy with a median survival of 14 months while the 17 patients with larger tumor volumes (37 cc versus 18 cc) treated with two fields had a median survival of 10.5 months [7].

At Harvard-MIT, a phase I trial was conducted between July 1996 and May 1999 and 24 patients with primary or metastatic brain tumors were entered into the trial (22 patients were irradiated at the MIT Nuclear reactor laboratory) [8]. Neutron irradiation was delivered with a 15-cm diameter epithermal beam. The treatment plans varied from 1 to 3 fields depending upon the size and location of the tumor. The ^{10}B carrier, amino acid boron phenylalanine-fructose (BPA-F) compound was infused through a central venous catheter at doses of 250 mg/kg over 1 h (10 subjects), 300 mg/kg over 1.5 h (2 subjects), or 350 mg/kg over 1.5-2 h (10 subjects). The pharmacokinetic profile of ^{10}B in blood was very reproducible and permitted a predictable model to be developed. A more recent phase I/II clinical trial was conducted at Harvard-MIT using a fission converter epithermal neutron beam [9]. Six GBM patients were treated with NCT by infusion of the BPA-F boron carrier at a dose of 14.0 g/m^2 body surface area over 90 min followed by irradiation by epithermal neutrons. The reported doses (in RBE Gy) were biologically weighted by applying the relative biologic effectiveness (RBE) factors for fast neutrons (3.2), thermal neutrons (3.2) and the compound biologic effectiveness factor (CBE) for the boron compound (3.8 for tumor and 1.3 for normal tissue). A dose reduction factor of 0.5 was applied for photon dose. Estimates of average tumor dose ranged from 33.7 to 83.4 RBE Gy (median 57.8 RBE Gy), a substantial improvement over the previous trials where the median value of the average tumor dose was 25.8 RBE Gy.

Between August 1968 and July 2001, 183 patients with different kinds of brain tumors were treated by BNCT using 6 different reactors in Japan. In the retrospective analysis of appropriate radiation dose of boron n-alpha reactions, 105 patients with glial tumors treated in Japan between 1978 and 1997 were included [10]. Only the absorbed doses from boron n-alpha reactions were considered important to clinical outcomes. The RBE of the heavy charged particles was not evaluated. Gamma and fast neutron doses were not estimated. When 105 patients were divided according to whether they survived for more (group 1; n=29) or less (Group 2; n=76) than 3 years, it was found that those with longer survival times had received a significantly higher tumor volume dose. In patients with grade 2 giloma, the dose was 11.4 Gy (Group 1) versus 7.1 Gy (Group2), in those with grade 3 it was 15.3 Gy (Group 1) versus 10.5 Gy (Group 2), and in patients with glioblastoma (grade 4) it was 15.6 Gy (group1) versus 9.5 (group 2). Yamamoto et al. [11] reported on the latest BNCT trial at the Japan Research Reactor 4 (JRR-4) which has a mixed thermal/epithermal neutron beam. Nine patients with high-grade gliomas (5 glioblastoma and 4 anaplastic astrocytomas) were treated with BSH-based intraoperative boron neutron capture therapy. The blood boron level at the time of irradiation averaged 29.9 (18.8-39.5) μg/g. The minimum boron dose for the tumor and target volume averaged 15.9 Gy (7.5-24.6 Gy) and 7.3 Gy (3.7-11.9Gy), respectively. At the time of the report, 7 (4 glioblastoma and 3 anaplastic astrocytoma) of the 9 patients had died. The median survival time was 23.3 months for glioblastoma and 25.9 months for anaplastic astrocytoma.

In Europe, a phase I clinical trial testing the tolerance of the central nervous system (CNS) to BSH-mediated BNCT was undertaken and 10 patients have been treated [12]. In the European clinical trial, photon therapy is replaced by BNCT which is administered 2-6 weeks after debulking surgery. The boronated drug used is sodium borocaptate (BSH). The radiations are performed using the epithermal neutron beam of the High Flux Reactor at the Joint Research Center (JRC) in Petten/The Netherlands. The clinical trial is based on extensive preclinical dog studies as well as on distribution studies of the BSH in tumor cells.

The reports from both the Harvard-MIT and BNL studies indicate that the use of BNCT on residual tumor volumes greater than 60 cm^3 leads to a greater incidence of neurological toxicity associated with increased intracranial pressure [8, 13]. This is an acute effect related to tumor cell killing and associated edema. Other than side effects related to the residual tumor volume, the most commonly observed neurological side effect was a somnolence syndrome. The combined data for 68 evaluated patients from the Harvard-MIT and BNL BNCT clinical studies indicated that the doses associated with a 50% incidence of the effect (ED_{50}±SE) were 6.2 ±1.0 and 14.1±1.8 Gy(w) for average whole-brain doses and peak brain doses, respectively [14]. The brain doses are expressed in weighted (Gy(w)) units using RBE and compound biological effectiveness (CBE) [15,16] factors reported by Coderre and Morris [17] and Coderre et al. [18].

Kageji et al. [19] concluded from their study that the maximum vascular dose should not exceed 12 Gy to avoid the delayed radiation injury. In particular, it should be less than 10 Gy if the tumor exists in the speech center. The doses here are expressed in boron neutron capture physical dose (Gy).

In clinical BNCT dosimetry, estimates of ^{10}B dose in normal healthy tissue are generally based on the ^{10}B concentration in blood as a surrogate for normal tissue [20-22]. Furthermore, in the trials using the BPA-F complex as the boron delivery agent, a temporally constant tumor-to-blood concentration ratio of approximately 3.5-4 to 1 is assumed for GBM [23-25]. These tumor-to-blood uptake ratios were measured by Coderre et al. 0.5-1.5 h after the end of infusion [26, 27]. A pharmacokinetic model to predict ^{10}B concentration in blood following the infusion of BPA-F, a schedule currently employed for BNCT treatment by Harvard-MIT group, has been developed by Kiger et al. [28, 29].

2.2 Fast Neutron Therapy

The study of biological effectiveness of neutrons started after the discovery of the neutron by Chadwick in 1932 [30]. In 1936 Lawrence et al. demonstrated that neutrons had a "selectively effect" in killing tumor tissue as opposed to health tissue when compared to x-rays [31]. In 1939, Stone began to treat patients using a neutron beam produced by 16-MeV deuterons on a beryllium target. He reported that the neutrons produced a beneficial tumor response, but the treatment resulted in unacceptable late skin and subcutaneous radiation changes. In 1948, Stone concluded that neutrons had no place in cancer treatment because the side effects he observed outweighed the clinical benefits [32]. Ten years later researchers reopened this question and found out that Stone had severely overdosed the early patients [33]. New clinical studies [34] were begun in 1966 and their encouraging results led to the development of neutron therapy clinical trials throughout the world.

Fast neutron beams are considered the treatment of choice for inoperable salivary gland tumors. Fast neutron therapy has demonstrated advantage over conventional photon therapy [35] for the treatments resulting in long-term survival in advanced prostate cancer, inoperable squamous-cell lung cancer, soft-tissue sarcoma and osteosarcoma. It is estimated that 10-20% [36] of all oncology radiation patients would benefit from fast neutron therapy.

It was presumed that the fast neutrons may be beneficial for the treatment of brain tumors due to the presence of hypoxic cells. The clinical trials on fast neutron therapy for brain tumors did not show any advantage over photon therapy [36, 37] considering the life quality and survival time of the patients. Autopsy studies revealed considerably greater tumor destruction in the neutron-treated patients compared with those receiving photon treatments, but survival was limited by the onset of fatal post-irradiation gliosis. This implied that no therapeutic window existed at which tumor control could be achieved without serious side effects.

2.3 Boron Neutron Capture Enhanced Fast Neutron Therapy

Boron neutron capture enhanced fast neutron therapy (BNCEFNT) was first proposed by Waterman et al. in 1978 [4]. In their proposal a boron containing drug would be used to selectively load the tumor cells with boron. Instead of irradiating the tumor with thermal or epithermal neutron beam, the tumor is irradiated with a fast neutron therapy beam. As a fast neutron beam penetrates the tissue some of the particles are degraded to thermal energies which can be captured by ^{10}B resulting in a highly-localized release of additional energy during a course of fast neutron therapy. The percent dose enhancement (PDE) of a neutron beam generated by bombarding a 50-MeV proton beam on a beryllium target is about 0.1% per ppm of boron concentration [39]. Since the fast neutron therapy beams are designed to minimize the thermal neutron spectral component, it needs to be modified to have a larger fraction of thermal/epithermal neutrons to enhance the boron neutron capture dose in the tumor and thus to set up a therapeutic window for the treatment of radiation-resistant tumors.

Several fast neutron therapy facilities worldwide, including the University of Washington (UW), Harper Hospital Fast Neutron Therapy facility, the Fermilab Neutron

Therapy Facility (NTF), National Accelerator Centre (iThemba), and the Biomedical Cyclotron of Nice, are investigating ways of increasing the boron neutron capture dose.

In the UW FNT facility protons are accelerated in a cyclotron to an energy of 50.5 MeV. The resulting proton beam is directed by a series of magnets and focusing devices onto the target. The standard target is a 10.5 mm beryllium target. The spectral character of the fast neutron beam was determined using activation foil technique [40]. A modified target specifically designed for BNCEFNT studies has been installed. The new target is composed of a 5-mm layer of beryllium, followed by a 2.5-mm layer of tungsten. The new target design produces essentially the same neutron flux above 40-MeV as the standard target, per unit proton current, but leads to a decreased fluence rate in the 10 to 40-MeV range and an increased fluence rate below 10 MeV. The new target produces a boron dose enhancement of 13% to 14% at a depth of about 6 cm for a 100 ppm boron-10 concentration and a 10x10 cm^2 beam. The standard target resulted in a boron dose enhancement of about 7% at the 6-cm depth [41, 42].

The Harper Hospital Fast Neutron Therapy Facility uses a superconducting cyclotron which accelerates deuterons to an energy of 48.5 MeV. The deuteron beam is incident on a beryllium target (14.9x20.1x3.1 mm) brazed to a channeled copper backing plate which is cooled with water [43]. The unmodified beam at this facility has a boron dose enhancement of 2.5% to 5% per 100-ppm ^{10}B [44]. Studies at this facility have investigated the use of steel, tungsten, lead, and aluminum as possible filter materials for a BNCEFNT beam [45]. They found that the steel and tungsten provided the highest dose enhancements. Burmeister et al. [46] used a 25-cm thick steel filter upstream of the beam to obtain a therapeutic gain factor (defined as the ratio of RBE-weighted tumor dose to RBE-weighted normal tissue dose) greater than 50% for a 15x15 cm^2 field at depths required to treat brain lesions. The modification of the beam resulted in RBE-weighted tumor dose rate of approximately 4 cGy/min at the depth of 2.5 cm, which is too low for clinical applications.

The Nice Biomedical cyclotron produces 60-MeV protons that are incident on a laminated target of 15-mm of beryllium followed by 9-mm of graphite. A percent dose enhancement of 4.6% per 100-ppm ^{10}B for a 10x10 cm^2 field and 10.4% for a 20x20 cm^2 field [47] has been calculated using FLUKA/MCNP-4A codes. Further studies to increase the PDE for the Nice Biomedical Cyclotron have focused on the addition of high atomic number material collimation near the patients head which is surrounded by a block of graphite. These studies concluded that a lead collimator placed near the head can produce PDE of 22% per 100-ppm ^{10}B [48].

The Fermilab Neutron Therapy Facility produces neutrons by bombarding a 2.21-cm-thick beryllium target with 66-MeV protons. The protons lose 49 MeV in the beryllium target and are stopped by a 0.5-mm gold backing [49, 50]. The percent dose enhancement (PDE) of the Fermilab NTF has been measured by Katja Langen using tissue-equivalent proportional counter loaded with 200-ppm ^{10}B [51]. These measurements were performed in a head-shaped Lucite phantom filled with water at a depth of 5 cm. A PDE of 1.5% per 100-ppm ^{10}B for the 10x10 cm^2 field of the standard treatment beam was measured. Langen also attempted to modify the beam to increase the dose enhancement by using 9.0 cm of tungsten filtration. The tungsten filter was placed near the head phantom and produced a dose enhancement of (2.5±0.1)% for 100-ppm ^{10}B. She reduced the proton energy to 37-MeV, and thus obtained a dose enhancement of (6.0±0.2)% using 20-cm thick steel blocks to form a 12 x 12 cm^2 beam and using the 9.0 thick tungsten filter.

Jeremy Sweezy investigated the modification of the standard fast neutron beam at Fermilab NTF to increase PDE by using different collimation and filter materials with the MCNPX code [52]. He chose iron from 86 materials studied for use as collimation and filter materials. He measured a boron dose enhancement of 16.3% per 100-ppm ^{10}B for a 20-cm diameter beam and 10.0% per 100-ppm of ^{10}B for a 10-cm diameter beam for this system. The dose rate of the modified beam was reduced to 4.4% of the dose rate of the standard treatment beam [53]. Sweezy also proposed the use of tungsten filter, tungsten collimator and graphite reflector around the head instead of using a filter and collimator up stream of the beam to increase the boron percent dose enhancement (PDE). He calculated a PDE of about 30% per 100 ppm ^{10}B with a 5-cm thick tungsten filter, a 10-cm-thick by 5.64-cm-inner-diameter tungsten collimator and a partial graphite reflector placed around a mathematical head phantom [53].

CHAPTER 3

DOSE MEASUREMENTS

Two tissue-equivalent ionization chambers manufactured by Exradin, now the Standard Image, Inc. [54], were available for the measurement of the fast neutron, photon and boron dose in the head phantom at Fermilab NTF. The chambers are 0.5-cm^3 Spokas thimble chambers composed of A-150 tissue-equivalent plastic. The two ion chambers are identical except that one of them is borated with 1000-ppm of natural boron in the tissue equivalent (TE) material. Since ^{10}B comprises 18.4 weight percent of natural boron, the borated detector contains 184-ppm of ^{10}B. For all measurements and calibrations in this work, the ionization chambers are filled with air.

3.1 Measurements of the absorbed dose

The technique of using ionization chamber to measure the absorbed dose is based on the application of the Bragg-Gray Principle, which states that the absorbed dose in a given material can be deduced from the ionization produced in a small gas-filled cavity within the material. This relationship is based on the assumption that the charged particles produced by the radiation in the wall material of an ionization chamber lose a negligible fraction of the energy in traversing the gas cavity. This requires the use of a small cavity or alternatively the use of a homogeneous chamber, i.e., a chamber with wall and gas of the same composition. Ion chambers collect charges liberated in the fill gas, chamber wall, and surrounding media. The charge collected for radiation type x, Q_x, is proportional to the absorbed dose in the chamber gas, which is in turn proportional to the absorbed dose in the chamber wall, $D_{w,x.}$ The absorbed dose can be expressed as

$$D_{w,x} = Q_x \cdot \frac{\overline{W}_x}{e} \cdot \left(S_{w,g}\right)_x \cdot \frac{1}{M_g} \tag{3.1}$$

where M_g = the mass of the gas in the cavity

$(S_{w,g})_x$ = ratio of stopping powers of wall to gas for secondary charged particles

$\overline{W}_x/e$ = the average energy required to produce an ion pair in the gas

e = the charge of the electron (1.6 x10^{-19} Coulomb)

The subscript x denotes the type of radiation. If the ion chamber is calibrated in a ^{60}Co field the subscript is C. If the ion chamber is used to measure a mixed radiation beam the subscript is T, for total. The subscript N is often used in place of T when the neutron component predominates the radiation field.

For determination of the absorbed dose in tissue or tissue-equivalent phantom, $D_{t,x}$, the ratio of the mass-energy absorption coefficient of muscle tissue to that of the material of the chamber wall (A-150), K_x, must be applied.

$$D_{t,x} = K_x \cdot D_{w,x} \tag{3.2}$$

For measuring the absorbed dose of tissue in a mixed fast neutron and gamma radiation beam, $D_{t,T}$, the following equation should be used.

$$D_{t,T} = Q_T \cdot \frac{1}{M_g} \cdot \frac{\overline{W_N}}{e} \cdot \left(S_{w,g}\right)_N \cdot K_N \cdot d_{NG} \tag{3.3}$$

where $K_N = K_t/K_w$ is ratio of neutron kerma factor for tissue to that of A-150, d_{NG} is the chamber displacement correction factor which accounts for the perturbation of the radiation field by the displacement of the phantom material by the ion chamber, $\overline{W}_N/e$ is the average energy (J/C) required to produce an ion pair in the chamber gas by secondary charged particles created by neutrons, and Q_T is the charge collected by the detector. In this work, the absorbed dose due to fast neutron and gammas is measured with the non-borated ion chamber and Q_T is replaced by Q_{NB}.

As seen in Equations (3.1) and (3.3), the mass of the gas, M_g, in the sensitive volume of the chamber is required. Generally, the sensitive volume of a chamber can not be computed with the designed accuracy from drawings. Therefore, the ion chamber is normally placed in a ^{60}Co field of known exposure for calibration. The absorbed dose of tissue from the known exposure to ^{60}Co is obtained by

$$\boldsymbol{D}_{t,C} = \boldsymbol{X}_c \cdot \boldsymbol{f}_{t,C} \cdot \boldsymbol{A}_{w,C} = \boldsymbol{Q}_C \cdot \frac{1}{\boldsymbol{M}_g} \cdot \frac{\overline{\boldsymbol{W}}_C}{\boldsymbol{e}} \left(\boldsymbol{S}_{w,g}\right)_C \cdot \boldsymbol{K}_C \tag{3.4}$$

where X_c is the known exposure (R) from the ^{60}Co source, $f_{t,C}$ is the tissue-dose-to-exposure conversion coefficient (Gy/R), $A_{w,C}$ is the photon attenuation and scattering correction factor for the chamber(unitless), and $\overline{W}_C /e$ is the average energy (J/C) required to produce an ion pair in the chamber gas by secondary electrons created by ^{60}Co gamma rays. Combining equation 3.3 and 3.4, Equation 3.5 is obtained

$$\boldsymbol{D}_{t,T} = \boldsymbol{Q}_T \cdot \boldsymbol{f}_{t,C} \cdot \boldsymbol{A}_{w,C} \cdot \boldsymbol{d}_{NG} \cdot \boldsymbol{N}_C \cdot \frac{\overline{\boldsymbol{W}}_N}{\overline{\boldsymbol{W}}_C} \cdot \frac{\left(\boldsymbol{S}_{w,g}\right)_N}{\left(\boldsymbol{S}_{w,g}\right)_C} \cdot \frac{\boldsymbol{K}_N}{\boldsymbol{K}_C} \tag{3.5}$$

where $N_c = X_C / Q_C$ is the ion chamber ^{60}Co calibration factor, (R/nC). The AAPM Report No. 7 recommended values and uncertainties [55] for these factors in Equation (3.5) are shown in Table 1. The value of the displacement correction factor, d_{NG}, shown in Table 1 for 0.5-cc chamber is the linear interpolation of 0.970 (1.0-cc chamber) and 0.989 (0.1-cc chamber). These parameters are used in this experiment. Using these values, Equation (3.5) becomes

$$\boldsymbol{D}_{t,T} = \boldsymbol{N}_C\left(\boldsymbol{R}/\boldsymbol{nC}\right) \cdot 0.985 \cdot 0.00957\left(\boldsymbol{Gy}/\boldsymbol{R}\right) \cdot 0.981 \cdot \frac{1.157}{1.142} \cdot \frac{35.8\left(\boldsymbol{J}/\boldsymbol{C}\right)}{33.7\left(\boldsymbol{J}/\boldsymbol{C}\right)} \cdot \frac{0.952}{1.004} \cdot \boldsymbol{Q}_T\left(\boldsymbol{nC}\right)$$

$$= 9.437 \times 10^{-3}\left(\boldsymbol{Gy}/\boldsymbol{R}\right) \cdot \boldsymbol{N}_C\left(\boldsymbol{R}/\boldsymbol{nC}\right) \cdot \boldsymbol{Q}_T\left(\boldsymbol{nC}\right) \tag{3.7}$$

The charge measured in mixed radiation, Q_T, should be corrected to the same temperature-pressure condition as that of the ion chamber ^{60}Co calibration factor, N_c. The uncertainty of the coefficient in Equation (3.7), 9.437x10^{-3} (Gy/R), is about 9%, which is the combination of the uncertainties listed in Table 1.

The response of the ion chamber is a function of the mass of the gas in the chamber volume. The mass of the air inside the chamber changes with the change of temperature and pressure, so a correction of the temperature and pressure must be applied to the measurement. The temperature and pressure correction factor, TPC, corrected to the standard condition, 0 °C and 1000 kPa is

$$TPC_x = \frac{273.15 + T_x}{273.15} \cdot \frac{1000\text{kPa}}{P_x} \tag{3.6}$$

where T_x is the temperature (°C) and P_x is the pressure (kPa), the subscript x denotes the environment of the measurement.

Table 1: AAPM recommend values and uncertainties [55] of the constants in Equation (3.5).

Constant	AAPM value	Uncertainty (%)	Unit
$A_{w,C}$	0.985	0.5	unitless
$f_{t,C}$	0.00957	0.2	Gy/R
d_{NG}	0.981	1	unitless
$(S_{w,g})_N$	1.157	4-5	unitless
$(S_{w,g})_C$	1.142	1.0	unitless
$\overline{W}_N /e$	35.8	6-8	J/C
$\overline{W}_C /e$	33.7	0.4	J/C
K_N	0.952	2	Unitless
K_C	1.004	0.2	unitless

3.2 Borated Ion Chamber Thermal Neutron Response

The dose due to the boron capture reaction is a function of the ^{10}B concentration and the thermal neutron flux. It can be measured using the borated and non-borated TE ion chamber. Because the alpha particles and lithium ions have a very short range in air the Bragg-Gray principle may not be satisfied for ion chambers with dimensions larger than the range of alpha particles and lithium ions. To overcome this problem the two ion chambers should be calibrated in a thermal neutron beam of known thermal neutron fluence rate.

The thermal neutron fluence is proportional to the difference of collected charges in the borated and non-borated ion chamber multiplied with a calibration factor.

$$\phi_{th} = N_{th} \cdot \left[Q_B - Q_{NB} \left(\frac{N_C^{NB}}{N_C^B} \right) \right] \tag{3.8}$$

where ϕ_{th} = the thermal neutron fluence (n/cm^2).

N_{th} = the ion chamber thermal neutron calibration factor (n/cm^2/nC)

Q_B = the charge collected by the borated chamber (nC)

Q_{NB} = the charge collected by the non-borated chamber (nC)

N_C^B = ^{60}Co calibration factor of the borated ion chamber (R/nC)

$N_C^{N\text{-}B}$ = ^{60}Co calibration factor of the non-borated ion (R/nC)

If the thermal neutron fluence is known, the thermal neutron calibration factor can be calculated

$$N_{th} = \frac{\phi_{th}}{\left[Q_B - Q_{NB} \left(\frac{N_C^{NB}}{N_C^B} \right) \right]} \tag{3.9}$$

The boron capture dose, or the boron neutron capture rate per unit mass, is proportional to the thermal neutron fluence rate. The boron capture dose can be calculated from the boron capture rate:

$$D_{B-10}(Gy) = \frac{\phi_{th} \sigma_{a_{th}}^{B-10} N_{B-10} Q}{\rho_{wall}} \tag{3.10}$$

where $\sigma_{a_{th}}^{B-10}$ = the average microscopic (n,α) cross section for thermal neutrons (cm^2).

$N_{B\text{-}10}$ = the atomic density of ^{10}B (atoms/cm^3).

Q = the energy imparted to the alpha and lithium ions from the (n,α) reaction (2.34 MeV).

ρ_{wall} = density of the wall material (g/cm^3).

The (n, α) cross section of the ^{10}B nuclide has a 1/*v*-behavior in thermal neutron region and the thermal reaction cross section, $\sigma_{a_{th}}^{B-10}$ can be related to the (n, α) cross section of 2200 m/s neutrons (0.0253 eV) by

$$\sigma_{a_{th}}^{B-10} = \frac{\sqrt{\pi}}{2} \cdot \sqrt{\frac{T_0}{T_n}} \cdot \sigma_a^{B-10}(E_0) \tag{3.11}$$

where T_0 and T_n are temperatures of the tabulated cross section (typically 293.46K) and the moderator for the measurement, respectively. $\sigma_a^{B-10}(E_0)$ is the microscopic (n, α) cross section for neutrons of energy E_0 (0.0253 eV). From the ENDF-VI [56] evaluation for ^{10}B, $\sigma_a^{B-10}(0.0253eV)$=3839 ± 6 barns, therefore $\sigma_{a_{th}}^{B-10}$=3402 ± 6 barns if $T_\mathrm{n} = T_0$.

The ^{10}B atomic density of the borated ion chamber can be calculated from

$$N_{B-10} = \frac{w_{B-10}\rho_{wall}N_a}{A_{B-10}} \tag{3.12}$$

where w_{B-10} =weight percent of ^{10}B, 184 ppm for the borated ion chamber used.

N_a = Avogadro's number, 6.022 x 10^{23}atoms/mole.

A_{B-10} = atomic weight of ^{10}B, 10.01293 g/mole.

Combining Equations (3.8), (3.10), and (3.12), we have

$$D_{B-10}(Gy) = N_{th} \cdot \left[Q_B - Q_{NB}\left(\frac{N_C^{NB}}{N_C^B}\right)\right] \cdot \sigma_{a_{th}}^{B-10} \cdot \frac{Q}{\rho_{wall}} \cdot \frac{w_{B-10}\rho_{wall}N_a}{A_{B-10}}$$

$$= N_{th} \cdot \left[Q_B - Q_{NB}\left(\frac{N_C^{NB}}{N_C^B}\right)\right] \cdot Q \cdot \sigma_{a_{th}}^{B-10} \cdot \frac{w_{B-10}N_a}{A_{B-10}} \tag{3.13}$$

Substituting the parameters in Equation 3.13, for the 184-ppm ^{10}B ion chamber, Equation (3.13) becomes

$$D_{B-10}(Gy) = N_{th}\left(\frac{\mathrm{n}}{\mathrm{cm}^2 \cdot \mathrm{nC}}\right) \cdot \left[Q_B(\mathrm{nC}) - Q_{NB}(nC)\left(\frac{6.709\left(R/_{nC}\right)}{7.055\left(R/_{nC}\right)}\right)\right] \cdot \left(3402 \times 10^{-24}\,\mathrm{cm}^2\right) \times$$

$$\frac{\left(184 \times 10^{-6}\right)\left(6.022 \times 10^{23}\ \mathrm{atoms}/_{\mathrm{mole}}\right)}{\left(10.01293\ \mathrm{g}/_{\mathrm{cm}^3}\right)}\left(2.34\mathrm{MeV}\right)\left(1.602 \times 10^{-13}\,\frac{\mathrm{J}}{\mathrm{MeV}}\right)\left(1000\,\frac{\mathrm{g}}{\mathrm{kg}}\right)$$

$$= 1.411 \times 10^{-11}\left(\frac{\mathrm{Gy}}{\mathrm{n}/_{\mathrm{cm}^2}}\right) \cdot \boldsymbol{N_{th}}\left(\frac{\boldsymbol{n/cm}^2}{\boldsymbol{nC}}\right) \cdot \left[\boldsymbol{Q_B}(\mathrm{nC}) - \boldsymbol{Q_{NB}}(\boldsymbol{nC})\left(\frac{\boldsymbol{N_C^{NB}}}{\boldsymbol{N_C^B}}\right)\right] \tag{3.14}$$

3.3 Dose Enhancement Due to Boron Neutron Capture

The percent dose enhancement (PDE) is defined as

$$PDE = \frac{D_{B-10}}{D_{n+\gamma}} \times 100(\%) \tag{3.15}$$

where $D_{n+\gamma}$ is the dose due to fast neutrons and gamma rays, which is the same as $D_{t,T}$ defined in Equation (3.7). Substituting Equations (3.7) and (3.14) into Equation (3.15), yields,

$$\boldsymbol{PDE} = 1.495\times10^{-9}\left(\frac{\mathrm{R}}{\mathrm{n/cm^2}}\right)\left(\frac{\boldsymbol{N_{th}}\left(\frac{\mathrm{n/cm^2}}{\mathrm{nC}}\right)}{\boldsymbol{N_C^{NB}}\left(\frac{\mathrm{R}}{\mathrm{nC}}\right)}\right)\left[\frac{\boldsymbol{Q_B}(\mathrm{nC}) - \boldsymbol{Q_{NB}}(\mathrm{nC})\left(\frac{\boldsymbol{N_C^{NB}}}{\boldsymbol{N_C^{B}}}\right)}{\boldsymbol{Q_{NB}}(\mathrm{nC})}\right]\times100\% \tag{3.16}$$

3.4 Calibration of the TE Ionization Chambers

3.4.1 Gamma-ray Calibration

The TE ion chambers used in this project were calibrated in NIST traceable ^{60}Co source field on several occasions and the calibration factors are consistent. The borated and non-borated ion chambers were calibrated at the University of Wisconsin-Madison Radiation Calibration Laboratory. The radiation Calibration Laboratory is a National Institute of Standards and Technology (NIST) accredited secondary standards laboratory and is also accredited by the American Association of Physicists in Medicine (AAPM). The ion chambers were calibrated against a NIST traceable source to determine the ^{60}Co calibration factor, N_C (R/nC). The borated ion chamber (SN #446) had a calibration factor of 7.055 R/nC ± 2%. And the non-borated TE ion chamber (SN #445) had a calibration factor of 6.709 R/nC ± 2%.

The two ion chambers were also calibrated against a NIST traceable ^{60}Co source at the Georgia Institute of Techmology (Georgia Tech) ^{60}Co Irradiation Facility. The exposure rate of the Georgia Tech ^{60}Co source had an uncertainty of 3.4%. The calibration factors for the borated and non-borated ion chamber were determined to be 6.972 (R/nC) ± 4% and 6.591 (R/nC) ± 4%, respectively. The calibration factors obtained in the two calibration facilities agreed within uncertainty.

Table 2: Gamma calibration results of the borated and non-borated ion chambers

Calibration Source	Calibration Facility	Calibration Date	NB-IC (SN#445)	B-IC (SN#446)	Ratio NB-IC/B-IC
^{60}Co	UW	04/06/2001	6.709	7.055	0.9510
	GIT	07/07/2004	6.552	6.978	0.9390
	GIT	08/19/2004	6.630	6.966	0.9518
^{137}Cs	NTF	05/06/1996	6.743	7.072	0.9535
	NTF	01/21/2001	6.885	7.279	0.9459
	UW	04/06/2001	6.846	7.180	0.9535
	NTF	11/30/2001	6.714	7.097	0.9460
	NTF	05/19/2006	6.808	7.101	0.9587
	Average		6.736	7.091	0.9499
	St. Dev.		0.111	0.102	0.0061
	Percent Error		1.6%	1.4%	0.6%

UW – University of Wisconsin-Madison Radiation Calibration Laboratory
NTF – Fermilab Neutron Therapy Facility
GIT – Georgia Tech Irradiation Facility

Before each set of measurements, the detectors were checked with a ^{137}Cs source located in the treatment room of the Fermilab Neutron Therapy Facility. The calibration factors from the ^{60}Co and ^{137}Cs sources are shown in Table 2. It shows that the responses of the detectors have been very stable over a long period of time. Since the calibrations performed at the University of Wisconsin-Madison Radiation Calibration Laboratory had the smallest uncertainty, the calibration factors for the borated (N_C^B) and the non-borated (N_C^{NB}) ion chambers, namely 7.055 R/nC ± 2% and 6.709 R/nC ± 2%, were used in the late measurements. The different responses of the two detectors implies that the gas volume of the borated ion chamber is smaller than that of the non-borated ion chamber by the following ratio

$$\frac{\boldsymbol{N_C^{NB}}}{\boldsymbol{N_C^B}} = \frac{6.709(\boldsymbol{R/nC})}{7.055(\boldsymbol{R/nC})} = 0.951 \tag{3.17}$$

This correction factor needs to be applied to the charge measured by the non-borated ion chamber before it is subtracted from the charge measured by the borated ion chamber to determine the charge due to boron capture reactions.

3.4.2 Thermal Neutron Calibration

Since alpha particles and lithium ions from the $^{10}B(n,\alpha)^{7}Li$ reactions have very short ranges in air, the Bragg-Gray principle may not be satisfied for the borated TE ion chamber. So this chamber has to be calibrated in a thermal neutron beam of known fluence rate.

Both the borated and non-borated ion chambers were calibrated in the thermal column of Oregon State University (OSU) research reactor in 2001. The thermal neutron fluence rate was determined to be 1.39×10^8 n/cm^2 /sec ± 13% using gold foil activation method. The calibration factor of the borated ion chamber was determined to be 1.76×10^9 n/cm^2 per nC ±13%. The large uncertainty associated with this calibration factor resulted in a large uncertainty of the boron dose enhancements reported by Sweezy [52, 57].

In order to reduce the uncertainty of the thermal neutron calibration factor of the borated ion chamber, the responses of the two ion chambers to thermal neutrons were calibrated again in the National Institute of Standards and Technology (NIST) reactor thermal column in 2004. The NIST thermal column has a very high fraction of thermal neutrons with a cadmium ratio greater than 400 determined by gold foil activation. The calibration of the borated TE ion chamber was performed at the center of the beam. The thermal neutron fluence rate was determined by a dual fission ion chamber [59] provided by NIST. The thermal neutron component of the beam can be substantially attenuated by placing an optically thick lithium slab at the opening of the beam port.

The conversion factor (n/cm^2 per count) of the dual fission ion chamber is calculated using the number of ^{235}U nuclei, the thermal neutron fission cross section and a series of corrections. The fission cross section of ^{235}U for thermal neutrons can be calculated by

$$\sigma_{th} = \frac{\sqrt{\pi}}{2} \cdot g(T) \cdot \sqrt{\frac{T_0}{T}} \cdot \sigma_f(E_0) \tag{3.18}$$

where $\sigma_f(E_0)$ is the microscopic fission cross section for neutrons of energy E_0, typically 0.0253 eV or 2200 m/s, $\sigma_f(0.0253\ eV)$=584 barn; T_0 is the temperature of the tabulated cross section, 294.61 K; T is the temperature of the moderator for the measurement, 303 K; $g(T)$ is the empirical correction factor of the departure from 1/v behavior of ^{235}U. At 303K, $g(T)$ is 0.974. Substituting the values of the parameters in equation (3.18), σ_{th}=496 b is obtained.

The upper chamber of the dual fission chamber has 378.5±1% μg of ^{235}U uniformly deposited over an area of 1.2668 cm^2, corresponding to 9.655x10^{17} ^{235}U nuclei per cm^2. The bottom chamber was not used in the measurements. The detection of the fission fragments is essentially 100% and the conversion factor (CF) of the fission chamber counts to thermal neutron fluence rate is

$$CF = \frac{1}{\sigma_{th} \cdot N} = 2079 \text{ cm}^{-2}/\text{ count} \tag{3.19}$$

The counter reading is the integral of the pulses above the low level discriminator threshold and the integral must be extrapolated to include count down to zero pulse-height. The extrapolation-to-zero correction is 1.0368, self-absorption correction is 1.0206, inscatter from substrate correction is 1/1.034, in-scatter correction from chamber is 1/1.023, out-scatter by chamber bottom and anode correction is 1.009. The total correction factor is the combination of the above, i.e. $(1.0368)(1.0206)\left(\frac{1}{1.034}\right)\left(\frac{1}{1.023}\right)(1.009) = 1.009$, so the corrected count-to-fluence conversion factor for the fission chamber is (2079)(1.009)=2099 cm^{-2}/count.

A correction for the dead time of the electronics must also be made. The width of each pulse is 2μs and the fraction of count loss due to dead time is (2μs/pulse)(# pulses/s). The count rate of the fission chamber at low neutron fluence rate was 2417 counts per second and at high neutron fluence rate were 20,426 counts per second, leading to a dead time losses of 0.005 and 0.0407, respectively. The conversion factor corrected for dead time, CF_f, are 2109.5 ± 5% n/cm^2 per count at the lower neutron fluence rate and 2184.4 ± 5% n/cm^2 per count at the higher neutron fluence rate. The thermal neutron fluence rate, ϕ_{th}, is determined by

$$\phi_{th} = C \cdot CF_f \tag{3.20}$$

where C is the count rate (cps) of the fission chamber for thermal neutrons. Substituting Equation (3.20) into Equation (3.9), the borated ion chamber thermal neutron calibration factor is obtained

$$N_{th} = \frac{C \cdot CF_f}{Q_T^B - Q_T^{NB}\left(\frac{N_C^{NB}}{N_C^B}\right)} \tag{3.21}$$

The subscript T in equation (3.21) stands for the total, including thermal neutrons, fast neutrons and gamma rays. All readings from the ion chambers are corrected to standard temperature and pressure of 273.15K and 100 kPa using Equation (3.6).

The ion chambers, the electrometer, and the high voltage unit were placed near the NIST thermal column beam. Since they are filled with ambient air, the ion chambers have the same temperature and pressure as the experimental environment. The temperature and the pressure in the room were recorded. The fission chamber was placed at the center of the neutron beam with its front surface perpendicular to the neutron beam. The position of the chamber stem was marked to ensure that the placement of the fission chamber was repeatable. The fission chamber was replaced with the ion chamber and the ion chamber was centered at the same location as the fission chamber.

The boron curtain on the thermal column beam was lifted until the thermal neutron fluence rate was around $5x10^6$ n/cm^2 based on the fission chamber readings. The readings of the fission chamber were recorded several times to reduce statistical uncertainties in the count rate. The fission chamber was then replaced with the borated ion chamber (446B). An electrometer was used in charge mode, and readings for integration times of 1 second, 10 seconds and 1 minute were taken at least six times. After the measurements the optically thick lithium plate was placed in the front of the neutron beam port to stop the thermal neutrons and the responses of the borated ion chamber to fast neutrons and gamma rays were recorded. The procedure was repeated for the non-borated chamber (445).

The boron curtain in the reactor was lifted higher to obtain a larger neutron fluence rate and the calibration procedure was repeated. When the measurements with the two TE ion chambers were finished, measurements were performed with the fission chamber at three positions along the neutron beam axis and three positions about the center line of the beam perpendicular to the neutron beam. These data were used to evaluate the uncertainties caused by positioning of the chambers.

The chambers were calibrated at the thermal neutron fluence rates of $5.10x10^6$ and $4.46x10^7$n cm^{-2}s^{-1}. The calibration factors of the borated ion chamber obtained from the lower and higher neutron fluence rates are 1.86 $x10^9$ and 1.81 $x10^9$ n/cm^2 per nC, respectively. The final calibration factor is the average, which is 1.83 $x10^9 \pm$ 5.5% n/cm^2 per nC at STP (0 ˚C and 1000 kPa) conditions. This result agrees with Sweezy's result within the uncertainty.

The dose due to the 184-ppm ^{10}B in the borated ion chamber Equation (3.14) can now be calculated as

$$\boldsymbol{D}_{\boldsymbol{B}-10}(\boldsymbol{Gy}) = 1.411 \times 10^{-11}\left(\frac{\mathrm{Gy}}{\mathrm{n/cm^2}}\right)\cdot 1.83\times 10^{9}\left(\frac{\mathrm{n/cm^2}}{\mathrm{nC}}\right)\cdot\left[\boldsymbol{Q}_{\boldsymbol{B}}(\mathrm{nC}) - 0.951\cdot \boldsymbol{Q}_{\boldsymbol{NB}}(\mathrm{nC})\right]$$

$$= 0.0258\left(\frac{\text{Gy}}{\text{nC}}\right)\cdot\left[\boldsymbol{Q_B}(\text{nC}) - 0.951\cdot\boldsymbol{Q_{NB}}(\text{nC})\right] \tag{3.22}$$

And the PDE can be determined from Equation (3.16) as

$$\boldsymbol{PDE} = 1.495\times10^{-9}\left(\frac{\text{R}}{\text{n/cm}^2}\right)\left(\frac{1.83\times10^9\left(\frac{\text{n/cm}^2}{\text{nC}}\right)}{6.705\left(\frac{\text{R}}{\text{nC}}\right)}\right)\left[\frac{\boldsymbol{Q_B}(\text{nC}) - (0.951)\boldsymbol{Q_{NB}}(\text{nC})}{\boldsymbol{Q_{NB}}(\text{nC})}\right]\times100\%$$

$$= 0.4080\cdot\left[\frac{\boldsymbol{Q_B}(\text{nC}) - (0.951)\boldsymbol{Q_{NB}}(\text{nC})}{\boldsymbol{Q_{NB}}(\text{nC})}\right]\times100\% \tag{3.23}$$

The error associated with the PDE correction factor in Equation (3.23), 0.4080, is about 11%. It comes from two major sources, the thermal neutron calibration factor, N_{th} (5.5%) and $\overline{W}_N/e$ (6-8%). The latter is the greatest error contributor to the error associated with the Bragg-Gray equation (9%). Substituting $N^{NB}{}_C$=6.709 R/nC ± 2% into Equation (3.7), the Bragg-Gray equation for the TE ion chamber (SN#445) is

$$\boldsymbol{D_{n+\gamma}}(\text{Gy}) = 9.437\times10^{-3}\left(\frac{\text{Gy}}{\text{R}}\right)\cdot 6.705\left(\frac{\text{R}}{\text{nC}}\right)\cdot\boldsymbol{Q_T^{NB}}(\text{nC})$$

$$= 0.0633(\text{Gy/nC})\cdot\boldsymbol{Q_T^{NB}}(\text{nC}) \tag{3.24}$$

The coefficient in Equation (3.24), 0.0633(Gy/nC) has an uncertainty of about 9% which comes mainly from $\overline{W}_N/e$ (6-8%).

CHAPTER 4

CALCULATION AND MEASUREMENTS OF THE NEUTRON SPECTRAL FLUENCE RATE

The Fermilab Neutron Therapy Facility (NTF) produces neutrons by bombarding a 2.21-cm-thick beryllium target with 66-MeV protons. The protons lose 49 MeV in the beryllium target and are stopped by a 0.5-mm gold backing [53]. The neutron beam is collimated to produce different field sizes by using different collimators. The neutron fluence rate is monitored by dual parallel plate ionization chambers during experiments and therapy. The ionization chambers are calibrated such that one monitor unit (MU) produces a dose of one gray at 10-cm deep in tissue for a 10x10 cm^2 collimator (standard treatment field size) at 190 cm source to axis distance (SAD).

The knowledge of the neutron spectral fluence rate is essential for Monte Carlo simulations. So a relationship between proton current or charge measured by the dual parallel plate ion chamber and the neutron fluence rate or fluence at the isocenter is required. Cupps et al. [57] measured the neutron fluence rate spectrum of the Fermilab NTF using gold and indium foil activations in 1996. Ross et al. [60] calculated the neutron spectrum using the LAHET and MCNP codes in 1997. The shapes of the calculated and measured neutron spectrum were in reasonable agreement. Since Ross et al. also calculated the neutron spectrum of the neutron therapy facility at the National Accelerator Centre (NAC) in South Africa, and their calculation agreed well with the extensive time-of-flight measurements of Jones et al. [61], the shape of the Fermilab NTF neutron spectra measured by Cupps et al. and calculated by Ross et al. should be reasonable.

J. Sweezy [53] modeled the Fermilab NTF neutron beam using MCNPX and the LA-150 neutron libraries [62]. A total of 6.0×10^9 source protons were tracked resulting in 9.0×10^6 neutrons incident on the face of the collimator, which were written to a surface source file for subsequent calculations. Sweezy calculated a total fluence of 2.58×10^{-7} neutrons/cm^2 per proton at the 190 cm isocenter of the Fermilab Fast Neutron Therapy facility using the MCNPX Bertini intranuclear cascade (INC) model and the LA-150 neutron library. Comparison of depth-dose measurements to the calculation indicated that MCNPX underestimated the total absorbed dose by approximately a factor of three. This discrepancy needed to be addressed before further simulations of BNCEFNT design could be conducted using the MCNPX code.

Due to the space limitation in the treatment room, the time-of-flight technique can not be used to measure the neutron spectral fluence rate at the Fermilab FNT facility. An active detector placed in the neutron beam will be saturated due to the intensity of the neutron beam. So foil activation techniques were used to measure the neutron spectral fluence rate for the neutron beam at the Fermilab NTF facility.

4.1 Activation Foils and Activation Products

Aluminum and copper foils were chosen to be the activation detectors because they have well evaluated neutron cross section data up to 150 MeV in the MCNPX library and their activation products have appropriate half-lives and gamma ray lines for counting. The Fermilab NTF neutron beam was moderated by polymethylmethachrylate (PMMA) slabs of various thicknesses before reaching the foils. The foils were attached to the center of the downstream wall of a moderator box made of PMMA material with dimensions of 30cm x 30cm x 15cm. The thickness of the box walls was 0.6 cm. Up to 12 PMMA slabs of various thicknesses were inserted into the box. The thickness of the moderator was varied from 1.2 cm (empty) to 14.5 cm (all slabs inserted) in these measurements. The center of the front surface of the moderator box was placed at the isocenter (SAD=190 cm).

Five reactions are considered for the experiment: $^{27}Al\ (n,\gamma)\ ^{28}Al$, $^{27}Al\ (n, p)^{27}Mg$, $^{27}Al\ (n,\alpha)^{24}Na$, $^{65}Cu(n,\gamma)^{66}Cu$ and $^{63}Cu(n,2n)^{62}Cu$. The decay data (half-life, gamma-ray energy and emission probability) of these activation products are shown in Table 3.

Table 3: Decay data of the Activation Products [63, 64]

Reactions	Radionuclide	$T_{1/2}$	E_γ (keV)	P_γ (%)
$^{27}Al\ (n,\gamma)\ ^{28}Al$	^{28}Al	2.2414 min	1778.9	100
$^{27}Al\ (n, p)^{27}Mg$	^{27}Mg	9.458 min	843.76	71.0
			1014.4	28.0
$^{27}Al\ (n,\alpha)^{24}Na$	^{24}Na	14.9512 h	1368.5	100
			2754.1	99.9
$^{65}Cu(n,\gamma)^{66}Cu$	^{66}Cu	9.67 min	875.71	0.15
$^{63}Cu(n,2n)^{62}Cu$	^{62}Cu	5.12 min	1039.2	7.4

Each irradiated foil was counted using an HPGe detector-based spectrometer and the activities of the activation products, ^{28}Al, ^{27}Mg, ^{24}Na, ^{66}Cu and ^{62}Cu, at the end of each irradiation were determined. The beam fluctuation was small and was assumed to be constant during the irradiation, the production rates of the activation products are also constant, the production rate was obtained by

$$\dot{P}_j = \frac{A_j(0)\lambda_j}{1-e^{-\lambda_j T}}\frac{1}{m} \tag{4.1}$$

where $\dot{P}_j$ is the production rate of radionuclide j (Bq/s/g), λ_j is its decay constant (s^{-1}), T (s) is the irradiation time, m is the mass of the foil (g) and $A_j(0)$ is the activity of radionuclide j at the end of irradiation (Bq), which is calculated by

$$A_j(0) = \frac{C_{ij}}{P_{ij}\varepsilon_i}\frac{\lambda_j}{1-e^{-\lambda_j T_R}}\frac{T_R}{T_L}\cdot e^{\lambda_j T_D} \tag{4.2}$$

where C_{ij} is the net full-energy peak counts for the gamma-ray line of energy E_i of radionuclide j, P_{ij} is the gamma-ray emission probability, ε_i is the detection efficiency, T_R

is the real time (s), T_L is the live time (s) and T_D (s) is the decay time (from the end of irradiation to the start of the counting).

4.2 HPGe Detector Calibration

The HPGe detector is calibrated using a NIST-traceable mixed gamma-ray point source. The foils must be counted on the surface of the detector because of the low activity in the foil. So the efficiencies for this geometry must be determined. Due to the cascading emission of two gamma rays from both ^{60}Co and ^{88}Y, summing effects were unavoidable in counting the standard point source. Thus the high energy part (above 889 keV) of the efficiency curve for the short source-to-detector distance geometry needs to be corrected for the summing effect. The MCNP code was used in the calculation of the true efficiency and the correction factor for the summing effects [65].

4.2.1 Modeling of the HPGe detector

The detector used in this work is an EG & G Ortec manufactured p-type HPGe detector (Model No. GEM-15190-P). For the 1.332 MeV ^{60}Co gamma rays, it has a relative efficiency of about 18.8% and has a 1.83-keV full width half-maximum (FWHM) at the full-energy peak. The detector was modeled using MCNP5 code based on the detector drawing provided by the manufacturer. A diagram of the MCNP5 modeled detector is displayed in Figure 2. The germanium dead layer and the distance between the surface of the crystal and the aluminum housing cap was adjusted to make the calculated full-energy peak efficiencies at 88, 122 and 662 keV to match the efficiencies of the three peaks calibrated using a NIST traceable mixed point source within 3.0%. After that, the efficiencies for other gamma rays were calculated and compared with the calibration obtained using the point source standard. Figure 3 shows the efficiency curves for the standard point source calibration and MCNP5 simulations. It is obvious that the summing effect is significant for the ^{60}Co and ^{88}Y gamma rays in this geometry. The peak efficiencies of gamma rays above 898 keV calibrated using ^{60}Co and ^{88}Y would be more than 20% lower if the correction were not applied than the true efficiencies.

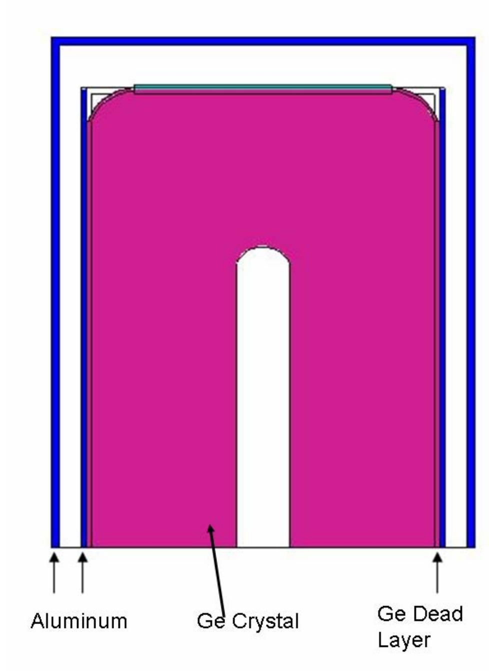

Figure 2: Diagram of the MCNP5 modeled HPGe detector. (drawing not to scale)

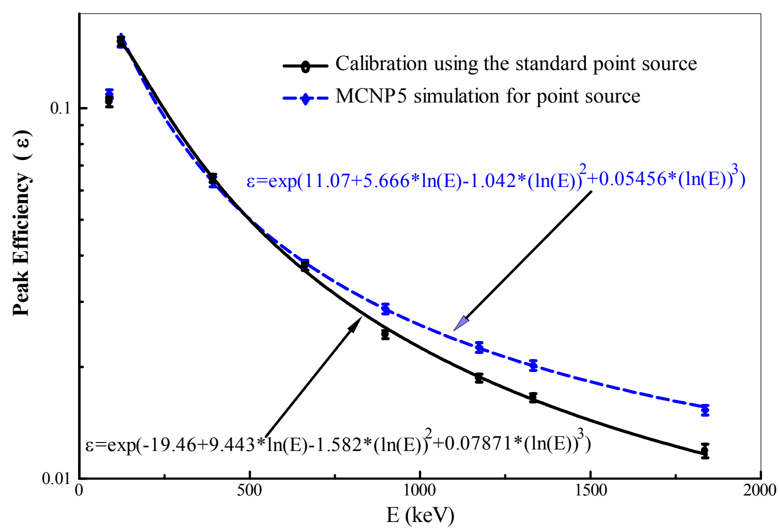

Figure 3: Peak efficiency curves calibrated with a standard point source placed on the surface center of the detector cap and modeled using MCNP5 for the same geometry. The lines are fit curves without the 88-keV data point.

Once the MCNP5 Model is validated, the detection efficiencies for gamma rays from the five activation products of interest were calculated. Radioisotopes were assumed uniformly distributed in the foils. Self-absorption is automatically corrected for in the calculation. The calculated peak efficiencies for the interested gamma rays are listed in Table 4. The efficiencies of the two ^{24}Na gamma rays were obtained using different methods from others because these two gamma rays have coincidence summing effect in the same way as gamma rays emitted by ^{60}Co and ^{88}Y.

Table 4: MCNP5 calculated peak efficiencies for gamma rays from the aluminum and copper foil activation products

Foil	E_γ (keV)	Peak efficiency (%)	Error (%)	
aluminum	1778.9	1.45	4.0	^{28}Al
	843.76	2.79	3.5	^{27}Mg
	1014.4	2.37	3.5	^{27}Mg
	1368.5	1.69	5.0	^{24}Na
	2754.1	0.847	5.0	^{24}Na
copper	875.71	2.72	3.5	^{66}Cu
	1039.2	2.35	3.5	^{62}Cu

4.2.2 Calculation of the efficiencies for gamma rays emitted by ^{24}Na

The simplified ^{24}Na decay scheme from Table of Isotopes [66] is shown in Figure 4. There is a chance that while the 2754-keV gamma ray is detected by the detector, the 1369-keV gamma ray may also interact in the detector. The signal processing inside the detector takes much longer time than 1.35 ps, so the detector can not differentiate the signals from the two gamma rays. The two gamma rays will result in a larger energy signal and either gamma ray line could lose a count in its full-energy peak if it happens to be a full energy event. If either gamma-ray peak gains a count from coincident summing of Compton scattering events of the two gamma rays, this count only contributes to the background of the peak and will be subtracted in peak analysis.

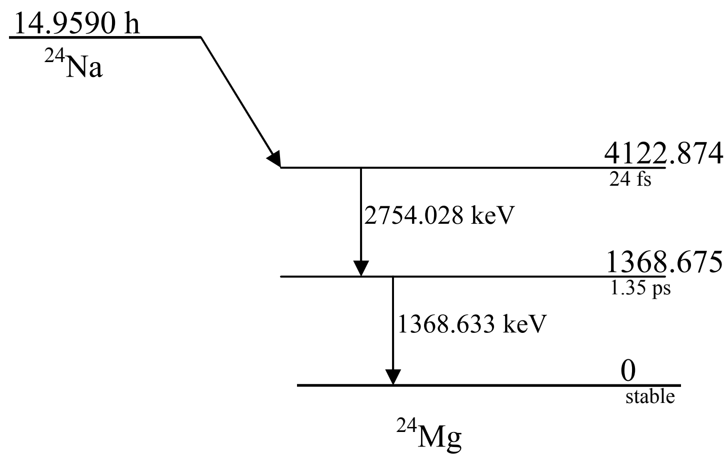

Figure 4: Simplified decay scheme of ^{24}Na.

If the total efficiencies of the 2754-keV and 1369-keV gamma rays are $\varepsilon_{t,h}$ and $\varepsilon_{t,l}$, respectively, their true (no-summing) full-energy peak efficiencies are designated as $\varepsilon_{p,h}$ and $\varepsilon_{p,l}$, the observed full-energy peak efficiencies of the 2754-keV and 1369-keV gamma rays emitted from ^{24}Na decay can be obtained from the following equations

$$\boldsymbol{\varepsilon}_{\boldsymbol{p}}(2754\boldsymbol{keV}) = \boldsymbol{\varepsilon}_{\boldsymbol{p},\boldsymbol{h}}(1-\boldsymbol{\varepsilon}_{\boldsymbol{t},\boldsymbol{l}}) \tag{4.3}$$

$$\boldsymbol{\varepsilon}_{\boldsymbol{p}}(1369\boldsymbol{keV}) = \boldsymbol{\varepsilon}_{\boldsymbol{p},\boldsymbol{l}}(1-\boldsymbol{\varepsilon}_{\boldsymbol{t},\boldsymbol{h}}) \tag{4.4}$$

Equations (4.3) and (4.4) are only valid for point sources. The efficiency for a disc source can be obtained in two steps. First, a set of total and peak efficiencies of 2754-keV and 1369-keV point sources placed on the detector surface moving along radial direction (from 0 to 0.85 cm) were calculated using MCNP5. The point source is actually a small cylinder with 1-mm diameter and 0.5-mm thickness because the aluminum foil used in this project is 0.5-mm thick. The observed peak efficiencies for 2754-keV and 1369-keV gamma rays at each point were computed using Equations (4.3) and (4.4). Then the observed peak efficiencies were plotted against the radial distance, r, and these data points were fitted using a quadratic equation, $\varepsilon(r)=a + br + cr^2$, as shown in Figure 5. The observed peak efficiency for a disc source with radius R is calculated by integrating $\varepsilon(r)dr$ from 0 to R and then divided by R, which is

$$\varepsilon_{disc} = \frac{\int_0^R \varepsilon(r)dr}{R} = \frac{\int_0^R (a + br + cr^2)dr}{R} = a + \frac{b}{2}R + \frac{2c}{3}R^2 \tag{4.5}$$

Substituting the radius of the aluminum foil R=0.85 cm and the fitted parameters (in Figure 5) into equation (4.5), the peak efficiencies for the 2754-keV and 1369-keV gamma rays emitted from ^{24}Na decay were obtained to be (0.847±0.042)% and (1.69±0.08)%, respectively.

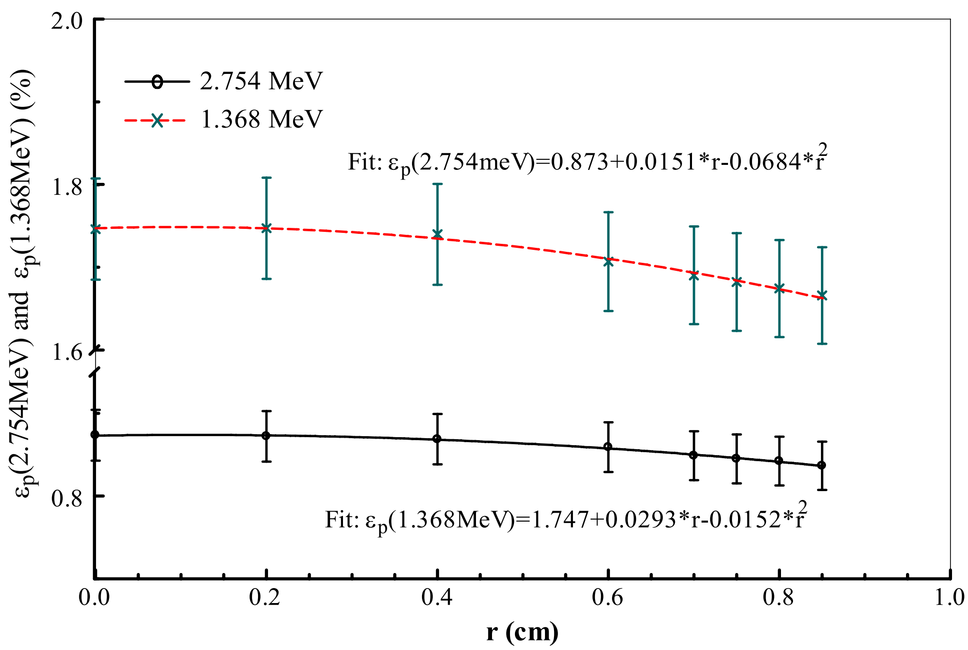

Figure 5: Observed peak efficiencies for a ^{24}Na point source moving along radial direction.

4.3 Neutron Spectrum Unfolding

The unfolding of neutron spectra is performed by using MXD_FC33 code [67]. The MAXED algorithm [68-70] used in the code is the maximum entropy algorithm. In principle, the spectral neutron flux rate desired can be solved from the following equations:

$$\dot{P}_j(k) + \varepsilon_j(k) = \sum_{l=1}^{n} \phi_l R_{lj}(k) \tag{4.3}$$

$$\sum_k \sum_j \frac{\varepsilon_j(k)^2}{\sigma_j(k)^2} = \Omega \quad \textbf{(4.4)}$$

where $\dot{P}_j(k)$ is the production rate of the radionuclide j of moderation k in unit of Bq/s/g, ϕ_l is the neutron flux rate of energy group l in unit of 1/cm^2/s, $R_{lj}(k)$ is the response matrix for radionuclide j of moderation k over energy group l in unit of Bq/g per n/cm^2 and Ω is a parameter set by the user (typically, Ω is set to the number of detectors) [57].

There are fewer equations than unknowns in equation (4.3) and no unique solution can be obtained. An initial guess for the spectrum is provided to the MXD_FC33 code for the unfolding process.

4.4 Calculation of the Response Matrices

The response matrices, $R_{lj}(k)$, for j = ^{28}Al, ^{27}Mg, ^{24}Na, ^{66}Cu and ^{62}Cu are calculated using MCNPX with the LA150N neutron cross section library. The energy scale is divided into 49 groups from 10^{-10} MeV to 70 MeV. The response functions for ^{28}Al, ^{27}Mg, ^{24}Na, ^{66}Cu and ^{62}Cu are shown in Figure 6 to 10, respectively. Only the responses for 6 different moderator thicknesses are shown in each figure.

The MCNPX input files modeled the experimental setup as exactly as possible. A 10 x 10 cm^2 field size of a parallel neutron beam is directed perpendicularly on the center of the front face of the PMMA box with the copper and aluminum foils mounted on the back face of the box. The density of the PMMA $(C_5H_8O_2)_n$ is 1.19 g/cm^3. The tally multiplication card (FM) and special treatment card (SCX) were used to tally the responses of neutrons for each incident energy bin in one MCNPX run.

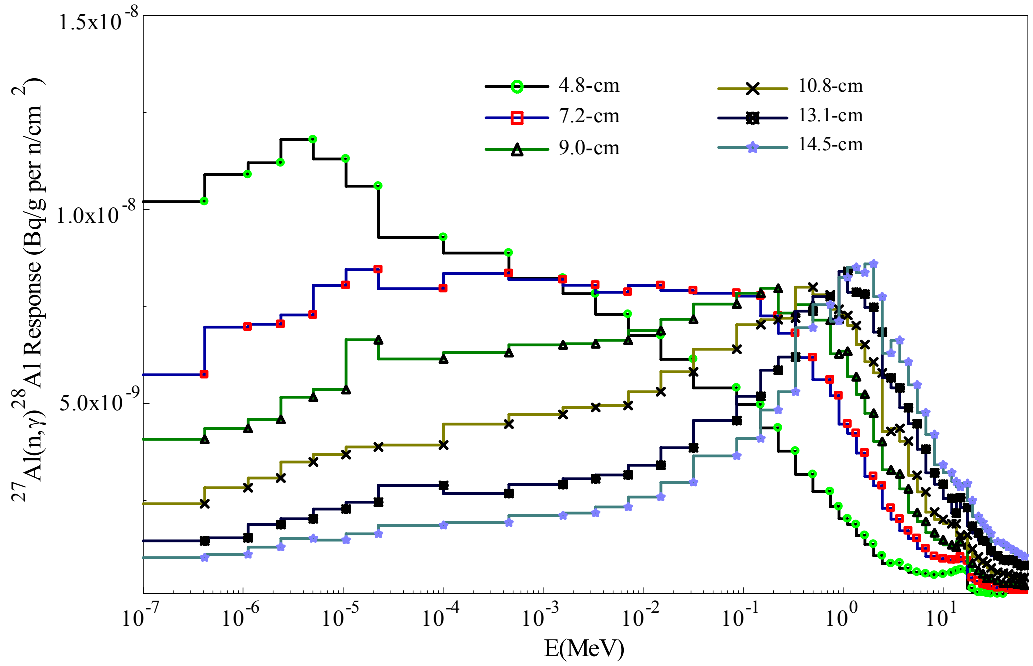

Figure 6: $^{27}Al(n,\gamma)^{28}Al$ Response functions behind various moderator thicknesses

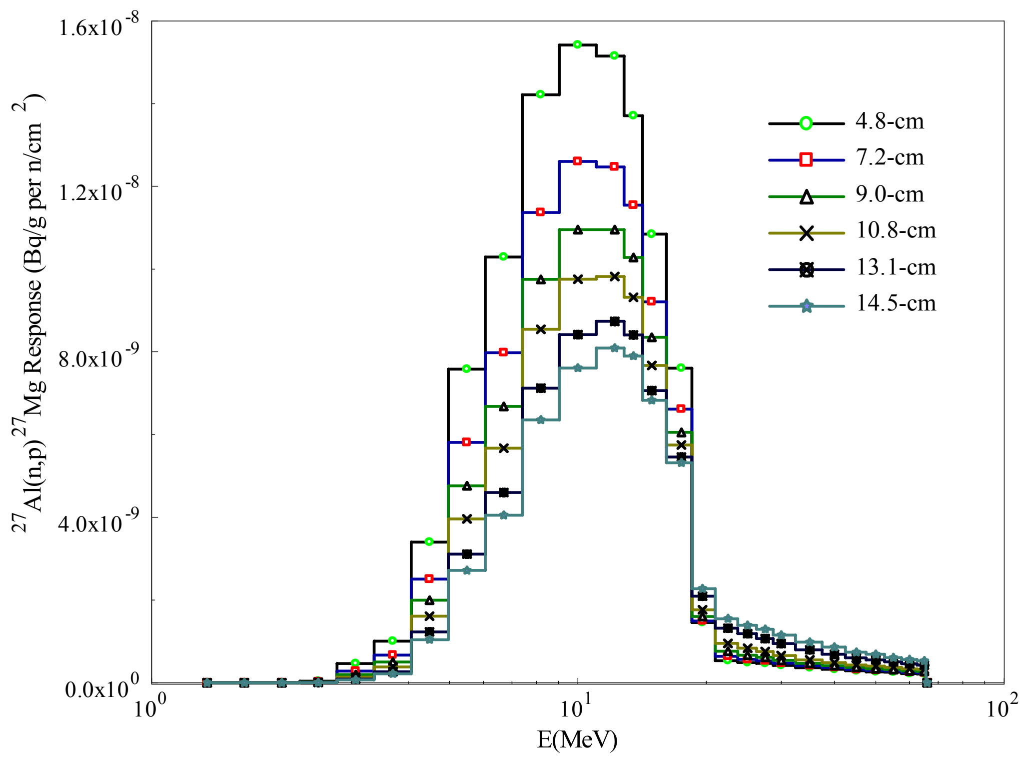

Figure 7: $^{27}Al(n,p)^{27}Mg$ Response functions behind various moderator thicknesses

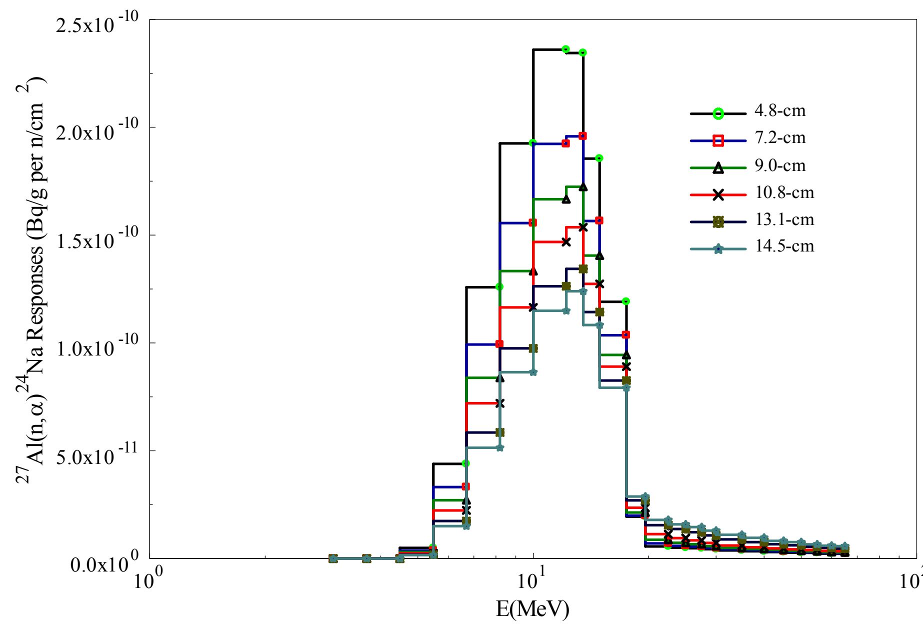

Figure 8: ^{27}Al(n,α)^{24}Na Response functions behind various moderator thicknesses

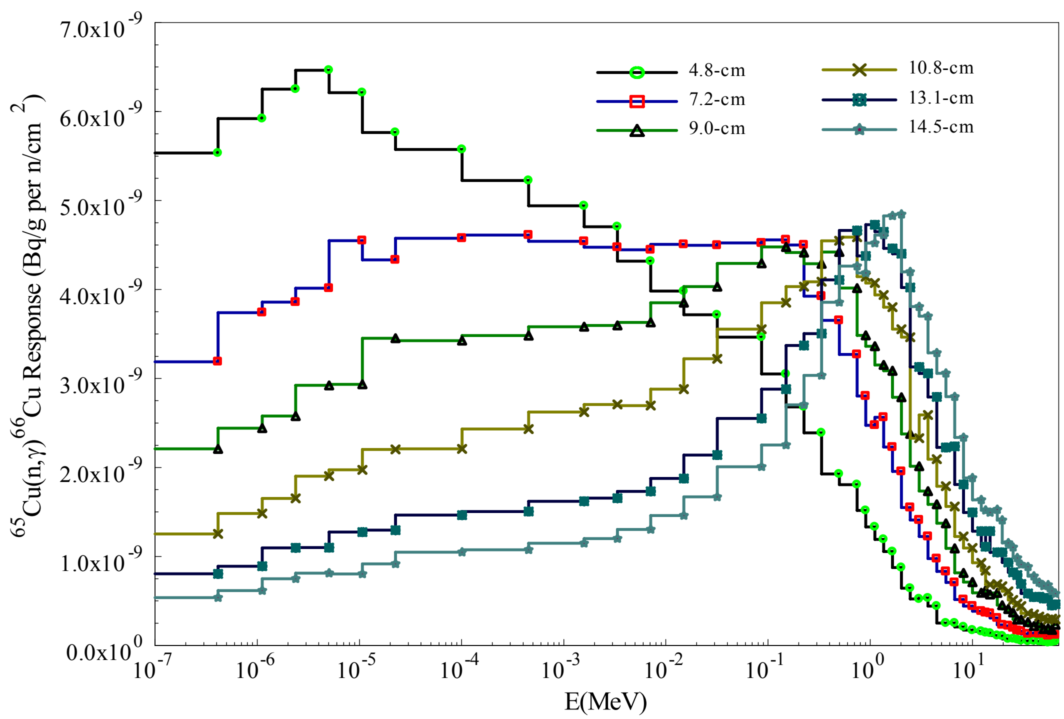

Figure 9: ^{65}Cu(n,γ) ^{66}Cu Response functions behind various moderator thicknesses

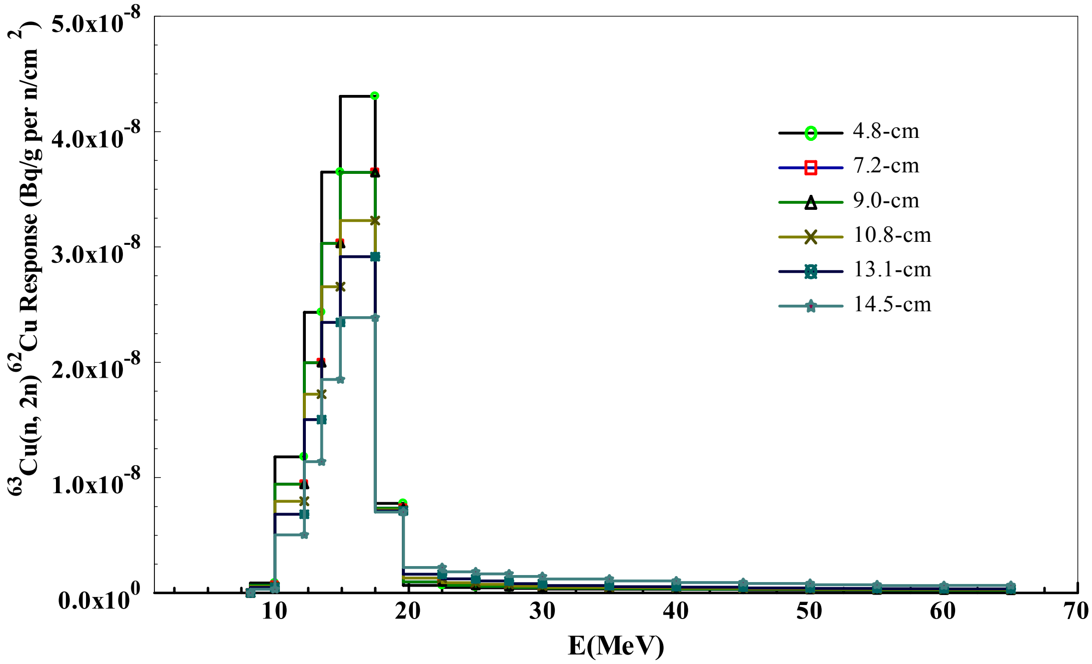

Figure 10: ^{63}Cu(n,2n) ^{62}Cu Response functions behind various moderator thicknesses

4.5 Foil Activation and Counting

Pure (99.99%) aluminum foils 1.693 cm in diameter and 0.1-cm thick and pure copper foil of the same diameter and 0.05-cm thick were placed at the center of the outside surface of the backside of the moderator. The copper foil is on the moderator wall. The front face of the moderator is at the isocenter (190 cm from the berillium target). The setup is the same as described in the MCNPX simulations. For each irradiation, a dose of 1 MU or 2 MU was preset, resulting in run times of 3.4 or 6.8 minutes. The start and stop time of the irradiation and other proton current information were recorded.

The foils were counted immediately after irradiation using an ORTEC manufactured HPGe detector (GEM20190) gamma spectrometer. The aluminum foil was counted first for less than 5 min to determine the activity of its short half-life (2.24 min) activation product ^{28}Al and then copper foil was counted for about 5 to 10 mins. A relatively long count of the aluminum foil was performed for the activity determinations of the longer lived activation products ^{27}Mg and ^{24}Na.

4.6 Results

The activity production rates for foils behind various moderation thicknesses are given in Table 5. Because of the short irradiation time, saturated activities of the activation products were not attained. So the activity production rates were calculated using equations (4.1) and (4.2). Because the unfolding of the spectrum is actually a spectral adjusting process, the accuracy of the result relies not only on the accuracy of the response matrices and foil activity determinations, but also on supplying a spectral shape of the initial guess spectrum that is similar in shape to the spectrum measured. Two starting spectra, the MCNPX-calculated NTF neutron spectrum and the spectrum measured by Cupps et al. [60] were used as the starting spectra for unfolding. The unfolded spectra and the MCNPX calculated spectrum are shown in Figure 11. For a better view, the spectrum is also plotted in lethargy in Figure 12. A comparison of this work and Cupps et al.[59] is shown in Figure 13.

The unfolded total neutron fluence rate at the isocenter for a $10x10cm^2$ field is $1.22x10^8$ n/cm^2-s for a beam current of $1.5x10^{14}$ proton/s. The fluence density measured in this work agrees with Cupps et al.[59], which yielded a total flux rate of $1.35x10^8$ n/cm^2-s for a beam current of $1.7x10^{14}$ proton/s.

An MCNPX calculation was performed for 10^9 proton particles and a fluence of $6.34x10^{-7}$ neutrons/cm^2 per proton at the 190 cm isocenter was calculated. This resulted in a total neutron fluence rate of $9.52x10^7$ n/cm^2-s for the beam current of $1.5x10^{14}$ proton/s. The ratio of the measured to the calculated flux is 1.29. The previous MCNPX input file of Sweezy [53] used an isotropic proton surface source instead of a parallel beam, causing half of the protons to not hit the beryllium target. Therefore, the previously observed factor of 3 was incorrect.

Table 5: Production rates (Bq/g/sec) for foils behind different moderation thickness

Moderation thickness	4.8 cm	7.2 cm	9 cm	10.8 cm	13.1 cm	14.5 cm
^{28}Al	12.51	19.91	26.30	32.11	37.33	41.45
^{27}Mg	30.69	25.75	24.01	22.36	22.14	21.13
^{24}Na	0.34	0.30	0.28	0.28	0.26	0.24
^{62}Cu	--	64.41	45.00	38.56	46.73	39.83
^{66}Cu	7.83	10.53	13.48	19.12	23.20	26.54

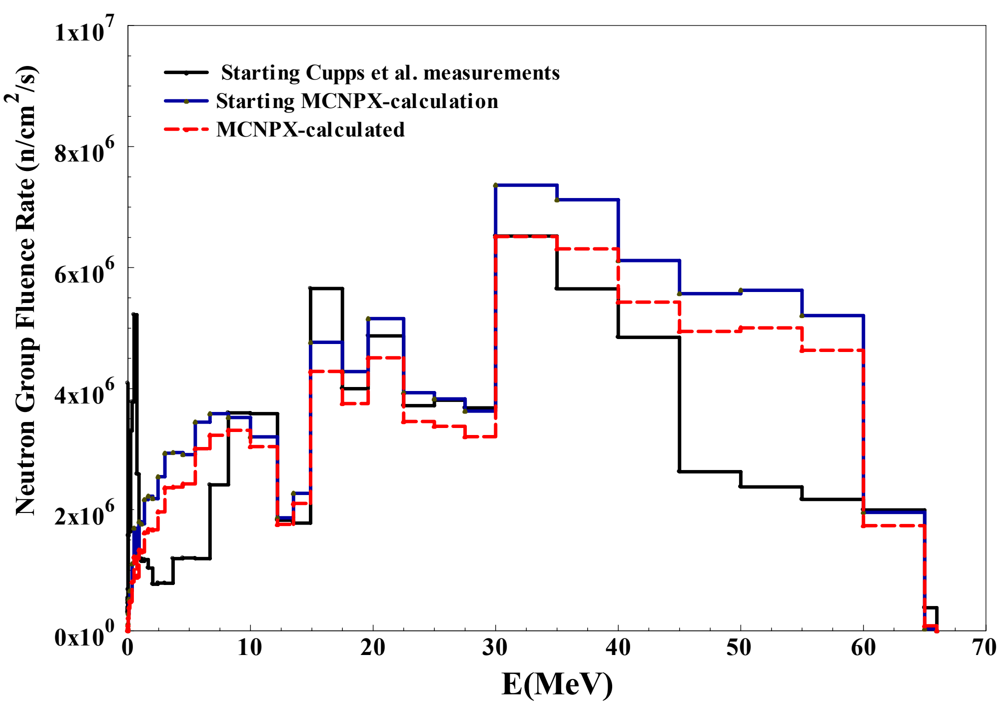

Figure 11: Fermilab NTF neutron spectrum at isocenter for a 10x10 cm^2 standard treatment beam. The fluence rate is corresponding to a proton current of 1.5x10^{14} p/s

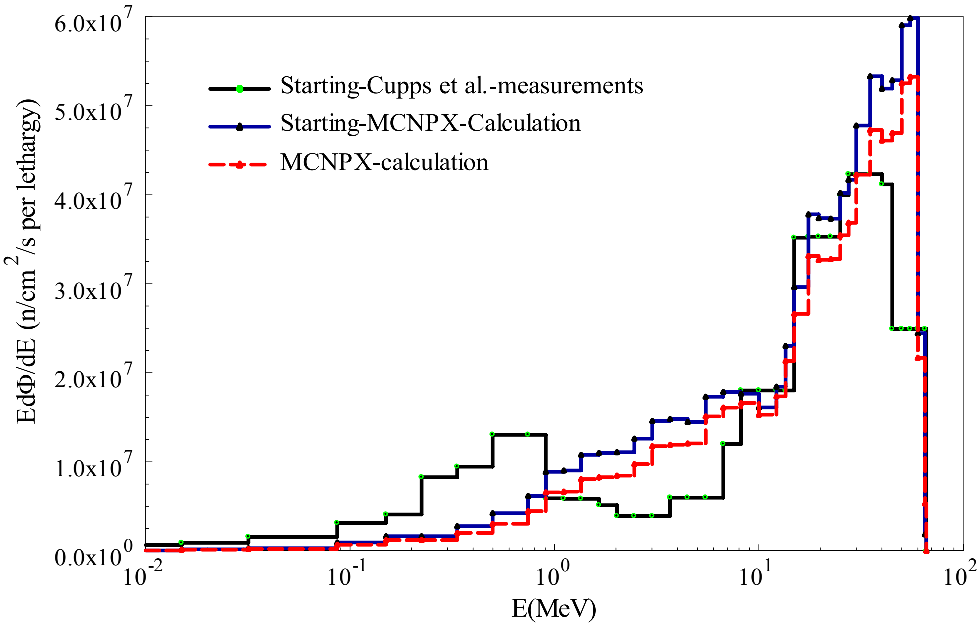

Figure 12: Fermilab NTF neutron spectrum at isocenter for a 10x10 cm^2 standard treatment beam displayed in lethargy. The fluence rate is corresponding to a proton current of $1.5x10^{14}$ p/s

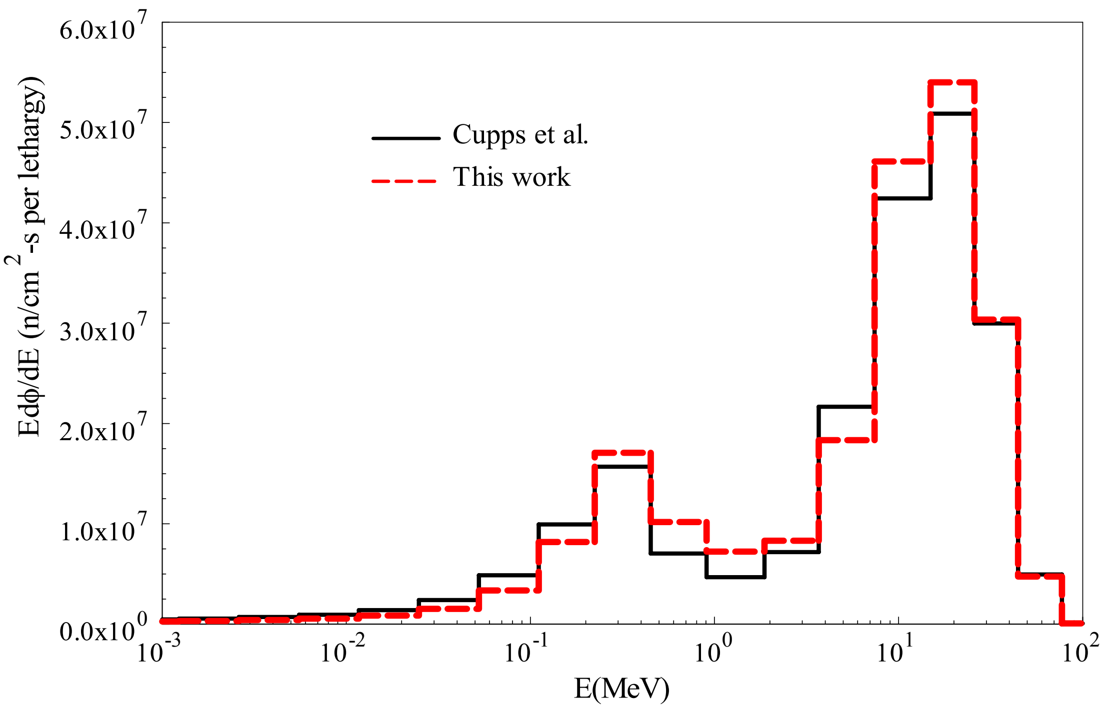

Figure 13: Comparison of the Fermilab NTF neutron spectra determined by Cupps et al. and this work starting with measured spectrum by Cupps et al.

Uncertainties in the measurement of the activities of the activation products ranged from 1 to 20% for counting statistics and for between 3.5-5.0% detector efficiencies. The production rates also suffer from the fluctuation of the proton current and the uncertainty in the determination of the proton current. The uncertainty in the unfolded neutron fluence density is about 15%.

The advantages in selection of aluminum and copper foils as the activation detectors are that the short half-lives of the activation products require short irradiation time and the gamma-ray energies and high gamma-ray emission probabilities make it easy to determine their activities.

From the response functions shown in Figure 6 to 10, one can see that the moderation thicknesses for the threshold reactions do not differentiate high energy neutrons very well (the peaks of the response functions does not shift significantly for different thickness). If some of the PMMA slabs were replaced by high-Z material, such as lead or tungsten, more energy-dependent features can be added to the responses.

CHAPTER 5

DESIGN OF THE BNCEFNT ASSEMBLY

The RSVP head phantom^{TM*} [71] was used to simulate the depth-dose and PDE distributions as a function of depth using MCNP5 code. It was also used to verify the design of the BNCEFNT reflective assembly. The shell of the RSVP phantom is formed from ¼ inch cellulose acetate butyrate (CAB) sheet, a transparent material chosen for its strength and low water absorption. The elemental composition of CAB is, by weight percentage, Hydrogen: 6.7125%, Carbon: 54.5403%, and Oxygen: 38.7472%. The shell is mounted on a polycarbonate end plate by water-tight seal. The details of the RSVP phantom, such as the nose, eyes, ears and etc., were not modeled. The phantom is filled with deionized water for the modeling.

Moderation and reflection of neutrons using graphite, water, or heavy water around the head phantom was studied by Pignol [48] for Boron Neutron Capture Enhanced Fast Neutron Therapy. He concluded that a graphite moderator produced the largest dose enhancement. Monte Carlo simulations performed for graphite, water, heavy water, and polyethylene at Fermilab Neutron Therapy facility supported Pignol's conclusion.

5.1 Selection of Material for the Filter and Collimator

The use of filtration, collimation and reflection near the head phantom was investigated using the Monte Carlo method for this study. A MCNP5 model of the moderator/reflector, heavy metal filter and collimator, and the simplified RSVP head

---

* Phantom Laboratory, Inc., 2727 State Route 29, Greenwich, NY 12834

phantom is shown in Figure 14. While Graphite was used as the moderator/reflector, the filter and collimator materials were studied for iron, tungsten, and lead in various combinations.

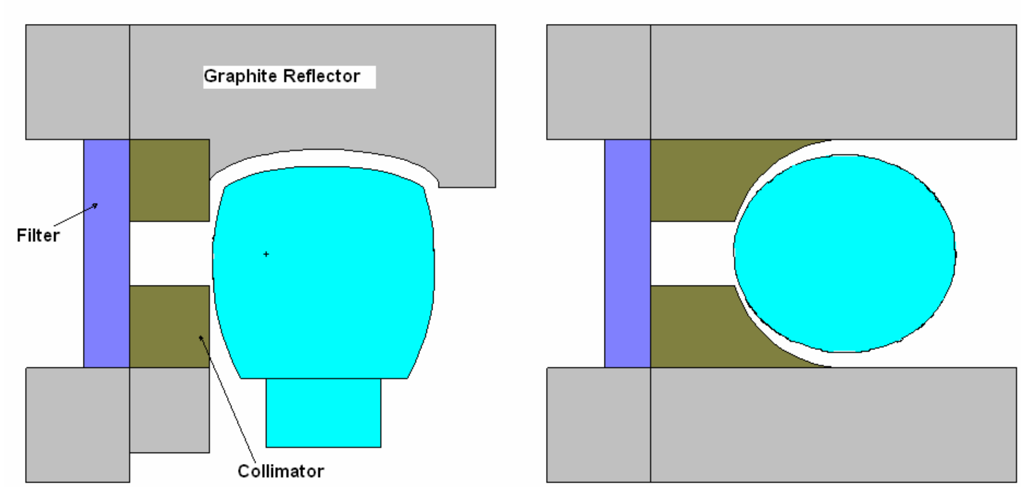

Figure 14: Diagram of the MCNP5 model of graphite moderator/reflector, iron, lead and tungsten filter and collimator combinations, and the simplified RSVP head phantom.

A parallel beam of 20 x 20 cm^2 size is directed perpendicularly to the 20 x 20 cm^2 filter surface and the centerline of the beam coincides with the axis of the collimator. The neutron spectrum determined in Chapter 4 was used as the source energy distribution in the SDEF card of MCNP input files. A relationship between the neutron fluence and proton, $8.13x10^{-7}$ n/cm^2 per proton determined in Chapter 4, was used for the normalization. A proton current of $1.7x10^{14}$ protons/sec (most common for the treatment) was used to normalize the MCNP5 calculated absorbed dose rates to the unit of Gy/min.

Figure 15 displays the Percent Dose Enhancement (PDE) per 100-ppm ^{10}B at 5-cm depth in the water-filled head phantom for various filter and collimator combinations. Figure 16 is the total dose rate at 5-cm depth in the water filled phantom for various combinations of iron, lead and tungsten as filter and collimator.

The relationship between PDE and the total dose rate in 5.0-cm depth of the water filled head phantom for various filter and collimator combinations studied is shown in Figure 17. In this study, the collimator, no matter what material it is made of, is the same size and shape, while the filter thickness varies. It is obvious from Figure 17 that tungsten is superior as both collimator and filter to other materials for the same total dose rate.

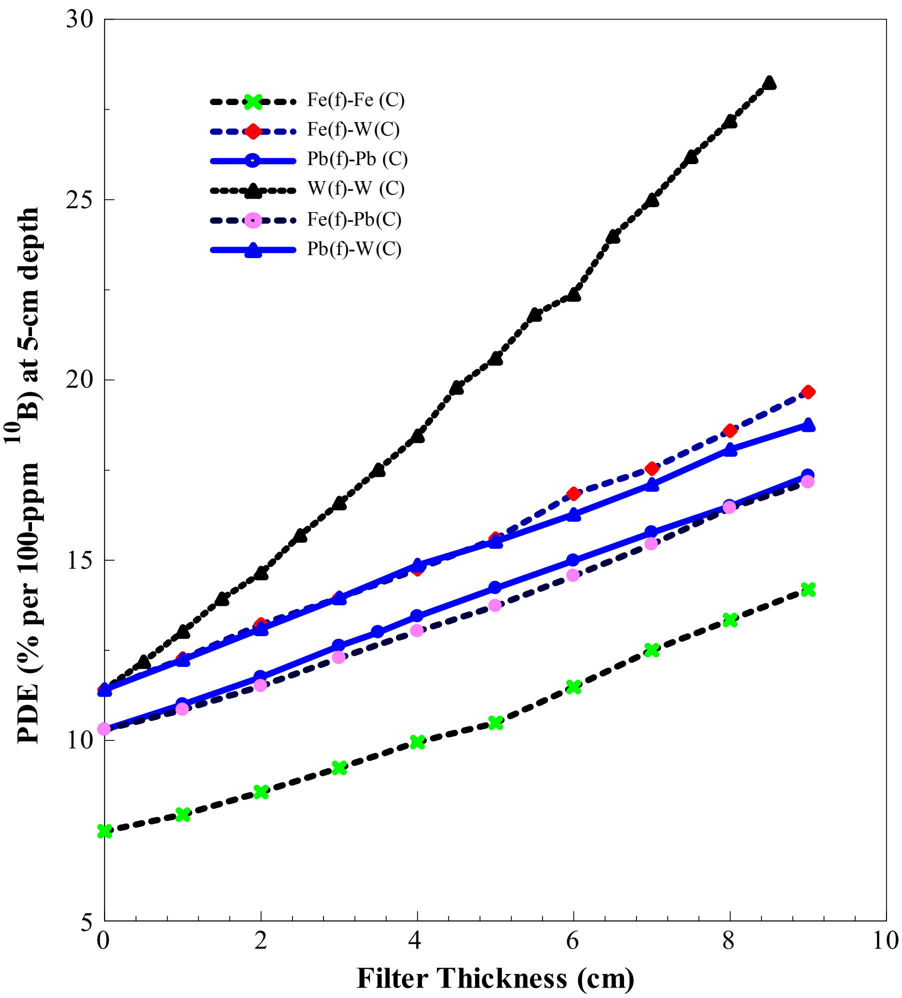

Figure 15: PDE at 5-cm depth in the head phantom for various filter and collimator combinations. In the legend, (f) stands for filter and (C) stands for collimator. A 20x10 cm^2 standard treatment beam field is used and the opening of the collimator is equivalent to 5x5 cm^2 size. The thickness of the collimator is 7 cm for all materials.

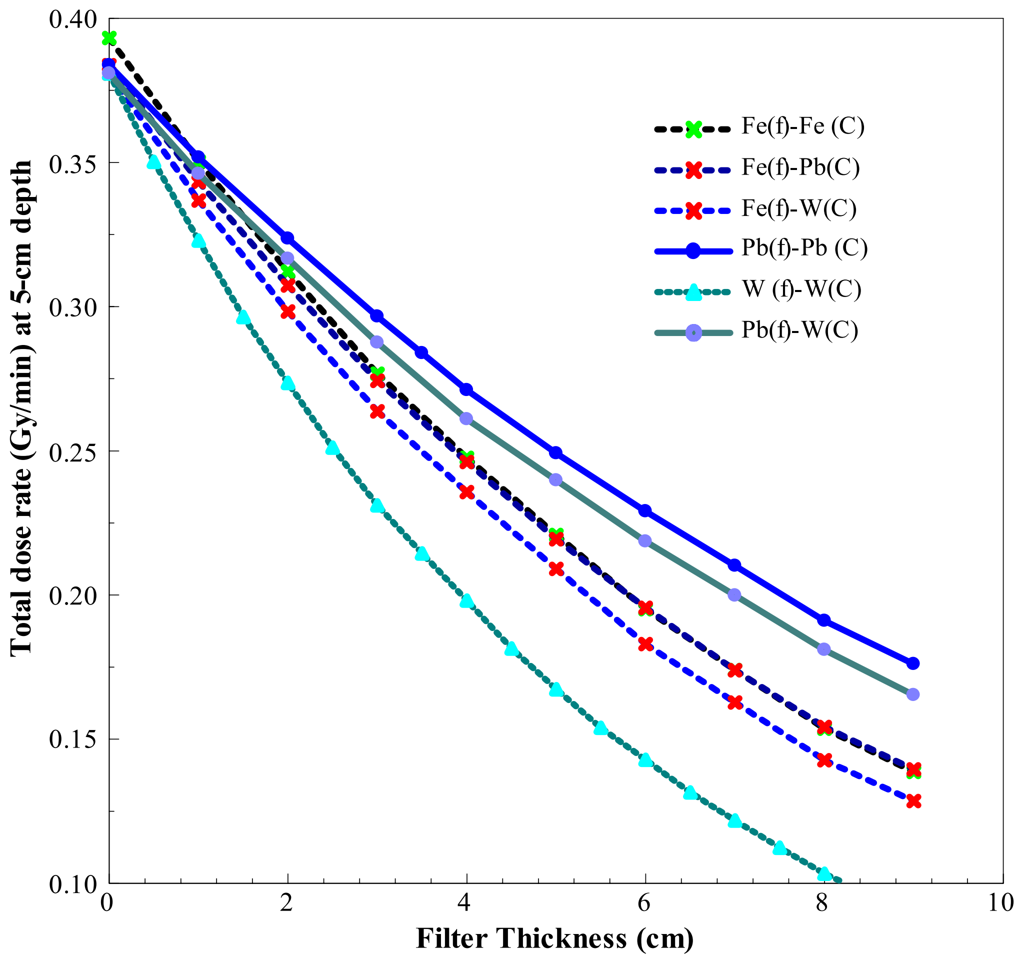

Figure 16: Total dose rate at 5-cm depth in the head phantom for various filter and collimator combinations. In the legend, (f) stands for filter and (C) stands for collimator. A 20x10 cm^2 standard treatment beam field is used and the opening of the collimator is equivalent to 5x5 cm^2 size. The thickness of the collimator is 7 cm for all materials. A proton current of 1.7x10^{14} protons/sec is assumed.

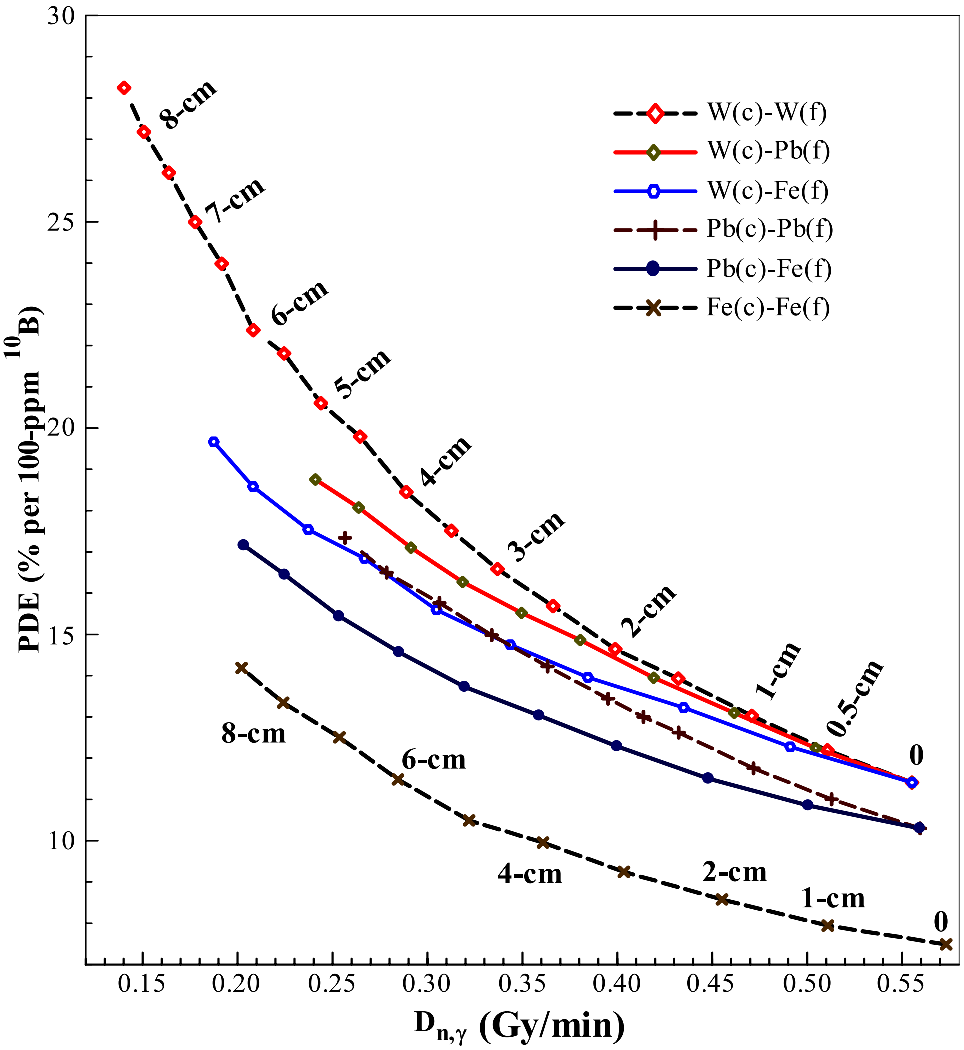

Figure 17: Relationship between PDE and total dose rate at 5-cm depth in the head phantom for various filter and collimator combinations. In the legend, (f) stands for filter and (C) stands for collimator. Values in the graph (1cm, 2 cm, etc.) indicate the filter thickness of the corresponding material. A 20x20 cm^2 standard treatment beam field is used and the opening of the collimator is equivalent to 5x5 cm^2 size. The thickness of the collimator is 10 cm for all materials. A proton current of 1.7x10^{14} protons/sec is assumed for the normalization of the MCNP results.

5.2 Characterizations of the Designed Assembly Using MCNP Simulations

The sizes of the graphite moderator/reflector, the tungsten collimator and filter were optimized by MCNP simulations for the purpose of obtaining the maximum PDE while retaining an acceptable total dose rate for treatment. It was found that 10-cm thick graphite reflector is sufficient and that further increasing of the reflector thickness will not result in a larger PDE.

Two collimator sizes were studied, one with a inner diameter of 5.64 cm (an area equivalent to 5 x 5 cm^2) and one with diameter of 11.29-cm (an area equivalent to 10 x10 cm^2). The MCNP5 model of the graphite reflector, 5.64-cm diameter and 7.0-cm tungsten collimator, and tungsten filter is shown in Figure 18.

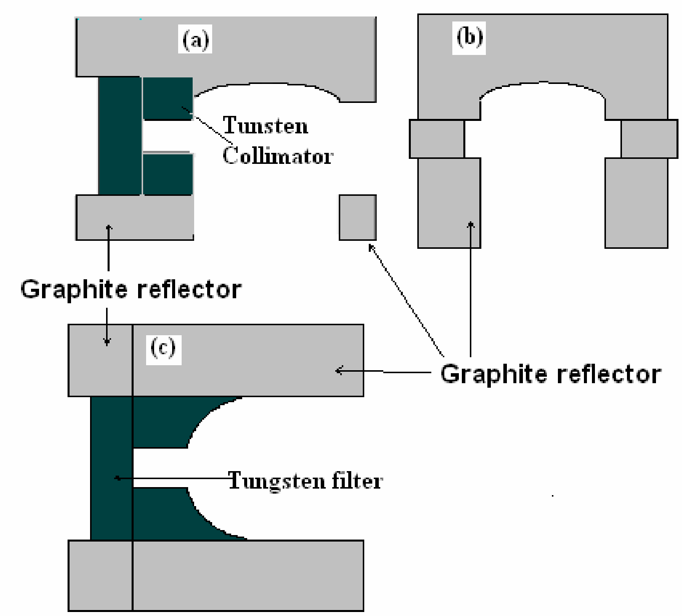

Figure 18: Diagram of the MCNP model of a tungsten filter, tungsten collimator and graphite reflector. These are cross-sectional views at the centerline of the collimator: (a) side view, (b) front view, and (c) top view. The thickness of the tungsten collimator and the graphite reflector are 10 cm

The isodose curve for neutrons and gamma rays in the head for the 4.0-cm tungsten filter, tungsten collimator and graphite reflector is given in Figure 19. This plot, produced using the mesh tally feature of MCNP5, shows that this design produces good collimation. The collimator projects a 5.64-cm diameter field at the isocenter, which is located at 5-cm depth from the back head and 7.5-cm from the top of the head phantom. The MCNP F6 tally, which yields kerma values, was used in the computation of neutron and photon doses. This resulted in higher dose values at shallow depths in the head than the true absorbed dose. Doses at depths shallower than 1.7 cm calculated by F6 tally are not correct due to the lack of charged particle equilibrium condition, i.e., the condition for kerma to be equal to absorbed dose.

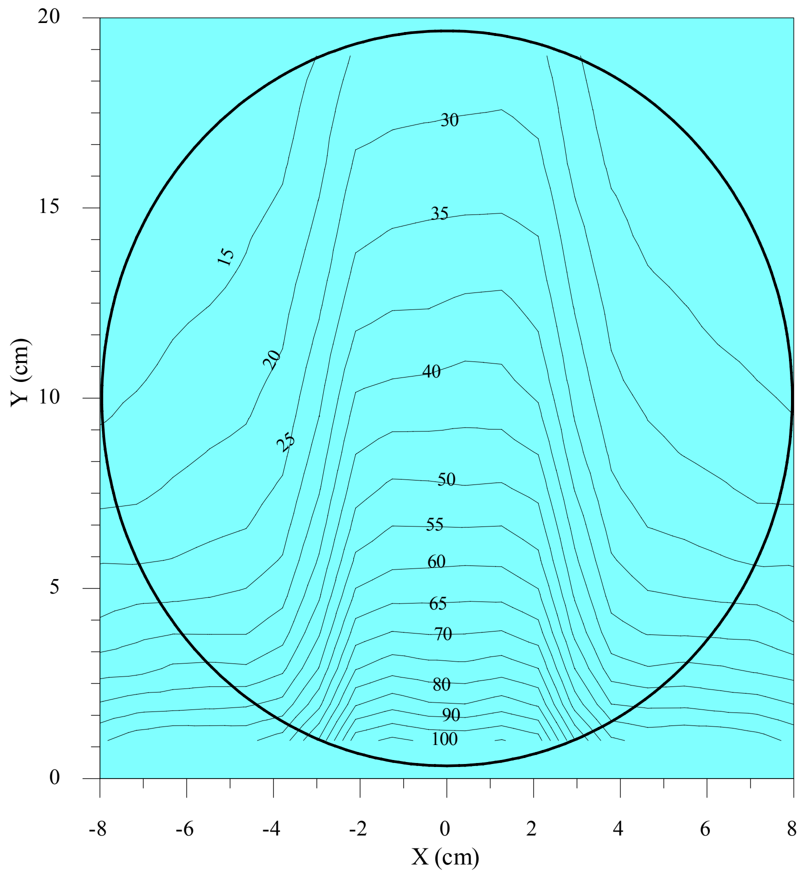

Figure 19: Calculated isokerma curve of the neutron and gamma dose for 5.64-cm diameter and 7.0-cm thick tungsten collimator, 4.0-cm tungsten filter and 10-cm thick graphite reflector as shown in Figure 18. The thick elliptical line is the outline of the head phantom. (Curves outside the head should be ignored)

The isodose curve for the boron capture dose alone is plotted in Figure 20. The ^{10}B concentration (100 μg/g) is assumed to be uniformly distributed in the head for the boron dose calculation. The peak of the boron capture dose is at 5-cm depth, around the beam centerline.

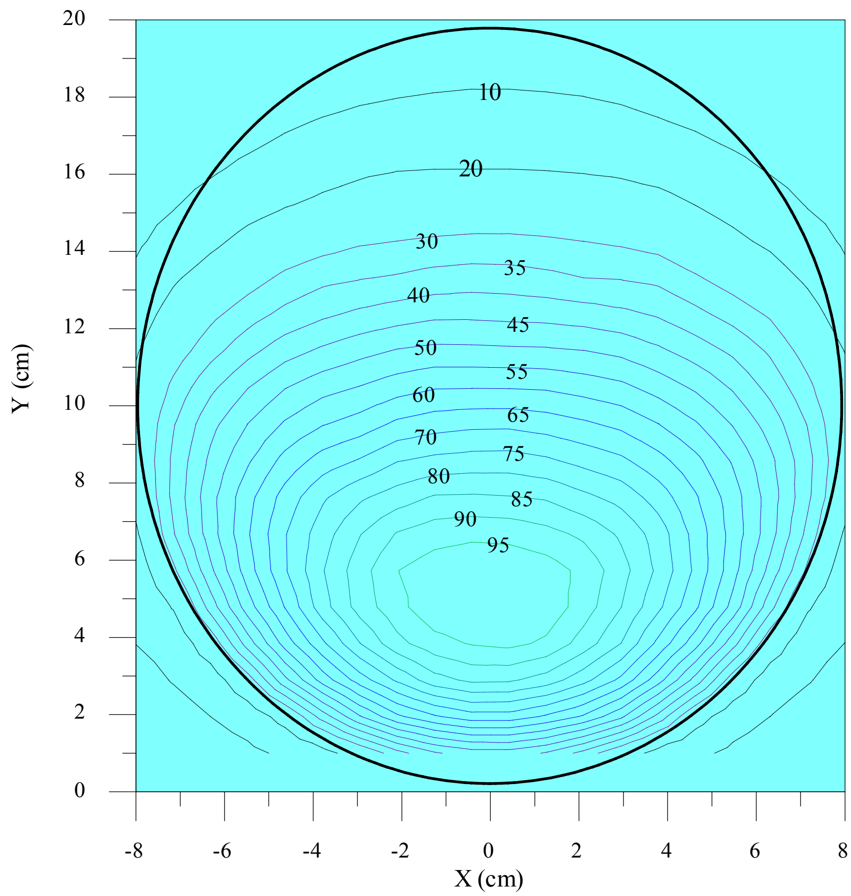

Figure 20: Calculated isodose curve of the boron capture dose (^{10}B concentration is uniformly distributed through the head) for 5.64-cm diameter and 7.0-cm thick tungsten collimator, 4.0-cm tungsten filter and 10-cm thick graphite reflector as shown in Figure 18. The thick elliptical line is the outline of the head phantom. (Curves outside the head should be ignored)

The total kerma rates due to neutrons and gammas and the PDEs for the 5.64-cm and 11.29-cm diameter collimators were calculated in various phantom depths for different filter thicknesses and the results are shown in Figure 21 and Figure 23. The boron capture dose rate in units of Gy/min as a function of depth for the 5.64-cm diameter collimator is shown in Figure 22. It is found that increase of filter thickness results in a decrease of the absolute boron capture dose. The reason that thicker filters have higher PDE values is that the neutron dose decreases much faster than does boron capture dose as the filter thickness increases.

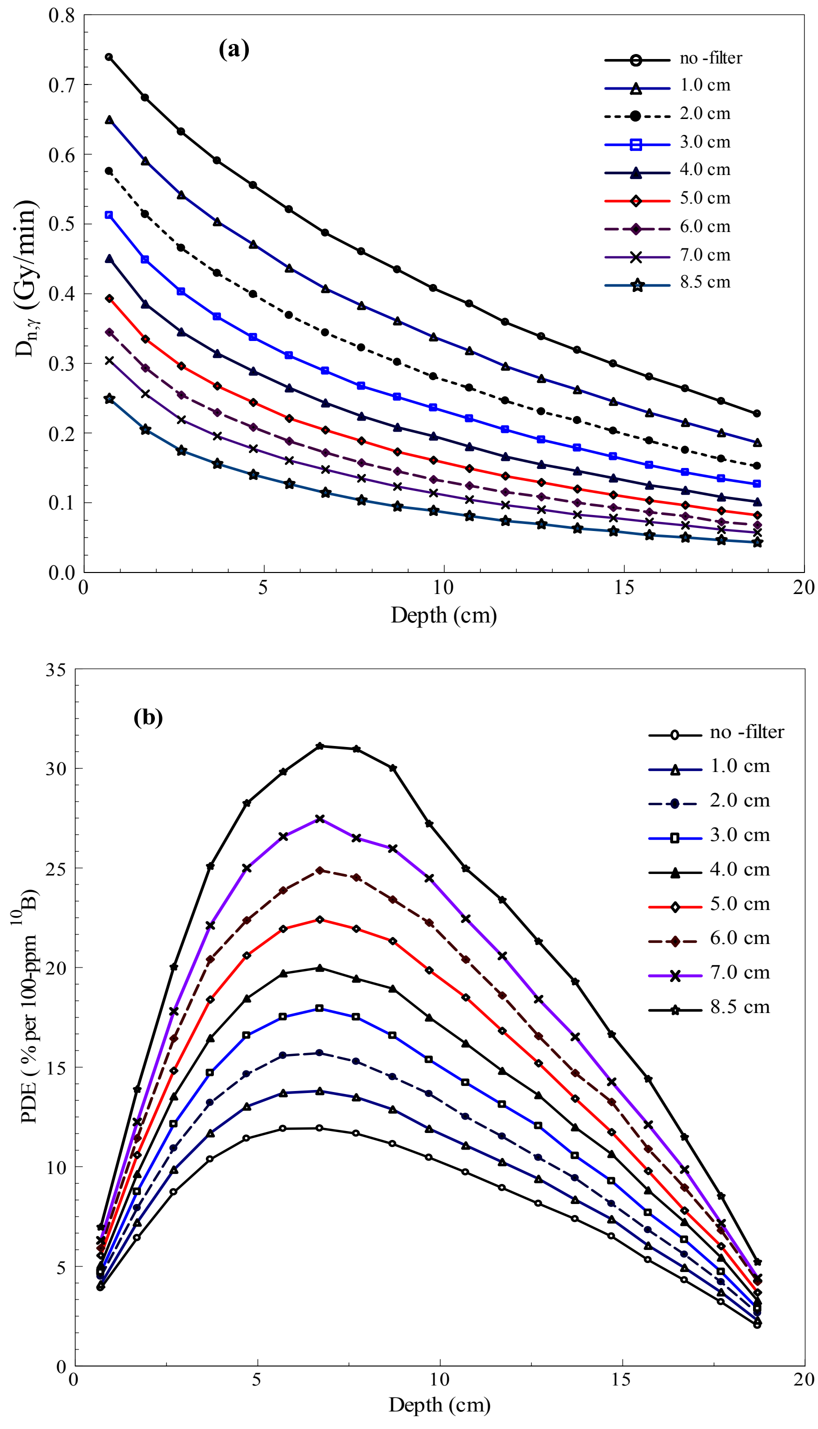

Figure 21: The MCNP calculated (a) depth-kerma distribution ($1.7x10^{14}$ protons/sec) and (b) depth-PDE distribution of the 5.64-cm collimator along the centerline for various thick filters.

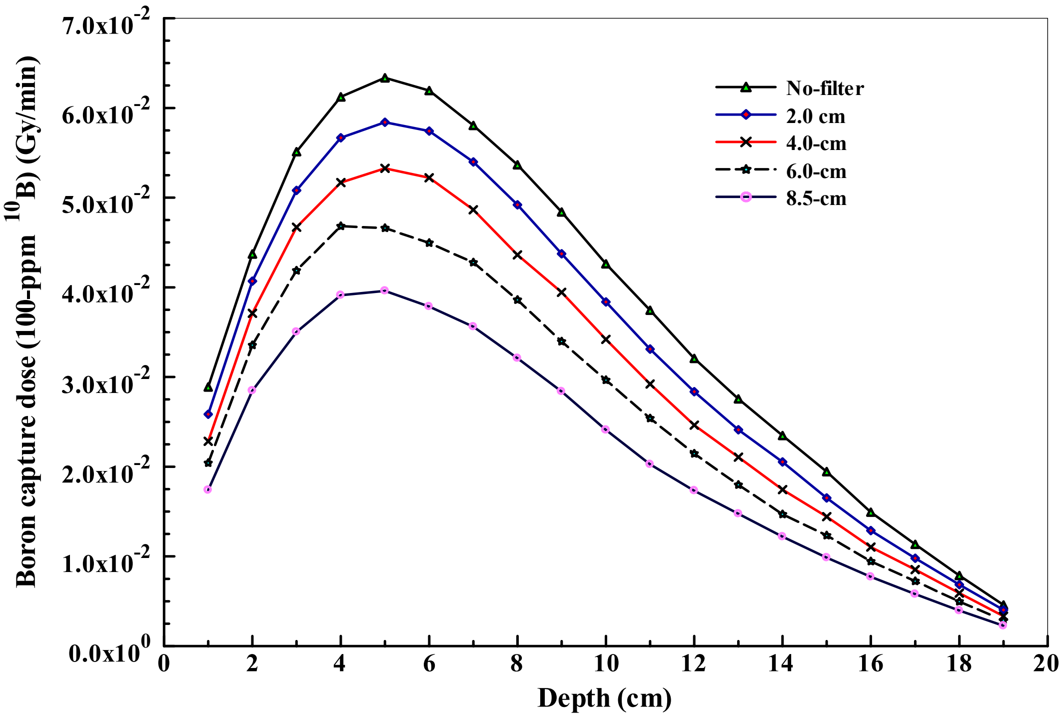

Figure 22: MCNP5 calculated depth-boron capture dose distribution of the 5.64-cm collimator along the centerline for various thick filters. 100-ppm ^{10}B uniformly distributed in the water-filled head phantom and 1.7x10^{14} protons/sec are assumed in the calculation. The error due to statistics is smaller than the symbol and the systematic error due to normalization is not considered here.

From the MCNP calculations shown in Figure 21 and Figure 23, the maximum values of PDE for any filter was found to be at depths in the phantom ranging from 5 to 9 cm. Increasing the filter thickness results in an increase in the PDE but a decrease in the total kerma rate. The relationship between PDE and total kerma rate as a function of the filter thickness is shown in Figure 24 for the 5.64-cm diameter collimator at 5.7-cm depth in the water-filled head phantom. The maximum PDE for the 5.64-cm diameter collimator with an 8.5-cm thick tungsten filter was found to be 31% while the total kerma rate at the corresponding location in the phantom was 0.11 Gy/min. The maximum PDE for the 11.29-cm diameter collimator with an 8.5-cm thick tungsten filter was found to be 29% while the total kerma rate at the corresponding location in the phantom was 0.14 Gy/min.

The gamma kerma depth distributions for various tungsten filters were also computed using MCNP simulation. The percentage of gamma dose in the total dose for several tungsten filters are shown in Figure 25. At 5.7-cm depth, the gamma percentage varies from 4.1% for no-filter to 8.5% for 8.5-cm tungsten filter.

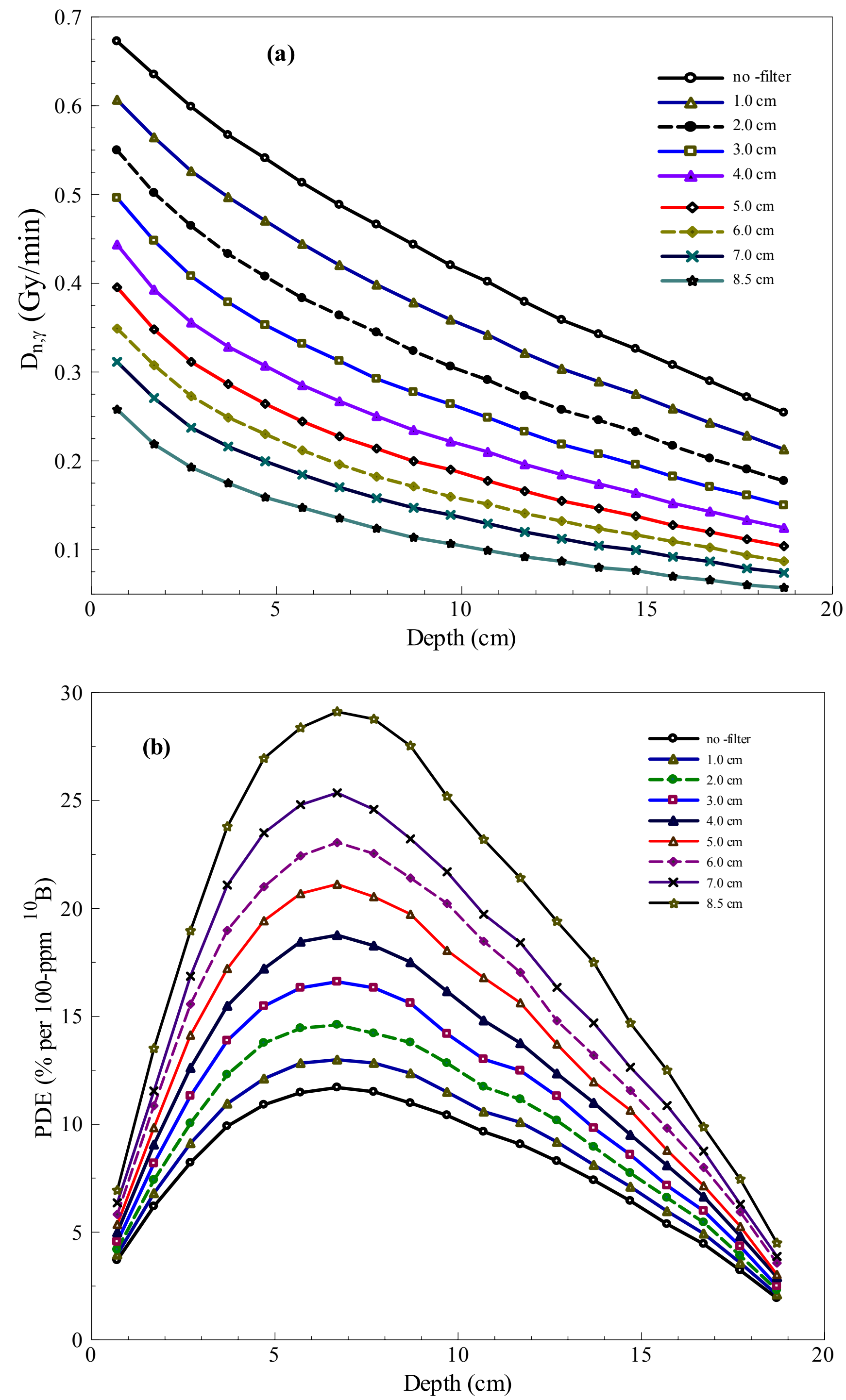

Figure 23: The MCNP5 calculated (a) depth-kerma distribution (1.7x10^{14} protons/sec) and (b) depth-PDE distribution of the 11.29-cm collimator along the centerline for various thick filters.

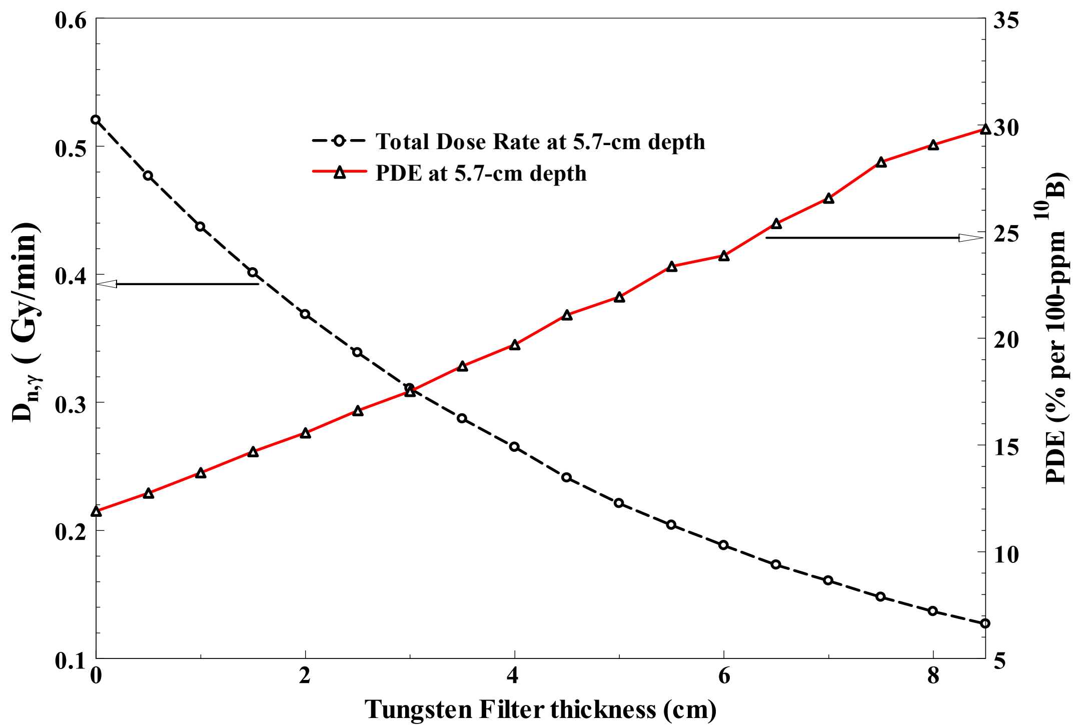

Figure 24: Relationship between PDE and total kerma rate as a function of filter thickness for the 5.64-cm collimator at 5.7-cm depth in the water filled head phantom.

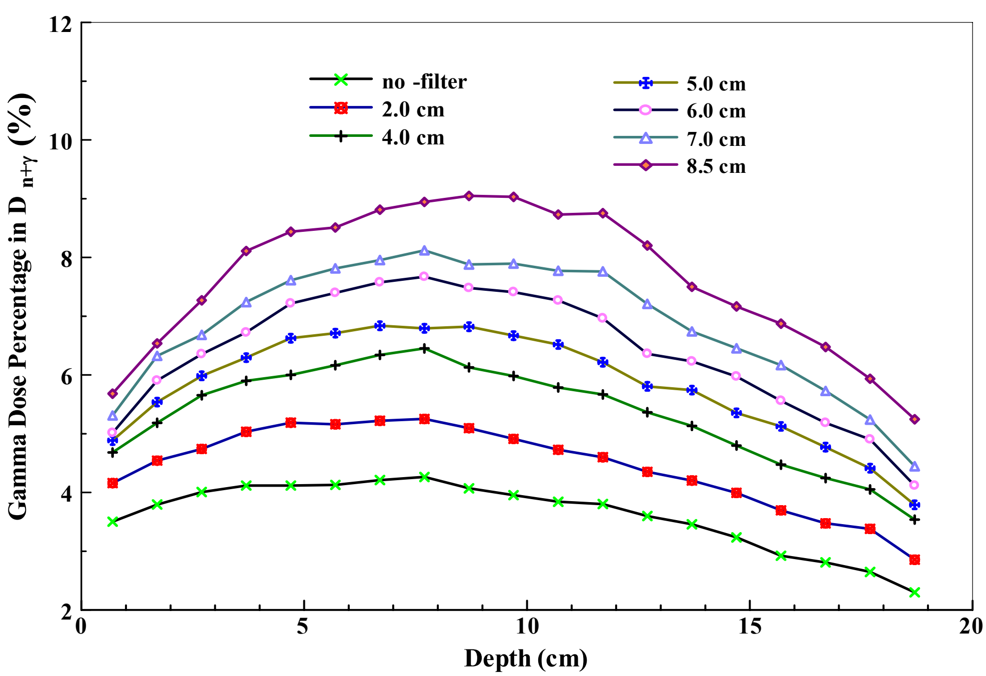

Figure 25: The percentage of gamma kerma in the total dose as a function of depth in the water-filled head phantom for various tungsten filter thickness. Statistic uncertainties range from 2% to 4%, not plot in the graph.

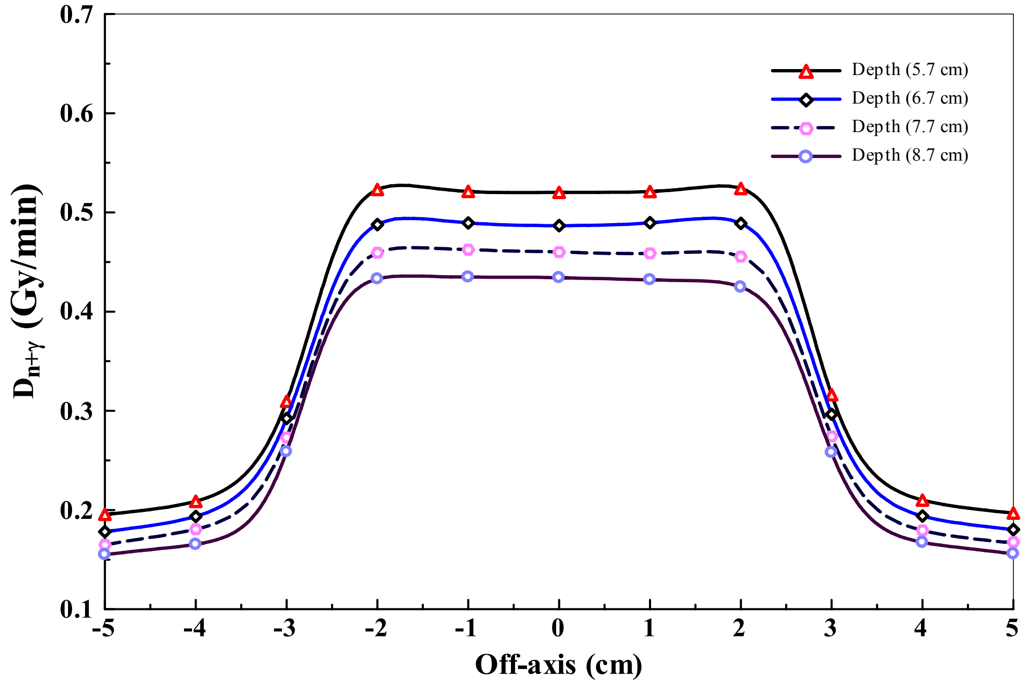

Figure 26: Total kerma rate off-axis profile at various depths in the water-filled head phantom in the designed BNCEFNT assembly with 5x5 cm^2 equivalent collimator and no-filter.

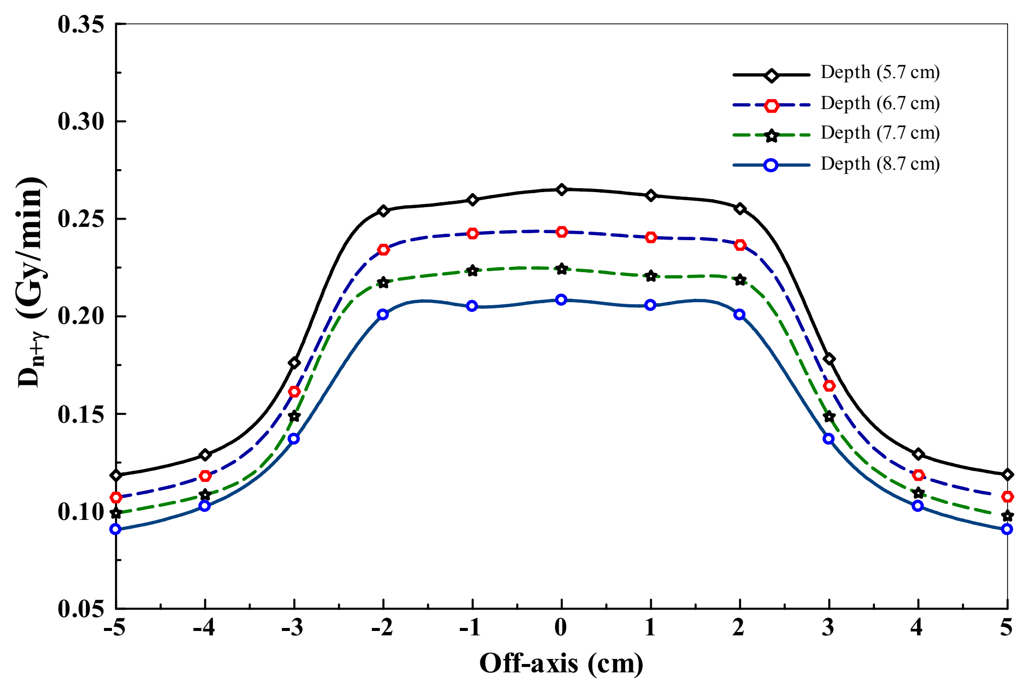

Figure 27: Total kerma rate off-axis profile at various depths in the water-filled head phantom in the designed BNCEFNT assembly with 5x5 cm^2 equivalent collimator and 4.0-cm thick tungsten filter.

The total kerma rate off-axis profiles at depth from 5.7 to 8.7 cm in the water-filled head phantom in the BNCEFNT assembly with 5.64-cm diameter collimator plus no-filter and 4.0-cm tungsten filter are shown in Figure 26 and Figure 27, respectively. They demonstrate the effect of the collimator. The kerma rates across the opening of the collimator are relatively flat; the ratios of the dose rate at the center to the dose rate at 2.0 cm off axis range from 0.992 to 1.01 for no-filter and from 1.03 to 1.04 for 4.0-cm tungsten filter. The statistical uncertainties in these ratios range from 1.2% to 1.6%. It is also noted that the collimator performs better when there is no filter.

The boron capture dose rate off-axis profiles at depths from 5.7 to 8.7 cm in the water-filled head phantom in the BNCEFNT assembly (5.64-cm diameter collimator plus no-filter and 4.0-cm tungsten filter) are shown in Figure 28 and Figure 29, respectively. The curves are more like a cosine function because they depend almost exclusively on the thermal neutron fluence rates, which can be explained using diffusion theory.

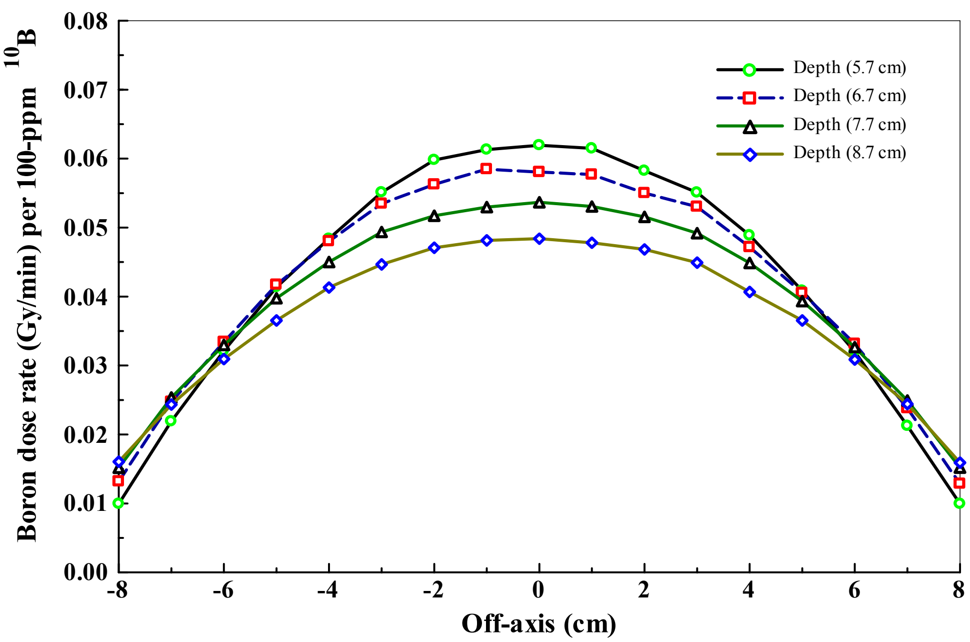

Figure 28: Boron dose rate off-axis profile per 100-ppm ^{10}B uniformly distributed in a water-filled head phantom in the designed BNCEFNT assembly with no-filter

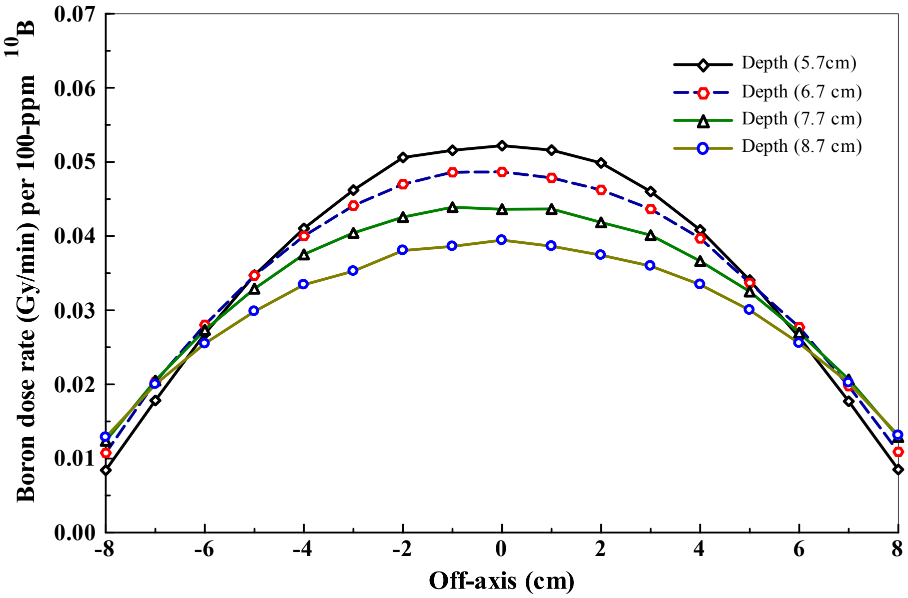

Figure 29: Boron dose rate off-axis profile per 100-ppm ^{10}B uniformly distributed in a water-filled head phantom in the designed BNCEFNT assembly with 4.0-cm tungsten filter

5.3 Validation of the Design

The MCNP-calculated PDE and total dose rate of the BNCEFNT assembly must be validated by experiments. According to the simulation, the system shown in Figure 18 will work. The exploded view of the assembly of the system is shown in Figure 30. The reflector (Figure 30(a)) is made of graphite. The largest cylinder in the center of the moderator is 22 cm in diameter with a curvature at the top to accommodate the head phantom. The cylindrical hole on the back of the moderator is 20-cm in diameter and for the insertion of the tungsten collimator. The two 10-cm diameter cylindrical holes on both sides of the moderator are for viewing and adjusting the position of the head and will be filled with two 10-cm diameter and 10-cm long graphite cylindrical plugs (Figure 30 (f)) after the head is positioned. The frame (Figure 30 (e)) is made of steel and serves as filter holder, collimator and reflector. Based on the MCNP calculations a frame made of tungsten results in higher PDE, but it is too heavy and expensive, so steel is used to substitute for tungsten. This leads to a PDE close to the PDE obtained by a tungsten frame. The collimator (Figure 30 (b) and (c)) is made of tungsten and consists two pieces for two different collimator diameters. The large piece should be always inserted in the moderator, and provides a 10-cm x 10-cm equivalent collimation if the small piece is not inserted. A 5-cm x 5-cm equivalent collimation can be obtained if the small piece is inserted into the larger one. The filter (Figure 30 (e)) is made of tungsten and is 20-cm in diameter and 1-cm thick (8 pieces) and 0.5 thick (1 piece) disks. The combination of these tungsten disks can make 16 filter thicknesses range from 0.5 to 8.5 cm.

For each collimator (5-cm x 5-cm and 10-cm x 10-cm), depth-dose distribution and depth-PDE distribution in the head phantom for a representative filter thickness should be measured using the borated and non-borated TE ion chamber as described in Chapter 3. This serves to validate the MCNP results shown in Figure 21, Figure 23, and Figure 24.

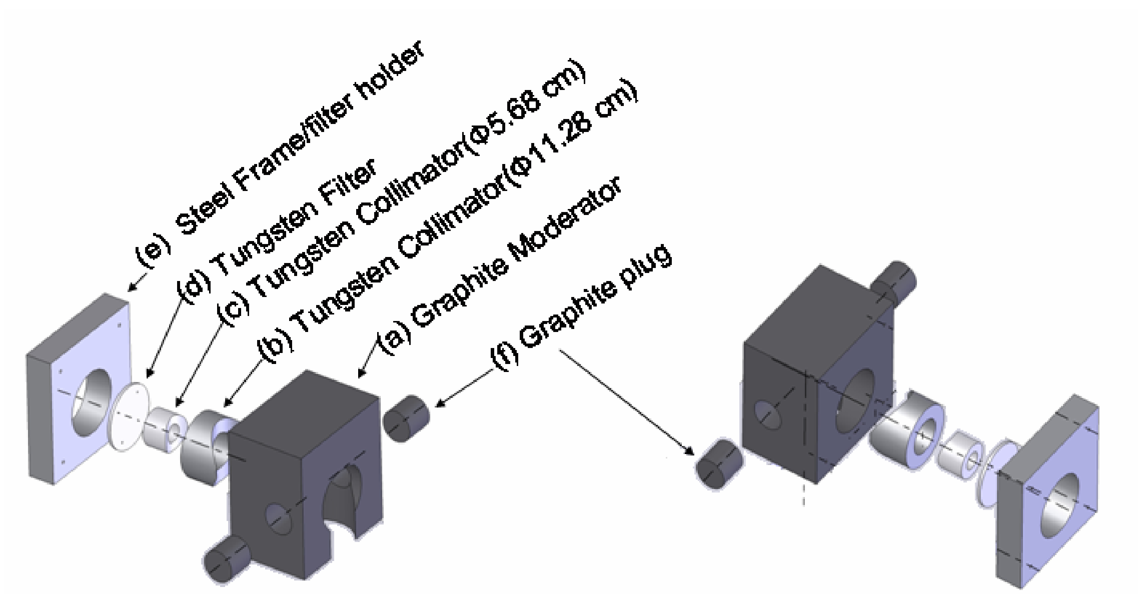

Figure 30: Drawings of the moderator, frame, collimator, and filter of the designed system

However, the cost of purchasing and machining tungsten is too prohibitive for a testing phase. So to validate the MCNP simulations, a simplified BNCEFNT assembly was built using tungsten plates (filter), lead bricks (collimator) and graphite blocks (reflector). The 5 cm x 5 cm collimator was made of four lead bricks is shown in Figure

31. The thickness of the collimator is 10 cm. The finished test assembly is shown in Figure 32. In order to reduce surface contamination, all the graphite bricks/blocks were wrapped with plastic foils. The center of the 5 cm x 5 cm collimator was aligned along the centerline of the 20 cm x 20 cm neutron beam (shown in Figure 32).

A picture of the RSVP head phantom used in the experiment is given in Figure 34. It was filled with deionized water and placed in the center of the built assembly in an upside down position.

An X-Y positioner is used to move the ion chamber remotely during the experiment. The small dimension of the neck of the head phantom makes it difficult to move the ion chamber inside the head phantom over a large range. Two ion chamber holders, one at an angle of 22˚ and one perpendicular to the X-Y table, were used in the experiment to move the ion chamber from 1 cm to 12.8 cm along the beam centerline (in the X axis), and to move the ion chamber laterally along the Y axis in a range of ±3.0 cm. X-Y positioner with the 22˚ angle ion chamber holder, the head phantom and the graphite reflective assembly is shown in Figure 35.

Figure 31: The 5 cm x 5 cm collimator made of four lead bricks (the brown colored in the center). The thickness of the collimator is 10 cm. The lead brick has a dimension of 20 cm x 10cm x 5 cm. The black bricks are graphite. The assembly is placed on a cart and between the assembly and cart is 10-cm thick polyethylene plate.

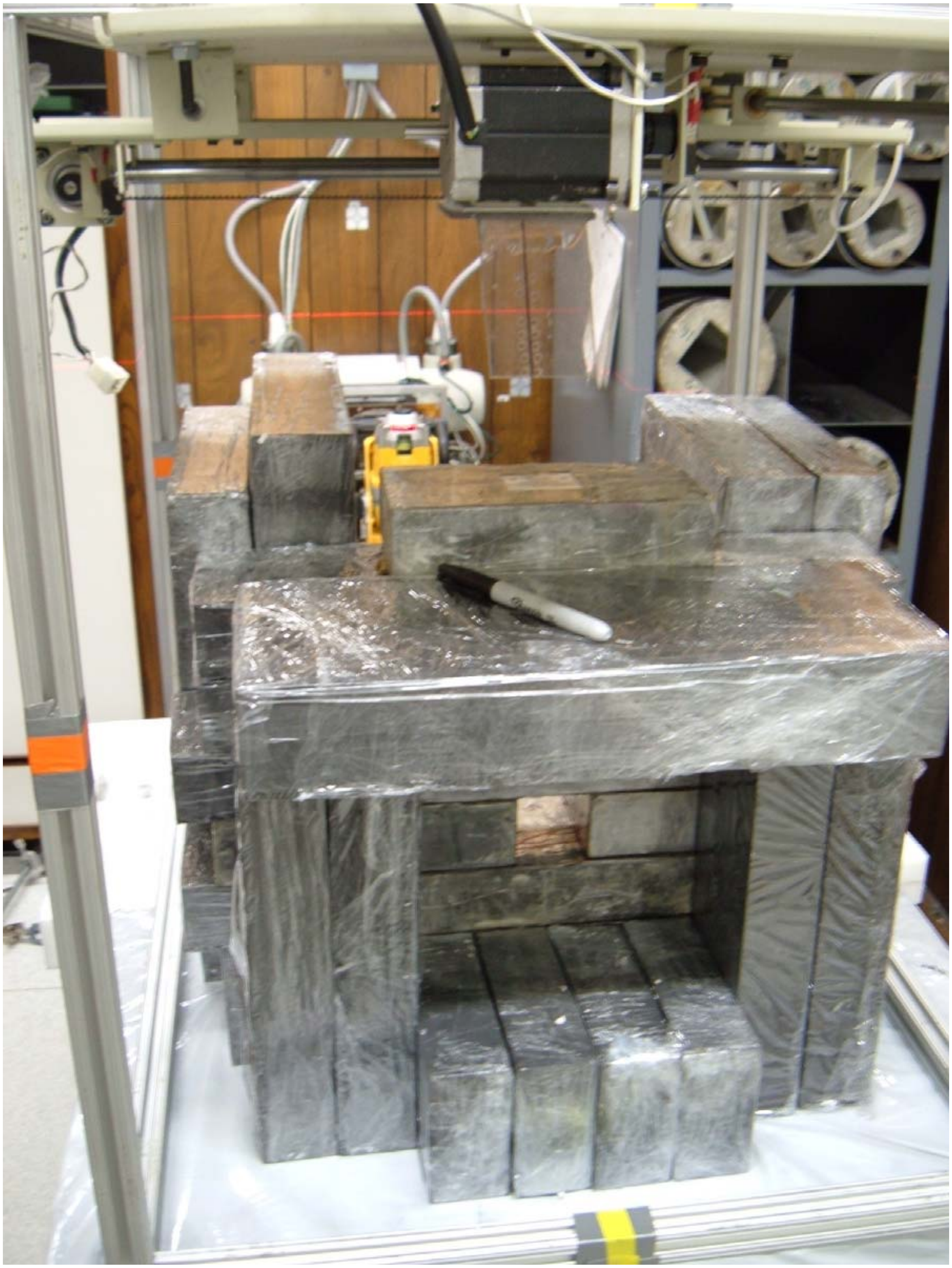

Figure 32: Picture of the simplified moderator/collimator assembly. The tungsten filter will be placed in the center. All graphite bricks are wrapped with plastic foil to avoid contamination.

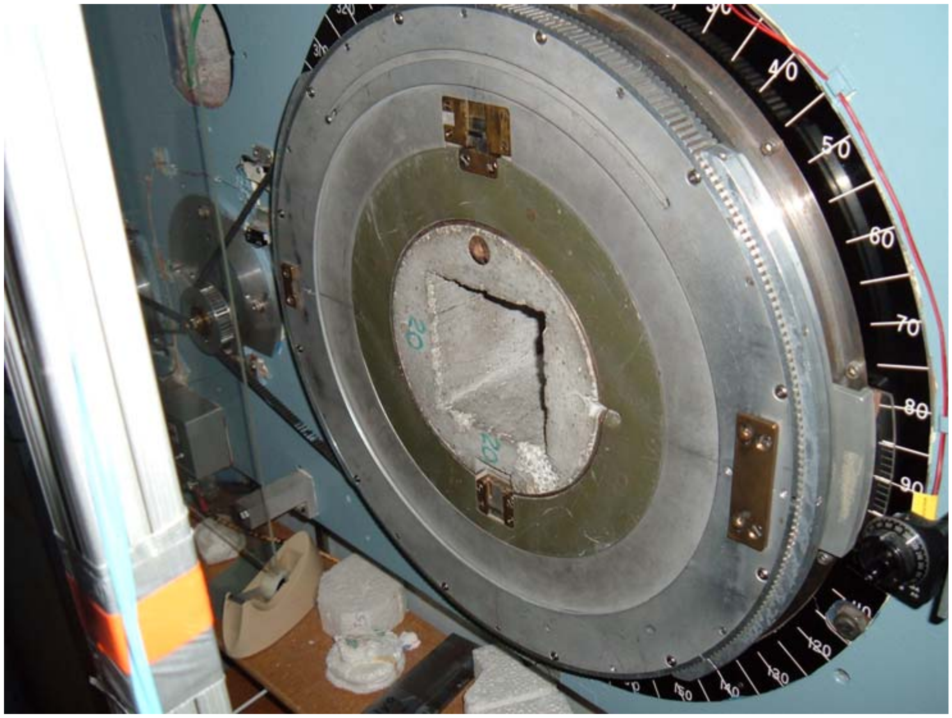

Figure 33: The standard 20 cm x 20 cm beam collimator used in the experiment.

Figure 34: Head phantom used in the experiment. It will be filled with deionized water and placed upside down during the experiment.

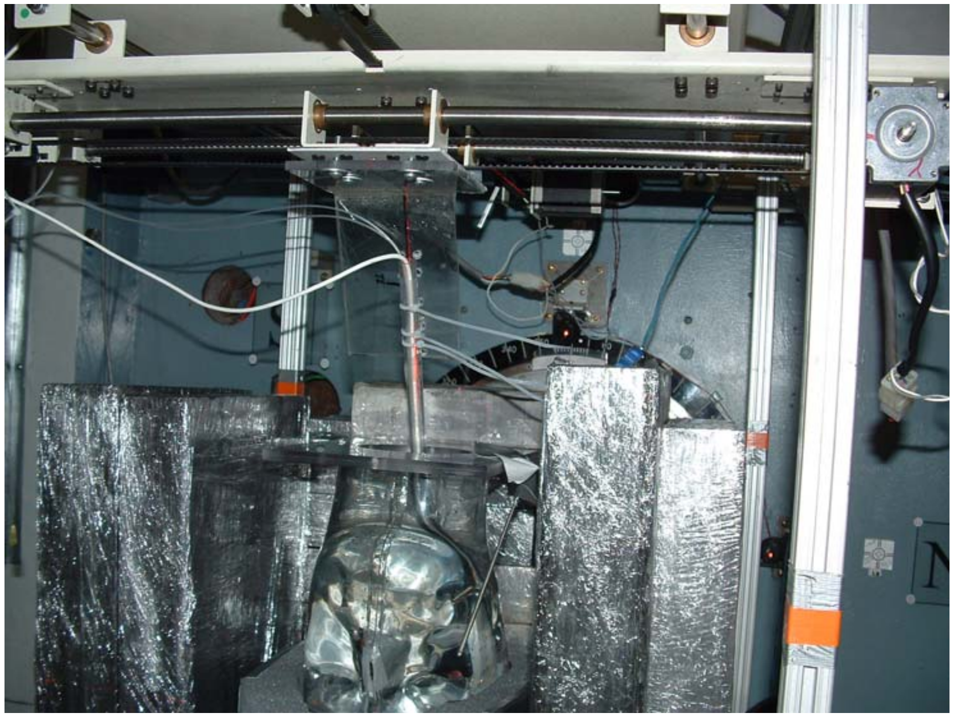

Figure 35: The head phantom filled with deionized water inside the assembly. The ion chamber is mounted on an X-Y positioner which can be remotely controlled to the designed position. The ion chamber holder has a 22° angle so that it can reach the wall of the head phantom.

The isocenter is at 5.8-cm depth (from back of the head) and 7.5 cm above the top of the head phantom (upside down), so the distance from the beryllium target to the rear surface of the head phantom is 184.2 cm. Six sets of dose data, no-filter and 1 to 5 cm thick tungsten filters, were taken using the borated and non-borated TE ion chambers. The irradiation ranged from 0.3 to 0.9 MU depending on the filter thickness and the ion chamber locations to ensure that the integrated charge measured by the Keithley 617 electrometer was more than 5.0 nC (with a few exceptions). This ensured good statistical data.

The neutron and gamma depth-dose distributions in the water-filled head phantom for the six different filter thickness were measured using the non-borated ion chamber and Equation (3.24). The boron capture dose was measured using the borated and non-borated ion chambers and Equation (3.22). The percent dose enhancement (PDE) was obtained using Equation (3.23). The boron capture dose was normalized to 100-ppm ^{10}B. The measurements of the depth-dose for no-filter, 1.0-cm to 5.0-cm filter are shown through Figure 36 to Figure 41, respectively. The measured total dose for each filter thickness, including the neutron, photon and boron capture doses, are also shown in Figure 36 to Figure 41. The MCNP5-calculated neutron and photon kermas for these filters are also shown in these figures for comparison. The relationship between the number of protons and the MU during the experiment was found to be 3.3×10^{16} protons/MU, which was used to normalize the MCNP5 results to Gy/MU.

From Figure 36 to Figure 41, the measured neutron and photon doses agree with the MCNP-calculated neutron and photon doses within uncertainties. The 9% error in the Bragg-Gray equation was not accounted in the error bar of the measured curves. The 15% error in the normalization factor for the MCNP5-calculated neutron and gamma dose was not included. The errors in the boron capture dose consist the 5.5% error from the thermal calibration factor and 3.5% error in the charge measured by the ion chambers. This charge error is mainly due to uncertainty in the ion chamber positioning.

It is also observed from Figure 36 to Figure 41 that the first data points of the MCNP calculated dose in all figures are consistently higher than the measured values. This is because the F6 MCNP tally is a kerma tally, not absorbed dose tally. Charged particle equilibrium does not exist at shallow depths in the head phantom, at these locations the kerma value is higher than the absorbed dose. For the Fermilab neutron beam, the maximum absorbed dose (D_{max}) is at 1.7 cm depth. So the MCNP-calculated kerma at positions deeper than 1.7 cm should be smaller than the absorbed dose. These phenomena were clearly seen in Figures 36 to 41.

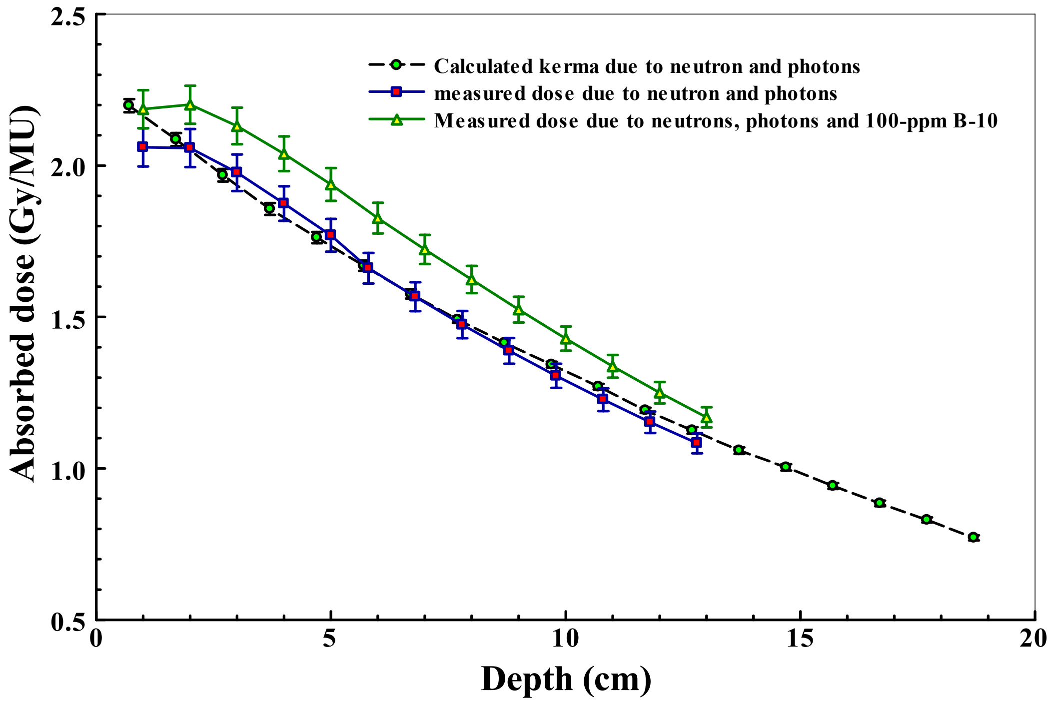

Figure 36: MCNP5 calculated and measured depth-dose distribution in the water filled head phantom for 0-cm filter. The measured (n+γ) dose is obtained using the non-borated ion chamber and equation (3.24); the (n+γ + boron) dose is measured using the borated and non borated ion chamber using equations (3.24) and (3.22).

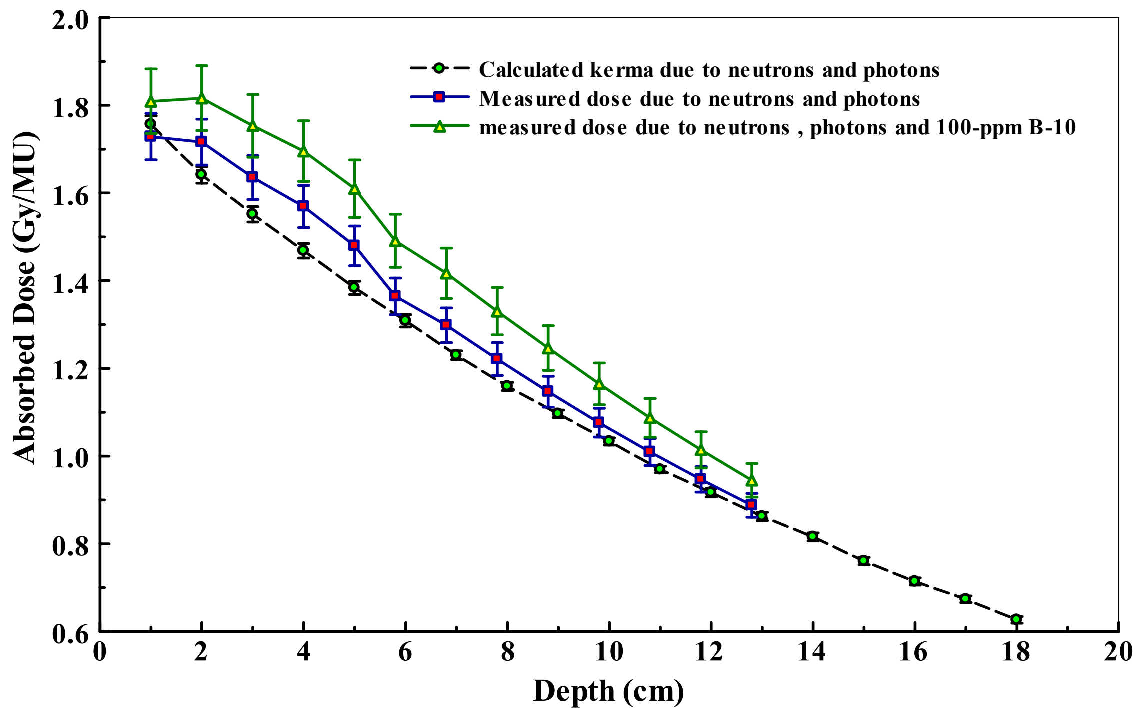

Figure 37: MCNP5 calculated and measured depth-dose distribution in the water filled head phantom for 1.0-cm filter. The measured (n+γ) dose is obtained using the non-borated ion chamber; the (n+γ + boron) dose is measured using the borated and non borated ion chamber.

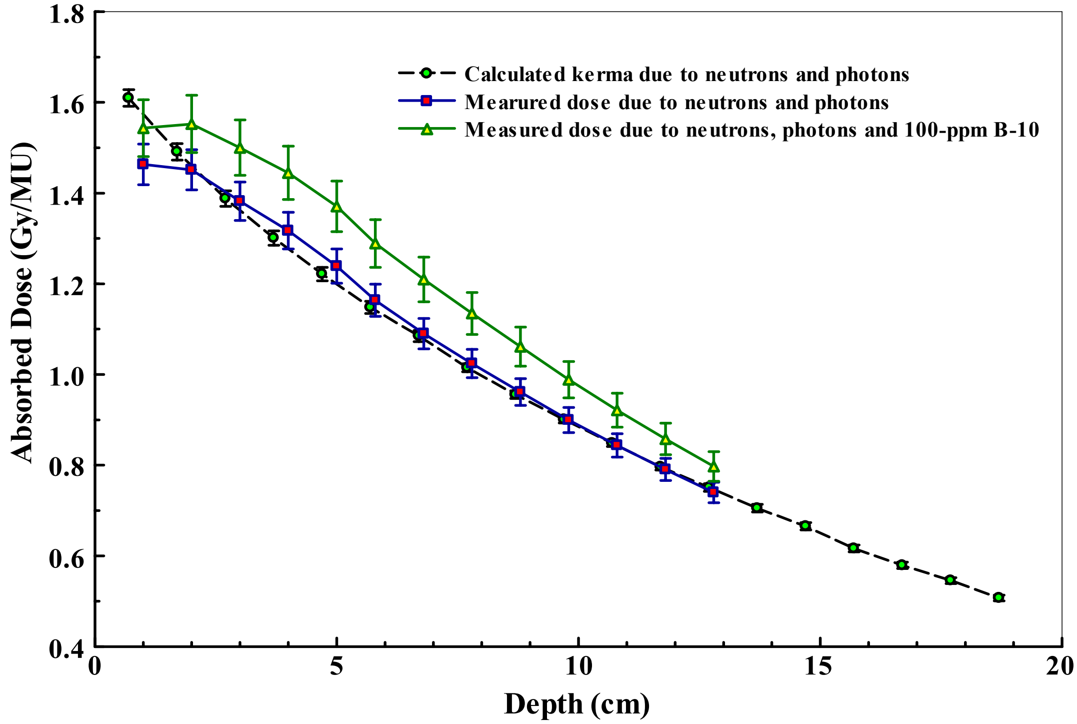

Figure 38: MCNP5 calculated and measured depth-dose distribution in the water filled head phantom for 2.0-cm filter. The measured (n+γ) dose is obtained using the non-borated ion chamber; the (n+γ + boron) dose is measured using the borated and non borated ion chamber.

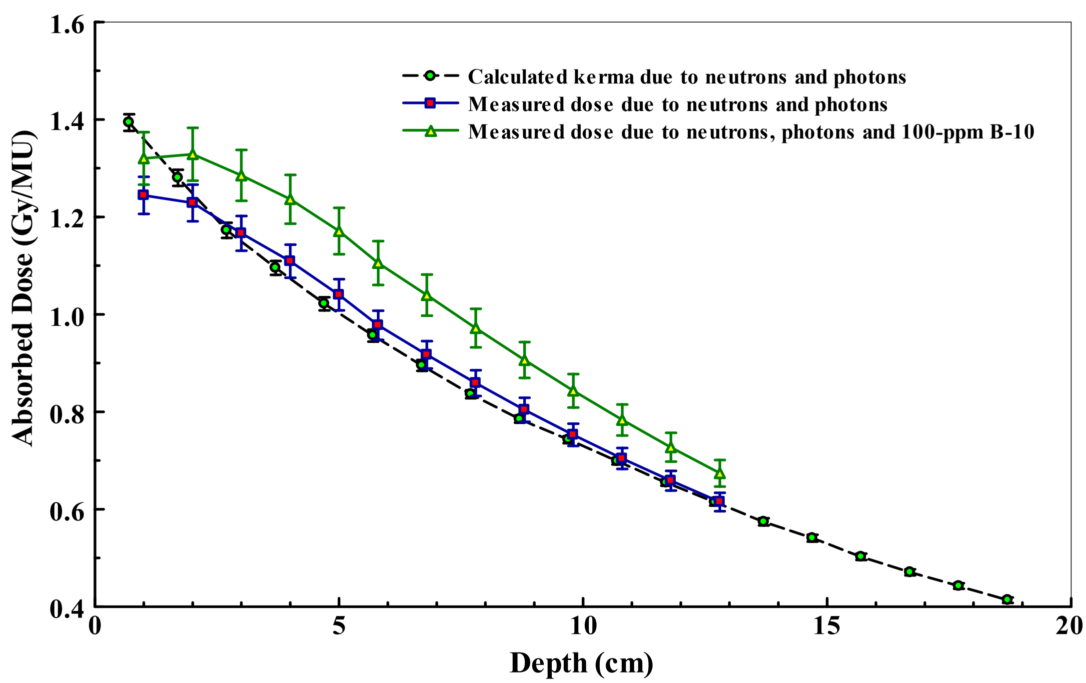

Figure 39: MCNP5 calculated and measured depth-dose distribution in the water filled head phantom for 3.0-cm filter. The measured (n+γ) dose is obtained using the non-borated ion chamber; the (n+γ + boron) dose is measured using the borated and non borated ion chamber.

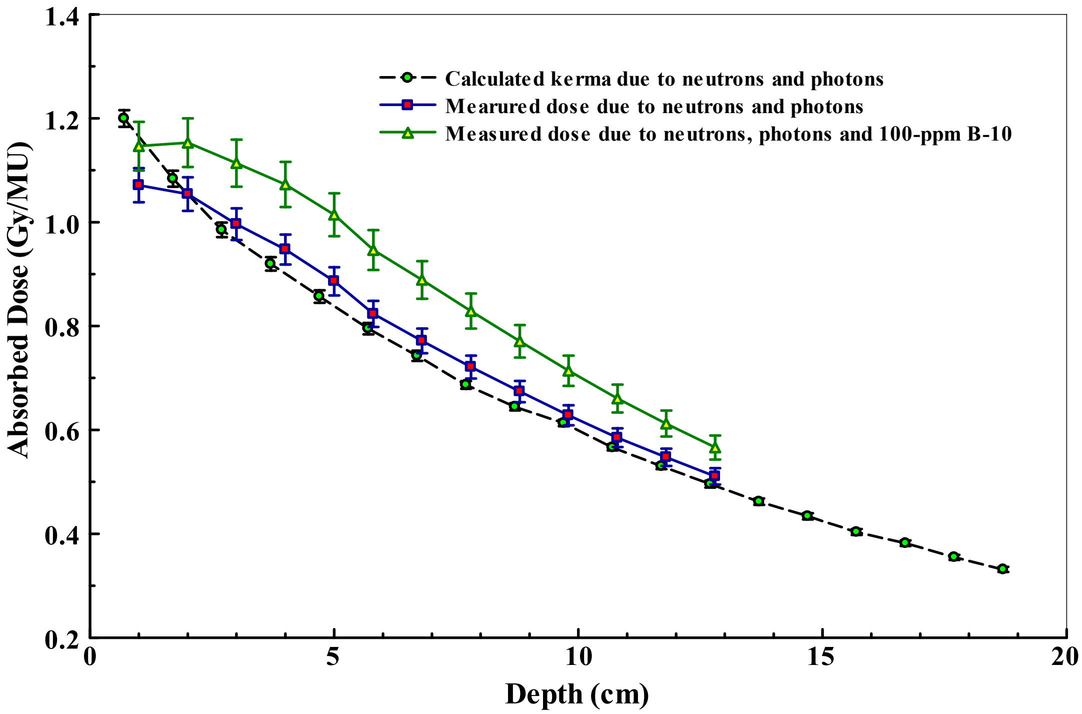

Figure 40: MCNP5 calculated and measured depth-dose distribution in the water filled head phantom for 4.0-cm filter. The measured (n+γ) dose is obtained using the non-borated ion chamber; the (n+γ + boron) dose is measured using the borated and non borated ion chamber.

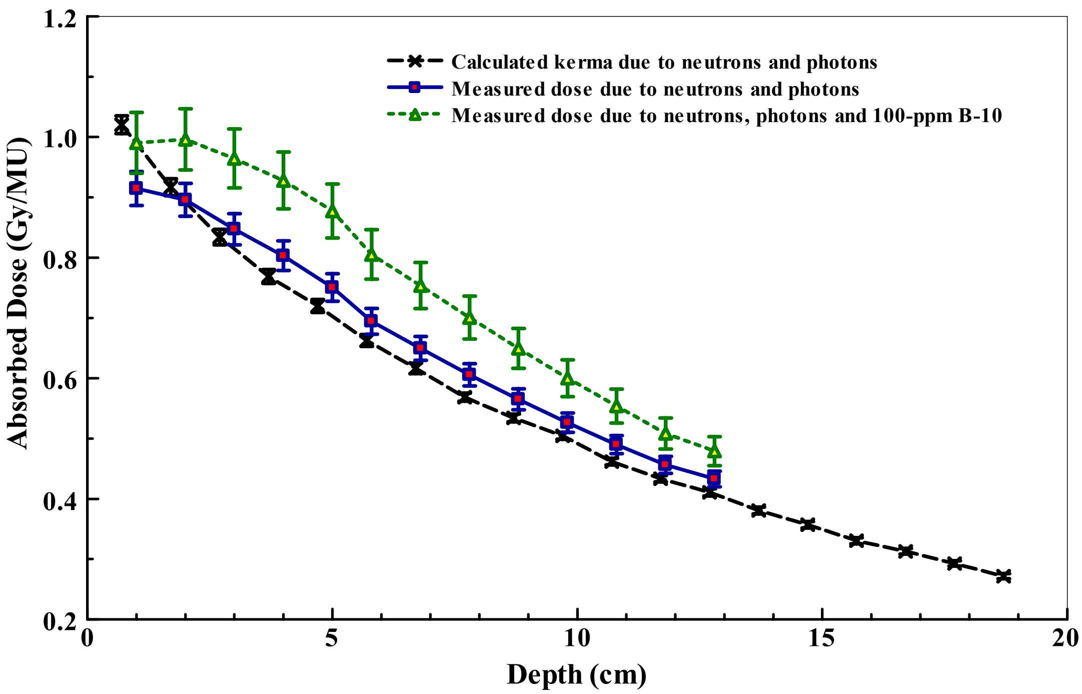

Figure 41: MCNP5 calculated and measured depth-dose distribution in the water filled head phantom for 5.0-cm filter. The measured (n+γ) dose is obtained using the non-borated ion chamber; the (n+γ + boron) dose is measured using the borated and non borated ion chamber.

The comparisons of measurements and calculations of the PDE values for the six conditions are shown in Figure 42 to Figure 47. The measurements and calculations agree within uncertainty. The error bars of the measurements do not include the 9% error from the Brag-Gray equation. The error consists of the 5.5% error from borated ion chamber thermal neutron calibration coefficient and about 4.0% error due to the positioning of the borated and non-borated ion chambers. The error in the calculated PDE is a combination of statistical uncertainties in boron, neutron and gamma dose calculations. The simplification of the head phantom and the neglecting of foams surrounding the head phantom in the simulation may also lead to uncertainty in the calculated PDE values, but this error is not included in the error bars.

The importance of the graphite reflector on both sides of the head phantom can be seen clearly from Figure 47. The PDE with the graphite reflector is 25% higher than the PDE with graphite reflector on both sides removed.

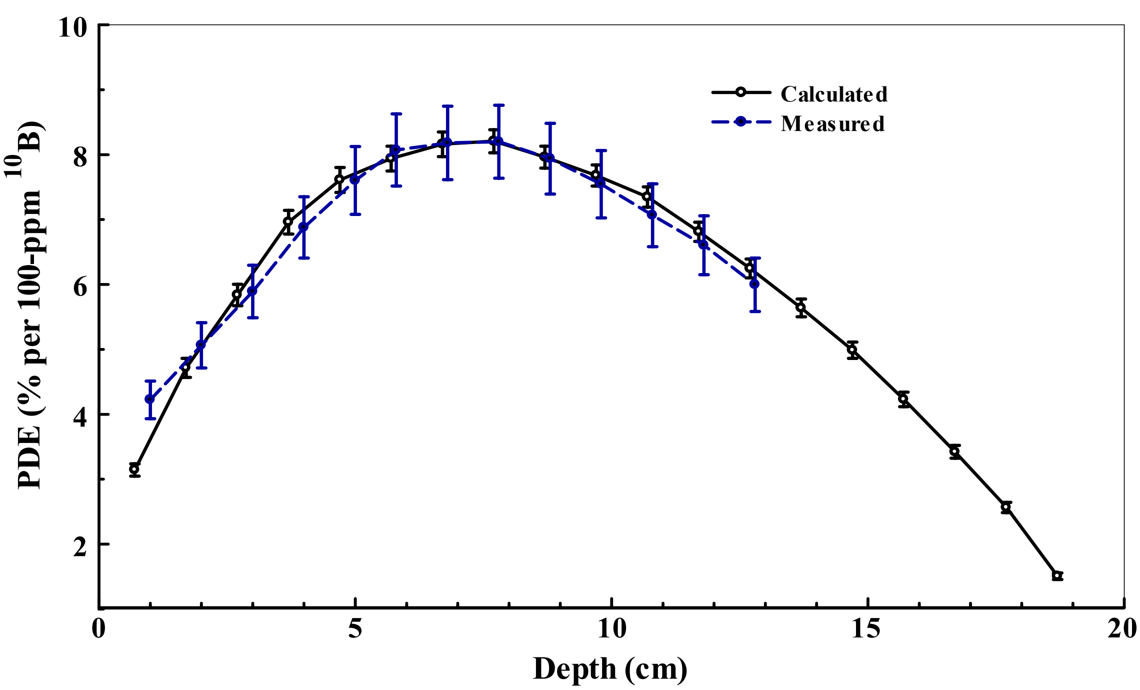

Figure 42: PDE for 100-ppm ^{10}B in the water filled head phantom for 0.0-cm filter. The measured PDE is obtained using Equation (3.23) and the borated and non-borated ion chamber readings.

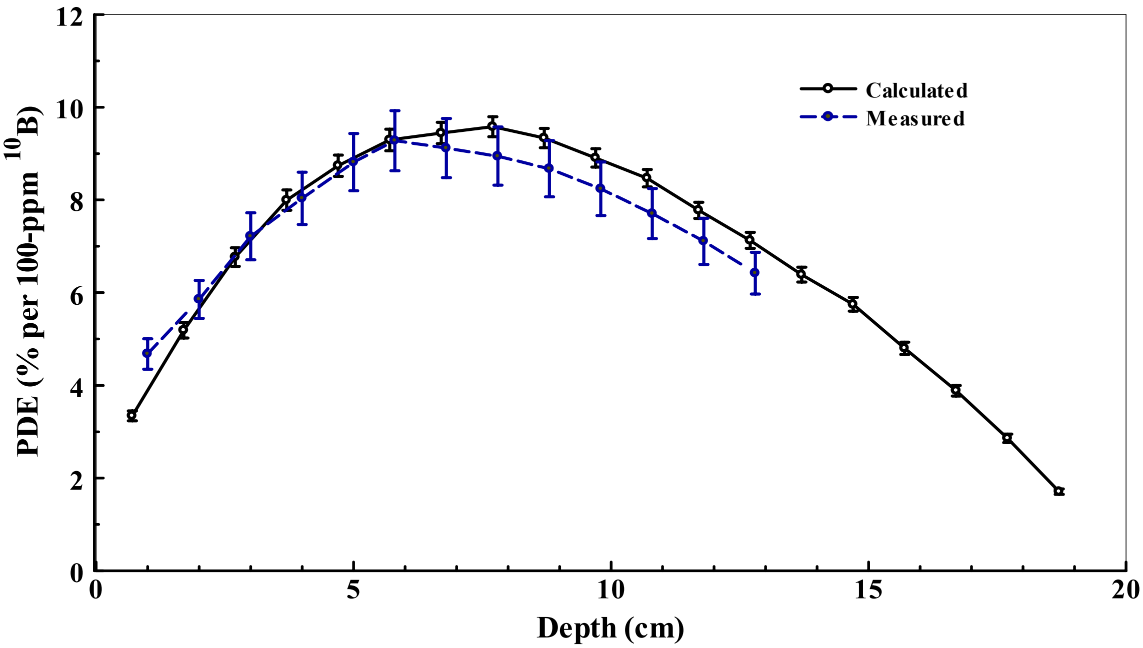

Figure 43: PDE for 100-ppm ^{10}B in the water filled head phantom for 1.0-cm filter. The measured PDE is obtained using Equation (3.23) and the borated and non-borated ion chamber readings.

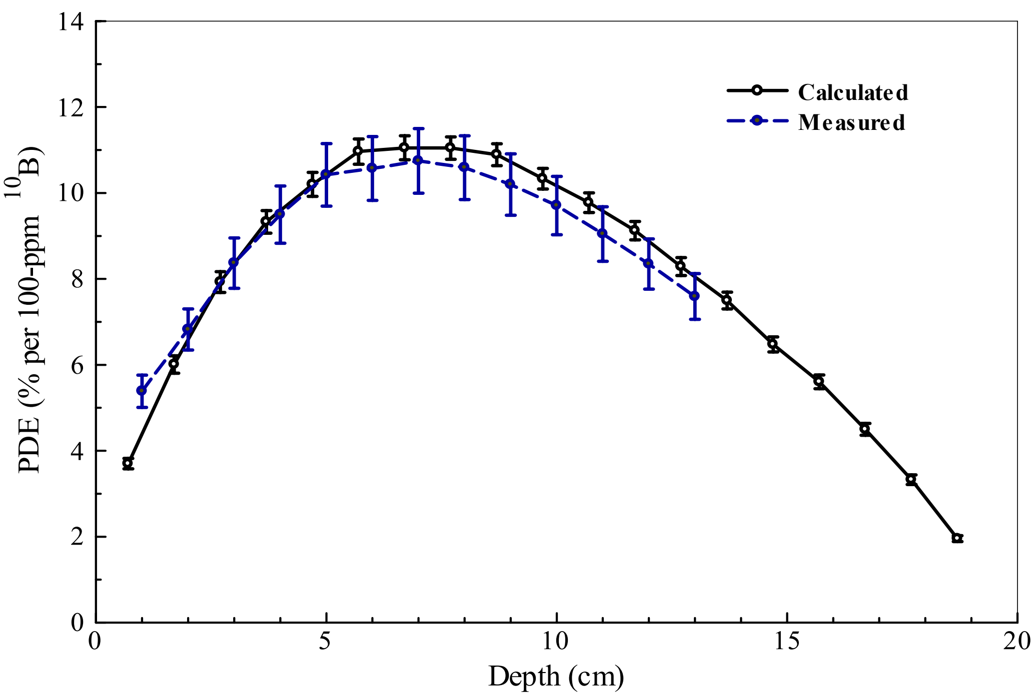

Figure 44: PDE for 100-ppm ^{10}B in the water filled head phantom for 2.0-cm filter. The measured PDE is obtained using Equation (3.23) and the borated and non-borated ion chamber readings.

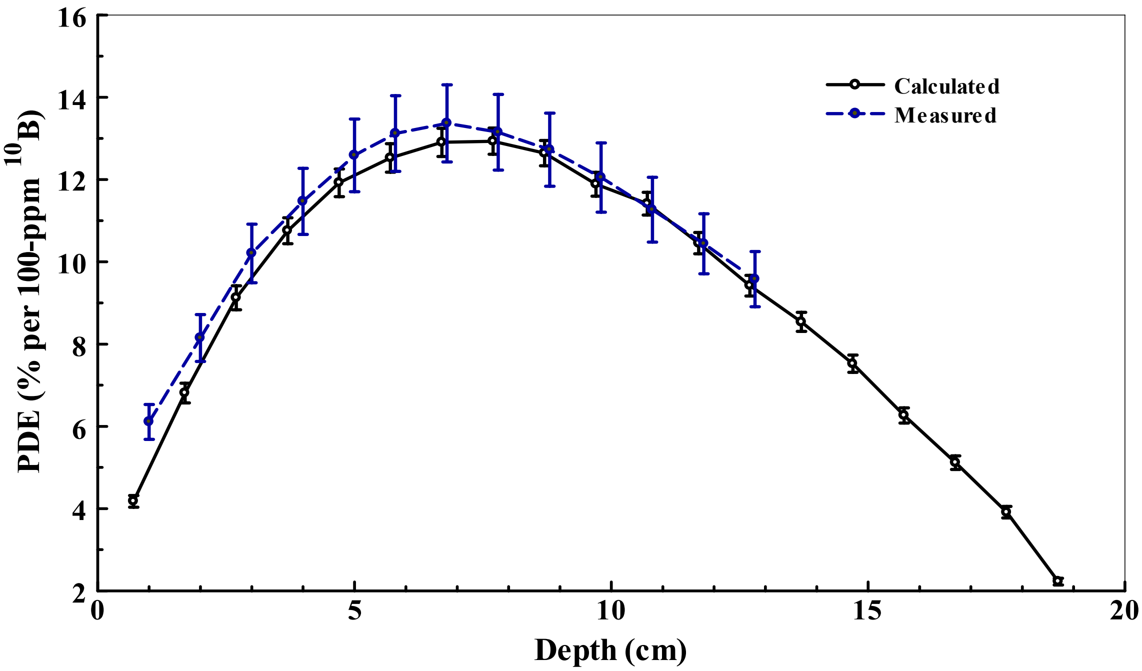

Figure 45: PDE for 100-ppm ^{10}B in the water filled head phantom for 3.0-cm filter. The measured PDE is obtained using Equation (3.23) and the borated and non-borated ion chamber readings.

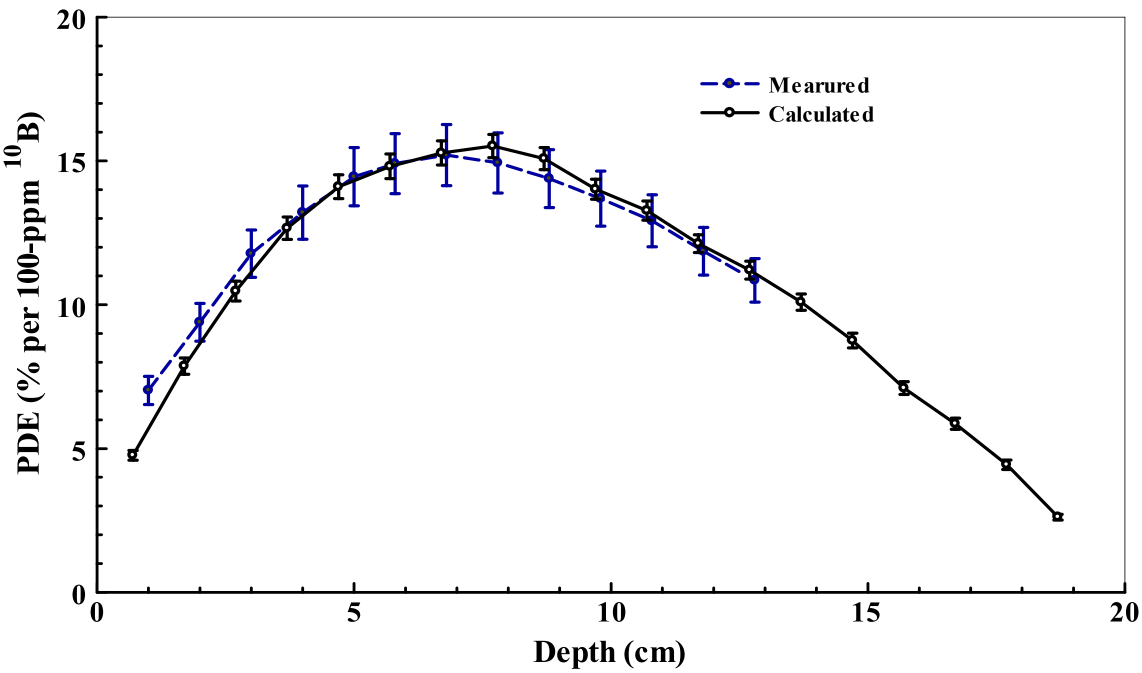

Figure 46: PDE for 100-ppm ^{10}B in the water filled head phantom for 4.0-cm filter. The measured PDE is obtained using Equation (3.23) and the borated and non-borated ion chamber readings.

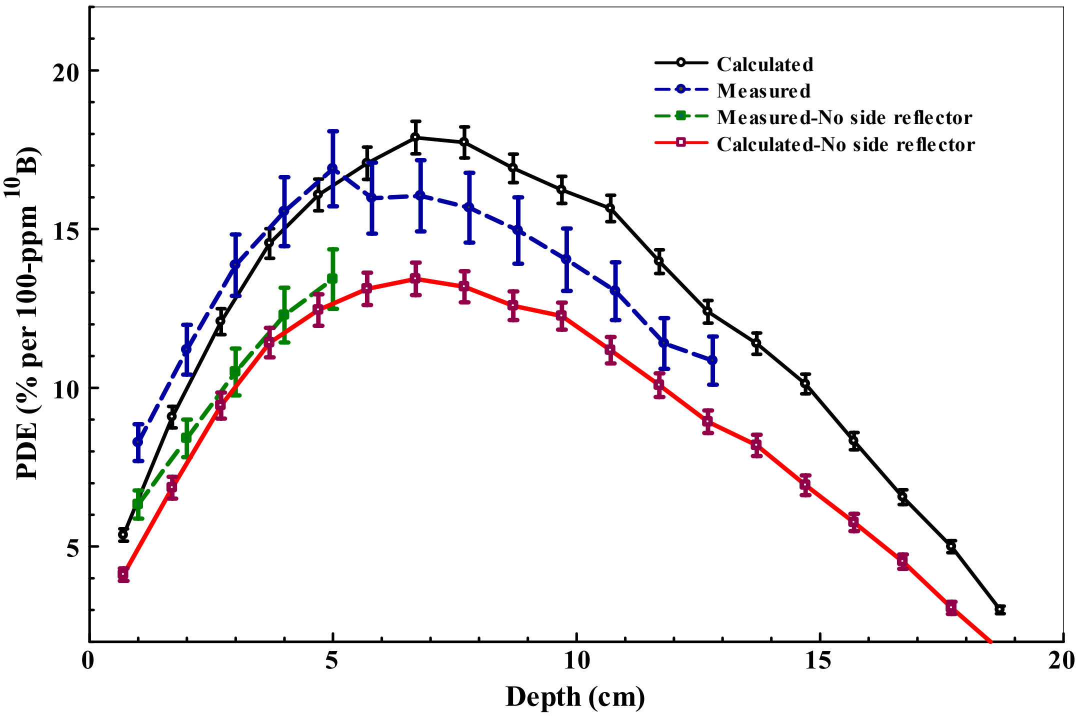

Figure 47: PDE for 100-ppm ^{10}B in the water filled head phantom for 5.0-cm filter. The measured PDE is obtained using Equation (3.23) and the borated and non-borated ion chamber readings. Graphite reflector on both sides were removed and the PDEs were measured at 1-cm to 5-cm depth to see their effects on PDEs. The present of the side graphite reflectors can increase PDE at 5.0-cm depth by more than 25%.

In Figure 47, the measured PDE curve behaves abnormally starting at position of 5.8-cm depth. Because the ion chamber holder was changed at this point, the author believes that this abnormality is due to the position recording of the borated ion chambers. Comparisons of the measured boron capture dose (from Equation (3.22)) and the MCNP-calculated boron capture dose for the 5.0-cm and 4.0-cm tungsten filter are shown in Figure 48 and Figure 49, respectively. The two figures imply that the measured boron doses for the 5.0-cm tungsten filter at depth of 5.8-cm and deeper in the head phantom are lower than they should be. Further analysis of the data suggests that the data might be misrecorded: the borated ion chamber readings of the 5.8-cm to 12.8-cm depth may be the readings for 6.8-cm to 12.8-cm depth, and the data point for 5.8-cm may have been missed. Figure 47 is re-plotted in Figure 51 according to the above argument. In this case the measurements and calculations agree much better after the data adjustment.

However, the measurements and calculations agree within uncertainty even before the data adjustment.

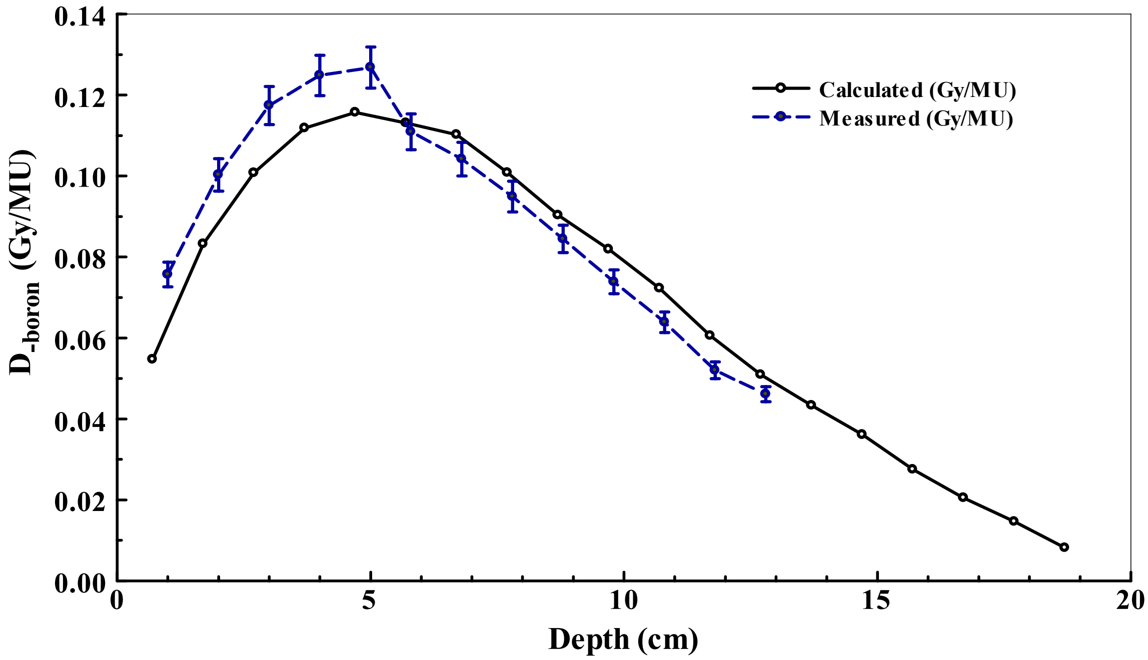

Figure 48: Comparison of the calculation and measurements of the boron dose distribution for 5.0-cm thick tungsten filter. Abnormality of the trend of the measured data occurs at the position where ion chamber holder was changed.

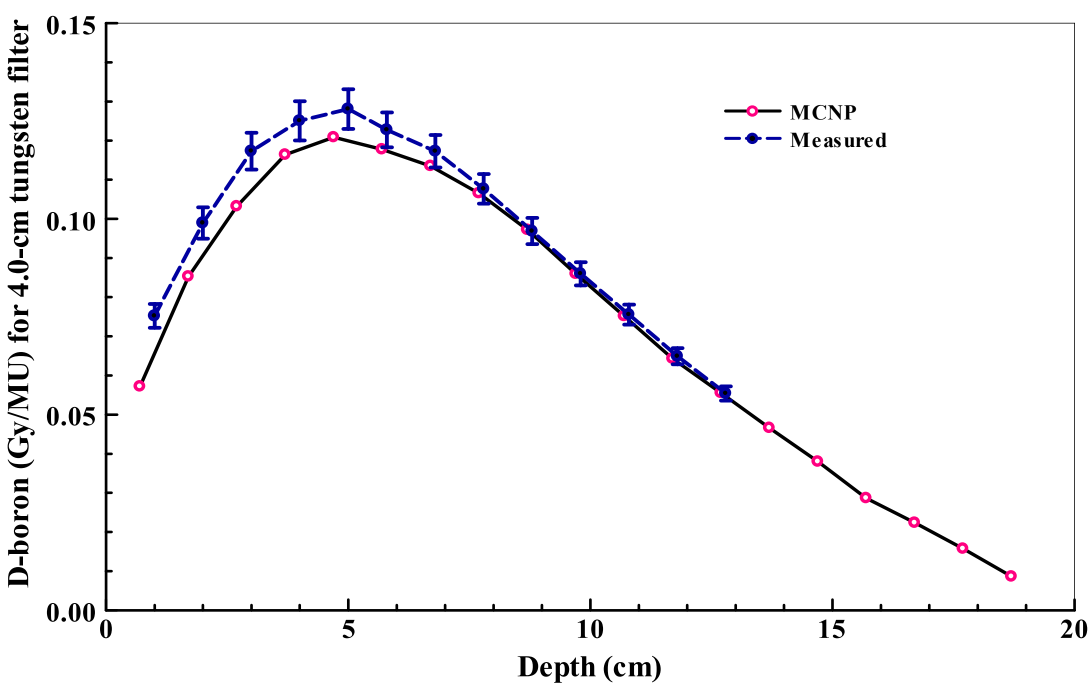

Figure 49: Comparison of the calculation and measurements of the boron dose distribution for 4.0-cm thick tungsten filter. Both measured and calculated curves vary smoothly with depth.

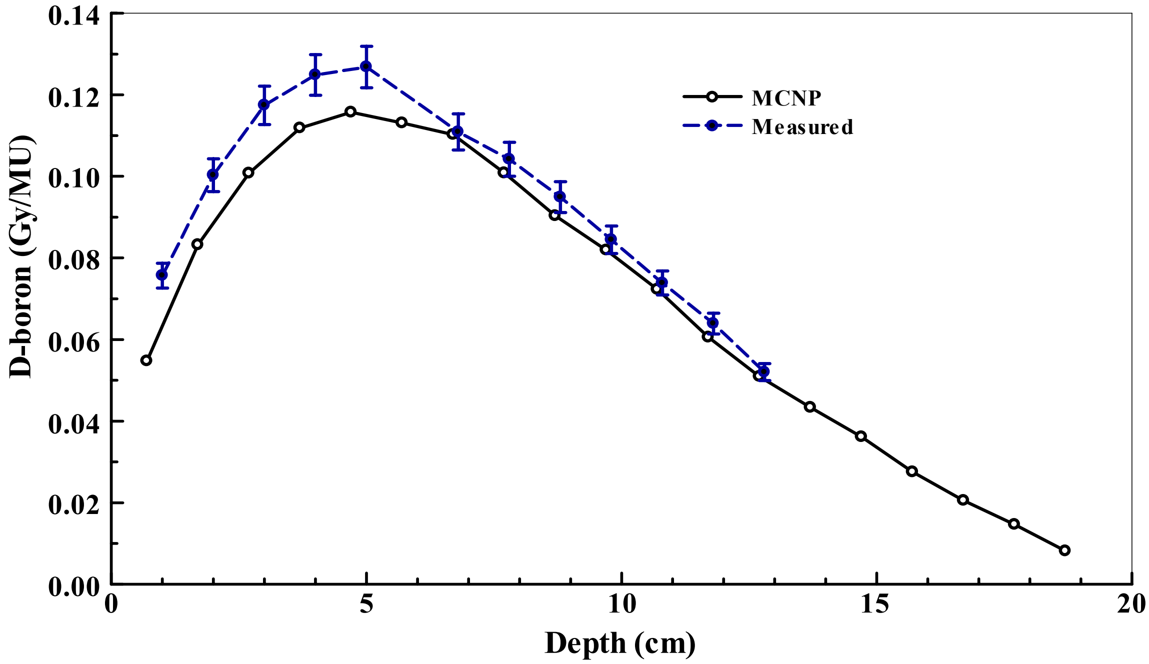

Figure 50: Comparison of the calculation and measurements of the boron dose distribution for 5.0-cm thick tungsten filter with adjusted data.

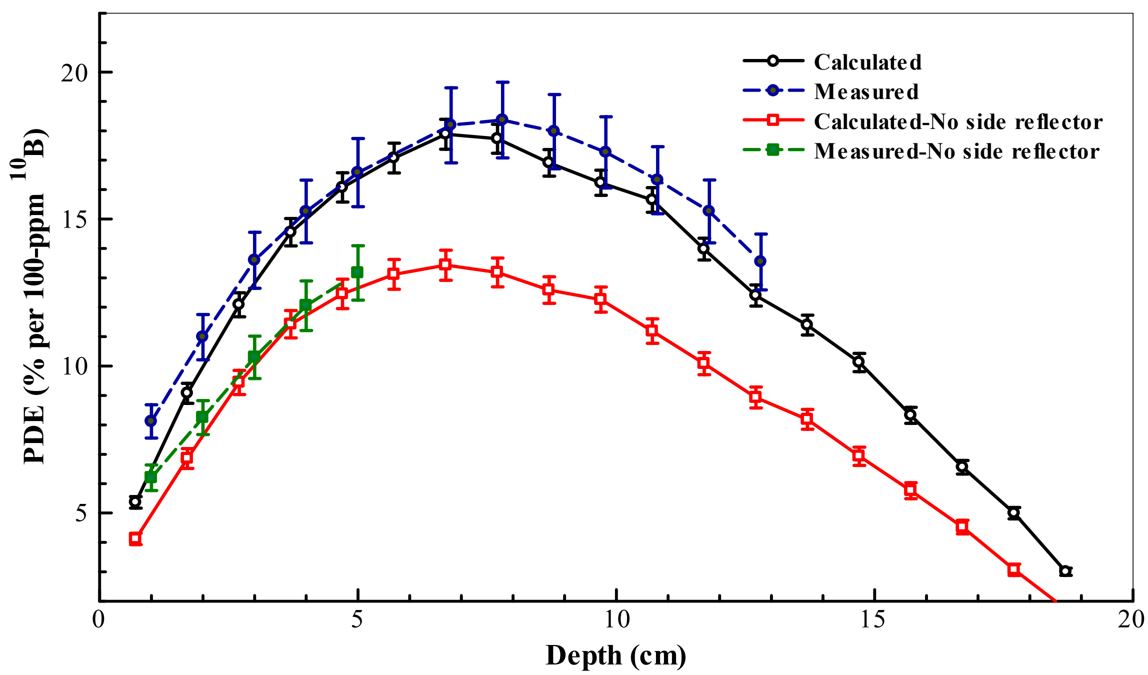

Figure 51: PDE for 100-ppm ^{10}B in the water filled head phantom for 5.0-cm filter after adjustment (a re-plot of Figure 47).

The off-axis total absorbed dose rate profiles of the MCNP calculations and the measurements at 8.8-cm depth in the water-filled head phantom in the simplified BNCEFNT assembly with no-filter and 5.0-cm tungsten filter are shown in Figure 52 and Figure 53, respectively. The 15% normalization error (from the neutron fluence rate) is not plotted for the MCNP data. The error bars of the measured data points are from the uncertainties in the positioning of ion chamber during the measurement and do not include the 9% error from the Bragg-Gray equation. The discrepancy at ±3.0 cm off axis position between the calculation and measurement are mainly due to the positioning of the ion chamber in the experiment.

The MCNP calculated results, the total absorbed dose, the boron dose and the PDE as a function of depth in the water filled head phantom, agree well with the measurements. The measurements have demonstrated that the MCNP5 simulations are valid.

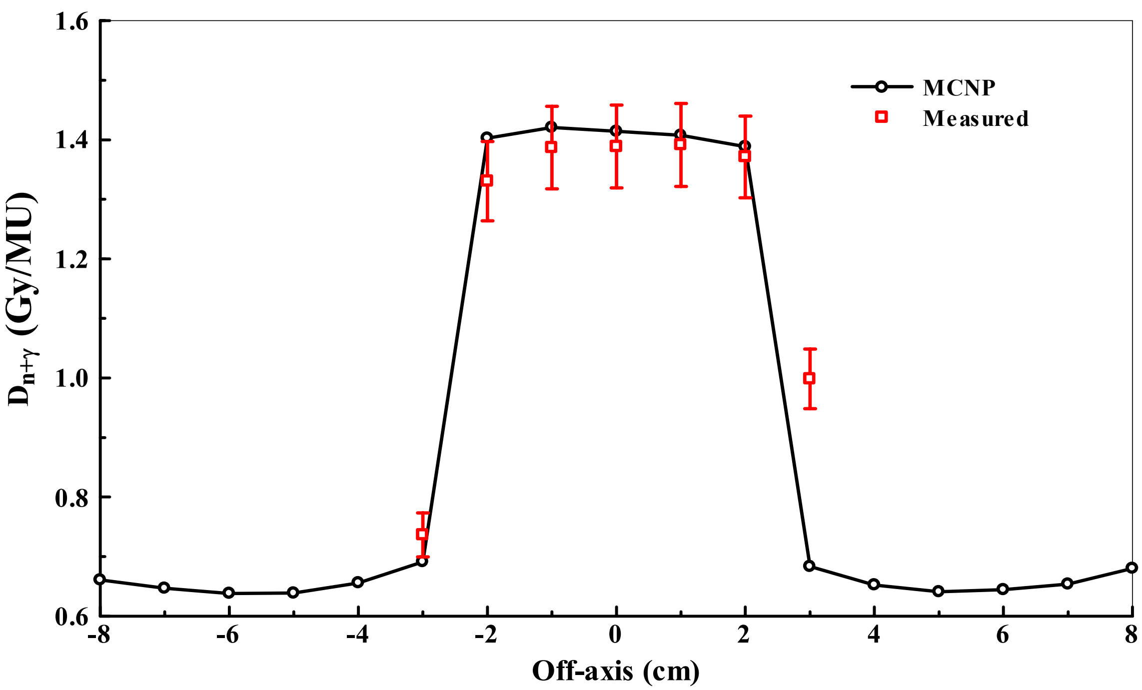

Figure 52: Comparison of the off-axis total dose rate profiles between MCNP calculations and the experiment at 8.8-cm depth in a water-filled head phantom in the simplified BNCEFNT assembly with no-filter. The error bars of the measured data do not include the 9% error from the Bragg-Gray equation. The 15% normalization error in the MCNP results is not plotted.

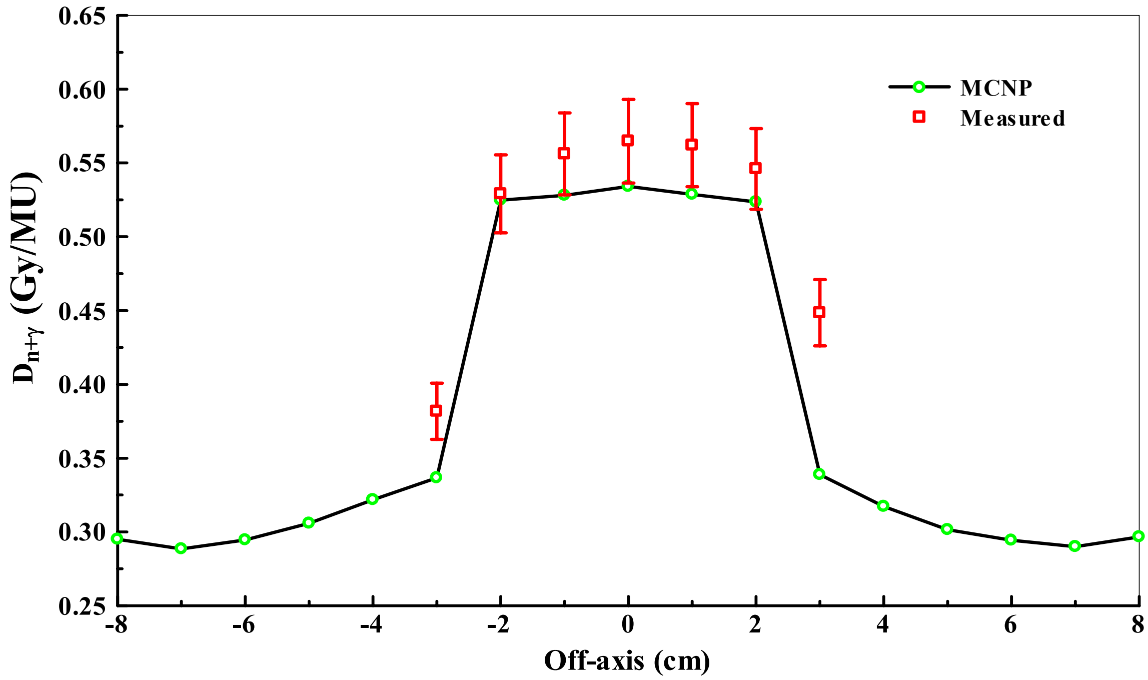

Figure 53: Comparison of the off-axis total dose rate profiles between MCNP calculations and the experiment at 8.8-cm depth in a water-filled head phantom in the simplified BNCEFNT assembly with 5.0-cm tungsten filter. The error bars of the measured data do not include the 9% error from the Bragg-Gray equation. The 15% normalization error in the MCNP results is not plotted.

5.4 Dose Enhancement Calculation in a Hypothetic Tumor

In the previous sections, all the boron percent dose enhancement (PDE) depth distribution were computed based on the assumption that the 100-ppm ^{10}B concentration were uniformly distributed in the water-filled head phantom. This assumption is useful in the characterization of the designed BNCEFNT assembly, but not suitable for determining the PDE at a tumor site.

A hypothetic tumor with a size of 4 x 4 x 2 cm^3 is placed in the water-filled head phantom model at 4.0-cm depth from the back. A BNCEFNT assembly with a 5 x 5 cm^2 tungsten collimator was used and the axis of the collimator coincides with the center of the tumor. 100-ppm of ^{10}B was uniformly distributed in the tumor and a 30 ppm ^{10}B concentration in the rest of the head. The isodose curve in the head was calculated for no-filter and 5.0-cm tungsten filter. Figure 54 shows the relative dose due to boron neutron capture reactions in the water filled head phantom inserted in the designed BNCEFNT assembly with a 5.64-cm diameter tungsten collimator and no filter. The relative boron dose curve for a 5.0-cm tungsten filter looks the same and is not shown here.

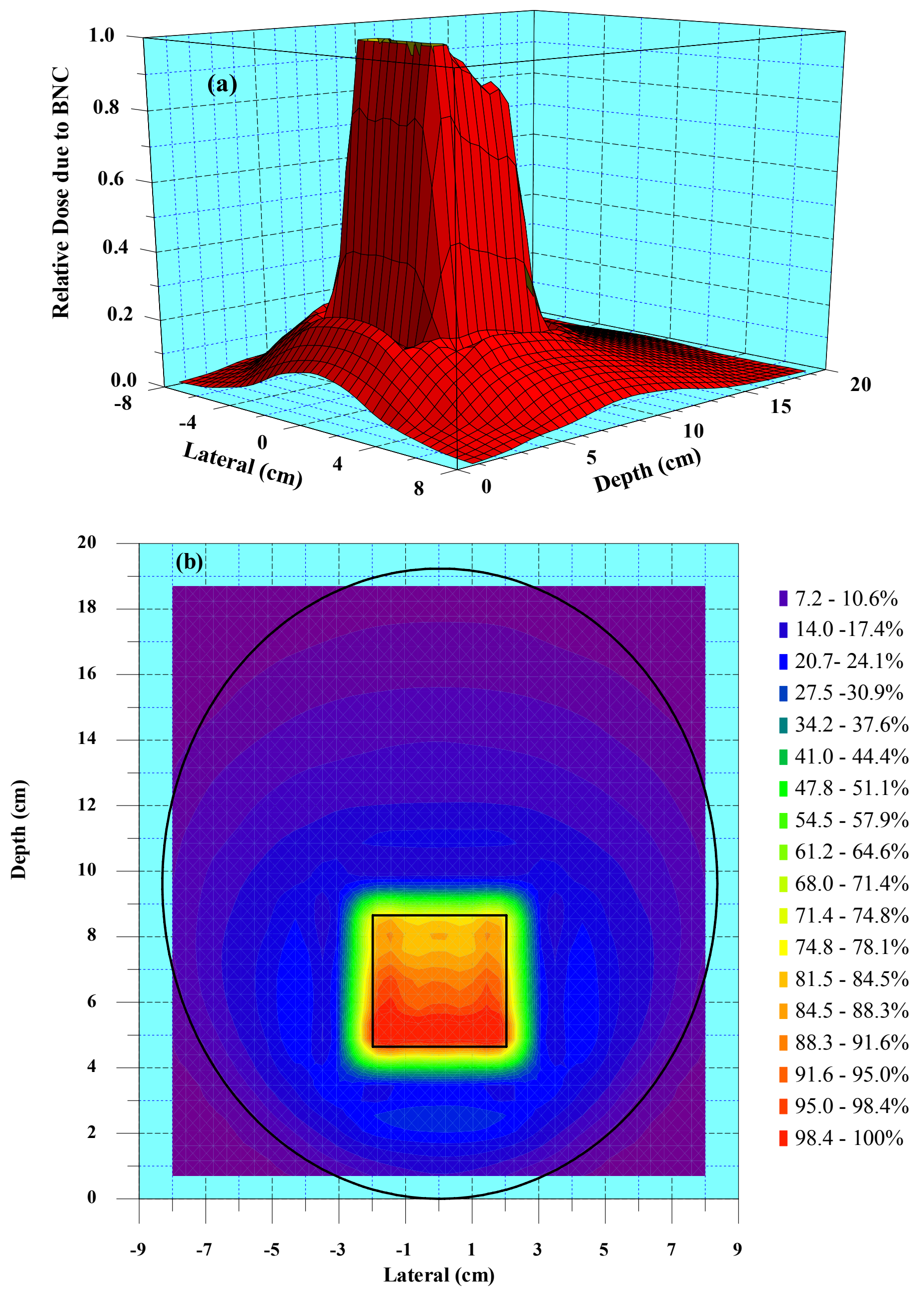

Figure 54: Relative dose due to boron neutron capture reaction in a water-filled head phantom inserted in the BNCEFNT assembly with 5x5 cm^2 tungsten collimator and no filter. The tumor size is 4x4x2 cm^3 (the black square in (b)) and has ^{10}B concentration of 100 ppm, the rest of the head has 30-ppm ^{10}B. (a) 3-D plot, (b) isodose plot.

The calculated isodose curves due to (n + γ), and due to (n + γ + BNC) in a water-filled head phantom for the BNCEFNT assembly of 5.64-cm diameter tungsten collimator and no filter are shown in Figure 55 (a) and (b), respectively. The calculated isodose curves due to (n + γ) and due to (n + γ + BNC) in a water-filled head phantom for the BNCEFNT assembly of 5.64-cm diameter tungsten collimator and 5.0-cm tungsten filter are shown in Figure 56 (a) and (b), respectively. From Figure 55 and Figure 56 it is very obvious that boron neutron capture enhanced the tumor total dose significantly. However, comparisons of Figure 55 (a) and Figure 56 (a), and of Figure 55 (b) and Figure 56 (b) indicate that the increase of tungsten filter thickness deteriorates the collimation effects, reduces the penetrating ability of the beam, and also decreases the tumor dose. In these calculations relative biological effectiveness (RBE) of boron neutron capture, fast neutrons and photons are not considered.

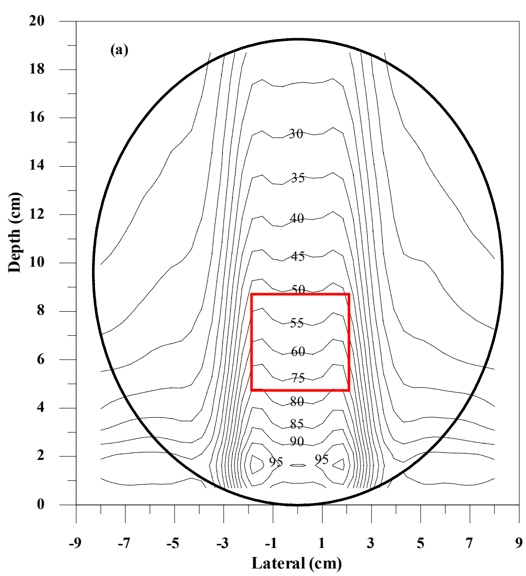

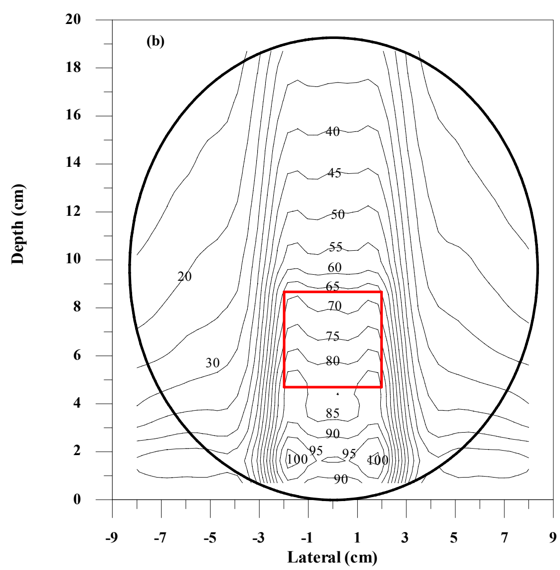

Figure 55: Calculated isodose curves for (a) (n + γ) and (b) (n + γ + BNC) in a water-filled head phantom for a BNCEFNT assembly with 5.64-cm diameter tungsten collimator and no filter. The red square is the tumor (4x4x2 cm^3) with 100-ppm ^{10}B, the rest is with 30-ppm ^{10}B. (Curves outside the head should be ignored)

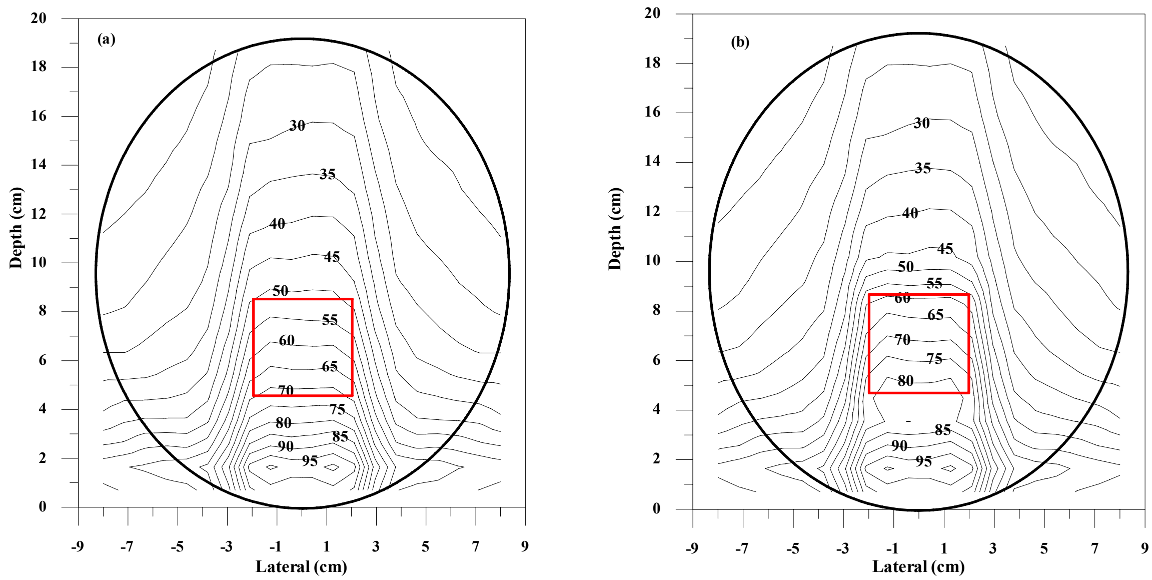

Figure 56: Calculated isodose curves for (a) (n + γ) and (b) (n + γ + BNC) in a water-filled head phantom for a BNCEFNT assembly with 5.64-cm diameter tungsten collimator and 5.0-cm tungsten filter. The red square is the tumor (4x4x2 cm^3) with 100-ppm ^{10}B, the rest is with 30-ppm ^{10}B. (Curves outside the head should be ignored)

Percent dose enhancements (PDE) calculated for the no-filter and 5.0-cm tungsten filter BNCEFNT assembly with 5.64-cm diameter tungsten collimator are shown in Figure 57 and Figure 58, respectively. As calculated in the previous sections, the tumor PDE with the 5.0-cm tungsten filter is much higher than the tumor PDE with no-filter. The PDE and absolute dose due to boron neutron capture reaction trend differently with tungsten filter thickness. An increase in the filter thickness will result in an increase of PDE but a decrease of the absolute boron capture dose. So the thickness of tungsten filter should be optimized based on the requirement of PDE and absolute boron capture dose enhancement.

The 100-ppm ^{10}B concentration in tumor is not attainable using the currently available boron delivery agent. However, if we use boronophenylalanine fructose (BPA-f) as the boron delivery agent, a ^{10}B concentration in blood of approximately 15 ppm within 0.5 to 1.5 h after infusion can be realized using the infusion schedule currently employed for BNCT treatments at the Massachusetts Institute of Technology, Cambridge, MA [28]. The boron concentration in the bloodstream is generally used as a surrogate for the concentration in normal healthy tissue since this quantity is difficult to measure. According to the observations by Coderre et al. [26-27], a tumor-to-blood uptake ratio of approximately 3.5-4 to 1 has been attained 0.5-1.5 h after infusion. So it is practical to assume ^{10}B concentration of 15 and 55 ppm for blood (normal brain tissue) and tumor, respectively. Based on this assumption and the tumor size and location described previously, the absorbed dose rate and PDE-depth distributions were calculated for the head phantom in a BNCEFNT assembly with a 5.64-cm diameter collimator and 7.5-cm tungsten filter and are shown in Figure 59. The minimum tungsten filter thickness required to attain a PDE of 15% was calculated to be 7.5 cm.

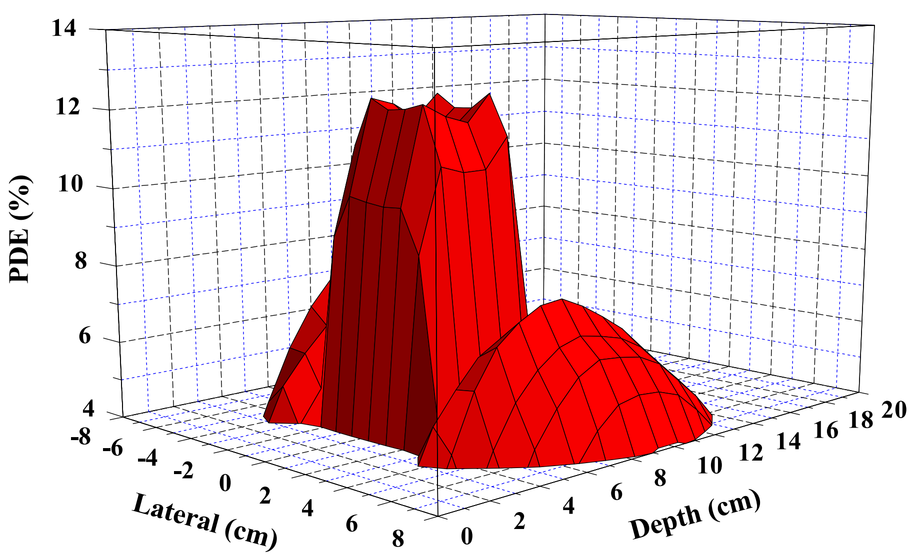

Figure 57: PDE for the water-filled head phantom inserted in the BNCEFNT assembly with 5.65-cm diameter tungsten collimator and no-filter. Tumor (4x4x2 cm^3) is located between depth 4.7 and 8.7 cm and centered in the collimator. Tumor has 100-ppm ^{10}B the rest of the head has 30-ppm ^{10}B.

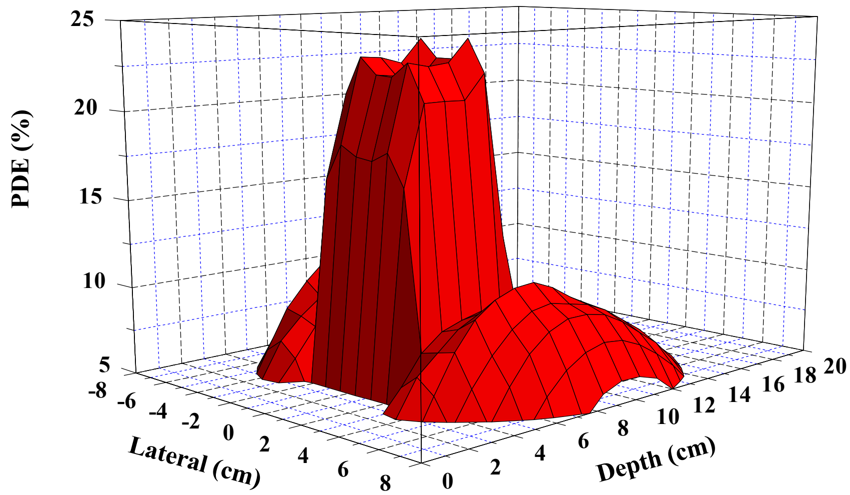

Figure 58: PDE for the water-filled head phantom inserted in the BNCEFNT assembly with 5.65-cm diameter tungsten collimator and 5.0-cm tungsten filter. Tumor (4x4x2 cm^3) is located between depth 4.7 and 8.7 cm and centered in the collimator. Tumor has 100-ppm ^{10}B the rest of the head has 30-ppm ^{10}B.

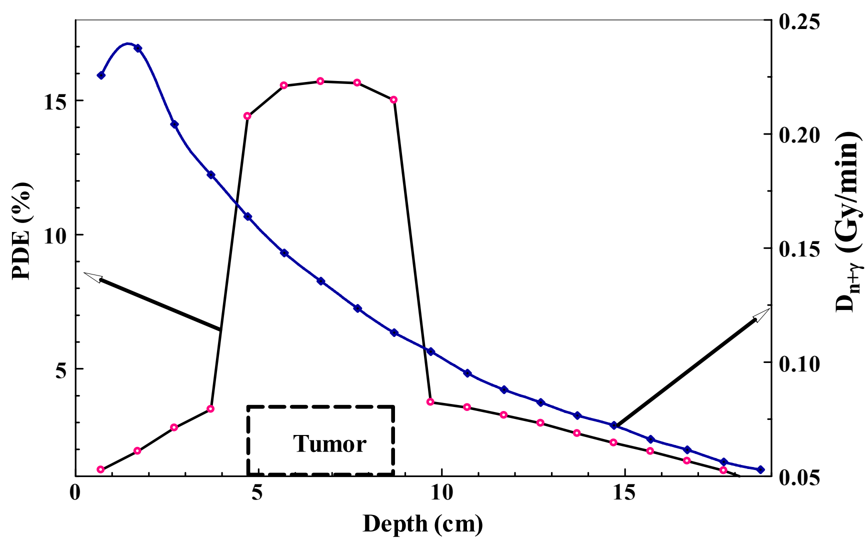

Figure 59: Absorbed dose rate and PDE-depth distribution in the head phantom in a BNCEFNT assembly with a 5.64-cm diameter collimator and a 7.5-cm tungsten filter. The tumor location is shown as the dashed box.

5.5 Discussion

The kerma-depth distribution in a water-filled head phantom in the BNCEFNT assembly calculated using MCNP5 code can result in misinterpretation of the dose enhancement effect of the assembly. Figure 60 is a re-plot of no-filter and 5.0-cm curves from Figures 21(a), which are normalized at 4.7-cm depth. The decrease of the kerma with the increase of depth is much faster for 5-cm tungsten filter than for no-filter. If a tumor is located at 4.7-cm depth, the tumor will receive much less kerma using 5.0-cm tungsten filter than kerma using no-filter.

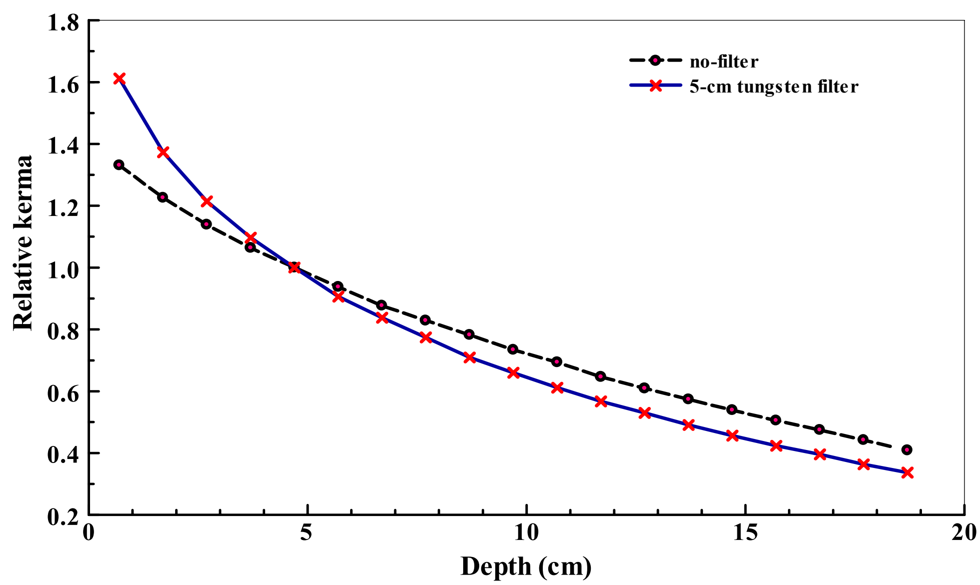

Figure 60: Relative kerma (n +γ) distributions in a water-filled head phantom in the BNCEFNT assembly with 5.64-cm diameter collimator for no-filter and 5.0-cm tungsten filter.

Fortunately, the decrease of the absorbed dose with the increase of depth in the head phantom is much slower than that of the kerma. The measured absorbed dose at shallow depth in the water-filled head phantom is much smaller than the kerma calculated using MCNP5 code, as shown in Figures 36 to 41. The relative measured absorbed dose distributions in the water-filled head phantom in the simplified BNCEFNT assembly for no-filter and 5-cm tungsten filter are shown in Figure 61. It is assumed that a tumor is located at depth ranging from 3 to 7 cm, and ^{10}B concentration is 100 ppm in tumor and 30 ppm in normal tissue. The relative (n + γ + ^{10}B capture) dose depth distributions for no-filter and 5.0-cm tungsten filter are shown in Figure 62. It is obvious that the dose enhancement effect for the 5.0-cm tungsten filter is better than that of no-filter. From the calculations and measurements, it is concluded that the BNCEFNT assembly works better for shallow (5 cm and less) tumors than deep-seated (greater than 7 cm) tumors in the tumor dose enhancement.

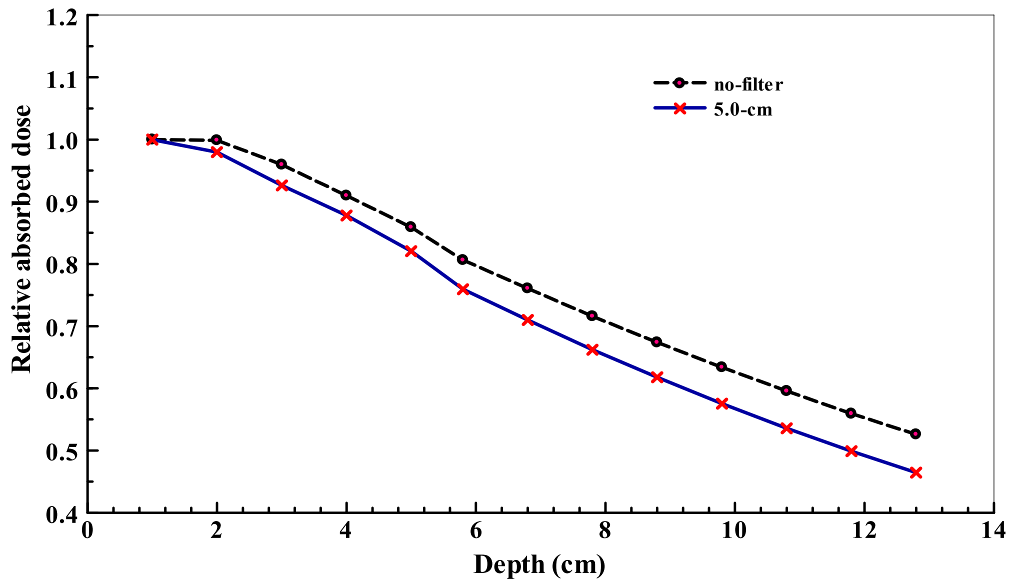

Figure 61: Relative measured absorbed dose (n +γ) distributions in the water-filled head phantom using the simplified BNCEFNT assembly for no-filter and 5.0-cm filter.

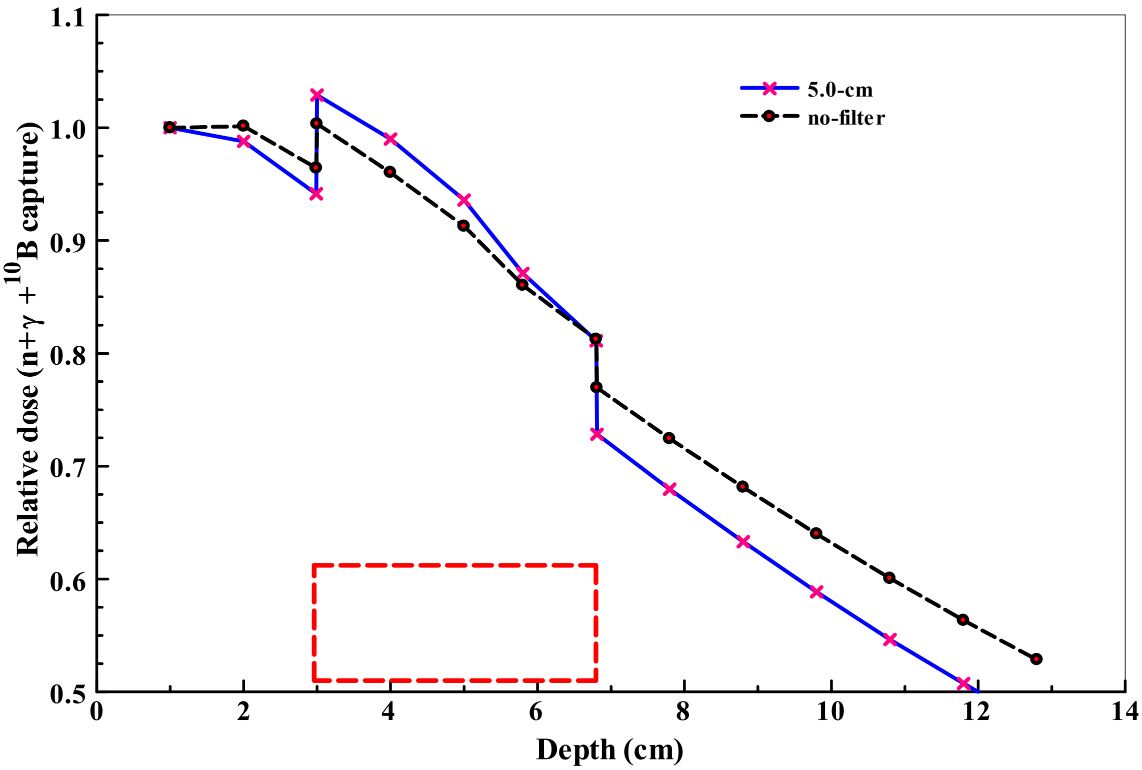

Figure 62: Demonstration of dose enhancement in tumor for the simplified BNCEFNT assembly with no-filter and 5.0-cm tungsten filter. The red box represents the tumor. ^{10}B concentration is 100 ppm in tumor and 30 ppm in normal tissue.

CHAPTER 6

EVALUATION OF THE ABSORBED DOSES IN OTHER ORGANS

In an effort to evaluate the absorbed dose in other organs for using BNCEFNT to treat brain tumors, two anthropomorphic phantoms of man and woman were created using the software package, BodyBuilder [72]. The models developed in this program are based on the Medical Internal Radiation Dose (MIRD) reports and are generated in an MCNP geometry format [73]. The phantom head is inserted into the designed reflective BNCEFNT assembly (Figure 30) as shown in Figure 63. Chair and tables or other supporting tools were not modeled.

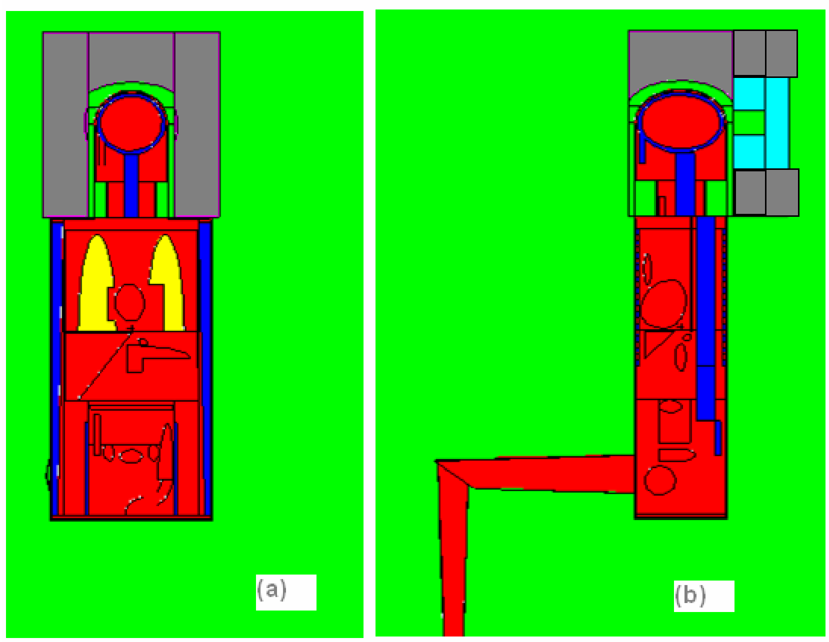

Figure 63: Cross-sectional view (a) from front and (b) from side, of an anthropomorphic phantom in a sitting posture with its head in the BNCEFNT reflective assembly for the computation of organ doses.

The doses in organs were calculated for two situations for male and female phantoms: (a) with the heads in the reflective BNCEFNT assembly of 5.64-cm diameter tungsten collimator and 5.0-cm tungsten filter in a 20 x 20 cm^2 beam field, and (b) with the above reflective BNCEFNT assembly removed from the heads in a 10 x 10 cm^2 standard treatment beam. The dose in each organ is shown in Table 6.

The average doses to the entire brain were normalized to 1000 cGy. The doses to all other organs were increased significantly due to the use of the reflective BNCEFNT assembly. The impact of the increased dose in other organs to the patient's health needs to be evaluated.

Table 6: Doses in other organs relative to brain dose.

	Total dose (cGy)					
	male phantom			female phantom		
organ	M+C+F5.0 [a]	air [b]	Ratio	M+C+F5.0	air	Ratio
head skin	843	271	3.1	860	302	2.8
neck skin	189	11.8	16.1	217	7.98	27.3
lower spine	1.97	0.06	32.8	2.91	0.07	41.6
middle spine	27.1	1.39	19.5	34.3	0.70	49.0
upper spine	266	80.5	3.3	280	21.3	13.2
skull	613	543	1.1	620	438	1.4
brain	1000	1000	1.0	1000	1000	1.0
bladder	2.46	0.11	22.4	3.60	0.12	30.0
stomach	3.28	0.15	21.9	4.80	0.17	28.2
small intestine	1.19	0.05	23.8	1.87	0.06	31.2
heart	9.51	0.55	17.3	12.9	0.45	28.6
kidney	3.13	0.1	31.3	4.64	0.12	38.7
liver	4.23	0.2	21.2	5.97	0.22	27.1
lung	19.2	1.22	15.7	23.7	0.82	28.9
pancreas	3.88	0.19	20.4	5.78	0.19	30.4
spleen	4.49	0.2	22.5	6.22	0.23	27.0
thyroid	95.5	9.81	9.7	109	6.80	16.0
testicles	1.13	0.07	16.1			
Uterus				1.13	0.04	28.3
breast				15.5	0.80	19.4

a. 20 x 20 cm^2 beam field + optimized 5.64-cm diameter BNCEFNT assembly with 5.0-cm filter
b. 10 x 10 cm^2 standard treatment beam

CHAPTER 7

RADIOACTIVITY GENERATED IN THE BNCEFNT ASSEMBLY AND THEIR DOSE CALCULATIONS

Radioactivity will be produced when material is irradiated in the neutron field. After the BNCEFNT assembly is used to treat a patient or phantom in the Fermilab Fast Neutron Therapy facility, a variety of radioisotopes will be produced. The photons emitted from these activation products will dose the patient and the medical personnel. While the dose to the patient is secondary importance compared to the dose from the neutron beam, this dose to the medical staff may be the major source of their dose. Therefore, it should be evaluated for radiation protection purposes. Procedures should be developed according to these dose rates.

Activities of the major activation products of tungsten and lead were calculated using MCNP5 code. Reactions such as (n, γ), (n, 2n), (n, 3n), (n, p), (n, d), (n, t), (n, n'p), (n, α) and (n, n'α) were considered if radioactive products have half-lives greater than 1 minute. The cross sections for the activation were taken from the LA150N library (with extension .24c in the material ID) if available and from ACTL [74] (material card with extension .30y) (an evaluated neutron activation cross section library from the Lawrence Livermore National Laboratory (LLNL)) if not available in the LA150N library.

After the activities of the activation products at the end of the irradiation (dose delivery) are calculated, the dose rate per unit activity of the radioisotope is computed using MCNP5 code. Since the half-lives of these radioisotopes range from minutes to years, the dose rate due to all of the activation products at different times after neutron beam delivery were calculated separately.

7.1 Calculation of the Activities of the Activation Products

7.1.1 Activities of the Activation Products in Tungsten Filter

The tungsten filter with the dimensions of 20cm x 20cm x 5 cm was used in the calculations. The 20cm x 20cm neutron beam with the spectrum determined in Chapter 4 was used in the calculations as was the simplified BNCEFNT assembly described in section 5.2. The particle weight in the SDEF card is set to 400 (the area of the neutron field) so that the results will be normalized to unit fluence on the filter (per neutron/cm^2). The filter is divided into 5 cells, each with the dimension of 20cm x 20cm x 1cm and were tallied separately. The constant C in the FM card is the number of target atoms in 1 gram of tungsten (units of atoms-barn/g) so that the result will be the number of radionuclide generated in 1 gram of tungsten per unit fluence on the filter. C is calculated as follows,

$$C = \frac{(1g)}{\left(W_A \frac{g}{mol}\right)} \cdot q \cdot \left(6.022 \times 10^{23} \frac{atoms}{mol}\right)\left(10^{-24} \frac{cm^2}{barn}\right) \tag{7.1}$$

where W_A is the atomic weight of tungsten, W_A =183.84 g/mol, and q is the abundance of the target nucleus.

The dose rate due to 16 radioisotopes produced in the tungsten filter were calculated and their resulting concentrations in nuclei per gram of tungsten per unit neutron fluence (neutron/cm^2) are displayed in Table 7. Assuming the proton current is 1.5x10^{14} protons/s, and the total mass of tungsten filter is 3.86x10^4 grams, the total activities (Bq) of the activation products at the end of 12, 20 and 100-minute irradiations were calculated and are displayed in Table 8.

Table 7: Number of nuclei of the activation products generated in 1 gram of tungsten per unit neutron fluence

Isotope	$T_{1/2}$	reactions	Layer 1	Layer 2	Layer 3	Layer 4	Layer 5	total
^{178}W	21.6 d	^{180}W(n,3n)	2.26^{-6} *	2.01^{-6}	1.76^{-6}	1.54^{-6}	1.33^{-6}	8.89^{-6}
^{179}W	37.05 m	^{180}W(n,2n)	2.97^{-6}	2.69^{-6}	2.38^{-6}	2.09^{-6}	1.81^{-6}	11.9^{-6}
^{181}W	121.2 d	^{180}W(n,γ) ^{182}W(n,2n) ^{183}W(n,3n)	3.10^{-4}	2.86^{-4}	2.56^{-4}	2.26^{-4}	1.97^{-4}	12.8^{-4}
^{185}W	75.1 d	^{184}W(n,γ) ^{186}W(n,2n)	4.17^{-4}	4.36^{-4}	4.29^{-4}	4.07^{-4}	3.84^{-4}	20.7^{-4}
^{187}W	23.72 h	^{186}W(n,γ)	4.43^{-4}	3.33^{-4}	2.97^{-4}	3.08^{-4}	4.58^{-4}	18.4^{-4}
^{179}Ta	1.82 y	^{180}W(n,n'p) ^{180}W(n,d)	7.92^{-9}	7.05^{-9}	6.18^{-9}	5.38^{-9}	4.65^{-9}	31.2^{-9}
^{180}Ta	8.152 h	^{180}W(n,p)	8.16^{-9}	7.36^{-9}	6.51^{-9}	5.69^{-9}	4.93^{-9}	32.7^{-9}
^{182}Ta	114.43 d	^{182}W(n,p) ^{183}W(n,n'p) ^{183}W(n,d)	1.57^{-6}	1.42^{-6}	1.26^{-6}	1.10^{-6}	0.944^{-6}	6.29^{-6}
^{183}Ta	5.1 d	^{183}W(n,p) ^{184}W(n,n'p) ^{184}W(n,d)	8.35^{-7}	7.50^{-7}	6.61^{-7}	5.75^{-7}	4.95^{-7}	33.2^{-7}
^{184}Ta	8.7 h	^{184}W(n,p)	10.0^{-7}	9.09^{-7}	8.05^{-7}	7.02^{-7}	6.06^{-7}	40.3^{-7}
^{185}Ta	49.4 m	^{186}W(n,d) ^{186}W(n,n'p)	5.55^{-7}	4.99^{-7}	4.39^{-7}	3.82^{-7}	3.29^{-7}	22.0^{-7}
^{186}Ta	10.5 m	^{186}W(n,p)						
^{179m}Hf	25.05 d	^{183}W(n,n'α)	2.75^{-8}	2.46^{-8}	2.16^{-8}	1.89^{-8}	1.63^{-8}	10.9^{-8}
^{181}Hf	42.39 d	^{184}W(n,α)	5.00^{-7}	4.52^{-7}	3.99^{-7}	3.48^{-7}	3.00^{-7}	20.0^{-7}
^{182m}Hf	61.5 m	^{186}W(n,n'α)	4.95^{-8}	4.41^{-8}	3.88^{-8}	3.37^{-8}	2.92^{-8}	19.5^{-8}
^{183}Hf	1.067 h	^{186}W(n,α)	2.66^{-7}	2.41^{-7}	2.13^{-7}	1.85^{-7}	1.60^{-7}	10.6^{-7}

* 2.26^{-6} stands for 2.26×10^{-6}

The total number of absorptions, (n, 2n) and (n, 3n) reactions in each 1-cm thickness 20x20 cm^2 tungsten filter per unit fluence of the 20x20 cm^2 neutron beam were also calculated and are shown in Figure 64. It is understandable that the (n, 2n) and (n, 3n) interactions decrease as neutrons penetrate deeper into the tungsten filter since they lose energy. For the absorption reactions, the interactions decrease slightly in the first 3 cm and then start to increase as neutrons go through more tungsten. This is because the low-energy neutrons accumulate deeper into the tungsten filter and the neutron capture reactions start to dominate in the absorption. The total number of absorptions, (n, 2n) and (n, 3n) reactions in the 5-cm thick tungsten filter per unit fluence are computed as 46.4, 31.6 and 8.32 reactions per n/cm^2, respectively. So on average, there are more neutrons produced than lost in the tungsten filter of 5-cm thickness. A neutron multiplication of 1.39 was obtained for 5-cm tungsten filter in the simplified BNCEFNT assembly.

Table 8: Total activities (Bq) produced in 5-cm tungsten filter for 12, 20 and 100 minutes

Isotope	Total Activity (Bq) for the irradiation time of		
	12 min	20 min	100 min
^{178}W	2.24E+03	3.73E+03	1.86E+04
^{179}W	2.26E+06	3.51E+06	9.51E+06
^{181}W	5.98E+04	9.97E+04	4.99E+05
^{185}W	1.50E+05	2.50E+05	1.25E+06
^{187}W	1.01E+07	1.68E+07	8.22E+07
^{179}Ta	2.55E-01	4.25E-01	2.13E+00
^{180}Ta	5.19E+02	8.59E+02	4.06E+03
^{182}Ta	2.99E+02	4.98E+02	2.49E+03
^{183}Ta	5.78E+03	9.62E+03	4.79E+04
^{184}Ta	5.99E+04	9.94E+04	4.71E+05
^{185}Ta	3.22E+05	5.08E+05	1.57E+06
^{186}Ta	2.07E+06	2.78E+06	3.79E+06
^{179m}Hf	2.36E+01	3.94E+01	1.97E+02
^{181}Hf	2.57E+02	4.28E+02	2.14E+03
^{182m}Hf	2.33E+04	3.71E+04	1.24E+05
^{183}Hf	1.22E+05	1.95E+05	6.63E+05

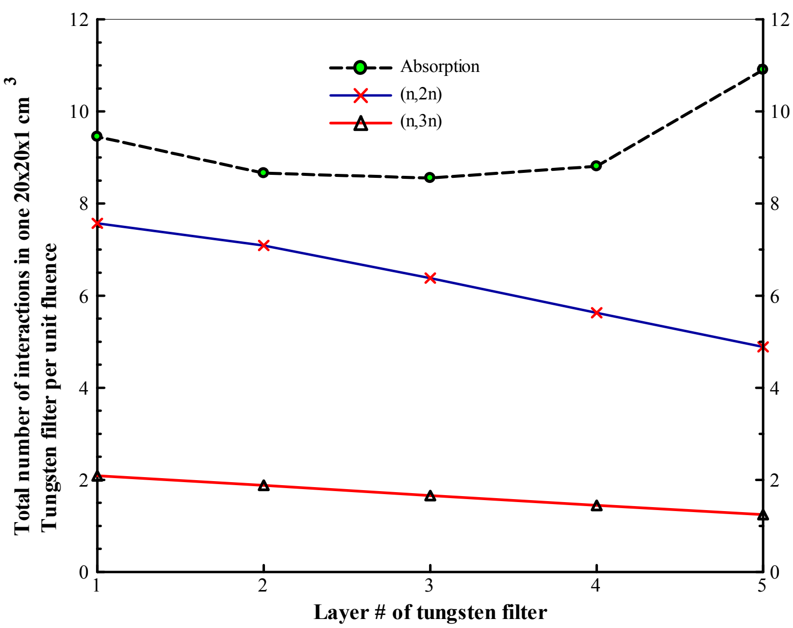

Figure 64: Number of absorption, (n, 2n) and (n, 3n) interactions in each 20x20x1 cm^3 tungsten filter per unit fluence in a 20x20 cm^2 standard neutron therapy beam. Layer #1 is at the upstream end of the beam.

7.1.2 Activities of the Activation Products in Lead Collimator

The lead collimator has an outer dimension of 20x20x10 cm^3 and an inner dimension of 5x5x10 cm^3. It was divided into 5 layers along the neutron beam direction. The activities of the activation products in lead were calculated following the same method as for tungsten. A total of 11 radioisotopes from activation products in the lead were calculated, and are listed in Table 9.

Table 9: Total activities (Bq) produced in the lead collimator for 21, 20 and 100 minute irradiation

radioisotope	T1/2	Total activities (Bq) produce in lead collimator		
		12-min	20-min	100-min
Pb-202	52.5e3 y	1.50E-02	2.50E-02	1.25E-01
Pb-203	51.873 h	1.36E+05	2.26E+05	1.12E+06
Pb-204m	67.2 m	6.71E+05	1.07E+06	3.71E+06
Pb-209	3.253 h	5.76E+05	9.46E+05	4.12E+06
Tl-202	12.23 d	7.67E-01	1.28E+00	6.38E+00
Tl204	3.78 y	1.82E+00	3.03E+00	1.51E+01
Tl-206	4.2 m	1.98E+06	2.21E+06	2.29E+06
Tl-207	4.77 m	9.78E+06	1.12E+07	1.19E+07
Tl-208	3.053 m	6.35E+06	6.72E+06	6.79E+06
Hg-203	46.612 d	4.38E+02	7.30E+02	3.65E+03
Hg-205	5.2 m	9.85E+05	1.15E+06	1.23E+06

7.2 Calculation of the dose rate for unit activity of the Activation Products

The dose rate at 50 cm from the BNCEFNT assembly on the side, back and front was calculated using the MCNP5 code. Dose rates due to beta particles was not considered because dose due to beta particle is not significant to the medical personnel compared with the gamma dose. The gamma energies and emission probabilities were taken from decay data of Rad Toolbox [75], which is based on ICRP-38 decay data [76]. For radionuclides produced in tungsten filter, the photon source was distributed in the five 1-cm layer tungsten plate as per section 7.1.1. A uniform distribution in each plate was assumed. For radioisotopes produced in the lead collimator, the same method is applied for each 2-cm thick lead layer. The Photon fluence rates at each location of interest per disintegration of each radionuclide were calculated and dose rates were computed using different photon flux-to-dose rate conversion factors. Photon flux-to-dose conversion factors as given in the ANSI/ANS-6.1.1 [77] and ICRP-21 reports [78] have been widely used in the past. These coefficients yield results in biological dose equivalent in rem, or they can be converted to physical dose in rad easily because the quality factor for photon is considered to be 1. These factors are used to convert MCNP calculated photon flux to rad-in-tissue. To determine the rad-in-air dose value from photon flux, the kerma factors for air are to be used. This is normally done using F6 tally or ICRP 74 [79] kerma factors for air. The differences in calculated dose rate resulted from using different conversion factors has been studied [80].

In the MCNP calculation for this work, photon flux-to-dose rate conversion factors of ANSI/ANS-C6.1.1(1977), ICRP-21(1971) and ANSI/ANS-C6.1.1(1991) were used to calculate dose rate-in-tissue per decay and ICRP-74(1996) conversion factors and the F6 tally were used to calculate dose rate-in-air per decay of the interested radionuclide. To convert the result of MCNP F6 tally (MeV/g per disintegration) to rad/h per Bq, one needs to multiply it by a constant, C. The constant can be calculated by

$$\boldsymbol{C} = 1\left(\frac{\boldsymbol{MeV/g}}{\boldsymbol{decay}}\right)\cdot\left(\frac{1.602\times10^{-8}\,(\boldsymbol{Rad})}{1(\boldsymbol{MeV/g})}\right)\left(\frac{\boldsymbol{decay/s}}{\boldsymbol{Bq}}\right)\left(\frac{3600\boldsymbol{s}}{1\boldsymbol{h}}\right) = 5.767\times10^{-5}\left(\frac{\boldsymbol{Rad/h}}{\boldsymbol{Bq}}\right) \quad (7.2)$$

The MCNP5-calculated dose rate at a distance of 50 cm from the back (upstream of neutron beam), the front (downstream of the neutron beam) and the side of the simplified BNCEFNT assembly due to 1 Bq of activation products in the 5-cm tungsten filter and in the 10-cm thick lead collimator are listed in Table 10 and Table 11, respectively.

Table 10: Calculated Dose rate by different conversion factors at 50 cm from back, front and side of the BNCEFNT assembly due to unit activity of the activation products in tungsten filter.

		rem/hr per Bq (tissue)			rad/hr per Bq (air)	
	Dose position	ANS6.1.1 (1977)	ANS6.1.1 (1991)	ICRP-21 (1971)	ICRP-74 (1996)	F6 tally
^{178}W	back	7.50E-15	3.69E-15	3.15E-15	2.99E-15	3.00E-15
	front	4.54E-18	2.06E-18	1.88E-18	1.81E-18	1.82E-18
	side	2.20E-16	8.57E-17	9.14E-17	8.92E-17	9.00E-17
^{179}W	back	2.60E-18	1.22E-18	1.07E-18	1.04E-18	1.06E-18
	front	2.24E-19	8.74E-20	9.09E-20	8.88E-20	8.94E-20
	side	9.36E-19	2.12E-19	4.04E-19	4.08E-19	4.15E-19
^{181}W	back	5.31E-18	1.85E-18	2.12E-18	2.08E-18	2.13E-18
	front	7.69E-21	4.46E-21	3.52E-21	3.27E-21	3.26E-21
	side	3.00E-18	7.87E-19	1.26E-18	1.26E-18	1.28E-18
^{185}W	back	3.14E-21	1.47E-21	1.29E-21	1.29E-21	1.26E-21
	front	1.43E-21	6.91E-22	5.99E-22	5.99E-22	5.79E-22
	side	5.98E-21	2.34E-21	2.44E-21	2.44E-21	2.41E-21
^{179}Ta	back	1.76E-14	8.43E-15	7.44E-15	7.09E-15	7.16E-15
	front	3.56E-17	1.44E-17	1.47E-17	1.43E-17	1.44E-17
	side	4.92E-16	1.88E-16	2.03E-16	1.99E-16	2.01E-16
^{180}Ta	back	5.60E-19	6.61E-19	1.54E-18	5.60E-19	6.59E-19
	front	9.01E-20	7.18E-20	1.75E-19	9.01E-20	6.80E-20
	side	3.64E-19	3.37E-19	8.26E-19	3.64E-19	3.27E-19
^{182}Ta	back	1.20E-11	9.51E-12	1.07E-11	9.68E-12	9.66E-12
	front	9.12E-14	7.27E-14	8.12E-14	7.33E-14	7.34E-14
	side	7.22E-13	5.76E-13	6.39E-13	5.77E-13	5.76E-13
^{183}Ta	back	4.23E-14	3.14E-14	3.15E-14	2.80E-14	2.81E-14
	front	1.59E-16	1.12E-16	1.12E-16	1.00E-16	1.01E-16
	side	7.95E-16	5.79E-16	5.85E-16	5.22E-16	5.15E-16
^{184}Ta	back	7.49E-12	7.49E-12	6.46E-12	5.83E-12	5.82E-12
	front	3.89E-14	3.89E-14	3.36E-14	3.03E-14	3.03E-14
	side	3.67E-13	3.67E-13	3.15E-13	2.85E-13	2.84E-13
^{185}Ta	back	2.48E-13	1.99E-13	2.11E-13	1.91E-13	1.90E-13
	front	1.26E-15	1.01E-15	1.07E-15	9.69E-16	9.68E-16
	side	1.17E-14	9.39E-15	9.91E-15	8.96E-15	8.95E-15
^{186}Ta	back	6.19E-12	4.92E-12	5.22E-12	4.73E-12	4.72E-12
	front	2.81E-14	2.23E-14	2.40E-14	2.17E-14	2.17E-14
	side	2.75E-13	2.17E-13	2.30E-13	2.09E-13	2.08E-13
^{179m}Hf	back	8.33E-13	6.31E-13	6.31E-13	5.80E-13	5.79E-13
	front	2.62E-15	1.98E-15	1.98E-15	1.82E-15	1.82E-15
	side	2.53E-14	1.91E-14	1.91E-14	1.74E-14	1.74E-14
^{181}Hf	back	1.05E-12	8.04E-13	8.04E-13	7.47E-13	7.45E-13
	front	3.15E-15	2.42E-15	2.42E-15	2.23E-15	2.23E-15
	side	3.34E-14	2.55E-14	2.55E-14	2.35E-14	2.35E-14
^{183}Hf	back	4.42E-12	3.54E-12	3.79E-12	3.43E-12	3.42E-12
	front	2.15E-14	1.71E-14	1.85E-14	1.67E-14	1.67E-14
	side	2.14E-13	1.70E-13	1.82E-13	1.65E-13	1.64E-13

To calculate the dose rate at the end of 12, 20, and 100-minute irradiation for the 5-cm thick tungsten filter and 10-cm thick lead collimator in the BNCEFNT assembly, one multiplies the activities of the activation products in Table 8 and Table 9 with the corresponding activity-to-dose rate coefficients in Table 10 and Table 11. For example, multiplying the activities with the coefficients in column 6 of Table 10 and Table 11, one can obtain the air kerma rates (rad/h) at the end of irradiation from all the activation products listed in the above tables, which are listed in Table 12.

Table 11: Calculated Dose rate by different conversion factors at 50 cm from back, front and side of the BNCEFNT assembly due to unit activity of the activation products in lead collimator.

		rem/hr per Bq (tissue)			rad/hr per Bq (air)	
	Dose position	ANS6.1.1 (1977)	ANS6.1.1 (1991)	ICRP-21 (1971)	ICRP-74 (1996)	F6 tally
^{203}Pb	back	4.94E-15	8.87E-15	5.57E-14	5.02E-14	5.03E-14
	front	7.11E-15	6.73E-15	6.42E-14	5.76E-14	5.76E-14
	side	6.17E-15	7.76E-15	7.31E-14	6.62E-14	6.61E-14
^{204m}Pb	back	3.42E-12	2.70E-12	2.81E-12	2.54E-12	2.53E-12
	front	4.12E-12	3.31E-12	3.47E-12	3.13E-12	3.13E-12
	side	4.42E-12	3.50E-12	3.64E-12	3.29E-12	3.28E-12
^{206}Tl	back	7.84E-17	6.05E-17	1.39E-12	5.62E-17	5.61E-17
	front	9.18E-17	7.22E-17	1.85E-12	6.76E-17	6.75E-17
	side	1.00E-16	7.73E-17	1.84E-12	7.21E-17	7.19E-17
^{207}Tl	back	4.04E-15	3.21E-15	3.34E-15	3.02E-15	3.01E-15
	front	4.76E-15	3.84E-15	4.03E-15	3.64E-15	3.64E-15
	side	5.17E-15	4.11E-15	4.28E-15	3.87E-15	3.86E-15
^{208}Tl	back	7.92E-12	6.53E-12	7.10E-12	6.40E-12	6.28E-12
	front	9.89E-12	8.23E-12	8.99E-12	8.09E-12	7.95E-12
	side	1.01E-11	8.35E-12	9.07E-12	8.17E-12	8.03E-12
^{203}Hg	back	7.04E-14	4.86E-14	4.53E-14	4.09E-14	4.10E-14
	front	7.47E-14	5.33E-14	5.05E-14	4.54E-14	4.54E-14
	side	8.74E-14	6.01E-14	5.59E-14	5.05E-14	5.05E-14
^{205}Hg	back	1.30E-15	9.19E-16	9.17E-16	8.31E-16	8.29E-16
	front	1.56E-15	1.15E-15	1.16E-15	1.05E-15	1.05E-15
	side	1.80E-15	1.24E-15	1.24E-15	1.12E-15	1.12E-15

The major contributors to the air kerma rate in Table 12 are ^{187}W, ^{186}Ta, and ^{208}Tl, which account for more than 95% of the calculated air kerma. From Table 12, one can see that the air kerma rate due to these known activation products is not significantly high. However, the dose rate due to activation of unknown impurities in graphite, lead and tungsten may predominate. One should measure the actual dose rate in the treatment room using a dosimeter for radiation protection purpose.

Table 12: Total photon air kerma rate (Rad/h) due to activation products in the tungsten filter and lead collimator at the end of 12, 20, and 100-minute irradiation

Dose position	Air Kerma (rad/h) at the end of irradiation		
	12-min	20-min	100-min
back	9.56E-05	1.28E-04	3.55E-04
front	5.38E-05	5.83E-05	6.87E-05
side	5.70E-05	6.30E-05	8.44E-05

CHAPTER 8

CONCLUSIONS AND FUTURE WORK

8.1 Conclusions

A reflective boron neutron capture enhanced fast neutron therapy (BNCEFNT) assembly has been designed for the Fermilab Neutron Therapy Facility. This assembly consists of a tungsten collimator of 20-cm outer diameter, 5.64-cm inner diameter and 10-cm thickness, a tungsten filter of 20x20 cm^2 area and various thicknesses, and a 10-cm thick graphite reflector around the patient's head. It is designed for a 20x20 cm^2 standard treatment beam. The MCNP5 calculated boron dose enhancement of the assembly at 5.7-cm depth in a water-filled head phantom was 21.9% and 29.8% per 100-ppm ^{10}B for 5.0-cm and 8.5-cm thick tungsten filter, respectively. The corresponding dose rate for the 5.0-cm and 8.5-cm thick filters were 0.22 and 0.13 Gy/min, respectively..

The design was validated with a simplified BNCEFNT assembly that was built using four lead bricks to form a 5x5 cm^2 collimator, five 1.0-cm thick 20x20 cm^2 tungsten plates as filter and graphite bricks and blocks as reflector. Measurements of the dose enhancement of the simplified assembly in a water-filled head phantom were performed using a pair of tissue equivalent ion chambers. One of the ion chambers is loaded with 1000-ppm natural boron (184-ppm ^{10}B) to measure dose due to boron neutron capture. The measured dose enhancement at 5.0-cm depth in the head phantom for the 5.0-cm thick tungsten filter is (16.6 ± 1.8)%, which agrees with the MCNP simulation of the simplified BNCEFNT assembly, 16.4%. The dose rate measured using the non-borated ion chamber is (0.765 ± 0.075) Gy/MU, about 61% of the total dose rate for the standard 10x10 cm^2 treatment beam (1.255 Gy/MU at 5.0-cm depth), which also agrees with the MCNP5 simulation, 0.701 Gy/MU, within uncertainty.

The measurements of the boron dose enhancement and total dose rate using the pair of TE ion chamber have shown that the MCNP5 code is a viable tool to design the BNCEFNT assembly. The excellent agreement between the measurements and the simulation indicates that the Fermilab NTF neutron spectral fluence rate determined by foil activation is reasonably accurate. The results also demonstrated that the calibration factors for the TE ion chambers are accurate.

The increased doses to other organs due to the use of the BNCEFNT assembly were calculated using MCNP5 and a MIRD phantom. There is a significant increase of dose to other organs using the BNCEFNT assembly compared to the standard beam treatment. The impact of these dose increases in other organs need to be evaluated.

8.2 Future Work

A BNCEFNT assembly more closely resembling the optimized design should be built and experiments to measure the boron dose enhancement and total dose-depth distribution in a head phantom should be performed. Skin dose measurements should also be evaluated. The photon dose contribution to the total dose in the head phantom with the BNCEFNT assembly should be measured.

The relative biological effectiveness (RBE) of the neutron beam with the use of the BNCEFNT assembly should be evaluated. The use of the BNCEFNT assembly changes the energy spectrum of the standard therapy beam and also changes the dose profile in the head. An evaluation of the effects of the altered neutron beam to brain tissue should be performed.

The neutron capture cross section of gadolinium-157 is 2.25×10^5 barns, about 60 times larger than that of ^{10}B. Investigation of the gadolinium capture dose enhancement using the designed assembly is of interest in finding a therapeutic window of fast neutron therapy for GBM patients.

APPENDIX A

TABLES OF NTF NEUTRON SPECTRUM AND RESPONSE MATRICES

Table 13: Measured and MCNPX calculated NTF neutron spectrum at isocenter

E (MeV)	Unfolded starting with Cupps et al	Unfolded starting with MCNPX-Calculated	MCNPX Calculated
1.00E-10			
4.14E-07	4.50E+06	1.11E+05	8.58E+04
1.12E-06	3.86E+05	9.64E+03	7.22E+03
2.38E-06	3.32E+05	5.74E+03	4.26E+03
5.04E-06	3.45E+05	5.21E+03	3.84E+03
1.07E-05	3.41E+05	4.32E+03	3.14E+03
2.26E-05	3.22E+05	3.53E+03	2.56E+03
1.01E-04	5.91E+05	1.09E+04	7.76E+03
4.54E-04	5.58E+05	9.21E+03	6.55E+03
1.58E-03	4.99E+05	1.59E+04	1.12E+04
3.35E-03	3.51E+05	1.00E+04	7.04E+03
7.10E-03	4.21E+05	2.92E+04	2.04E+04
1.50E-02	5.36E+05	4.27E+04	2.99E+04
3.18E-02	7.48E+05	1.30E+05	8.98E+04
8.65E-02	1.73E+06	3.12E+05	2.13E+05
1.50E-01	1.89E+06	5.69E+05	3.83E+05
2.24E-01	1.80E+06	7.25E+05	4.82E+05
3.34E-01	3.63E+06	7.26E+05	4.81E+05
4.98E-01	4.16E+06	1.22E+06	8.08E+05
7.43E-01	5.74E+06	1.86E+06	1.22E+06
9.06E-01	2.85E+06	1.34E+06	8.83E+05
1.11E+00	1.32E+06	1.98E+06	1.33E+06
1.35E+00	1.26E+06	1.94E+06	1.30E+06
1.65E+00	1.29E+06	2.38E+06	1.62E+06
2.02E+00	1.14E+06	2.45E+06	1.67E+06
2.46E+00	8.45E+05	2.40E+06	1.67E+06
3.01E+00	8.66E+05	2.80E+06	1.97E+06
3.68E+00	8.63E+05	3.23E+06	2.36E+06
4.49E+00	1.31E+06	3.24E+06	2.37E+06
5.49E+00	1.32E+06	3.20E+06	2.43E+06
6.70E+00	1.31E+06	3.79E+06	3.01E+06
8.19E+00	2.65E+06	3.95E+06	3.23E+06
1.00E+01	3.96E+06	3.88E+06	3.31E+06
1.22E+01	3.94E+06	3.52E+06	3.04E+06
1.35E+01	2.01E+06	2.05E+06	1.76E+06
1.49E+01	1.96E+06	2.50E+06	2.10E+06
1.75E+01	6.22E+06	5.24E+06	4.28E+06
1.96E+01	4.40E+06	4.71E+06	3.75E+06
2.25E+01	5.36E+06	5.67E+06	4.51E+06
2.50E+01	4.09E+06	4.32E+06	3.46E+06
2.75E+01	4.19E+06	4.21E+06	3.38E+06
3.00E+01	4.05E+06	3.99E+06	3.21E+06
3.50E+01	7.17E+06	8.10E+06	6.51E+06
4.00E+01	6.21E+06	7.83E+06	6.31E+06
4.50E+01	5.33E+06	6.73E+06	5.43E+06
5.00E+01	2.89E+06	6.13E+06	4.94E+06
5.50E+01	2.61E+06	6.19E+06	5.00E+06
6.00E+01	2.39E+06	5.73E+06	4.63E+06
6.50E+01	2.20E+06	2.15E+06	1.74E+06
6.60E+01	4.19E+05	3.12E+04	8.16E+04
Total	1.15E+08	1.22E+08	9.52E+07

Table 14: Al-28 response matrix (Bq/g per n/cm^2)

	Moderator thickness					
E(MeV)	4.8 cm	7.2 cm	9.0 cm	10.8 cm	13.1 cm	14.5 cm
1.00E-10						
4.14E-07	7.03E-07	4.20E-07	2.53E-07	1.58E-07	1.09E-07	6.14E-08
1.12E-06	1.02E-06	5.74E-07	4.08E-07	2.42E-07	1.46E-07	1.03E-07
2.38E-06	1.09E-06	6.97E-07	4.36E-07	2.83E-07	1.54E-07	1.11E-07
5.04E-06	1.12E-06	7.04E-07	4.59E-07	3.08E-07	1.88E-07	1.30E-07
1.07E-05	1.18E-06	7.28E-07	5.16E-07	3.49E-07	2.03E-07	1.52E-07
2.26E-05	1.13E-06	8.04E-07	5.36E-07	3.68E-07	2.28E-07	1.48E-07
1.01E-04	1.06E-06	8.45E-07	6.64E-07	3.88E-07	2.46E-07	1.64E-07
4.54E-04	9.28E-07	7.96E-07	6.15E-07	3.93E-07	2.89E-07	1.86E-07
1.58E-03	8.88E-07	8.35E-07	6.31E-07	4.47E-07	2.68E-07	1.93E-07
3.35E-03	8.23E-07	8.19E-07	6.51E-07	4.72E-07	2.91E-07	2.11E-07
7.10E-03	7.83E-07	8.05E-07	6.54E-07	4.90E-07	3.06E-07	2.18E-07
1.50E-02	7.30E-07	7.87E-07	6.63E-07	4.95E-07	3.16E-07	2.33E-07
3.18E-02	6.75E-07	8.04E-07	6.88E-07	5.30E-07	3.41E-07	2.59E-07
8.65E-02	6.14E-07	7.91E-07	7.17E-07	5.82E-07	3.86E-07	2.97E-07
1.50E-01	5.40E-07	7.84E-07	7.56E-07	6.40E-07	4.56E-07	3.65E-07
2.24E-01	4.97E-07	7.77E-07	7.84E-07	7.03E-07	5.19E-07	4.10E-07
3.34E-01	4.37E-07	7.26E-07	7.97E-07	7.16E-07	5.86E-07	4.83E-07
4.98E-01	3.77E-07	6.81E-07	7.33E-07	7.20E-07	6.20E-07	5.30E-07
7.43E-01	3.17E-07	6.18E-07	7.55E-07	8.00E-07	7.38E-07	6.95E-07
9.06E-01	2.73E-07	5.61E-07	7.15E-07	7.80E-07	7.75E-07	7.55E-07
1.11E+00	2.34E-07	5.20E-07	6.28E-07	7.43E-07	7.17E-07	7.12E-07
1.35E+00	2.03E-07	4.47E-07	6.35E-07	7.27E-07	8.41E-07	8.25E-07
1.65E+00	1.88E-07	4.23E-07	5.69E-07	7.01E-07	7.87E-07	8.51E-07
2.02E+00	1.60E-07	3.72E-07	5.24E-07	6.52E-07	7.82E-07	8.37E-07
2.46E+00	1.37E-07	3.12E-07	4.75E-07	6.07E-07	7.48E-07	8.60E-07
3.01E+00	1.08E-07	2.88E-07	4.02E-07	5.79E-07	6.84E-07	7.75E-07
3.68E+00	8.76E-08	2.30E-07	3.29E-07	4.28E-07	5.66E-07	6.30E-07
4.49E+00	8.92E-08	2.02E-07	3.19E-07	4.36E-07	5.40E-07	6.63E-07
5.49E+00	7.58E-08	1.72E-07	2.80E-07	4.03E-07	4.89E-07	6.07E-07
6.70E+00	6.51E-08	1.52E-07	2.19E-07	3.15E-07	4.48E-07	5.48E-07
8.19E+00	6.12E-08	1.26E-07	1.96E-07	2.72E-07	3.82E-07	4.77E-07
1.00E+01	5.77E-08	1.06E-07	1.67E-07	2.20E-07	3.21E-07	4.20E-07
1.22E+01	5.97E-08	9.95E-08	1.49E-07	2.01E-07	2.92E-07	3.42E-07
1.35E+01	6.39E-08	9.69E-08	1.36E-07	1.90E-07	2.56E-07	3.22E-07
1.49E+01	6.90E-08	9.74E-08	1.30E-07	1.90E-07	2.18E-07	2.99E-07
1.75E+01	7.19E-08	1.04E-07	1.44E-07	1.60E-07	2.57E-07	2.85E-07
1.96E+01	6.85E-08	9.43E-08	1.36E-07	1.61E-07	2.32E-07	2.94E-07
2.25E+01	2.36E-08	5.06E-08	8.87E-08	1.25E-07	1.84E-07	2.50E-07
2.50E+01	1.32E-08	4.23E-08	6.99E-08	1.05E-07	1.66E-07	2.09E-07
2.75E+01	1.26E-08	3.47E-08	6.17E-08	9.39E-08	1.47E-07	1.94E-07
3.00E+01	1.10E-08	3.17E-08	4.95E-08	8.79E-08	1.45E-07	1.78E-07
3.50E+01	1.01E-08	2.88E-08	5.10E-08	7.61E-08	1.21E-07	1.65E-07
4.00E+01	9.27E-09	2.49E-08	4.39E-08	6.52E-08	1.08E-07	1.44E-07
4.50E+01	8.75E-09	2.61E-08	3.78E-08	6.26E-08	9.75E-08	1.40E-07
5.00E+01	7.83E-09	2.22E-08	3.76E-08	6.07E-08	9.50E-08	1.30E-07
5.50E+01	7.47E-09	1.94E-08	3.79E-08	5.47E-08	9.85E-08	1.23E-07
6.00E+01	6.82E-09	1.94E-08	3.43E-08	5.49E-08	8.74E-08	1.17E-07
6.50E+01	6.65E-09	2.00E-08	3.42E-08	5.23E-08	8.18E-08	1.11E-07
6.60E+01	7.01E-09	1.90E-08	3.13E-08	5.16E-08	8.30E-08	1.06E-07

Table 15: Mg-27 response matrix (Bq/g per n/cm^2)

	Moderator thickness					
E(MeV)	4.8 cm	7.2 cm	9.0 cm	10.8 cm	13.1 cm	14.5 cm
1.00E-10	-	-	-	-	-	-
4.14E-07	-	-	-	-	-	-
1.12E-06	-	-	-	-	-	-
2.38E-06	-	-	-	-	-	-
5.04E-06	-	-	-	-	-	-
1.07E-05	-	-	-	-	-	-
2.26E-05	-	-	-	-	-	-
1.01E-04	-	-	-	-	-	-
4.54E-04	-	-	-	-	-	-
1.58E-03	-	-	-	-	-	-
3.35E-03	-	-	-	-	-	-
7.10E-03	-	-	-	-	-	-
1.50E-02	-	-	-	-	-	-
3.18E-02	-	-	-	-	-	-
8.65E-02	-	-	-	-	-	-
1.50E-01	-	-	-	-	-	-
2.24E-01	-	-	-	-	-	-
3.34E-01	-	-	-	-	-	-
4.98E-01	-	-	-	-	-	-
7.43E-01	-	-	-	-	-	-
9.06E-01	-	-	-	-	-	-
1.11E+00	-	-	-	-	-	-
1.35E+00	-	-	-	-	-	-
1.65E+00	-	-	-	-	-	-
2.02E+00	1.43E-13	7.95E-14	5.13E-14	3.37E-14	1.92E-14	1.35E-14
2.46E+00	3.95E-11	2.40E-11	1.66E-11	1.16E-11	7.24E-12	5.49E-12
3.01E+00	3.77E-09	2.29E-09	1.57E-09	1.10E-09	6.92E-10	5.20E-10
3.68E+00	4.67E-08	2.80E-08	1.95E-08	1.39E-08	8.93E-09	6.75E-09
4.49E+00	1.01E-07	6.72E-08	5.05E-08	3.84E-08	2.70E-08	2.19E-08
5.49E+00	3.40E-07	2.50E-07	2.00E-07	1.61E-07	1.23E-07	1.04E-07
6.70E+00	7.58E-07	5.81E-07	4.76E-07	3.96E-07	3.11E-07	2.71E-07
8.19E+00	1.03E-06	7.98E-07	6.68E-07	5.67E-07	4.60E-07	4.05E-07
1.00E+01	1.42E-06	1.14E-06	9.75E-07	8.54E-07	7.12E-07	6.35E-07
1.22E+01	1.54E-06	1.26E-06	1.10E-06	9.76E-07	8.42E-07	7.61E-07
1.35E+01	1.52E-06	1.25E-06	1.10E-06	9.82E-07	8.74E-07	8.09E-07
1.49E+01	1.37E-06	1.15E-06	1.03E-06	9.32E-07	8.41E-07	7.90E-07
1.75E+01	1.08E-06	9.21E-07	8.35E-07	7.67E-07	7.06E-07	6.83E-07
1.96E+01	7.60E-07	6.62E-07	6.05E-07	5.75E-07	5.46E-07	5.32E-07
2.25E+01	1.46E-07	1.49E-07	1.60E-07	1.76E-07	2.09E-07	2.27E-07
2.50E+01	5.31E-08	6.39E-08	7.64E-08	9.53E-08	1.32E-07	1.55E-07
2.75E+01	4.88E-08	5.64E-08	6.68E-08	8.36E-08	1.19E-07	1.39E-07
3.00E+01	4.72E-08	5.29E-08	6.15E-08	7.55E-08	1.07E-07	1.29E-07
3.50E+01	4.16E-08	4.73E-08	5.41E-08	6.59E-08	9.48E-08	1.15E-07
4.00E+01	3.61E-08	4.08E-08	4.67E-08	5.56E-08	8.00E-08	9.83E-08
4.50E+01	3.23E-08	3.67E-08	4.16E-08	4.86E-08	6.85E-08	8.63E-08
5.00E+01	2.89E-08	3.20E-08	3.72E-08	4.32E-08	6.00E-08	7.37E-08
5.50E+01	2.64E-08	3.00E-08	3.38E-08	4.02E-08	5.55E-08	6.87E-08
6.00E+01	2.57E-08	2.85E-08	3.17E-08	3.73E-08	5.08E-08	6.05E-08
6.50E+01	2.24E-08	2.54E-08	2.87E-08	3.36E-08	4.61E-08	5.59E-08
6.60E+01	2.15E-08	2.39E-08	2.73E-08	3.24E-08	4.29E-08	5.31E-08

Table 16: Na-24 response matrix (Bq/g per n/cm^2)

	Moderator thickness					
E(MeV)	4.8 cm	7.2 cm	9.0 cm	10.8 cm	13.1 cm	14.5 cm
1.00E-10	-	-	-	-	-	-
4.14E-07	-	-	-	-	-	-
1.12E-06	-	-	-	-	-	-
2.38E-06	-	-	-	-	-	-
5.04E-06	-	-	-	-	-	-
1.07E-05	-	-	-	-	-	-
2.26E-05	-	-	-	-	-	-
1.01E-04	-	-	-	-	-	-
4.54E-04	-	-	-	-	-	-
1.58E-03	-	-	-	-	-	-
3.35E-03	-	-	-	-	-	-
7.10E-03	-	-	-	-	-	-
1.50E-02	-	-	-	-	-	-
3.18E-02	-	-	-	-	-	-
8.65E-02	-	-	-	-	-	-
1.50E-01	-	-	-	-	-	-
2.24E-01	-	-	-	-	-	-
3.34E-01	-	-	-	-	-	-
4.98E-01	-	-	-	-	-	-
7.43E-01	-	-	-	-	-	-
9.06E-01	-	-	-	-	-	-
1.11E+00	-	-	-	-	-	-
1.35E+00	-	-	-	-	-	-
1.65E+00	-	-	-	-	-	-
2.02E+00	-	-	-	-	-	-
2.46E+00	-	-	-	-	-	-
3.01E+00	-	-	-	-	-	-
3.68E+00	2.82E-28	1.64E-28	1.12E-28	7.66E-29	4.68E-29	3.45E-29
4.49E+00	4.67E-16	3.07E-16	2.27E-16	1.68E-16	1.07E-16	8.44E-17
5.49E+00	6.10E-12	4.43E-12	3.47E-12	2.74E-12	2.02E-12	1.69E-12
6.70E+00	4.97E-10	3.75E-10	3.04E-10	2.49E-10	1.90E-10	1.63E-10
8.19E+00	4.40E-09	3.32E-09	2.71E-09	2.24E-09	1.75E-09	1.50E-09
1.00E+01	1.26E-08	9.92E-09	8.39E-09	7.20E-09	5.85E-09	5.14E-09
1.22E+01	1.93E-08	1.56E-08	1.33E-08	1.16E-08	9.74E-09	8.64E-09
1.35E+01	2.36E-08	1.92E-08	1.67E-08	1.47E-08	1.26E-08	1.15E-08
1.49E+01	2.34E-08	1.96E-08	1.72E-08	1.54E-08	1.34E-08	1.24E-08
1.75E+01	1.85E-08	1.57E-08	1.41E-08	1.27E-08	1.14E-08	1.08E-08
1.96E+01	1.19E-08	1.04E-08	9.45E-09	8.90E-09	8.26E-09	7.93E-09
2.25E+01	1.95E-09	2.00E-09	2.14E-09	2.36E-09	2.70E-09	2.88E-09
2.50E+01	5.66E-10	7.07E-10	8.78E-10	1.13E-09	1.56E-09	1.80E-09
2.75E+01	5.05E-10	6.00E-10	7.36E-10	9.57E-10	1.37E-09	1.59E-09
3.00E+01	4.83E-10	5.58E-10	6.69E-10	8.49E-10	1.22E-09	1.46E-09
3.50E+01	4.37E-10	5.03E-10	5.84E-10	7.28E-10	1.08E-09	1.30E-09
4.00E+01	3.79E-10	4.35E-10	5.03E-10	6.09E-10	8.98E-10	1.10E-09
4.50E+01	3.44E-10	3.94E-10	4.51E-10	5.34E-10	7.70E-10	9.68E-10
5.00E+01	3.08E-10	3.45E-10	4.07E-10	4.76E-10	6.72E-10	8.26E-10
5.50E+01	2.78E-10	3.19E-10	3.64E-10	4.35E-10	6.16E-10	7.66E-10
6.00E+01	2.72E-10	3.01E-10	3.40E-10	4.01E-10	5.51E-10	6.66E-10
6.50E+01	2.31E-10	2.66E-10	3.04E-10	3.57E-10	4.99E-10	6.03E-10
6.60E+01	2.23E-10	2.49E-10	2.88E-10	3.45E-10	4.63E-10	5.85E-10

Table 17: Cu-66 response matrix (Bq/g per n/cm^2)

	Moderator thickness					
E(MeV)	4.8 cm	7.2 cm	9.0 cm	10.8 cm	13.1 cm	14.5 cm
1.00E-10						
4.14E-07	3.97E-07	2.23E-07	1.38E-07	8.83E-08	6.10E-08	3.29E-08
1.12E-06	5.53E-07	3.19E-07	2.21E-07	1.25E-07	8.05E-08	5.37E-08
2.38E-06	5.92E-07	3.74E-07	2.44E-07	1.48E-07	8.90E-08	6.17E-08
5.04E-06	6.25E-07	3.86E-07	2.58E-07	1.65E-07	1.10E-07	7.51E-08
1.07E-05	6.46E-07	4.01E-07	2.92E-07	1.90E-07	1.10E-07	8.12E-08
2.26E-05	6.21E-07	4.55E-07	2.93E-07	1.97E-07	1.27E-07	8.02E-08
1.01E-04	5.76E-07	4.33E-07	3.45E-07	2.20E-07	1.30E-07	9.16E-08
4.54E-04	5.57E-07	4.58E-07	3.43E-07	2.21E-07	1.46E-07	1.05E-07
1.58E-03	5.23E-07	4.61E-07	3.48E-07	2.43E-07	1.50E-07	1.08E-07
3.35E-03	4.94E-07	4.54E-07	3.58E-07	2.62E-07	1.62E-07	1.15E-07
7.10E-03	4.71E-07	4.47E-07	3.60E-07	2.71E-07	1.66E-07	1.20E-07
1.50E-02	4.32E-07	4.45E-07	3.63E-07	2.70E-07	1.73E-07	1.30E-07
3.18E-02	3.98E-07	4.51E-07	3.85E-07	2.88E-07	1.88E-07	1.46E-07
8.65E-02	3.72E-07	4.50E-07	4.03E-07	3.22E-07	2.14E-07	1.67E-07
1.50E-01	3.46E-07	4.52E-07	4.29E-07	3.55E-07	2.55E-07	2.01E-07
2.24E-01	3.05E-07	4.56E-07	4.48E-07	3.85E-07	2.88E-07	2.25E-07
3.34E-01	2.68E-07	4.50E-07	4.42E-07	4.03E-07	3.37E-07	2.70E-07
4.98E-01	2.39E-07	3.93E-07	4.29E-07	4.09E-07	3.50E-07	3.04E-07
7.43E-01	1.93E-07	3.65E-07	4.42E-07	4.55E-07	4.11E-07	3.86E-07
9.06E-01	1.81E-07	3.27E-07	4.02E-07	4.59E-07	4.66E-07	4.26E-07
1.11E+00	1.52E-07	2.80E-07	3.48E-07	4.14E-07	4.38E-07	4.19E-07
1.35E+00	1.33E-07	2.48E-07	3.36E-07	4.07E-07	4.73E-07	4.52E-07
1.65E+00	1.19E-07	2.56E-07	3.15E-07	3.94E-07	4.65E-07	4.61E-07
2.02E+00	1.05E-07	2.23E-07	3.09E-07	3.80E-07	4.46E-07	4.83E-07
2.46E+00	8.76E-08	1.95E-07	2.79E-07	3.55E-07	4.40E-07	4.85E-07
3.01E+00	6.43E-08	1.55E-07	2.38E-07	3.46E-07	4.02E-07	4.20E-07
3.68E+00	5.24E-08	1.41E-07	2.01E-07	2.33E-07	3.13E-07	3.81E-07
4.49E+00	5.33E-08	1.23E-07	1.73E-07	2.59E-07	3.06E-07	3.70E-07
5.49E+00	4.42E-08	9.76E-08	1.59E-07	2.09E-07	2.79E-07	3.29E-07
6.70E+00	2.51E-08	8.32E-08	1.37E-07	1.79E-07	2.22E-07	3.06E-07
8.19E+00	2.51E-08	7.07E-08	1.09E-07	1.56E-07	2.24E-07	2.80E-07
1.00E+01	2.08E-08	5.15E-08	8.15E-08	1.22E-07	1.81E-07	2.34E-07
1.22E+01	1.73E-08	4.43E-08	7.13E-08	1.10E-07	1.50E-07	1.88E-07
1.35E+01	1.58E-08	3.85E-08	5.92E-08	9.28E-08	1.28E-07	1.64E-07
1.49E+01	1.44E-08	3.69E-08	6.21E-08	8.39E-08	1.11E-07	1.52E-07
1.75E+01	1.38E-08	3.60E-08	5.72E-08	6.84E-08	1.28E-07	1.49E-07
1.96E+01	1.11E-08	3.08E-08	5.89E-08	6.89E-08	1.05E-07	1.53E-07
2.25E+01	1.07E-08	2.30E-08	4.52E-08	6.65E-08	1.05E-07	1.41E-07
2.50E+01	7.28E-09	2.21E-08	4.10E-08	6.09E-08	9.33E-08	1.15E-07
2.75E+01	7.58E-09	1.97E-08	3.70E-08	5.11E-08	8.22E-08	1.10E-07
3.00E+01	6.50E-09	1.68E-08	2.93E-08	4.71E-08	7.92E-08	9.84E-08
3.50E+01	5.36E-09	1.61E-08	2.89E-08	4.42E-08	6.92E-08	9.11E-08
4.00E+01	4.78E-09	1.30E-08	2.63E-08	3.61E-08	5.84E-08	8.84E-08
4.50E+01	5.04E-09	1.38E-08	2.19E-08	3.49E-08	5.44E-08	7.79E-08
5.00E+01	4.67E-09	1.30E-08	2.51E-08	3.25E-08	5.48E-08	7.09E-08
5.50E+01	4.19E-09	1.46E-08	1.84E-08	3.07E-08	5.27E-08	6.70E-08
6.00E+01	3.20E-09	1.10E-08	1.93E-08	2.89E-08	5.35E-08	6.81E-08
6.50E+01	3.56E-09	1.22E-08	1.75E-08	2.99E-08	4.51E-08	6.13E-08
6.60E+01	4.52E-09	1.17E-08	2.34E-08	2.93E-08	4.63E-08	5.82E-08

Table 18: Cu-62 response matrix (Bq/g per n/cm^2)

	Moderator thickness					
E(MeV)	4.8 cm	7.2 cm	9.0 cm	10.8 cm	13.1 cm	14.5 cm
1.00E-10	-	-	-	-	-	-
4.14E-07	-	-	-	-	-	-
1.12E-06	-	-	-	-	-	-
2.38E-06	-	-	-	-	-	-
5.04E-06	-	-	-	-	-	-
1.07E-05	-	-	-	-	-	-
2.26E-05	-	-	-	-	-	-
1.01E-04	-	-	-	-	-	-
4.54E-04	-	-	-	-	-	-
1.58E-03	-	-	-	-	-	-
3.35E-03	-	-	-	-	-	-
7.10E-03	-	-	-	-	-	-
1.50E-02	-	-	-	-	-	-
3.18E-02	-	-	-	-	-	-
8.65E-02	-	-	-	-	-	-
1.50E-01	-	-	-	-	-	-
2.24E-01	-	-	-	-	-	-
3.34E-01	-	-	-	-	-	-
4.98E-01	-	-	-	-	-	-
7.43E-01	-	-	-	-	-	-
9.06E-01	-	-	-	-	-	-
1.11E+00	-	-	-	-	-	-
1.35E+00	-	-	-	-	-	-
1.65E+00	-	-	-	-	-	-
2.02E+00	-	-	-	-	-	-
2.46E+00	-	-	-	-	-	-
3.01E+00	-	-	-	-	-	-
3.68E+00	-	-	-	-	-	-
4.49E+00	-	-	-	-	-	-
5.49E+00	-	-	-	-	-	-
6.70E+00	-	-	-	-	-	-
8.19E+00	-	-	-	-	-	-
1.00E+01	-	-	-	-	-	-
1.22E+01	8.61E-08	6.75E-08	5.59E-08	4.75E-08	3.80E-08	3.23E-08
1.35E+01	1.18E-06	9.42E-07	7.95E-07	6.81E-07	5.62E-07	5.04E-07
1.49E+01	2.43E-06	2.00E-06	1.72E-06	1.50E-06	1.26E-06	1.14E-06
1.75E+01	3.65E-06	3.03E-06	2.66E-06	2.35E-06	2.02E-06	1.85E-06
1.96E+01	4.31E-06	3.65E-06	3.23E-06	2.92E-06	2.56E-06	2.39E-06
2.25E+01	7.77E-07	7.35E-07	7.21E-07	7.12E-07	7.07E-07	7.02E-07
2.50E+01	6.63E-08	9.71E-08	1.28E-07	1.62E-07	2.02E-07	2.21E-07
2.75E+01	4.76E-08	6.53E-08	8.96E-08	1.22E-07	1.64E-07	1.84E-07
3.00E+01	4.48E-08	5.66E-08	7.53E-08	1.04E-07	1.43E-07	1.66E-07
3.50E+01	3.98E-08	4.77E-08	5.90E-08	8.05E-08	1.20E-07	1.43E-07
4.00E+01	3.39E-08	4.15E-08	4.96E-08	6.40E-08	9.87E-08	1.21E-07
4.50E+01	3.24E-08	3.81E-08	4.53E-08	5.57E-08	8.52E-08	1.05E-07
5.00E+01	2.99E-08	3.42E-08	4.10E-08	5.00E-08	7.42E-08	8.99E-08
5.50E+01	2.60E-08	3.01E-08	3.55E-08	4.34E-08	6.51E-08	8.21E-08
6.00E+01	2.40E-08	2.74E-08	3.26E-08	3.94E-08	5.73E-08	7.06E-08
6.50E+01	2.22E-08	2.59E-08	3.07E-08	3.62E-08	5.29E-08	6.41E-08
6.60E+01	2.14E-08	2.38E-08	2.90E-08	3.55E-08	4.92E-08	6.56E-08

APPENDIX B

MEASUREMENTS AND MCNP5 CALCULATIONS OF THE ABSORBED DOSE, BORON DOSE AND PDE

B.1 MCNP5 calculations for the optimized design of the BNCEFNT assembly: 10-cm graphite reflector, 10-cm thick tungsten collimator with 20-cm outer diameter and 5.64-cm inner diameter, 20x20 cm^2 standard therapy beam. Normalization of the MCNP results is based on a proton current of 1.7×10^{14} protons/s and 8.13×10^{-7} n/cm^2 per proton obtained in chapter 4.

Table 19: MCNP5 calculated kerma rate (neutrons and gammas) distributions in the simplified water filled head phantom for different thickness of tungsten filter

Depth	Kerma (Gy/min)								
(cm)	no -filter	0.5 cm	1.0 cm	1.5 cm	2.0 cm	2.5 cm	3.0 cm	3.5 cm	4.0 cm
0.7	0.739	0.694	0.650	0.612	0.575	0.543	0.512	0.481	0.450
1.7	0.680	0.634	0.590	0.551	0.514	0.481	0.448	0.416	0.385
2.7	0.632	0.583	0.542	0.502	0.465	0.433	0.403	0.373	0.345
3.7	0.590	0.544	0.503	0.466	0.429	0.398	0.367	0.339	0.314
4.7	0.555	0.511	0.471	0.432	0.399	0.366	0.337	0.313	0.289
5.7	0.520	0.477	0.437	0.401	0.369	0.339	0.311	0.287	0.265
6.7	0.487	0.445	0.407	0.373	0.344	0.315	0.289	0.264	0.243
7.7	0.460	0.421	0.383	0.352	0.322	0.294	0.267	0.244	0.224
8.7	0.434	0.397	0.361	0.330	0.301	0.275	0.251	0.228	0.208
9.7	0.407	0.372	0.338	0.308	0.281	0.258	0.236	0.215	0.196
10.7	0.385	0.350	0.318	0.290	0.265	0.242	0.221	0.200	0.180
11.7	0.359	0.326	0.296	0.271	0.246	0.225	0.205	0.184	0.166
12.7	0.338	0.307	0.278	0.254	0.231	0.210	0.190	0.171	0.155
13.7	0.319	0.289	0.262	0.239	0.218	0.197	0.178	0.160	0.146
14.7	0.299	0.271	0.245	0.224	0.203	0.183	0.166	0.150	0.136
15.7	0.280	0.253	0.229	0.208	0.189	0.171	0.154	0.139	0.125
16.7	0.263	0.238	0.215	0.195	0.175	0.159	0.143	0.129	0.118
17.7	0.245	0.222	0.201	0.181	0.163	0.149	0.134	0.120	0.108
18.7	0.227	0.206	0.187	0.168	0.152	0.140	0.127	0.113	0.101

Table 19: MCNP5 calculated kerma rate (neutrons and gammas) distributions in the simplified water filled head phantom for different thickness of tungsten filter (continue)

Depth	kerma (Gy/min)								
(cm)	4.5 cm	5.0 cm	5.5 cm	6.0 cm	6.5 cm	7.0 cm	7.5 cm	8.0 cm	8.5 cm
0.7	0.419	0.393	0.369	0.345	0.322	0.304	0.284	0.267	0.249
1.7	0.360	0.335	0.312	0.293	0.273	0.256	0.238	0.221	0.205
2.7	0.318	0.296	0.273	0.255	0.234	0.219	0.204	0.189	0.175
3.7	0.289	0.267	0.246	0.229	0.211	0.196	0.182	0.168	0.156
4.7	0.265	0.244	0.224	0.208	0.192	0.178	0.164	0.151	0.140
5.7	0.241	0.221	0.204	0.188	0.173	0.161	0.148	0.137	0.127
6.7	0.223	0.204	0.188	0.172	0.159	0.148	0.135	0.125	0.114
7.7	0.206	0.189	0.172	0.157	0.145	0.135	0.124	0.114	0.104
8.7	0.189	0.173	0.159	0.145	0.133	0.123	0.113	0.105	0.095
9.7	0.176	0.161	0.146	0.133	0.124	0.114	0.105	0.097	0.088
10.7	0.163	0.149	0.136	0.124	0.114	0.105	0.095	0.089	0.081
11.7	0.151	0.138	0.126	0.115	0.105	0.097	0.088	0.081	0.074
12.7	0.141	0.129	0.119	0.109	0.098	0.090	0.082	0.076	0.069
13.7	0.132	0.120	0.110	0.100	0.091	0.083	0.077	0.071	0.063
14.7	0.122	0.111	0.102	0.093	0.085	0.078	0.072	0.067	0.059
15.7	0.114	0.103	0.094	0.087	0.079	0.073	0.066	0.061	0.054
16.7	0.106	0.097	0.088	0.081	0.074	0.068	0.062	0.056	0.050
17.7	0.097	0.089	0.081	0.073	0.067	0.062	0.056	0.051	0.046
18.7	0.091	0.082	0.076	0.068	0.062	0.057	0.053	0.048	0.043

Table 20: MCNP5 calculated PDE distribution for different thickness of tungsten filter

Depth	PDE								
(cm)	no -filter	0.5 cm	1.0 cm	1.5 cm	2.0 cm	2.5 cm	3.0 cm	3.5 cm	4.0 cm
0.7	3.9%	4.0%	4.1%	4.3%	4.5%	4.6%	4.7%	4.9%	5.1%
1.7	6.4%	6.8%	7.2%	7.5%	7.9%	8.3%	8.7%	9.2%	9.6%
2.7	8.7%	9.2%	9.9%	10.4%	10.9%	11.5%	12.1%	12.7%	13.5%
3.7	10.4%	11.1%	11.7%	12.4%	13.2%	14.0%	14.7%	15.5%	16.5%
4.7	11.4%	12.2%	13.0%	13.9%	14.6%	15.7%	16.6%	17.5%	18.5%
5.7	11.9%	12.7%	13.7%	14.7%	15.6%	16.6%	17.5%	18.7%	19.7%
6.7	11.9%	12.8%	13.8%	14.7%	15.7%	16.7%	17.9%	19.1%	20.0%
7.7	11.7%	12.6%	13.5%	14.3%	15.3%	16.3%	17.5%	18.7%	19.4%
8.7	11.1%	12.0%	12.9%	13.7%	14.5%	15.6%	16.6%	17.9%	18.9%
9.7	10.5%	11.1%	11.9%	12.7%	13.7%	14.3%	15.4%	16.5%	17.5%
10.7	9.7%	10.4%	11.1%	11.9%	12.5%	13.4%	14.2%	15.1%	16.2%
11.7	8.9%	9.6%	10.2%	10.9%	11.5%	12.3%	13.1%	14.1%	14.8%
12.7	8.1%	8.8%	9.4%	9.9%	10.5%	11.2%	12.0%	12.9%	13.6%
13.7	7.4%	7.9%	8.3%	8.8%	9.4%	10.1%	10.5%	11.3%	12.0%
14.7	6.5%	6.9%	7.4%	7.8%	8.1%	8.7%	9.3%	9.8%	10.6%
15.7	5.3%	5.7%	6.0%	6.3%	6.8%	7.5%	7.7%	8.3%	8.8%
16.7	4.3%	4.6%	4.9%	5.1%	5.6%	6.1%	6.3%	6.7%	7.2%
17.7	3.2%	3.4%	3.7%	3.9%	4.2%	4.5%	4.7%	5.0%	5.4%
18.7	2.0%	2.1%	2.3%	2.4%	2.6%	2.7%	2.9%	3.1%	3.3%

Table 20: MCNP5 calculated PDE distribution for different thickness of tungsten filter (continue)

Depth	PDE								
(cm)	4.5 cm	5.0 cm	5.5 cm	6.0 cm	6.5 cm	7.0 cm	7.5 cm	8.0 cm	8.5 cm
0.7	5.4%	5.6%	5.7%	5.9%	6.3%	6.3%	6.5%	6.7%	7.0%
1.7	10.1%	10.6%	10.8%	11.4%	11.8%	12.2%	12.8%	13.3%	13.9%
2.7	14.5%	14.8%	15.7%	16.4%	17.2%	17.8%	18.7%	19.0%	20.0%
3.7	17.7%	18.4%	19.5%	20.4%	21.5%	22.1%	23.3%	23.9%	25.1%
4.7	19.8%	20.6%	21.8%	22.4%	24.0%	25.0%	26.2%	27.2%	28.2%
5.7	21.1%	21.9%	23.4%	23.9%	25.4%	26.6%	28.3%	29.1%	29.8%
6.7	21.6%	22.4%	23.6%	24.9%	25.9%	27.5%	28.6%	29.4%	31.1%
7.7	21.1%	21.9%	23.3%	24.5%	25.5%	26.5%	28.4%	29.1%	31.0%
8.7	20.2%	21.3%	22.7%	23.4%	24.8%	26.0%	27.3%	28.4%	30.0%
9.7	18.7%	19.9%	21.3%	22.3%	23.1%	24.5%	25.0%	26.0%	27.2%
10.7	17.2%	18.5%	19.4%	20.4%	21.6%	22.5%	23.7%	24.1%	25.0%
11.7	15.7%	16.8%	17.5%	18.6%	19.9%	20.6%	21.8%	22.5%	23.4%
12.7	14.3%	15.2%	15.7%	16.6%	17.8%	18.4%	19.8%	20.3%	21.3%
13.7	12.7%	13.4%	13.9%	14.7%	16.0%	16.5%	17.3%	17.9%	19.3%
14.7	11.2%	11.7%	12.6%	13.3%	13.6%	14.3%	14.9%	15.7%	16.6%
15.7	9.3%	9.8%	10.4%	10.9%	11.3%	12.1%	12.8%	13.5%	14.4%
16.7	7.6%	7.8%	8.7%	9.0%	9.3%	9.9%	10.4%	10.8%	11.5%
17.7	6.0%	6.0%	6.5%	6.8%	7.1%	7.2%	8.1%	8.0%	8.5%
18.7	3.6%	3.7%	3.9%	4.2%	4.3%	4.4%	4.8%	4.8%	5.2%

Table 21: MCNP5 calculated gamma kerma percentage in the total kerma for different thickness of tungsten filter

Depth	Gamma Dose Percentage								
(cm)	no -filter	0.5 cm	1.0 cm	1.5 cm	2.0 cm	2.5 cm	3.0 cm	3.5 cm	4.0 cm
0.7	3.5%	3.7%	3.8%	4.0%	4.2%	4.3%	4.4%	4.5%	4.7%
1.7	3.8%	4.0%	4.2%	4.3%	4.5%	4.7%	4.8%	5.0%	5.2%
2.7	4.0%	4.2%	4.3%	4.5%	4.7%	5.0%	5.2%	5.4%	5.7%
3.7	4.1%	4.3%	4.6%	4.8%	5.0%	5.2%	5.4%	5.7%	5.9%
4.7	4.1%	4.4%	4.6%	4.9%	5.2%	5.5%	5.6%	5.8%	6.0%
5.7	4.1%	4.3%	4.6%	4.9%	5.2%	5.4%	5.6%	5.9%	6.2%
6.7	4.2%	4.4%	4.7%	4.9%	5.2%	5.5%	5.8%	6.1%	6.3%
7.7	4.3%	4.5%	4.8%	5.0%	5.2%	5.5%	5.8%	6.1%	6.4%
8.7	4.1%	4.3%	4.6%	4.9%	5.1%	5.3%	5.5%	5.9%	6.1%
9.7	4.0%	4.1%	4.5%	4.7%	4.9%	5.0%	5.4%	5.7%	6.0%
10.7	3.8%	4.1%	4.3%	4.6%	4.7%	4.9%	5.1%	5.5%	5.8%
11.7	3.8%	4.0%	4.3%	4.5%	4.6%	4.9%	5.1%	5.4%	5.7%
12.7	3.6%	3.8%	4.0%	4.2%	4.4%	4.6%	4.8%	5.1%	5.4%
13.7	3.5%	3.7%	3.9%	4.1%	4.2%	4.4%	4.7%	5.0%	5.1%
14.7	3.2%	3.5%	3.7%	3.9%	4.0%	4.2%	4.5%	4.5%	4.8%
15.7	2.9%	3.1%	3.3%	3.5%	3.7%	3.8%	4.0%	4.3%	4.5%
16.7	2.8%	3.1%	3.1%	3.3%	3.5%	3.7%	3.8%	4.1%	4.2%
17.7	2.6%	2.8%	2.9%	3.1%	3.4%	3.5%	3.5%	3.8%	4.1%
18.7	2.3%	2.4%	2.5%	2.7%	2.9%	3.0%	3.0%	3.4%	3.5%

Table 21: MCNP5 calculated gamma kerma percentage in the total kerma for different thickness of tungsten filter (continue)

Depth	Gamma Dose Percentage								
(cm)	4.5 cm	5.0 cm	5.5 cm	6.0 cm	6.5 cm	7.0 cm	7.5 cm	8.0 cm	8.5 cm
0.7	4.7%	4.9%	4.9%	5.0%	5.2%	5.3%	5.4%	5.5%	5.7%
1.7	5.4%	5.5%	5.6%	5.9%	6.1%	6.3%	6.4%	6.5%	6.5%
2.7	5.8%	6.0%	6.1%	6.4%	6.6%	6.7%	7.1%	7.2%	7.3%
3.7	6.1%	6.3%	6.5%	6.7%	7.0%	7.2%	7.6%	7.8%	8.1%
4.7	6.2%	6.6%	6.9%	7.2%	7.4%	7.6%	8.0%	8.2%	8.4%
5.7	6.5%	6.7%	7.1%	7.4%	7.8%	7.8%	8.2%	8.4%	8.5%
6.7	6.6%	6.8%	7.2%	7.6%	7.9%	8.0%	8.4%	8.6%	8.8%
7.7	6.6%	6.8%	7.1%	7.7%	7.7%	8.1%	8.4%	8.8%	8.9%
8.7	6.4%	6.8%	7.2%	7.5%	7.8%	7.9%	8.3%	8.5%	9.0%
9.7	6.2%	6.7%	7.1%	7.4%	7.6%	7.9%	8.3%	8.4%	9.0%
10.7	6.2%	6.5%	6.8%	7.3%	7.4%	7.8%	7.9%	8.3%	8.7%
11.7	6.1%	6.2%	6.6%	7.0%	7.2%	7.8%	7.8%	8.1%	8.7%
12.7	5.6%	5.8%	6.2%	6.4%	6.7%	7.2%	7.5%	7.6%	8.2%
13.7	5.4%	5.7%	6.0%	6.2%	6.5%	6.7%	6.9%	7.0%	7.5%
14.7	5.0%	5.4%	5.7%	6.0%	6.1%	6.5%	6.7%	6.8%	7.2%
15.7	4.8%	5.1%	5.2%	5.6%	5.8%	6.2%	6.2%	6.3%	6.9%
16.7	4.5%	4.8%	5.0%	5.2%	5.3%	5.7%	5.7%	6.1%	6.5%
17.7	4.2%	4.4%	4.6%	4.9%	5.2%	5.2%	5.4%	5.8%	5.9%
18.7	3.5%	3.8%	4.0%	4.1%	4.5%	4.4%	4.8%	5.0%	5.2%

B.2 MCNP5 calculations of kerma and PDE distributions in a water-filled head phantom using the simplified BNCEFNT assembly as the measurements. 12.5-cm graphite reflector, 5x5 cm^2 size with 10-cm thick lead collimator made of four 20x10x5 cm^3 lead bricks, 20x20 cm^2 standard therapy beam. Normalization of the MCNP results is based on a proton current of 3.3x10^{16} protons/MU and 8.13x10^{-7} n/cm^2 per proton obtained in chapter 4.

Table 22: Calculated absorbed dose distribution (Gy/MU) for different thick tungsten filter as in the measurements

Depth	kerma (Gy/MU)						
(cm)	0-cm	1.0-cm	2.0-cm	3.0-cm	4.0-cm	5.0-cm	5.0-cm/NSGR*
0.7	2.198	1.875	1.610	1.394	1.199	1.020	0.953
1.7	2.086	1.756	1.491	1.280	1.084	0.917	0.870
2.7	1.968	1.641	1.388	1.172	0.985	0.834	0.796
3.7	1.857	1.551	1.301	1.095	0.920	0.769	0.737
4.7	1.762	1.469	1.222	1.022	0.857	0.720	0.689
5.7	1.670	1.384	1.148	0.956	0.795	0.663	0.639
6.7	1.576	1.309	1.085	0.895	0.743	0.616	0.593
7.7	1.491	1.230	1.015	0.836	0.687	0.569	0.555
8.7	1.414	1.159	0.956	0.785	0.644	0.534	0.518
9.7	1.343	1.096	0.901	0.743	0.613	0.504	0.481
10.7	1.270	1.034	0.849	0.699	0.566	0.462	0.448
11.7	1.192	0.970	0.796	0.655	0.530	0.433	0.422
12.7	1.126	0.917	0.751	0.615	0.496	0.411	0.396
13.7	1.059	0.863	0.705	0.574	0.462	0.381	0.369
14.7	1.003	0.816	0.665	0.541	0.434	0.357	0.345
15.7	0.942	0.761	0.616	0.502	0.403	0.331	0.321
16.7	0.884	0.714	0.579	0.470	0.382	0.313	0.305
17.7	0.830	0.674	0.546	0.442	0.355	0.293	0.284
18.7	0.771	0.627	0.507	0.413	0.331	0.272	0.266

* Side Graphite Reflectors Removed

Table 23: Calculated boron dose per 100-ppm ^{10}B

Depth	Absorbed dose (Gy/MU)						
(cm)	0-cm	1.0-cm	2.0-cm	3.0-cm	4.0-cm	5.0-cm	5.0-cm/NSGR*
0.7	0.069	0.063	0.060	0.058	0.057	0.055	0.039
1.7	0.098	0.091	0.090	0.087	0.085	0.083	0.060
2.7	0.115	0.111	0.110	0.107	0.103	0.101	0.075
3.7	0.129	0.124	0.121	0.118	0.116	0.112	0.084
4.7	0.134	0.128	0.125	0.122	0.121	0.116	0.086
5.7	0.133	0.129	0.126	0.120	0.118	0.113	0.084
6.7	0.129	0.124	0.120	0.116	0.113	0.110	0.080
7.7	0.122	0.118	0.112	0.108	0.107	0.101	0.073
8.7	0.113	0.108	0.104	0.099	0.097	0.090	0.065
9.7	0.103	0.098	0.093	0.088	0.086	0.082	0.059
10.7	0.093	0.088	0.083	0.080	0.075	0.072	0.050
11.7	0.081	0.075	0.073	0.068	0.064	0.061	0.043
12.7	0.070	0.065	0.062	0.058	0.056	0.051	0.035
13.7	0.060	0.055	0.053	0.049	0.047	0.043	0.030
14.7	0.050	0.047	0.043	0.041	0.038	0.036	0.024
15.7	0.040	0.037	0.035	0.031	0.029	0.028	0.018
16.7	0.030	0.028	0.026	0.024	0.022	0.021	0.014
17.7	0.021	0.019	0.018	0.017	0.016	0.015	0.009
18.7	0.012	0.011	0.010	0.009	0.009	0.008	0.005

* Side Graphite Reflectors Removed

Table 24: Calculated PDE distribution for different thick tungsten filter as in the measurements

Depth	PDE						
(cm)	0-cm	1.0-cm	2.0-cm	3.0-cm	4.0-cm	5.0-cm	5.0-cm/NSGR*
0.7	3.1%	3.3%	3.7%	4.2%	4.8%	5.4%	4.1%
1.7	4.7%	5.2%	6.0%	6.8%	7.9%	9.1%	6.9%
2.7	5.8%	6.8%	7.9%	9.1%	10.5%	12.1%	9.4%
3.7	7.0%	8.0%	9.3%	10.8%	12.7%	14.5%	11.4%
4.7	7.6%	8.7%	10.2%	11.9%	14.1%	16.1%	12.5%
5.7	7.9%	9.3%	11.0%	12.5%	14.8%	17.1%	13.1%
6.7	8.2%	9.4%	11.1%	12.9%	15.3%	17.9%	13.4%
7.7	8.2%	9.6%	11.0%	12.9%	15.5%	17.7%	13.2%
8.7	8.0%	9.3%	10.9%	12.6%	15.1%	16.9%	12.6%
9.7	7.7%	8.9%	10.3%	11.9%	14.0%	16.2%	12.3%
10.7	7.3%	8.5%	9.8%	11.4%	13.3%	15.7%	11.2%
11.7	6.8%	7.8%	9.1%	10.5%	12.1%	14.0%	10.1%
12.7	6.2%	7.1%	8.3%	9.4%	11.2%	12.4%	8.9%
13.7	5.6%	6.4%	7.5%	8.5%	10.1%	11.4%	8.2%
14.7	5.0%	5.7%	6.5%	7.5%	8.8%	10.1%	6.9%
15.7	4.2%	4.8%	5.6%	6.3%	7.1%	8.3%	5.8%
16.7	3.4%	3.9%	4.5%	5.1%	5.9%	6.6%	4.5%
17.7	2.6%	2.9%	3.3%	3.9%	4.4%	5.0%	3.1%
18.7	1.5%	1.7%	2.0%	2.2%	2.6%	3.0%	1.7%

* Side Graphite Reflectors Removed

B.2 Measurements of absorbed dose and PDE distributions in a water-filled RSVP head phantom using the simplified BNCEFNT assembly as described in Chapter 5. 12.5-cm graphite reflector, 5x5 cm^2 size with 10-cm thick lead collimator made of four 20x10x5 cm^3 lead bricks, 20x20 cm^2 standard therapy beam.

Table 25: Measurements of the absorbed dose in the water-filled head phantom using non-borated ion chamber (SN:445) and Equation (3.24)

Depth	Absorbed dose (Gy/MU)						
(cm)	0-cm	1.0-cm	2.0-cm	3.0-cm	4.0-cm	5.0-cm	5.0-cm/NSGR*
1.0	2.060	1.728	1.463	1.244	1.071	0.915	0.902
2.0	2.058	1.716	1.452	1.229	1.054	0.896	0.890
3.0	1.977	1.635	1.382	1.166	0.996	0.847	0.843
4.0	1.874	1.569	1.317	1.109	0.947	0.803	0.787
5.0	1.770	1.480	1.239	1.040	0.886	0.751	0.733
5.8	1.661	1.364	1.164	0.977	0.824	0.694	
6.8	1.567	1.298	1.090	0.917	0.772	0.649	
7.8	1.475	1.221	1.024	0.859	0.721	0.606	
8.8	1.388	1.147	0.961	0.804	0.674	0.565	
9.8	1.305	1.076	0.900	0.753	0.628	0.526	
10.8	1.227	1.009	0.844	0.704	0.585	0.490	
11.8	1.152	0.947	0.791	0.658	0.547	0.456	
12.8	1.083	0.888	0.740	0.615	0.511	0.425	

* Side Graphite Reflectors Removed

Table 26: Measured boron-10 dose using the borated (SN#446) and the non-borated ion chambers and Equation (3.22)

Depth	Absorbed dose (Gy/MU)						
(cm)	0-cm	1.0-cm	2.0-cm	3.0-cm	4.0-cm	5.0-cm	5.0-cm/NSGR*
1.0	0.087	0.081	0.080	0.076	0.075	0.076	0.057
2.0	0.104	0.100	0.101	0.100	0.099	0.100	0.075
3.0	0.116	0.118	0.118	0.119	0.117	0.117	0.089
4.0	0.129	0.126	0.128	0.127	0.125	0.125	0.097
5.0	0.135	0.130	0.132	0.131	0.128	0.127	0.098
5.8	0.134	0.127	0.125	0.128	0.123	0.111	
6.8	0.128	0.118	0.119	0.123	0.117	0.104	
7.8	0.121	0.109	0.111	0.113	0.108	0.095	
8.8	0.110	0.099	0.100	0.102	0.097	0.084	
9.8	0.098	0.089	0.089	0.091	0.086	0.074	
10.8	0.087	0.078	0.078	0.079	0.076	0.064	
11.8	0.076	0.067	0.067	0.069	0.065	0.052	
12.8	0.065	0.057	0.057	0.059	0.055	0.046	

* Side Graphite Reflectors Removed

Table 27: Measured PDE Normalized to 100-ppm ^{10}B using the borated and non-borated ion chambers and Equation (3.23)

Depth	PDE per 100-ppm ^{10}B						
(cm)	0-cm	1.0-cm	2.0-cm	3.0-cm	4.0-cm	5.0-cm	5.0-cm/NSGR*
1.0	4.2%	4.7%	5.5%	6.1%	7.0%	8.3%	6.3%
2.0	5.1%	5.9%	7.0%	8.1%	9.4%	11.2%	8.4%
3.0	5.9%	7.2%	8.5%	10.2%	11.8%	13.9%	10.5%
4.0	6.9%	8.0%	9.7%	11.5%	13.2%	15.6%	12.3%
5.0	7.6%	8.8%	10.6%	12.6%	14.4%	16.9%	13.4%
5.8	8.1%	9.3%	10.8%	13.1%	14.9%	16.0%	
6.8	8.2%	9.1%	11.0%	13.4%	15.2%	16.0%	
7.8	8.2%	8.9%	10.8%	13.2%	14.9%	15.7%	
8.8	7.9%	8.7%	10.4%	12.7%	14.4%	15.0%	
9.8	7.5%	8.2%	9.9%	12.0%	13.7%	14.0%	
10.8	7.1%	7.7%	9.2%	11.3%	12.9%	13.0%	
11.8	6.6%	7.1%	8.5%	10.4%	11.9%	11.4%	
12.8	6.0%	6.4%	7.7%	9.6%	10.8%	10.9%	

* Side Graphite Reflectors Removed

APPENDIX C

RAW MEASUREMENT DATA

C.1 Measurements using the normal TE ion chamber (SN # 445)

Table 28: Non-borated ion chamber measurement data for the simplified BNCEFNT assembly: 5 x 5 cm^2 collimator with no-filter using the 20 x 20 cm^2 standard therapy beam. Measurements made May, 2006.

Electrometer: Keithley 617 SN: 507703 Ion Chamber SN: 445 (normal) High Voltage = +400V

Cint/X1= 5.483E+14 protons/X1

Depth (cm)	Off Axis (cm)	Charge (nC)	Monitor Units (MU)	Beam Time (min)	X1	X1 TPCX	Pressure (mB)	Temperature (˚C)	Notes
1.0	0.0	8.957	0.3022	0.95	18.09	1.027	988.7	23.5	22˚ IC holder
2.0	0.0	8.940	0.3020	0.96	18.08	1.027	988.7	23.5	
3.0	0.0	8.576	0.3016	0.95	18.05	1.027	988.7	23.4	
4.0	0.0	8.113	0.3009	0.95	18.00	1.027	988.7	23.4	
5.0	0.0	7.664	0.3011	0.95	18.02	1.027	988.5	23.5	
1.5	0.0	8.953	0.3015	0.94	18.04	1.027	988.5	23.5	
1.5	1.0	8.940	0.3013	0.94	18.03	1.027	988.5	23.4	
1.5	2.0	9.001	0.3021	0.94	18.08	1.027	988.5	23.4	
1.5	2.5	8.785	0.3009	0.94	18.00	1.027	988.5	23.4	
1.5	3.0	6.554	0.3003	0.96	18.07	1.028	988.5	23.4	
1.5	-1.0	9.030	0.3016	0.96	18.07	1.027	988.5	23.4	
1.5	-2.0	8.513	0.3010	0.96	18.04	1.028	988.5	23.4	
1.5	-2.5	6.040	0.3016	0.96	18.00	1.028	988.5	23.4	
3.0	1.0	8.499	0.3001	0.96	18.05	1.028	988.5	23.4	
3.0	2.0	8.548	0.3021	0.97	18.07	1.028	988.5	23.4	
3.0	2.5	8.379	0.3022	0.96	18.07	1.028	988.5	23.4	
3.0	3.0	6.445	0.3021	0.96	18.07	1.028	988.5	23.5	
3.0	-1.0	8.492	0.3015	0.96	18.03	1.028	988.5	23.5	
3.0	-2.0	7.908	0.2992	0.95	17.89	1.028	988.5	23.5	
3.0	-2.5	5.733	0.3004	0.96	17.97	1.028	988.5	23.5	
3.0	-3.0	3.842	0.2993	0.95	17.89	1.028	988.5	23.5	
5.8	0.0	10.016	0.4207	1.34	25.14	1.029	983.6	22.84	Perpendicular
5.8	0.0	10.045	0.4216	1.34	25.19	1.029	983.6	22.84	IC holder
6.8	0.0	9.461	0.4209	1.34	25.14	1.029	983.6	22.84	
6.8	0.0	9.479	0.4220	1.34	25.21	1.029	983.6	22.84	
7.8	0.0	8.874	0.4195	1.38	25.02	1.031	983.6	22.84	
7.8	0.0	8.895	0.4207	1.38	25.09	1.031	983.6	22.84	
8.8	0.0	8.364	0.4201	1.33	25.05	1.031	983.6	22.84	
8.8	0.0	8.366	0.4203	1.33	25.02	1.032	983.6	22.84	
9.8	0.0	7.883	0.4210	1.33	25.08	1.032	983.6	22.84	
9.8	0.0	7.881	0.4211	1.33	25.08	1.032	983.6	22.84	
10.8	0.0	7.396	0.4203	1.36	25.03	1.032	983.6	22.84	
11.8	0.0	6.960	0.4212	1.36	25.07	1.033	983.6	22.84	
12.8	0.0	6.530	0.4204	1.36	25.02	1.033	983.6	22.84	
8.8	0.0	8.391	0.4212	1.38	25.07	1.033	983.6	22.84	
8.8	1.0	8.415	0.4216	1.38	25.08	1.033	983.6	22.84	
8.8	2.0	8.276	0.4207	1.37	25.02	1.034	983.6	22.84	
8.8	2.5	7.908	0.4216	1.33	25.08	1.034	983.0	22.84	
8.8	3.0	6.033	0.4212	1.36	25.06	1.033	983.5	22.84	
8.8	3.5	4.244	0.4209	1.32	25.05	1.033	983.5	22.84	
8.8	-1.0	8.364	0.4210	1.37	25.06	1.033	983.5	23.20	
8.8	-2.0	8.043	0.4219	1.35	25.08	1.034	983.5	23.20	
8.8	-2.5	6.520	0.4212	1.38	25.04	1.034	983.5	23.20	
8.8	-3.0	7.407	0.7018	2.29	41.72	1.034	983.5	23.20	

Table 29: Non-borated ion chamber measurement data for the simplified BNCEFNT assembly: 5 x 5 cm^2 collimator with 1.0-cm tungsten filter using the 20 x 20 cm^2 standard therapy beam. Measurements made May, 2006.

Electrometer: Keithley 617 SN: 507703 Ion Chamber SN: 445 (normal) High Voltage = +400V

Cint/X1= 5.483E+14 protons/X1

Depth (cm)	Off Axis (cm)	Charge (nC)	Monitor Units (MU)	Beam Time (min)	X1	X1 TPCX	Pressure (mB)	Temperature (˚C)	Notes
1.0	0.0	7.433	0.2991	0.96	17.88	1.029	988.4	23.50	22˚ IC holder
2.0	0.0	7.404	0.3001	0.97	17.94	1.029	988.4	23.50	
3.0	0.0	7.052	0.2998	0.96	17.92	1.029	988.4	23.36	
4.0	0.0	6.777	0.3002	0.96	17.94	1.029	988.4	23.36	
5.0	0.0	6.389	0.3002	0.97	17.94	1.029	988.4	23.36	
1.5	0.0	7.507	0.3006	0.96	17.96	1.029	988.4	23.36	
1.5	2.5	7.260	0.2997	0.96	17.91	1.029	988.3	23.36	
1.5	3.0	5.525	0.2995	0.96	17.89	1.029	988.4	23.36	
1.5	-2.5	5.209	0.2994	0.97	17.88	1.029	988.4	23.36	
1.5	-3.0	3.663	0.2990	0.96	17.91	1.029	988.4	23.36	
5.8	0.0	9.907	0.5070	1.63	29.83	1.034	983.5	23.20	Perpendicular IC holder
6.8	0.0	9.336	0.5017	1.63	29.84	1.034	983.5	22.98	
7.8	0.0	8.760	0.5005	1.63	29.77	1.034	983.5	22.98	
8.8	0.0	8.243	0.5014	1.63	29.81	1.034	983.5	22.98	
9.8	0.0	7.729	0.5011	1.63	29.80	1.034	983.5	22.98	
10.8	0.0	7.252	0.5013	1.63	29.81	1.034	983.5	22.98	
11.8	0.0	6.803	0.5013	1.64	29.81	1.034	983.5	22.98	
12.8	0.0	6.386	0.5019	1.64	29.82	1.035	983.5	22.98	
8.8	1.0	8.216	0.5003	1.64	29.82	1.035	983.5	22.98	
8.8	2.0	8.084	0.5019	1.64	29.81	1.035	983.5	22.98	
8.8	2.5	7.780	0.5011	1.63	29.76	1.035	983.5	22.98	
8.8	3.0	9.928	0.7998	2.61	47.52	1.035	983.5	22.98	

Table 30: Non-borated ion chamber measurement data for the simplified BNCEFNT assembly: 5 x 5 cm^2 collimator with 2.0-cm tungsten filter using the 20 x 20 cm^2 standard therapy beam. Measurements made May, 2006.

Electrometer: Keithley 617 SN: 507703 Ion Chamber SN: 445 (normal) High Voltage = +400V

Cint/X1= 5.483E+14 protons/X1

Depth (cm)	Off Axis (cm)	Charge (nC)	Monitor Units (MU)	Beam Time (min)	X1	X1 TPCX	Pressure (mB)	Temperature (˚C)	Notes
1.0	0.0	8.435	0.4008	1.25	23.93	1.029	988.4	23.36	22˚ IC holder
2.0	0.0	7.310	0.3501	1.13	20.91	1.029	988.4	23.36	
3.0	0.0	6.965	0.3503	1.13	20.92	1.029	988.4	23.36	
4.0	0.0	6.631	0.3500	1.12	20.90	1.029	988.4	23.36	
5.0	0.0	6.248	0.3506	1.13	20.93	1.029	988.4	23.36	
3.0	2.5	6.688	0.3510	1.12	20.96	1.029	988.4	23.36	
3.0	3.0	5.715	0.3710	1.19	22.15	1.030	988.4	23.36	
3.0	-2.5	4.924	0.3509	1.12	20.95	1.030	988.4	23.36	
3.0	-3.0	3.884	0.3719	1.19	22.20	1.030	988.4	23.36	
5.8	0.0	13.360	0.8012	2.60	47.60	1.035	983.5	22.98	Perpendicular IC holder
6.8	0.0	7.833	0.5014	1.62	29.79	1.035	983.5	22.98	
7.8	0.0	7.352	0.5009	1.62	29.75	1.035	983.5	22.98	
8.8	0.0	7.591	0.5510	1.78	32.75	1.035	983.5	22.98	
9.8	0.0	7.757	0.6016	1.94	35.73	1.035	983.5	22.98	
10.8	0.0	7.266	0.6010	1.94	35.69	1.035	983.5	22.98	
11.8	0.0	6.813	0.6013	1.96	35.71	1.036	983.5	22.98	
12.8	0.0	6.911	0.6517	2.11	38.68	1.036	983.5	22.98	
8.8	1.0	7.544	0.5501	2.11	38.68	1.036	983.5	22.98	
8.8	2.0	8.081	0.6090	1.93	35.66	1.036	983.5	22.98	
8.8	2.5	7.783	0.6016	1.93	35.69	1.036	983.5	22.98	
8.8	3.0	6.346	0.6022	1.94	35.72	1.036	983.5	22.98	

Table 31: Non-borated ion chamber measurement data for the simplified BNCEFNT assembly: 5 x 5 cm^2 collimator with 3.0-cm tungsten filter using the 20 x 20 cm^2 standard therapy beam. Measurements made May, 2006.

Electrometer: Keithley 617 SN: 507703 Ion Chamber SN: 445 (normal) High Voltage = +400V

Cint/X1= 5.483E+14 protons/X1

Depth (cm)	Off Axis (cm)	Charge (nC)	Monitor Units (MU)	Beam Time (min)	X1	X1 TPCX	Pressure (mB)	Temperature (˚C)	Notes
1.0	0.0	5.371	0.3001	0.96	17.91	1.030	988.4	23.36	22˚ IC holder
2.0	0.0	7.085	0.4009	1.28	23.93	1.030	988.4	23.36	
3.0	0.0	6.720	0.4006	1.27	23.90	1.030	988.4	23.36	
4.0	0.0	6.402	0.4013	1.27	23.93	1.030	988.4	23.36	
5.0	0.0	6.001	0.4011	1.27	23.93	1.030	988.4	23.36	
1.5	0.0	7.167	0.4004	1.27	23.88	1.030	988.4	23.36	
1.5	2.5	6.821	0.4012	1.27	23.93	1.031	988.4	23.36	
1.5	3.0	5.464	0.4009	1.27	23.91	1.031	988.4	23.36	
1.5	-2.5	5.225	0.4011	1.27	23.92	1.031	988.4	23.36	
1.5	-3.0	3.985	0.4011	1.27	23.92	1.031	988.4	23.36	Perpendicular
5.8	0.0	8.436	0.6019	1.96	35.69	1.037	984.1	22.98	IC holder
6.8	0.0	7.898	0.6007	1.94	35.63	1.037	984.1	22.98	
7.8	0.0	7.403	0.6011	1.94	35.64	1.037	984.0	22.98	
8.8	0.0	6.945	0.6024	1.94	35.73	1.037	984.1	22.98	
9.8	0.0	5.014	0.4659	1.97	35.73	1.037	984.1	22.98	
10.8	0.0	6.727	0.6213	1.97	36.85	1.037	984.2	22.98	
11.8	0.0	6.560	0.6498	2.12	38.54	1.037	984.2	22.98	
12.8	0.0	6.437	0.6816	2.22	40.42	1.037	984.2	22.98	
8.8	0.0	6.186	0.7014	2.27	41.60	1.037	984.2	22.98	

Table 32: Non-borated ion chamber measurement data for the simplified BNCEFNT assembly: 5 x 5 cm^2 collimator with 4.0-cm tungsten filter using the 20 x 20 cm^2 standard therapy beam. Measurements made May, 2006.

Electrometer: Keithley 617 SN: 507703 Ion Chamber SN: 445 (normal) High Voltage = +400V

Cint/X1= 5.483E+14 protons/X1

Depth (cm)	Off Axis (cm)	Charge (nC)	Monitor Units (MU)	Beam Time (min)	X1	X1 TPCX	Pressure (mB)	Temperature (˚C)	Notes
1.0	0.0	6.966	0.4521	1.45	26.95	1.031	988.4	23.36	22˚ IC holder
2.0	0.0	6.838	0.4510	1.44	26.88	1.031	988.4	23.36	
3.0	0.0	6.476	0.4519	1.44	26.93	1.031	988.4	23.36	
4.0	0.0	6.168	0.4526	1.45	26.98	1.031	988.4	23.36	
5.0	0.0	5.769	0.4525	1.44	26.96	1.031	988.4	23.36	
3.0	2.5	6.083	0.4491	1.43	26.75	1.032	988.4	23.36	
3.0	3.0	5.096	0.4492	1.43	26.75	1.032	988.4	23.36	
3.0	-2.5	5.276	0.5008	1.59	29.83	1.032	988.4	23.36	
3.0	-3.0	4.175	0.5004	1.59	29.80	1.032	988.4	23.36	
5.8	0.0	7.103	0.6014	1.89	35.67	1.037	984.2	22.98	Perpendicular
6.8	0.0	6.651	0.6011	1.94	35.65	1.037	984.2	22.98	IC holder
7.8	0.0	6.219	0.6012	1.94	35.66	1.036	984.3	22.98	
8.8	0.0	5.815	0.6017	1.93	35.69	1.037	984.3	22.98	
9.8	0.0	5.853	0.6497	2.09	38.52	1.037	984.3	22.98	
10.8	0.0	5.894	0.7022	2.25	41.52	1.037	984.6	22.98	
11.8	0.0	5.902	0.7516	2.43	44.57	1.037	984.7	22.98	
12.8	0.0	5.879	0.8022	2.59	47.57	1.037	984.7	22.98	

Table 33: Non-borated ion chamber measurement data for the simplified BNCEFNT assembly: 5 x 5 cm^2 collimator with 5.0-cm tungsten filter using the 20 x 20 cm^2 standard therapy beam. Measurements made May, 2006.

Electrometer: Keithley 617 SN: 507703 Ion Chamber SN: 445 (normal) High Voltage = +400V

Cint/X1= 5.483E+14 protons/X1

Depth (cm)	Off Axis (cm)	Charge (nC)	Monitor Units (MU)	Beam Time (min)	X1	X1 TPCX	Pressure (mB)	Temperature (˚C)	Notes
1.0	0.0	6.581	0.5002	1.58	29.21	1.032	988.4	23.36	22˚ IC holder
2.0	0.0	6.446	0.5002	1.58	29.78	1.033	988.4	23.36	
3.0	0.0	5.476	0.4494	1.42	26.76	1.033	988.4	23.36	
4.0	0.0	5.787	0.5010	1.42	26.76	1.033	988.4	23.36	
5.0	0.0	5.401	0.5003	1.58	29.82	1.033	988.4	23.36	
1.5	0.0	6.571	0.5006	1.57	29.78	1.033	988.4	23.36	
1.5	1.0	6.528	0.5007	1.58	29.80	1.033	988.4	23.36	
1.5	2.0	6.384	0.5012	1.58	29.79	1.033	988.3	23.36	
1.5	2.5	6.138	0.5005	1.58	29.81	1.033	988.3	23.36	
1.5	3.0	5.120	0.5020	1.59	29.85	1.034	987.9	23.36	
1.5	-1.0	6.496	0.5016	1.58	29.82	1.034	987.9	23.36	
1.5	-2.0	6.021	0.5017	1.58	29.83	1.034	987.9	23.36	
1.5	-2.5	4.934	0.5018	1.58	29.83	1.034	987.8	23.36	
1.5	-3.0	4.758	0.6006	1.89	35.70	1.034	987.8	23.36	
3.0	1.0	5.492	0.4506	1.42	26.78	1.034	987.8	23.36	
3.0	2.0	5.989	0.5019	1.58	29.82	1.035	987.8	23.36	
3.0	2.5	5.781	0.5012	1.60	29.78	1.035	987.8	23.36	
3.0	3.0	4.918	0.5016	1.58	29.80	1.035	987.9	23.36	
3.0	-1.0	6.038	0.5012	1.59	29.76	1.035	987.9	23.36	
3.0	-2.0	5.584	0.5018	1.60	29.80	1.035	987.9	23.36	
3.0	-2.5	4.776	0.5209	1.66	30.93	1.035	987.8	23.36	
3.0	-3.0	4.106	0.5512	1.74	32.73	1.036	987.8	23.36	Perpendicular
5.8	0.0	6.981	0.7006	2.19	54.54	1.037	984.8	22.98	IC holder
6.8	0.0	6.525	0.7002	2.25	41.50	1.037	984.8	22.98	
7.8	0.0	6.087	0.7003	2.25	41.51	1.037	984.8	22.98	
8.8	0.0	5.839	0.7202	2.31	42.68	1.037	984.8	22.98	
9.8	0.0	6.043	0.8001	2.59	47.39	1.038	984.8	22.98	
10.8	0.0	5.782	0.8223	2.65	48.72	1.038	984.8	22.98	
11.8	0.0	5.903	0.9013	2.91	53.39	1.038	984.8	22.98	
12.8	0.0	5.490	0.9001	2.90	53.31	1.038	985.0	22.98	
8.8	1.0	6.061	0.7506	2.49	44.51	1.037	985.5	22.98	
8.8	1.5	6.239	0.7799	2.59	46.27	1.036	985.5	22.98	
8.8	2.0	6.128	0.7811	2.58	46.34	1.036	985.7	22.98	
8.8	2.5	5.888	0.7804	2.58	46.29	1.036	985.7	22.98	
8.8	3.0	5.162	0.8007	2.65	47.50	1.036	986.0	22.98	
8.8	-1.0	6.006	0.7513	2.50	44.57	1.036	986.0	22.98	
8.8	-1.5	5.911	0.7516	2.48	44.57	1.037	986.0	22.98	
8.8	-2.0	6.102	0.8024	2.65	47.59	1.036	986.0	22.98	
8.8	-2.5	5.395	0.8019	2.65	47.56	1.037	986.0	22.98	
8.8	-3.0	4.398	0.8015	2.66	47.53	1.037	986.0	22.98	
1.0	0.0	6.492	0.5004	1.55	29.71	1.033	987.8	23.36	Graphite
2.0	0.0	6.408	0.5007	1.59	29.73	1.033	987.8	23.36	reflector on
3.0	0.0	6.058	0.4998	1.58	29.67	1.033	987.8	23.36	both sides
4.0	0.0	5.666	0.5006	1.58	29.73	1.033	987.8	23.36	removed
5.0	0.0	5.503	0.5219	1.65	30.98	1.033	987.8	23.36	

C.2 Measurements using the borated TE ion chamber (SN # 446)

Table 34: Borated ion chamber measurement data for the simplified BNCEFNT assembly: 5 x 5 cm^2 collimator with no-filter using the 20 x 20 cm^2 standard therapy beam. Measurements made May, 2006.

Electrometer: Keithley 617 SN: 507703 Ion Chamber SN: 446 (Borated) High Voltage = +400V

Cint/X1= 5.483E+14 protons/X1

Depth (cm)	Off Axis (cm)	Charge (nC)	Monitor Units (MU)	Beam Time (min)	X1	X1 TPCX	Pressure (mB)	Temperature (˚C)	Notes
1.0	0.0	16.936	0.5007	1.57	29.72	1.036	987.4	23.07	22˚ IC holder
2.0	0.0	10.447	0.2993	0.96	17.76	1.036	987.3	23.07	
3.0	0.0	10.948	0.3165	0.96	17.76	1.036	987.3	23.07	
4.0	0.0	10.211	0.3003	0.94	17.82	1.036	987.3	23.07	
5.0	0.0	16.483	0.5004	1.58	29.70	1.036	987.5	23.07	
1.5	0.0	10.349	0.3004	0.95	17.83	1.036	987.4	23.07	
1.5	1.0	10.268	0.2994	0.95	17.77	1.036	987.4	23.07	
1.5	2.0	10.275	0.30	0.95	17.80	1.036	987.3	23.07	
1.5	2.5	10.187	0.2998	0.95	17.79	1.036	987.2	23.07	
1.5	3.0	9.559	0.3005	0.95	17.83	1.036	987.2	23.07	
1.5	-1.0	10.185	0.2994	0.95	17.77	1.036	987.2	23.07	
1.5	-2.0	6.325	0.3008	0.95	17.84	1.036	987.2	23.07	
3.0	3.0	10.240	0.3021	0.94	17.93	1.035	987.2	23.07	
3.0	2.8	10.340	0.3019	0.95	17.92	1.035	986.9	23.07	
3.0	2.6	10.275	0.2993	0.95	17.77	1.035	986.7	23.07	
3.0	2.4	10.395	0.3004	0.97	17.83	1.036	986.7	23.07	
3.0	2.2	10.338	0.2996	0.95	17.78	1.036	986.7	23.07	
3.0	2.0	10.396	0.3005	0.96	17.83	1.036	986.6	23.07	
3.0	-0.6	10.225	0.2997	0.95	17.78	1.036	986.6	23.07	
3.0	-0.8	10.158	0.2997	0.95	17.78	1.036	986.6	23.07	
3.0	-1.0	9.998	0.3004	0.95	17.83	1.036	986.7	23.07	
3.0	-1.2	9.466	0.3005	0.96	17.84	1.036	986.6	23.07	
3.0	-1.4	8.652	0.3007	0.96	17.84	1.036	986.7	23.07	
3.0	-1.6	7.537	0.3000	0.95	17.80	1.036	986.8	23.07	
3.0	-1.8	6.577	0.3002	0.95	17.81	1.036	986.8	23.07	
3.0	-2.0	5.868	0.3007	0.95	17.84	1.036	986.6	23.07	
3.0	-2.2	5.490	0.3001	0.94	17.81	1.036	986.6	23.07	
3.0	-2.4	5.363	0.3002	0.95	17.81	1.036	986.6	23.07	
3.0	-2.6	5.260	0.3002	0.95	17.81	1.036	986.6	23.07	
3.0	1.0	10.45	0.3021	0.99	17.94	1.035	986.0	23.07	Re-adjusted
3.0	2.0	10.284	0.3018	1.02	17.92	1.035	986.0	23.07	the ion
3.00	2.5	9.634	0.3013	1.02	17.93	1.035	986.0	23.07	chamber
3.00	3.0	7.292	0.302	1.02	17.93	1.035	986.0	23.07	positioning
3.00	-1.0	10.426	0.3019	1.01	17.91	1.035	986.0	23.07	
3.00	-2.0	10.094	0.3016	1.01	17.88	1.035	986.0	23.07	
3.00	-2.5	8.382	0.3016	1.02	17.9	1.035	986.0	23.07	
3.00	-3.0	6.099	0.3015	0.99	17.94	1.035	986.0	23.07	
5.8	0.0	12.603	0.4207	1.30	23.85	1.036	986.0	22.84	Perpendicular
6.8	0.0	9.428	0.3003	0.99	17.81	1.036	986.0	22.85	IC holder
6.8	0.0	8.913	0.2998	0.99	17.78	1.036	986.0	22.85	
7.8	0.0	8.386	0.2995	0.99	17.77	1.036	986.0	22.85	
8.8	0.0	7.839	0.3001	0.99	17.80	1.036	986.0	22.85	
9.8	0.0	7.291	0.3009	0.99	17.84	1.036	986.0	22.85	
10.8	0.0	6.713	0.2997	0.98	17.78	1.036	986.1	22.85	
11.8	0.0	6.202	0.2998	0.99	17.79	1.036	986.1	22.85	
12.8	0.0	5.721	0.3008	0.98	17.85	1.036	986.1	22.85	
8.8	1.0	7.777	0.2992	0.96	17.75	1.036	986.1	22.85	
8.8	2.0	7.651	0.3007	1.00	17.84	1.036	986.1	22.85	
8.8	2.5	7.288	0.3002	0.96	17.81	1.036	986.1	22.85	
8.8	3.0	5.907	0.3002	0.97	17.81	1.036	986.0	22.85	
8.8	3.5	4.682	0.2998	0.96	17.79	1.036	986.1	22.85	
8.8	-1.0	7.761	0.2997	0.96	17.78	1.036	986.1	22.85	
8.8	-2.0	7.498	0.2997	0.96	17.78	1.036	986.1	22.85	
8.8	-2.5	6.646	0.2996	0.96	17.78	1.036	986.1	22.85	
8.8	-3.0	5.180	0.3001	0.96	17.83	1.036	986.1	22.85	

Table 35: Borated ion chamber measurement data for the simplified BNCEFNT assembly: 5 x 5 cm^2 collimator with 1.0-cm tungsten filter using the 20 x 20 cm^2 standard therapy beam. Measurements made May, 2006.

Electrometer: Keithley 617 SN: 507703 Ion Chamber SN: 446 (Borated) High Voltage = +400V

Cint/X1= 5.483E+14 protons/X1

Depth (cm)	Off Axis (cm)	Charge (nC)	Monitor Units (MU)	Beam Time (min)	X1	X1 TPCX	Pressure (mB)	Temperature (˚C)	Notes
1.0	0.0	8.660	0.3002	1.01	17.88	1.035	986.0	23.07	22˚ IC holder
2.0	0.0	9.014	0.3010	1.01	17.88	1.035	986.0	23.07	
3.0	0.0	8.991	0.2999	1.00	17.80	1.035	986.0	23.07	
4.0	0.0	8.938	0.3019	1.01	17.93	1.035	986.0	23.07	
5.0	0.0	8.634	0.3013	1.01	17.89	1.035	985.9	23.07	
1.5	0.0	8.961	0.3027	1.02	17.97	1.035	985.9	23.07	
1.5	-2.5	8.084	0.3024	1.02	17.96	1.035	986.0	23.07	
1.5	-3.0	6.049	0.3020	1.02	17.93	1.035	986.0	23.07	
1.5	2.5	7.227	0.3021	1.02	17.94	1.035	986.0	23.07	
1.5	3.0	5.296	0.3020	1.02	17.93	1.035	986.0	23.07	
5.8	0.0	8.059	0.3000	0.96	17.8	1.036	986.1	22.85	Perpendicular
6.8	0.0	7.609	0.2992	0.96	17.75	1.036	986.1	22.82	IC holder
7.8	0.0	7.124	0.2995	0.95	17.77	1.036	986.3	22.82	
8.8	0.0	6.626	0.2993	0.96	17.76	1.036	986.2	22.82	
9.8	0.0	6.152	0.3006	0.97	17.84	1.036	986.1	22.82	
10.8	0.0	5.656	0.3001	0.96	17.8	1.036	986.2	22.82	
11.8	0.0	5.180	0.2992	0.99	17.75	1.036	986.2	22.82	
12.8	0.0	4.759	0.3005	0.99	17.83	1.036	986.2	22.82	
8.8	1.0	6.426	0.2992	0.99	17.76	1.036	986.3	22.82	
8.8	2.0	4.864	0.3000	0.99	17.8	1.036	986.4	22.82	
8.8	2.5	4.144	0.2994	0.99	17.77	1.036	986.5	22.82	
8.8	3.0	3.920	0.2999	0.98	17.79	1.036	986.3	22.82	
8.8	3.0	6.537	0.5005	1.65	29.69	1.036	986.4	22.82	

Table 36: Borated ion chamber measurement data for the simplified BNCEFNT assembly: 5 x 5 cm^2 collimator with 2.0-cm tungsten filter using the 20 x 20 cm^2 standard therapy beam. Measurements made May, 2006.

Electrometer: Keithley 617 SN: 507703 Ion Chamber SN: 446 (Borated) High Voltage = +400V

Cint/X1= 5.483E+14 protons/X1

Depth (cm)	Off Axis (cm)	Charge (nC)	Monitor Units (MU)	Beam Time (min)	X1	X1 TPCX	Pressure (mB)	Temperature (˚C)	Notes
1.0	0.0	7.602	0.3018	1.02	17.92	1.035	986.0	23.07	22˚ IC holder
2.0	0.0	7.900	0.2996	1.01	17.78	1.035	986.0	23.07	
3.0	0.0	7.935	0.2992	1.01	17.76	1.035	986.0	23.07	
4.0	0.0	7.854	0.2992	1.01	17.76	1.036	985.9	23.07	
5.0	0.0	7.622	0.2995	1.01	17.78	1.036	986.0	23.07	
3.0	-2.5	7.280	0.2991	1.02	17.75	1.036	986.0	23.07	
3.0	-3.0	5.921	0.3000	1.01	17.81	1.036	986.0	23.07	
3.0	2.5	6.566	0.3004	1.01	17.83	1.036	986.0	23.07	
3.0	3.0	5.210	0.2993	1.01	17.76	1.036	986.0	23.07	
5.8	0.0	9.656	0.4016	1.33	23.83	1.036	986.3	22.82	Perpendicular
6.8	0.0	9.093	0.4014	1.33	23.78	1.036	986.3	22.82	IC holder
7.8	0.0	8.490	0.4009	1.33	23.85	1.036	986.3	22.82	
8.8	0.0	7.889	0.4020	1.33	23.75	1.037	986.1	22.82	
9.8	0.0	7.237	0.4004	1.33	23.75	1.037	986.1	22.82	
10.8	0.0	6.834	0.4122	1.36	24.45	1.037	986.2	22.82	
11.8	0.0	6.538	0.4309	1.42	25.56	1.036	986.2	22.82	
12.8	0.0	6.246	0.4516	1.5	26.78	1.037	986.2	22.82	
8.8	1.0	7.808	0.4017	1.32	23.82	1.036	986.4	22.82	
8.8	2.0	7.571	0.4014	1.34	23.8	1.037	986.4	22.82	
8.8	2.5	7.054	0.4008	1.33	23.77	1.036	986.4	22.82	
8.8	3.0	6.601	0.4505	1.49	26.71	1.037	986.4	22.82	
8.8	-1.0	7.814	0.4021	1.33	23.84	1.037	986.4	22.82	
8.8	-2.0	7.582	0.4024	1.33	23.85	1.037	986.5	22.82	

Table 37: Borated ion chamber measurement data for the simplified BNCEFNT assembly: 5 x 5 cm^2 collimator with 3.0-cm tungsten filter using the 20 x 20 cm^2 standard therapy beam. Measurements made May, 2006.

Electrometer: Keithley 617 SN: 507703 Ion Chamber SN: 446 (Borated) High Voltage = +400V

Cint/X1= 5.483E+14 protons/X1

Depth (cm)	Off Axis (cm)	Charge (nC)	Monitor Units (MU)	Beam Time (min)	X1	X1 TPCX	Pressure (mB)	Temperature (˚C)	Notes
1.0	0.0	6.580	0.3002	0.99	17.82	1.036	986.0	23.07	22˚ IC holder
2.0	0.0	6.980	0.3000	1.01	17.78	1.036	986.0	23.07	
3.0	0.0	7.082	0.2996	1.01	17.75	1.036	986.0	23.07	
4.0	0.0	6.996	0.2992	1.01	17.78	1.036	985.6	23.07	
5.0	0.0	6.797	0.2997	1.01	17.78	1.036	985.6	23.07	
1.5	0.0	6.859	0.3001	1.01	17.80	1.036	985.6	23.07	
1.5	-2.5	6.072	0.2993	1.00	17.75	1.036	985.6	23.07	
1.5	-3.0	4.890	0.3003	1.01	17.81	1.036	985.6	23.07	
1.5	2.5	5.646	0.2994	1.00	17.76	1.036	985.6	23.07	
1.5	3.0	4.493	0.3003	1.00	17.81	1.036	985.6	23.07	Perpendicular
5.8	0.0	13.035	0.6003	1.93	36.02	1.025	988.5	23.05	IC holder
6.8	0.0	8.238	0.4015	1.26	24.09	1.024	988.6	23.05	
7.8	0.0	7.667	0.4014	1.26	24.08	1.025	988.6	23.05	
8.8	0.0	7.075	0.4007	1.26	24.04	1.025	988.6	23.05	
9.8	0.0	6.491	0.4007	1.25	24.04	1.025	988.5	23.05	
10.8	0.0	5.926	0.4006	1.25	24.03	1.025	988.6	23.05	
11.8	0.0	6.074	0.4504	1.41	27.02	1.025	988.7	23.05	
12.8	0.0	6.143	0.5014	1.58	30.07	1.025	988.8	23.05	

Table 38: Borated ion chamber measurement data for the simplified BNCEFNT assembly: 5 x 5 cm^2 collimator with 4.0-cm tungsten filter using the 20 x 20 cm^2 standard therapy beam. Measurements made May, 2006.

Electrometer: Keithley 617 SN: 507703 Ion Chamber SN: 446 (Borated) High Voltage = +400V

Cint/X1= 5.483E+14 protons/X1

Depth (cm)	Off Axis (cm)	Charge (nC)	Monitor Units (MU)	Beam Time (min)	X1	X1 TPCX	Pressure (mB)	Temperature (˚C)	Notes
1.0	0.0	5.855	0.3003	1.01	17.82	1.036	985.6	23.07	22˚ IC holder
2.0	0.0	6.238	0.2998	1.01	17.79	1.036	985.9	23.07	
3.0	0.0	6.345	0.2992	1.01	17.75	1.036	985.9	23.07	
4.0	0.0	6.327	0.3007	1.01	17.84	1.036	985.9	23.07	
5.0	0.0	6.114	0.2997	1.01	17.78	1.036	985.9	23.07	
3.0	-2.5	5.770	0.2994	1.00	17.76	1.037	985.5	23.07	
3.0	-3.0	4.903	0.2993	1.01	17.75	1.037	985.5	23.07	
3.0	2.5	5.371	0.3003	1.01	17.82	1.037	985.5	23.07	
3.0	3.0	4.519	0.3000	1.00	17.80	1.037	985.5	23.07	
5.8	0.0	9.654	0.5013	1.57	30.06	1.025	988.8	23.05	Perpendicular
6.8	0.0	9.116	0.5012	1.59	30.05	1.025	988.7	23.05	IC holder
7.8	0.0	8.451	0.5008	1.57	30.02	1.025	988.7	23.05	
8.8	0.0	7.772	0.5006	1.56	30.01	1.025	988.7	23.05	
9.8	0.0	7.119	0.5017	1.56	30.08	1.025	988.7	23.05	
10.8	0.0	6.469	0.5006	1.55	30.01	1.025	988.7	23.05	
11.8	0.0	6.461	0.5516	1.72	33.05	1.026	988.7	23.05	
12.8	0.0	6.378	0.6020	1.88	36.07	1.026	988.7	23.05	

Table 39: Borated ion chamber measurement data for the simplified BNCEFNT assembly: 5 x 5 cm^2 collimator with 5.0-cm tungsten filter using the 20 x 20 cm^2 standard therapy beam. Measurements made May, 2006.

Electrometer: Keithley 617 SN: 507703 Ion Chamber SN: 446 (norated) High Voltage = +400V

Cint/X1= 5.483E+14 protons/X1

Depth (cm)	Off Axis (cm)	Charge (nC)	Monitor Units (MU)	Beam Time (min)	X1	X1 TPCX	Pressure (mB)	Temperature (˚C)	Notes
1.0	0.0	5.206	0.2994	1.00	17.76	1.037	985.5	23.07	22˚ IC holder
2.0	0.0	5.631	0.3007	1.01	17.83	1.037	985.5	23.07	
3.0	0.0	5.770	0.3010	1.01	17.85	1.037	985.5	23.07	
4.0	0.0	5.730	0.3008	1.01	17.84	1.037	985.5	23.07	
5.0	0.0	5.543	0.3003	1.01	17.81	1.037	985.5	23.07	
1.5	1.0	5.397	0.2996	1.00	17.77	1.037	985.5	23.07	
1.5	2.0	5.162	0.2999	1.01	17.79	1.036	985.7	23.07	
1.5	2.5	4.814	0.2994	1.01	17.76	1.036	985.8	23.07	
1.5	3.0	4.051	0.2998	1.01	17.78	1.036	985.5	23.07	
1.5	-1.0	5.428	0.2997	0.98	17.77	1.036	985.5	23.07	
1.5	-2.0	5.191	0.301	1.01	17.85	1.036	985.4	23.07	
1.5	-2.5	5.386	0.3507	1.19	20.79	1.036	985.4	23.07	
3.0	1.0	5.685	0.2995	1.01	17.76	1.037	985.4	23.07	
3.0	2.0	5.485	0.2995	1.00	17.76	1.037	985.4	23.07	
3.0	2.5	5.204	0.3004	1.00	17.81	1.037	985.4	23.07	
3.0	3.0	4.493	0.2997	1.00	17.77	1.037	985.4	23.07	
3.0	-1.0	5.698	0.3009	1.01	17.84	1.037	985.4	23.07	
3.0	-2.0	6.348	0.3512	1.17	20.82	1.037	985.4	23.07	
3.0	-2.5	5.751	0.3516	1.18	20.84	1.037	985.4	23.07	
3.0	-3.0	4.937	0.3504	1.17	20.77	1.037	985.4	23.07	
5.8	0.0	7.697	0.4611	1.51	27.34	1.037	986.5	22.82	
6.8	0.0	7.200	0.4603	1.51	27.29	1.037	986.5	22.82	Perpendicular IC holder
7.8	0.0	6.645	0.4601	1.50	27.28	1.037	986.5	22.82	
8.8	0.0	6.229	0.4716	1.55	27.29	1.037	986.5	22.82	
8.8	0.0	6.367	0.4822	1.57	28.59	1.037	986.4	22.82	
9.8	0.0	5.770	0.4813	1.57	28.53	1.037	986.3	22.82	
10.8	0.0	5.424	0.5001	1.64	29.63	1.037	986.3	22.82	
11.8	0.0	5.187	0.5396	1.72	31.38	1.037	986.0	22.82	
12.8	0.0	6.169	0.7010	2.29	41.54	1.038	986.0	22.82	
9.0	1.0	6.130	0.4827	1.57	28.59	1.038	986.0	22.82	
9.0	1.5	5.698	0.4797	1.57	28.42	1.038	986.0	22.82	
9.0	2.0	5.270	0.5012	1.63	29.69	1.038	986.0	22.82	
9.0	2.5	5.820	0.6000	1.95	35.54	1.038	986.0	22.82	
9.0	3.0	6.476	0.7021	2.29	41.58	1.038	986.0	22.82	
9.0	-1.0	6.393	0.4800	1.56	28.43	1.038	986.0	22.82	
9.0	-1.5	6.523	0.4899	1.60	29.01	1.038	986.0	22.82	
9.0	-2.0	6.771	0.5118	1.67	30.3	1.038	986.0	22.82	
9.0	-2.5	7.244	0.5528	1.80	32.72	1.038	986.0	22.82	
9.0	-3.0	9.000	0.7012	2.28	41.5	1.038	986.0	22.82	
1.0	0.0	4.814	0.3006	0.98	17.81	1.037	985.2	23.02	Graphite reflector on both sides removed
2.0	0.0	8.510	0.5006	1.66	29.64	1.037	985.2	23.02	
3.0	0.0	8.622	0.5001	1.67	29.65	1.037	985.2	23.02	
4.0	0.0	8.514	0.5005	1.67	29.66	1.037	985.2	23.02	
5.0	0.0	8.208	0.501	1.67	29.69	1.037	985.0	23.02	

C.3 Comparison of neutron spectra before and after 5.0-cm tungsten filter in the simplified BNCEFNT assembly

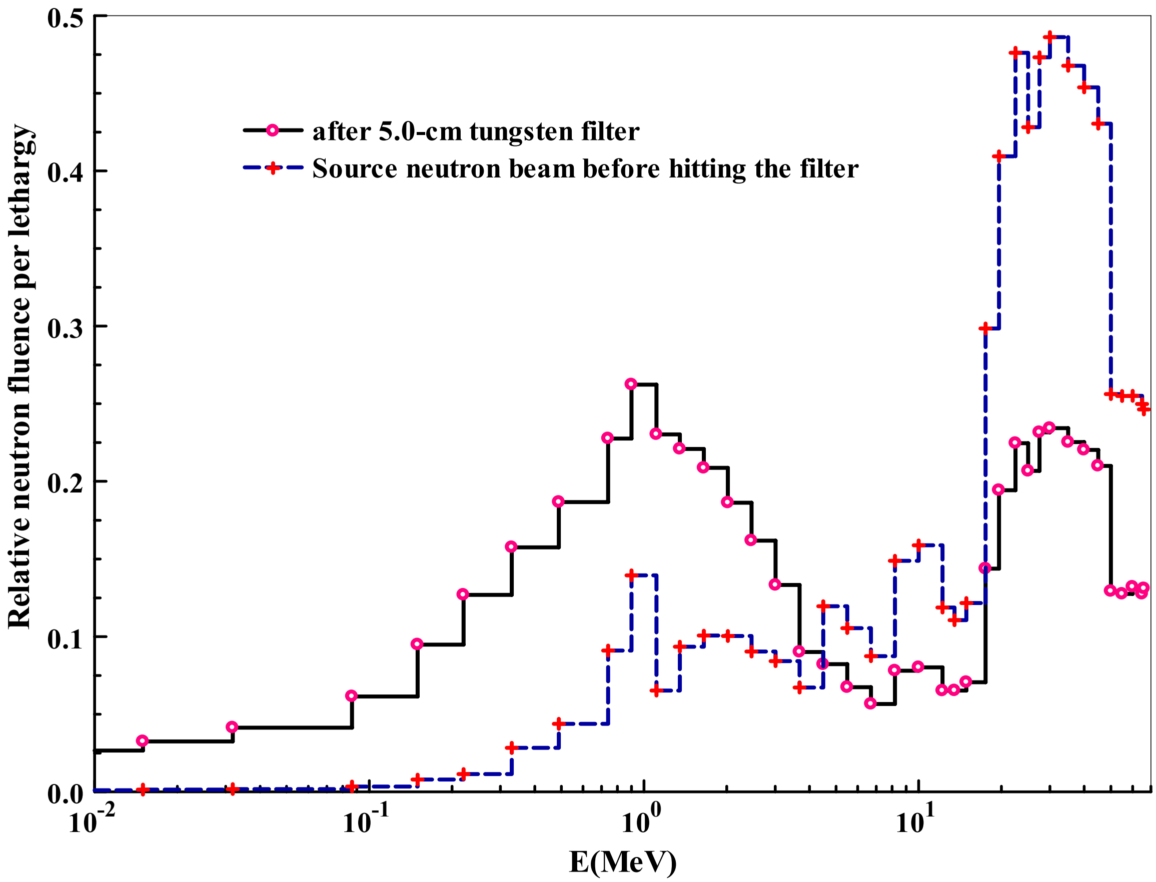

Figure 65: Comparison of source neutron spectrum and neutron spectrum after 5.0-cm tungsten filter in the simplified BNCEFNT assembly (lethargy).

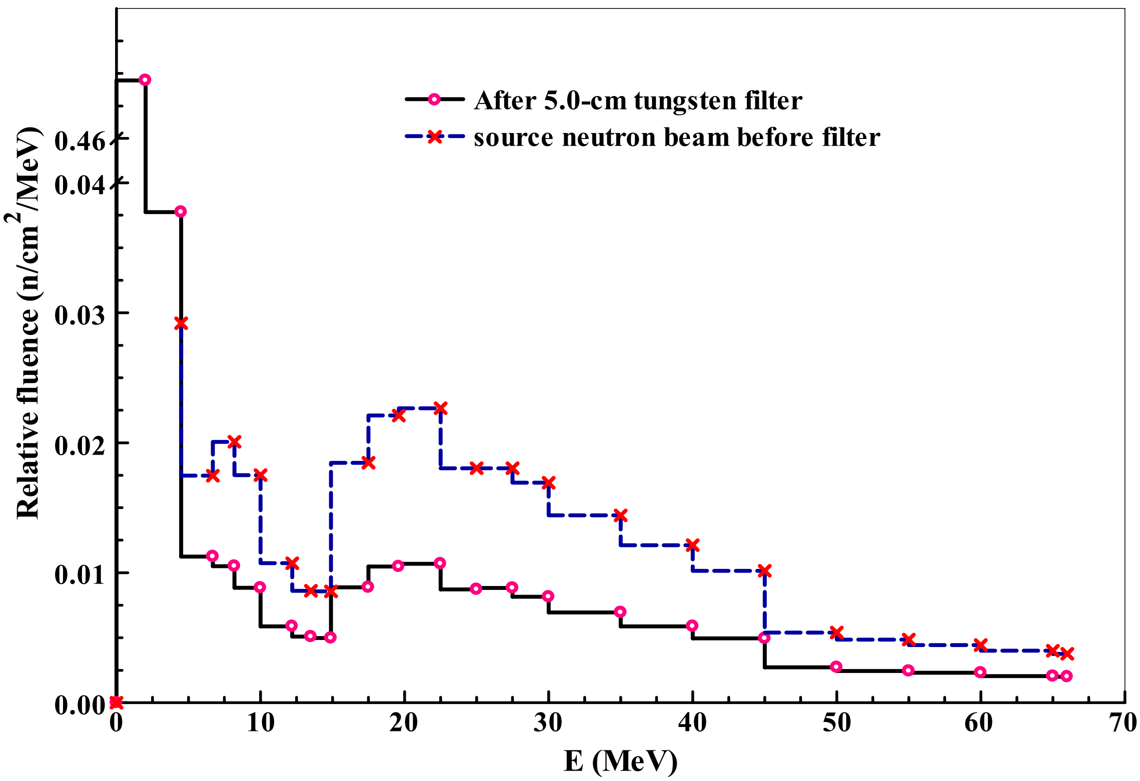

Figure 66: Comparison of source neutron spectrum and neutron spectrum after 5.0-cm tungsten filter in the simplified BNCEFNT assembly (linear). Notice that the energy intervals are not evenly divided, and the area under the curve represents the fraction of neutron fluence in each energy group.

APPENDIX D

SELECTED MCNPX AND MCNP5 INPUT FILES

D1. MCNPX input file

D1.1 Neutron source calculation model

```
Fermi Neutron Therapy Target Model - To calculate source neutron spectrum
 c Modified from Sweezy's code by changing cell 12 and 113 to VOID.  And
 c  Corrected his SDEF card by adding DIR=1
 c    Be Target
 1     1 -1.802  8 -9 -22                  $Be Target
 2     2 -19.32  9 -10 -22               $Gold Disk
 3     3 -2.7  (7 42 -11 -26 22):(-22 10 -11):(6 -7 23 -26):(41 -6 23 -24):
             (1 -41 23 -25) $Target Housing
 4     4 -4.5  (21 -22 6 -8):(6 -7 22 -23)  $Clamp
 5     5 -16.6  20 -23 4 -6                   $Proton Collimator
 6     6 -1  -42                                    $Water Cooling Channel
 7     7 -7.87  5 -12 27 -28                 $ Targe Housing collar
 8     8 -7.87  12 -13 40 -28               $Primary Collimator
 9     3 -2.7  (104 -105 -107):(-104 -107 106 100):(100 -103 107 -108):
             (101 -102 -106)  $ Transmission Chamber Housing
 10    3 -2.7 (110 -111 -116):(112 -113 -116):(114 -115 -116)   $High Voltage
Plate
 11    11 -2.7 (117 -118 -116):(119 -120 -116):(121 -122 -116):
             (123 -124 -116):(125 -126 -116):(127 -128 -116) $Signal Plates
 12    0 130 -131 132 -133                               $ Void the Neutron
Entrance
 c
 c Area's of Vacuum or Air tbat are inside of a part
 100   0   (1 -4 -23):(4 -6 -20):(6 -8 -21)       $Vacuum Chamber Before Target
 108   100 -0.001293  (-22 11 -12):(12 -13 -40):(100 -101 -106) $Air in Primary
C
 109   100 -0.001293  102 -104 -106 #10 #11
 112   100 -0.001293  (105 -130 -132)                    $Air in Neutron
Entrance
 113   0  (130 -131 -132)                     $Neutron Entrance Port set to
void
 c Area's of Vacuum or Air that are outside of a part
 203   100 -0.001293  (11 -12 22 -27):(-27 26 -11 6):(-6 -27 24 3):
                      (-3 24 41 -25):(25 -3 1 -27):(1 -5 27 -28)  $Air Around
Tar
 c                     Note Change the last -28 to incorporate a larger radius
 212   100 -0.001293  (132 -130 105 -133):(-105 103 107 -133):
                      (-103 100 108 -133):(-100 1 28 -133) $Air outside of
Target
 c
 1000  0 -1:131:133

 1        pz    -3.9243 $Target Housing Flange Upsteam Face (3)
 2        pz    -3.3655 $Target Housing slope point (not used)
 3        pz    -3.1115 $Target Housing slope point (not used)
 4        pz   -2.16408 $Proton Collimator Front Face (5)
 5        pz   -1.82118 $Target Housing Colliar Front Face (7)
 6        pz    -1.7018 $Target Housing Front Face        (3)
 7        pz    -1.3843 $Clamp (4) Downstream Face        (4)
 8        pz    -1.1049 $Target Upstream Face             (1)
 9        pz     1.1049 $Target Downstream Face           (1)
 10        pz     1.1557 $Gold Disk (2) Downstream Face    (2)
```

```
 11         pz     1.4732 $Target Housing (3) Downstream Face
 12         pz    1.67132 $Primary Collimator (8) Upstream Face
 13         pz   14.37132 $Primary Collimator (8) Downstream Face
 20         cz    0.79375 $Proton Collimator (5) Inter-Radius
 21         cz     1.1938 $Clamp (4) inter-radius
 22         cz       1.27 $Clamp (4) Collar outer-radius/ Target Radius
 23         cz      2.225 $Proton Collimator (5) & (4) outer-radius
 24         cz       2.54 $Target Housing (3) Intermediate Radius
 25         cz      3.302 $Target Housing (3) Flange outerradius
 26         cz     4.7625 $Target Housing (3) Outer Radius
 27         cz       5.08 $Target Housing Collar (7) Inter Radius
 28         cz      10.16 $Primary Collimator (8) & (7) outerradius
 40         kz  -0.027312  0.0262993          1 $Primary Collimator Opening (8)
 c 41         kz   -0.89167    58.0644         -1 $Target Housing Flange
Downstrea
 41          z     -3.3655 3.302 -3.1115 2.54

one-sheet cone
 42         tz   0.2032 0 0 2.54 0.3175 0.3175    $Outside of Water cooling
channe
 c
 c Aluminium Transmission Chamber (9)
 100        pz  14.37132              $ Chamber Flange Upstream Face
 101        pz  14.51864              $ Chamber Upsteam Face Outside wall
 102        pz  14.59484              $ Chamber Upsteam Face Inside Wall
 103        pz  15.48384              $ Chamber Flange Downstream Face
 104        pz  17.78                 $ Chamber Downstream Face Inside Wall
 105        pz  17.78762              $ Chamber Downstream Face Outside Wall
 106        cz  7.3025                $ Chamber Inside Surface
 107        cz  7.62                  $ Chamber Outside Surface
 108        cz  8.89                  $ Chamber Flange Outside Surface
 c
 c Aluminium Transmission Chamber High Voltage Plates (10)
 110        pz  14.87678
 111        pz  14.95552
 112        pz  15.79626
 113        pz  15.875
 114        pz  16.96974
 115        pz  17.04848
 116        cz  5.715
 c
 c Aluminium Transmission Chamber Signal Plates (11)
 117        pz 14.95806
 118        pz 14.98346
 119        pz 15.23492
 120        pz 15.26032
 121        pz 15.51686
 122        pz 15.54226
 123        pz 16.129
 124        pz 16.1544
 125        pz 16.4084
 126        pz 16.4338
 127        pz 16.6878
 128        pz 16.7132
 c
 c Starting Collimation
 c First Neutron Entrance Port (12)
 130  pz 24.3205                  $Neutron Entrance Port Upstream Wall (12)
 131  pz 31.3055                  $Neutron Entrance Port Downstream Wall (12)
 132  z  24.3205 4.24688 31.3055 5.1689   $Inside of Neutron Entrance Port (12)
 133  cz 15.24                    $Outside Radius of Neutron Entrance Port (12)
 c
 c Tally Surface segments in degrees as seen from center of target @ 31.3055 cm
```

```
9000 cz 0.54644 $1 deg
9001 cz 1.09321 $2 deg
9002 cz 1.64065 $3 deg
9003 cz 2.18909 $4 deg
9004 cz 2.73888 $5 deg
9005 cz 3.16890 $5.78 deg

c ********IMPORTANCE REGIONS****************
c            1   2   3   4   5   6   7   8   9
c       10  11  12
c      100                             108 109
c             112 113
c                 203
c             212
c     1000
imp:n        1   1   0.5   1   1   1   1   0.5   1       $1-9
         1   1   0                                   $10-19
         1                               1   1       $100-109
                 1   1                               $110-119
                     1                               $200-209
                 1                                   $210-219
         0                                           $1000
imp:p        1   1   1   1   1   1   1   1   1       $1-9
         1   1   0                                   $10-19
         1                               1   1       $100-109
                 1   1                               $110-119
                     1                               $200-209
                 1                                   $210-219
         0                                           $1000
imp:h        1   1   0.5   1   1   1   1   0.5   0.5       $1-9
         1   1   0                                   $10-19
         1                               1   1       $100-109
                 1   1                               $110-119
                     1                               $200-209
                 1                                   $210-219
         0                                           $1000
c *************************************************
mode n p h
c *************SOURCE DEF**************************
sdef sur=8 erg=69 rad=d1 vec=0 0 1 dir=1 pos= 0 0 -1.1049 par=9
si1 0.25
c *************************************************
c
c *************MATERIALS***************************
m1   4009.24c  1         $Beryllium
c
m2   79197.60c 1         $Gold
c
m3                       $ 6061-T6 Aluminum
     13027.24c  -0.995 $ Al
     12000.60c  -0.01 $ Mg
     14028.24c  -0.00551  14029.24c -0.000289 14030.24c -0.000199 $ Si -0.006
     29063.24c  -0.00137  29065.24c -0.000630                     $ Cu -0.002
     24050.24c  -0.000102 24052.24c -0.002055 24053.24c -0.000237
     24054.24c -0.000060                                           $ Cr -0.003
c
m4   22000.60c         1 $ Titanium
c
m5   73181.60c         1 $ Tantalum
c
m6                       $ Water
     1001.24c          1.9996886 $ H-1 0.9998443 % of H
     1002.24c          3.114e-4  $ H-2 0.0001557 % of H
```

```
     8016.24c          1         $ O
c
m7                      $ 1010-1020 Steel
     26054.24c -0.08178 26056.24c -0.91435 26057.24c -0.02181
      6000.24c    -0.001 $ C
     25055.60c    -0.004 $ Mn
c
m8                     $ 1010-1020 Steel & Tungsten
     26054.24c -0.08001 26056.24c -0.89551 26057.24c -0.02136
     74182.24c -0.0045566 74183.24c -0.0024866
     74184.24c -0.0053649 74186.24c -0.0050694                $ W - Tungsten
     24050.24c  -0.000273 24052.24c -0.005479 24053.24c -0.000633
     24054.24c -0.000161                                      $ Cr -0.008
c
m11                      $ 2024-T4 Aluminum
     13027.24c    -0.934                         $ Al
     29063.24c -0.0308264 29065.24c -0.1417334   $ Cu  -0.045
     12000.60c    -0.015                         $ Mg
     25055.60c    -0.006                         $ Mn
c
m100                    $ Air - density= -.001293
     7014.24c 0.7843     $ N
     8016.24c 0.2109     $ O
     6000.24c 0.0001     $ C
c
c
c ************TALLY ENERGY STRUCTURE**************
E0 1e-5 1e-4 1e-3 1e-2 8i 1e-1 8i 1 8i 10 8i 100
c ************TALLIES*****************************
F1:n 131
FC1 Neutron tally as function of energy on surface 131
c
F11:n 131
E11 1e-5 100
FS11 -9000 -9001 -9002 -9003 -9004 -9005
SD11 9.56960e-4 2.87059e-3 4.78334e-3 6.69461e-3 8.6039e-3 8.0348e-3 1
FC11 Neutron tally as function of angle.
c ***********************************************
c
SSW 130 (113) PTY=N
phys:n 71 j 0 -1 20 0 0
cut:n j 1e-6 j j j
cut:h j 1.0 j j j
prdmp j j j 3
CTME 1200
```

D2.2 10 x10 cm^2 standard treatment beam model

```
    Fermilab NTF Collimator w 10x10 standard inserts.
c
c CELLS
12 1 -7.87 200 -202 400 -302
13 1 -7.87 202 401 300 -301
14 1 -7.87 (-203 202 301 -304):(302 -304 200 -202)
15 2 -1.37 (203 402 -304 301):(-402 303 -304 -208)
19 3 -2.699 -304 303 208 -209
20 3 -2.699 304 -305 207 -209
21 1 -7.87 306 -309 205 -206
22 1 -7.87 304 -306 200 -206
24 1 -7.87 200 -201 306 -309
25 5 -3.53 306 -307 201 -205
26 5 -3.53 308 -309 201 -204
27 4 -2.35 308 -309 204 -205
28 1 -7.87 201 -205 307 -308
c Phantom set to Air
100 6 -0.001293 -310 210 -211 u=3 $Tally Cell
101 6 -0.001293 320 -321 210 -211 u=3 $Tally Cell
102 6 -0.001293 322 -323 210 -211 u=3 $Tally Cell
115 6 -0.001293  -210:211:(310 -320):(321 -322):323 u=3 $Remaining Phantom
c
116 0 -311 227 -228 fill=3 $Phantom
c
117 6 -.001293 (209 -227 -309):(207 -209 305 -309):(206 -207 304 -309):
               (227 -228 311 -309):(228 -226 -309) $ Air
c
200 0 230 -200 -309 $Source Region
c
300 0 (200 -202 -400):(202 -203 -301 #13):(203 -209 -303 #15) fill=1 $Filter
301 2 -1.37 (604 -605 610):(605 -606 601):(606 -607 611):(607 -608 602):
            (608 -609 612) u=1 $Benelox Removable Liner
302 8 -1.50 ((604 -605 -610):(605 -606 -601):(606 -607 -611):(607 -608 -602):
            (608 -609 -612)) 603 u=1 $Concrete/Poly Removable Liner
303 6 -0.001293 (604 -609 -603):(613 -202) u=1
c
1000 0 -230:226:309 $Outside universe

c SURFACES
c
200 pz 24.3205
201 pz 25.5905
202 pz 31.3055
203 pz 60.198
204 pz 97.028
205 pz 103.378
206 pz 104.648
207 pz 107.188
208 pz 109.093
209 pz 109.728
c
210 pz 176
211 pz 177
c
226 pz 230
c
c ***CHANGE to move phantom
227 pz 175
228 pz 211.6
```

```
c
230 pz -1
c
300 cz 7.62
301 cz 12.7
302 cz 15.24
303 cz 15.875
304 cz 22.225
305 cz 24.13
306 cz 25.4
307 cz 31.59125
308 cz 34.29
309 cz 76.2
310 cz 1
311 cz 22.88
c
320 cz 4.75
321 cz 5.25
322 cz 9.75
323 cz 10.25
c
400 z 24.3205 4.24688 31.3055 5.1689
401 z 43.7134 7.62 48.768 12.7
402 z 75.438 12.7 79.248 15.875
c
601 z  52.578 4.445 56.388 5.715
602 z  75.438 5.715 79.248 6.985
c
c Inside of collimator - sized to have equivalent diameter of 10x10 beam stop.
603 z  31.3055 0.930 109.728 3.258
c
604 pz 31.3055
605 pz 52.578
606 pz 53.388
607 pz 75.438
608 pz 79.248
609 pz 120
610 cz 4.445
611 cz 5.715
612 cz 6.985
613 pz 0
c

c tr1 0 0 24.3205
c *************IMPORTANCES************************
c         12  13  14  15  19  20  21  22  24  25
c         26  27  28
c         100 101 102
c         115 116 117
c         200
c         300 301 302 303
c         1000
imp:n     1   1   1   1   1   1   1   1   1   1
          1   1   1
          1   1   1
          1   1   1
          1
          1   1   1   1
          0
imp:p     1   1   1   1   1   1   1   1   1   1
          1   1   1
          1   1   1
          1   1   1
```

```
         1
         1   1   1   1
         0
imp:h    1   1   1   1   1   1   1   1   1   1
         1   1   1
         1   1   1
         1   1   1
         1
         1   1   1   1
         0
imp:e    0   0   0   0   0   0   0   0   0   0
         0   0   0
         1   1   1
         1   1   1
         0
         0   0   0   0
         0
imp:a    0   0   0   0   0   0   0   0   0   0
         0   0   0
         1   1   1
         1   1   1
         0
         0   0   0   0
         0
imp:d    0   0   0   0   0   0   0   0   0   0
         0   0   0
         1   1   1
         1   1   1
         0
         0   0   0   0
         0
imp:t    0   0   0   0   0   0   0   0   0   0
         0   0   0
         1   1   1
         1   1   1
         0
         0   0   0   0
         0
imp:s    0   0   0   0   0   0   0   0   0   0
         0   0   0
         1   1   1
         1   1   1
         0
         0   0   0   0
         0
c ************************************************
mode n p h e d t s a
c ************SOURCE DEF*************************
SDEF pos= 0 0 24.3205 sur=200 dir=d1 vec=0 0 1
     rad=d2 erg fdir d3
Si1 0 0.766    0.866    0.991   0.999   1.0
sp1 0 0.016868 0.062467 0.53666 0.33367 0.050335
si2    4.24688
ds3 s 4 5 6 7 8
# si0      sp4         sp5           sp6        sp7        sp8
1.00E-05 0.0000E+00 5.2538E-07   3.3031E-06 0.0000E+00 0.0000E+00
1.00E-04 6.1381E-07 7.3765E-06   2.6295E-05 4.0030E-06 0.0000E+00
1.00E-03 1.0365E-05 3.6884E-05   1.7612E-04 3.2848E-05 2.5300E-06
1.00E-02 1.5590E-04 4.7790E-04   1.7679E-03 2.1207E-04 3.3084E-05
1.90E-02 6.7473E-05 2.4887E-04   1.0583E-03 2.2615E-04 3.1562E-05
2.80E-02 1.0251E-04 5.8347E-04   3.3660E-03 6.9145E-04 7.4531E-05
3.70E-02 6.3123E-05 1.5630E-04   4.9629E-04 8.8040E-05 1.6123E-05
4.60E-02 8.3844E-05 2.7879E-04   1.1680E-03 2.1383E-04 3.4286E-05
```

```
5.50E-02 8.2559E-05 2.8929E-04   1.2017E-03 2.2869E-04 4.0206E-05
6.40E-02 1.0318E-04 3.6976E-04   1.4423E-03 2.8620E-04 4.0410E-05
7.30E-02 1.3553E-04 5.5712E-04   2.6536E-03 4.9670E-04 7.7955E-05
8.20E-02 1.6422E-04 3.8229E-04   1.9109E-03 3.4672E-04 7.3713E-05
9.10E-02 6.7815E-05 2.0296E-04   8.9114E-04 1.5583E-04 3.2857E-05
1.00E-01 7.3264E-05 2.0604E-04   9.9176E-04 1.6933E-04 2.4154E-05
1.90E-01 1.2515E-03 3.8771E-03   1.9801E-02 4.1875E-03 5.3799E-04
2.80E-01 9.5044E-04 3.1914E-03   1.6299E-02 3.4632E-03 4.6618E-04
3.70E-01 1.2152E-03 4.1743E-03   2.2296E-02 4.6575E-03 6.1054E-04
4.60E-01 9.5745E-04 3.0331E-03   1.5078E-02 3.1497E-03 4.3781E-04
5.50E-01 9.5612E-04 3.3023E-03   1.5472E-02 3.3853E-03 4.5884E-04
6.40E-01 1.2117E-03 4.0752E-03   2.0916E-02 4.3245E-03 5.6796E-04
7.30E-01 8.7505E-04 3.2507E-03   1.8314E-02 3.8109E-03 5.4318E-04
8.20E-01 7.5467E-04 2.4727E-03   1.2013E-02 2.5783E-03 3.5385E-04
9.10E-01 6.1951E-04 2.2228E-03   1.2492E-02 2.9975E-03 4.0873E-04
1.00E+00 4.9143E-04 2.1497E-03   1.2876E-02 3.2528E-03 4.8308E-04
1.90E+00 3.1760E-03 1.2211E-02   7.4837E-02 2.2463E-02 3.0212E-03
2.80E+00 1.2372E-03 5.0355E-03   3.5927E-02 1.3829E-02 2.0106E-03
3.70E+00 5.6907E-04 2.3749E-03   2.1024E-02 9.6944E-03 1.4195E-03
4.60E+00 3.3170E-04 1.4425E-03   1.5046E-02 8.3997E-03 1.2384E-03
5.50E+00 1.8680E-04 9.1799E-04   1.2088E-02 7.4178E-03 1.1535E-03
6.40E+00 1.4347E-04 6.1411E-04   1.0272E-02 6.9033E-03 9.7869E-04
7.30E+00 8.8363E-05 4.7921E-04   9.0870E-03 6.3086E-03 9.9166E-04
8.20E+00 7.6872E-05 3.5122E-04   8.2054E-03 6.0328E-03 9.2154E-04
9.10E+00 5.6953E-05 2.8812E-04   7.4916E-03 5.8717E-03 8.8488E-04
1.00E+01 5.3195E-05 2.5295E-04   6.7617E-03 5.4780E-03 8.3688E-04
1.38E+01 1.7216E-04 7.1528E-04   2.3997E-02 2.1413E-02 3.2138E-03
1.75E+01 1.0850E-04 5.8977E-04   2.1307E-02 2.1367E-02 3.2399E-03
2.13E+01 9.0139E-05 4.4138E-04   1.9973E-02 2.2590E-02 3.4526E-03
2.50E+01 3.5289E-05 2.7924E-04   1.7341E-02 2.1209E-02 3.3110E-03
2.88E+01 3.2220E-05 2.1634E-04   1.4824E-02 1.9814E-02 2.9366E-03
3.25E+01 2.4549E-05 1.6724E-04   1.2816E-02 1.7477E-02 2.7694E-03
3.63E+01 2.4549E-05 1.2888E-04   1.0901E-02 1.6086E-02 2.6190E-03
4.00E+01 1.6877E-05 1.1814E-04   8.9526E-03 1.4551E-02 2.2953E-03
4.38E+01 2.3014E-05 8.7455E-05   7.4091E-03 1.3011E-02 2.1511E-03
4.75E+01 9.2058E-06 6.9043E-05   5.5986E-03 1.1091E-02 1.8120E-03
5.13E+01 6.1372E-06 6.9043E-05   4.2914E-03 8.9311E-03 1.4069E-03
5.50E+01 7.6715E-06 3.8357E-05   2.8354E-03 6.8537E-03 1.1338E-03
5.88E+01 1.5343E-06 1.8412E-05   1.7875E-03 4.6781E-03 7.1192E-04
6.25E+01 1.5343E-06 1.3809E-05   9.2671E-04 2.5930E-03 3.9125E-04
6.63E+01 1.5343E-06 0.0000E+00   2.4549E-04 6.4747E-04 8.4386E-05
7.00E+01 0.0000E+00 0.0000E+00   0.0000E+00 3.0686E-06 0.0000E+00
C SSR OLD 130 NEW 200
c sdef erg=d2 dir=d3 vec=0 0 1 pos=0 0 0 par=1
c si2  1.00000e-05 1.00000e-04 1.00000e-03 1.00000e-02 2.00000e-02 3.00000e-02
c     4.00000e-02 5.00000e-02 6.00000e-02 7.00000e-02 8.00000e-02 9.00000e-02
c     1.00000e-01 2.00000e-01 3.00000e-01 4.00000e-01 5.00000e-01 6.00000e-01
c     7.00000e-01 8.00000e-01 9.00000e-01 1.00000e+00 2.00000e+00 3.00000e+00
c     4.00000e+00 5.00000e+00 6.00000e+00 7.00000e+00 8.00000e+00 9.00000e+00
c     1.00000e+01 2.00000e+01 3.00000e+01 4.00000e+01 5.00000e+01 6.00000e+01
c     7.00000e+01
c sp2  0.00000e+00 1.15826e-07 9.56867e-07 8.15276e-06 6.54268e-06 2.91185e-05
c     3.59253e-06 7.84624e-06 7.55651e-06 1.61060e-05 1.28825e-05 1.48511e-05
c     5.70329e-06 1.55085e-04 1.48989e-04 2.13710e-04 1.14516e-04 1.38239e-04
c     2.00873e-04 1.08475e-04 9.69866e-05 1.07365e-04 5.23179e-04 1.98955e-04
c     1.05525e-04 6.76163e-05 5.34447e-05 4.83748e-05 3.89503e-05 4.02425e-05
c     4.04447e-05 3.07750e-04 3.44128e-04 2.34320e-04 1.54216e-04 7.21327e-05
c     1.09715e-05
c si3  -1 .984808   .996195   .997564    .998630    .999391    .999848
c      1
c sp3   0 0         2.97998E-3 1.68559e-2 1.74814e-2 1.93356e-2 1.31190e-2
c      1.90276e-2
c ************MATERIALS*********************
```

```
m1                       $ 1010-1020 Steel den=
      26054.24c 0.0581
      26056.24c 0.9175
      26057.24c 0.0215
m2                          $ Benelex
      6000.24c  6                         $ C
      1001.24c  9.998443 1002.24c .001557  $ H
      8016.24c  5                         $ O
m3                          $Aluminum
      13027.24c 1
m4                     $ Ord. Concrete den=2.35 see Chilton p.374
      1001.24c -1.2998e-2 1002.24c -2.0241e-6
      8016.24c -1.165
      13027.24c -0.153
      14028.24c -6.7973e-1  14029.24c -3.4416e-2 14030.24c -2.2854e-2
      20000.24c -.194
      26054.24c -5.81e-2 26056.24c -2.6608e-2 26057.24c -6.235e-4
m5                     $ Magnetite Concrete
      1001.24c -1.0998e-2 1002.24c -1.7127e-6
      8016.24c -1.168
      13027.24c -0.116
      14028.24c -8.854e-2 14029.24c -4.483e-3 14030.24c -2.9769e-3
      20000.24c -.251
      24050.24c -9.0815e-3 24052.24c -1.7512e-1 24053.24c -1.9856e-2
      24054.24c -4.9422e-3
      26054.24c -9.7782e-2 26056.24c -1.5442 26057.24c -3.6185e-2
c
m6   7014.24c .7843 8016.24c .2109
     6000.24c .0001  $ Air @ STP
c
m7                     $ Water
      1001.24c     2 $ H
      8016.24c     1 $ O
mt7   lwtr.01t
c
m8     $ Concrete w/ Poly den=1.5 see Chilton p.374 and Fermilab
      1001.24c -0.21697 1002.24c -3.3787e-5
      6000.24c -1.2241
      8016.24c -1.165
      13027.24c -0.153
      14028.24c -6.7973e-1  14029.24c -3.4416e-2 14030.24c -2.2854e-2
c
m9    $ A-150
      1001.24c  -.102
      6000.24c  -.768
      8016.24c  -.059
      7014.24c  -.036
      20000.24c -.018
      20000.24c -.194
      26054.24c -5.81e-2 26056.24c -2.6608e-2 26057.24c -6.235e-4
mt8   poly.01t
c
m999  5010.50c    1 $ B-10
c ******************************************
c
c ************TALLIES*****************************
f4:n 100 101 102
FC4 Neutron tally as function of energy
# E4
1e-10
4.14e-7
1.12e-6
2.38e-6
```

```
5.04e-6
1.07e-5
2.26e-5
1.01e-4
4.54e-4
1.58e-3
3.35e-3
7.10e-3
1.50e-2
3.18e-2
8.65e-2
0.15
0.224
0.334
0.498
0.743
0.906
1.11
1.35
1.65
2.02
2.46
3.01
3.68
4.49
5.49
6.70
8.19
10.0
12.2
13.5
14.9
17.5
19.6
22.5
25
27.5
30
35
40
45
50
55
60
65
70
80
90
100
110
c
c f14:n 100 101 102
c FM14  1.35234e-7 999 207 $Convert to MeV/g for B-10 neutron capture
c Per ppm Boron.  Using 1.04 g/cc and 2.34 MeV per capture.
c
c +f6 100 101 102
c ********************************************
phys:n 71 j 71
prdmp j j j 3
print
nps 10000
tmesh
cmesh3 total
```

```
cora3 0.001 0.25 0.5 1 1.5 2 3 4 5 6 7 8 9 10 11 12 13 14 15
corb3  175 175.1 175.5 176 176.5 177 178 179 181 182 183 184 185
       186 187 188 189 191 193 195 197 199 201 203 205 207 209
       211 213 215
corc3 360
endmd
```

D1.3 Response matrix calculations

```
  c     This is the model for the calculation of response function of aluminum
  c     and copper foils behind moderator box. Thickness change is by changing
  c     material and density of the cell card
  c    This is for Plate # 12 inserted in the box, total 3.6 cm PMMA moderation
    1     1   -8.96 -14 4 -12                          $    Copper Foil
    2     2 -2.6987 12 -13 -14                         $    Al Foil
    3     3   -1.19 1 -2 -17 18 -21 22                 $    Front Wall
    4     3   -1.19 2 -5 18 -17 -21 22                 $    #12 plate
    5     6 -0.001293 5 -6 18 -17 -21 22               $    #7 plate
    6     6 -0.001293 6 -7 18 -17 -21 22               $    #11
    7     6 -0.001293 7 -8 18 -17 -21 22               $    #9 plate
    8     6 -0.001293 8 -9 18 -17 -21 22               $    #10
    9     6 -0.001293 9 -10 18 -17 -21 22              $    #8+6+5
   10     6 -0.001293 10 -11 18 -17 -21 22             $     #1+2+3+4
   11     6 -0.001293 11 -3 -17 18 -21 22              $    Air gap
   12     3   -1.19 3 -4 18 -17 -21 22                 $    Back wall
   13     3   -1.19 (1 -4 -15 16 20 -19 )(-22 :21 :17 :-18 )      $ side wall
   23     6 -0.001293 4 -13 -15 16 14 20 -19
   24     6 -0.001293 23 -1 -15 16 20 -19
   25     0         -23 :13 :15 :-16 :-20 :19

    1        px 0
    2        px 0.6
    3        px 14.4
    4        px 15
    5        px 3          $4Ca #12 plate
    6        px 4.2        $5ca #12+7
    7        px 6.6        $7ca #12+7+11
    8        px 8.4        $8ca #12+7+11+9
    9        px 10.2       $9ca #12+7+11+9+10
   10        px 12.5       $10ca #12+7+11+9+10+8+6+5
   11        px 13.9       $11ca # all plates
   12        px 15.05
   13        px 15.15
   14        cx 0.84667
   15        py 15
   16        py -15
   17        py 14.4
   18        py -14.4
   19        pz 15.5
   20        pz -15.5
   21        pz 14.9
   22        pz -14.9
   23        px -80

mode  n
imp:n 1 14r 0
c Material Cards
m1    29063.24c        0.6917 $ Copper
      29065.24c        0.3083
m2    13027.24c            -1 $Al foil
```

```
m3    1001.24c       -0.080538 $ PolymethylMethaCralate
      6000.24c       -0.599848 8016.24c       -0.319614
m4    29063.24c             -1 $Cu-63
m5    29065.24c             -1 $Cu-65
m6    7014.24c      -0.7653795 $ Air
      8016.24c      -0.2346205
c
mt3 poly.01t
c Source definition, the measured neutron spectrum from Chapter 4
sdef par=1 x=-80 y=d1 z=d2 erg=d3 dir=1 vec 1 0 0 sur=23
si1 -5 5
sp1  0 1
si2 -5 5
sp2  0 1
# SI3          SP3         sb3
1.00e-10      0.00E+00      0
4.14e-07      8.32E-05     1
1.12e-06      3.37E-05     1
2.38e-06      4.46E-05     1
5.04e-06      2.36E-05     1
1.07e-05      3.82E-05     1
2.26e-05      4.50E-05     1
1.01e-04      4.50E-05     1
4.54e-04      1.13E-04     1
1.58e-03      2.00E-04     10
3.35e-03      7.07E-05     10
7.10e-03      2.02E-04     10
1.50e-02      2.87E-04     10
3.18e-02      9.21E-04     10
8.65e-02      2.07E-03     10
1.50e-01      3.12E-03     10
2.24e-01      3.62E-03     10
3.34e-01      5.69E-03     10
4.98e-01      8.49E-03     10
7.43e-01      1.38E-02     10
9.06e-01      7.32E-03     10
1.11e+00      1.06E-02     1
1.35e+00      1.17E-02     1
1.65e+00      1.36E-02     1
2.02e+00      1.51E-02     40
2.46e+00      1.71E-02     10
3.01e+00      1.71E-02     1
3.68e+00      1.81E-02     1
4.49e+00      2.13E-02     1
5.49e+00      2.46E-02     1
6.70e+00      2.74E-02     1
8.19e+00      2.98E-02     20
1.00e+01      3.86E-02     1
1.22e+01      4.22E-02     1
1.35e+01      2.12E-02     1
1.49e+01      2.39E-02     1
1.75e+01      4.78E-02     1
1.96e+01      3.93E-02     1
2.25e+01      5.58E-02     10
2.50e+01      4.70E-02     10
2.75e+01      4.49E-02     10
3.00e+01      3.97E-02     10
3.50e+01      8.23E-02     40
4.00e+01      7.43E-02     10
4.50e+01      6.78E-02     10
5.00e+01      5.28E-02     10
5.50e+01      3.72E-02     10
6.00e+01      2.39E-02     10
```

```
6.50e+01       8.26E-03     10
6.60e+01       2.65E-04     10
c
e4 1.00E-10 4.14E-07 1.12E-06 2.38E-06 5.04E-06 1.07E-05 2.26E-05
     1.01e-04 4.54E-04 1.58E-03 3.35E-03 7.10E-03 1.50E-02 3.18E-02
     8.65e-02 1.50E-01 2.24E-01 3.34E-01 4.98E-01 7.43E-01 9.06E-01
     1.11e+00 1.35E+00 1.65E+00 2.02E+00 2.46E+00 3.01E+00 3.68E+00
     4.49e+00 5.49E+00 6.70E+00 8.19E+00 1.00E+01 1.22E+01 1.35E+01
     1.49e+01 1.75E+01 1.96E+01 2.25E+01 2.50E+01 2.75E+01 3.00E+01
     3.50e+01 4.00E+01 4.50E+01 5.00E+01 5.50E+01 6.00E+01 6.50E+01
     6.60e+01
c
c Tally Cards
f4:n  1 2
c
f14:n 1
fc14  Cu-63 (n,2n) Cu-62 total # of Cu-22 nuclei generated in the foil
fm14 6.61354E-03 4 16                 $# of Cu-62 atoms produced
ft14 scx 3
c
c
f24:n 1
fc24  Cu-65(n,gamma)Cu-66 total # of Cu-66 nuclei generated in the foil
fm24   2.94774E-03 5 102               $# of Cu-66 atoms produced
ft24  scx 3
c
f34:n 2
fc34 Al-27(n,gamma)Al-28, total # of Al-28 nuclei generated in the foil
fm34 1.35657E-02 2 102        $Al-27 capture
ft34 scx 3
c
f44:n 2
fc44  Al-27(n,p)Mg-27, total # of Mg-27 nuclei generated in the foil
fm44 1.35657E-02 2 103         $ total # of Mg-27 nuclei generated in the foil
ft44 scx 3
c
f54:n 2
fc54  Al-27 (n,alpha)Na-24, total # of Na-24 nuclei generated in the foil
fm54 1.35657E-02 2 107                           $Al-27(n,alpha)
ft54 scx 3
c
print
nps 1.2e9
```

D2. MCNP5 input files

D2.1 Depth-dose and PDE calculation for the BNCEFNT assembly

```
c  BNCEFNT assembly: 10-cm thick tungsten collimator with 5.64-cm diameter
c   5.0-cm thick tungsten filter; steel filter holder.
    1     1  -1         (-2  3  ):(4  -1  -800  ):(700  -1  -3  ) $head
    2     1  -1         -4  -5  6               $neck
    3     2  -0.001293  (-3  -8  4  1  ):(3  -10  2  -8  ):(5  -4  6  -8  )
    4     4  -1.6       (-20  8  22  -23  ):(-20  -8  10  3  ):
            (-20  8  23  3  ):(-20  8  23  -3  22  )
    5     3  -19.3      -20  -22  21  8  -23 $ collimator
    6     2  -0.001293  -20  8  -22  23  -3
    7     2  -0.001293  -21  -20  8  -23
    8     2  -0.001293  -20  -6  -8
    9     5  -7.87      -101  22  $ filter frame
   10     3  -19.3      -101  -22 24 $ filter
   11     2  -0.001293  -101 -22 -24
   12     2  -0.001293  (-100  20  ) #9 #10 #11
   13    0 100
 101     1  -1         -1  -700  800  -26  53  -56
  102     1  -1         -1  -700  800  -29  60
  103     1  -1         -1  -700  800  -30  61
  104     1  -1         -1  -700  800  -31  30  61
  105     1  -1         -1  -700  800  31  -34  62
  106     1  -1         -1  -700  800  63  34  -37
  107     1  -1         -1  -700  800  37  62
  108     1  -1         -1  -700  800  40  61  -62
  109     1  -1         -1  -700  800  42  60
  110     1  -1         -1  -700  800  45  53  -56
  111     1  -1         -1  -700  800  -49  42
  112     1  -1         -1  -700  800  -48  40  47
  113     1  -1         -1  -700  800  -47  37  46
  114     1  -1         -1  -700  800  -47  -34  46
  115     1  -1         -1  -700  800  -48  -31  47
  116     1  -1         -1  -700  800  -49  -29
  117     1  -1         -1  -700  800  -46
c     X=-9 ;Y=-2 to 2
  118     1  -1         -1  -700  800  -27  -53
  119     1  -1         -700  800  26  -27  53  -54
  120     1  -1         -700  800  26  -27  54  -55
  121     1  -1         -700  800  26  -27  55  -56
  122     1  -1         -1  -700  800  -27  56
c     x=-8; y=-4 to 4
  123     1  -1         -1  -700  800  27  -28  -51  49
  124     1  -1         -700  800  27  -28  51  -52
  125     1  -1         -700  800  27  -28  52  -53
  126     1  -1         -700  800  27  -28  53  -54
  127     1  -1         -700  800  27  -28  54  -55
  128     1  -1         -700  800  27  -28  55  -56
  129     1  -1         -700  800  27  -28  56  -57
  130     1  -1         -700  800  27  -28  57  -58
  131     1  -1         -1  -700  800  27  -28  58  -60
  c x=-7; y=-5 to 5
  132     1  -1         -700  800  28  -29  49  -50  -1
  133     1  -1         -700  800  28  -29  50  -51
  134     1  -1         -700  800  28  -29  51  -52
  135     1  -1         -700  800  28  -29  52  -53
```

```
136     1  -1         -700  800  28  -29  53  -54
137     1  -1         -700  800  28  -29  54  -55
138     1  -1         -700  800  28  -29  55  -56
139     1  -1         -700  800  28  -29  56  -57
140     1  -1         -700  800  28  -29  57  -58
141     1  -1         -700  800  28  -29  58  -59
142     1  -1         -700  800  28  -29  59  -60  -1
c x=-6; y=-6 to 6
143     1  -1         -700  800  29  -30  48  -49  -1
144     1  -1         -700  800  29  -30  49  -50
145     1  -1         -700  800  29  -30  50  -51
146     1  -1         -700  800  29  -30  51  -52
147     1  -1         -700  800  29  -30  52  -53
148     1  -1         -700  800  29  -30  53  -54
149     1  -1         -700  800  29  -30  54  -55
150     1  -1         -700  800  29  -30  55  -56
151     1  -1         -700  800  29  -30  56  -57
152     1  -1         -700  800  29  -30  57  -58
153     1  -1         -700  800  29  -30  58  -59
154     1  -1         -700  800  29  -30  59  -60
155     1  -1         -700  800  29  -30  60  -61  -1
c x=-5; y=-6 to 6
156     1  -1         -700  800  30  -31  48  -49
157     1  -1         -700  800  30  -31  49  -50
158     1  -1         -700  800  30  -31  50  -51
159     1  -1         -700  800  30  -31  51  -52
160     1  -1         -700  800  30  -31  52  -53
161     1  -1         -700  800  30  -31  53  -54
162     1  -1         -700  800  30  -31  54  -55
163     1  -1         -700  800  30  -31  55  -56
164     1  -1         -700  800  30  -31  56  -57
165     1  -1         -700  800  30  -31  57  -58
166     1  -1         -700  800  30  -31  58  -59
167     1  -1         -700  800  30  -31  59  -60
168     1  -1         -700  800  30  -31  60  -61
c x=-4; y=-7 to 7
169     1  -1         -700  800  31  -32  47  -48
170     1  -1         -700  800  31  -32  48  -49
171     1  -1         -700  800  31  -32  49  -50
172     1  -1         -700  800  31  -32  50  -51
173     1  -1         -700  800  31  -32  51  -52
174     1  -1         -700  800  31  -32  52  -53
175     1  -1         -700  800  31  -32  53  -54
176     1  -1         -700  800  31  -32  54  -55
177     1  -1         -700  800  31  -32  55  -56
178     1  -1         -700  800  31  -32  56  -57
179     1  -1         -700  800  31  -32  57  -58
180     1  -1         -700  800  31  -32  58  -59
181     1  -1         -700  800  31  -32  59  -60
182     1  -1         -700  800  31  -32  60  -61
183     1  -1         -700  800  31  -32  61  -62
c x=-3; y=-7 to 7
184     1  -1         -700  800  32  -33  47  -48
185     1  -1         -700  800  32  -33  48  -49
186     1  -1         -700  800  32  -33  49  -50
187     1  -1         -700  800  32  -33  50  -51
188     1  -1         -700  800  32  -33  51  -52
189     1  -1         -700  800  32  -33  52  -53
190     1  -1         -700  800  32  -33  53  -54
191     1  -1         -700  800  32  -33  54  -55
192     1  -1         -700  800  32  -33  55  -56
193     1  -1         -700  800  32  -33  56  -57
194     1  -1         -700  800  32  -33  57  -58
```

```
  195     1  -1         -700  800  32  -33  58  -59
  196     1  -1         -700  800  32  -33  59  -60
  197     1  -1         -700  800  32  -33  60  -61
  198     1  -1         -700  800  32  -33  61  -62
  c  x=-2 ; y=-7 to 7
  199     1  -1         -700  800  33  -34  47  -48
  200     1  -1         -700  800  33  -34  48  -49
  201     1  -1         -700  800  33  -34  49  -50
  202     1  -1         -700  800  33  -34  50  -51
  203     1  -1         -700  800  33  -34  51  -52
  204     1  -1         -700  800  33  -34  52  -53
  205     1  -1         -700  800  33  -34  53  -54
  206     1  -1         -700  800  33  -34  54  -55
  207     1  -1         -700  800  33  -34  55  -56
  208     1  -1         -700  800  33  -34  56  -57
  209     1  -1         -700  800  33  -34  57  -58
  210     1  -1         -700  800  33  -34  58  -59
  211     1  -1         -700  800  33  -34  59  -60
  212     1  -1         -700  800  33  -34  60  -61
  213     1  -1         -700  800  33  -34  61  -62
  c x=-1; y=-8 to 8
  214     1  -1         -700  800  34  -35  46  -47
  215     1  -1         -700  800  34  -35  47  -48
  216     1  -1         -700  800  34  -35  48  -49
  217     1  -1         -700  800  34  -35  49  -50
  218     1  -1         -700  800  34  -35  50  -51
  219     1  -1         -700  800  34  -35  51  -52
  220     1  -1         -700  800  34  -35  52  -53
  221     1  -1         -700  800  34  -35  53  -54
  222     1  -1         -700  800  34  -35  54  -55
  223     1  -1         -700  800  34  -35  55  -56
  224     1  -1         -700  800  34  -35  56  -57
  225     1  -1         -700  800  34  -35  57  -58
  226     1  -1         -700  800  34  -35  58  -59
  227     1  -1         -700  800  34  -35  59  -60
  228     1  -1         -700  800  34  -35  60  -61
  229     1  -1         -700  800  34  -35  61  -62
  230     1  -1         -700  800  34  -35  62  -63
  c x=0; y=-8 to 8
  231     1  -1         -700  800  35  -36  46  -47
  232     1  -1         -700  800  35  -36  47  -48
  233     1  -1         -700  800  35  -36  48  -49
  234     1  -1         -700  800  35  -36  49  -50
  235     1  -1         -700  800  35  -36  50  -51
  236     1  -1         -700  800  35  -36  51  -52
  237     1  -1         -700  800  35  -36  52  -53
  238     1  -1         -700  800  35  -36  53  -54
  239     1  -1         -700  800  35  -36  54  -55
  240     1  -1         -700  800  35  -36  55  -56
  241     1  -1         -700  800  35  -36  56  -57
  242     1  -1         -700  800  35  -36  57  -58
  243     1  -1         -700  800  35  -36  58  -59
  244     1  -1         -700  800  35  -36  59  -60
  245     1  -1         -700  800  35  -36  60  -61
  246     1  -1         -700  800  35  -36  61  -62
  247     1  -1         -700  800  35  -36  62  -63
c x=1 ;y=-8 to 8
  248     1  -1         -700  800  36  -37  46  -47
  249     1  -1         -700  800  36  -37  47  -48
  250     1  -1         -700  800  36  -37  48  -49
  251     1  -1         -700  800  36  -37  49  -50
  252     1  -1         -700  800  36  -37  50  -51
  253     1  -1         -700  800  36  -37  51  -52
```

```
 254     1  -1         -700  800  36  -37  52  -53
 255     1  -1         -700  800  36  -37  53  -54
 256     1  -1         -700  800  36  -37  54  -55
 257     1  -1         -700  800  36  -37  55  -56
 258     1  -1         -700  800  36  -37  56  -57
 259     1  -1         -700  800  36  -37  57  -58
 260     1  -1         -700  800  36  -37  58  -59
 261     1  -1         -700  800  36  -37  59  -60
 262     1  -1         -700  800  36  -37  60  -61
 263     1  -1         -700  800  36  -37  61  -62
 264     1  -1         -700  800  36  -37  62  -63
c x=2; y=-8 to 8
 265     1  -1         -700  800  37  -38  47  -48
 266     1  -1         -700  800  37  -38  48  -49
 267     1  -1         -700  800  37  -38  49  -50
 268     1  -1         -700  800  37  -38  50  -51
 269     1  -1         -700  800  37  -38  51  -52
 270     1  -1         -700  800  37  -38  52  -53
 271     1  -1         -700  800  37  -38  53  -54
 272     1  -1         -700  800  37  -38  54  -55
 273     1  -1         -700  800  37  -38  55  -56
 274     1  -1         -700  800  37  -38  56  -57
 275     1  -1         -700  800  37  -38  57  -58
 276     1  -1         -700  800  37  -38  58  -59
 277     1  -1         -700  800  37  -38  59  -60
 278     1  -1         -700  800  37  -38  60  -61
 279     1  -1         -700  800  37  -38  61  -62
c x=3; y=-8 to 8
 280     1  -1         -700  800  38  -39  47  -48
 281     1  -1         -700  800  38  -39  48  -49
 282     1  -1         -700  800  38  -39  49  -50
 283     1  -1         -700  800  38  -39  50  -51
 284     1  -1         -700  800  38  -39  51  -52
 285     1  -1         -700  800  38  -39  52  -53
 286     1  -1         -700  800  38  -39  53  -54
 287     1  -1         -700  800  38  -39  54  -55
 288     1  -1         -700  800  38  -39  55  -56
 289     1  -1         -700  800  38  -39  56  -57
 290     1  -1         -700  800  38  -39  57  -58
 291     1  -1         -700  800  38  -39  58  -59
 292     1  -1         -700  800  38  -39  59  -60
 293     1  -1         -700  800  38  -39  60  -61
 294     1  -1         -700  800  38  -39  61  -62
c x= 4 ; y=-7 to 7
 295     1  -1         -700  800  39  -40  47  -48
 296     1  -1         -700  800  39  -40  48  -49
 297     1  -1         -700  800  39  -40  49  -50
 298     1  -1         -700  800  39  -40  50  -51
 299     1  -1         -700  800  39  -40  51  -52
 300     1  -1         -700  800  39  -40  52  -53
 301     1  -1         -700  800  39  -40  53  -54
 302     1  -1         -700  800  39  -40  54  -55
 303     1  -1         -700  800  39  -40  55  -56
 304     1  -1         -700  800  39  -40  56  -57
 305     1  -1         -700  800  39  -40  57  -58
 306     1  -1         -700  800  39  -40  58  -59
 307     1  -1         -700  800  39  -40  59  -60
 308     1  -1         -700  800  39  -40  60  -61
 309     1  -1         -700  800  39  -40  61  -62
c x=5; y=-6 to 6
 310     1  -1         -700  800  40  -41  48  -49
 311     1  -1         -700  800  40  -41  49  -50
 312     1  -1         -700  800  40  -41  50  -51
```

```
 313     1  -1         -700  800  40  -41  51  -52
 314     1  -1         -700  800  40  -41  52  -53
 315     1  -1         -700  800  40  -41  53  -54
 316     1  -1         -700  800  40  -41  54  -55
 317     1  -1         -700  800  40  -41  55  -56
 318     1  -1         -700  800  40  -41  56  -57
 319     1  -1         -700  800  40  -41  57  -58
 320     1  -1         -700  800  40  -41  58  -59
 321     1  -1         -700  800  40  -41  59  -60
 322     1  -1         -700  800  40  -41  60  -61
c  x=6; y=-6 to 6
 323     1  -1         -700  800  41  -42  48  -49  -1
 324     1  -1         -700  800  41  -42  49  -50
 325     1  -1         -700  800  41  -42  50  -51
 326     1  -1         -700  800  41  -42  51  -52
 327     1  -1         -700  800  41  -42  52  -53
 328     1  -1         -700  800  41  -42  53  -54
 329     1  -1         -700  800  41  -42  54  -55
 330     1  -1         -700  800  41  -42  55  -56
 331     1  -1         -700  800  41  -42  56  -57
 332     1  -1         -700  800  41  -42  57  -58
 333     1  -1         -700  800  41  -42  58  -59
 334     1  -1         -700  800  41  -42  59  -60
 335     1  -1         -700  800  41  -42  60  -61  -1
c x=7 ; y=-5 to 5
 336     1  -1         -700  800  42  -43  49  -50  -1
 337     1  -1         -700  800  42  -43  50  -51
 338     1  -1         -700  800  42  -43  51  -52
 339     1  -1         -700  800  42  -43  52  -53
 340     1  -1         -700  800  42  -43  53  -54
 341     1  -1         -700  800  42  -43  54  -55
 342     1  -1         -700  800  42  -43  55  -56
 343     1  -1         -700  800  42  -43  56  -57
 344     1  -1         -700  800  42  -43  57  -58
 345     1  -1         -700  800  42  -43  58  -59
 346     1  -1         -700  800  42  -43  59  -60  -1
c x=8 ; y=-3 to 3
 347     1  -1         -1  -700  800  -51  43  -44
 348     1  -1         -700  800  43  -44  51  -52
 349     1  -1         -700  800  43  -44  52  -53
 350     1  -1         -700  800  43  -44  53  -54
 351     1  -1         -700  800  43  -44  54  -55
 352     1  -1         -700  800  43  -44  55  -56
 353     1  -1         -700  800  43  -44  56  -57
 354     1  -1         -700  800  43  -44  57  -58
 355     1  -1         -1  -700  800  43  58  -44
 356     1  -1         -1  -700  800  44  -53
 357     1  -1         -700  800  44  -45  53  -54
 358     1  -1         -700  800  44  -45  54  -55
 359     1  -1         -700  800  44  -45  55  -56
 360     1  -1         -1  -700  800  44  56

   1        sq     0.0106     0.0133     0.0045         0          0
                0          -1          0          0         -1
   2        sq     0.0115     0.0145      0.115         0          0
                0          -1          0          0        4.7
   3        pz        5.8
   4        pz        -11
   5        sq       0.04      0.029          0         0          0
                0          -1          0          0          0
   6        pz        -17
   8        cz         10
  10        sq     0.0098     0.0098       0.09         0          0
```

```
                0          -1           0           0         5.8
   20        rpp         -20         15         -20          20         -20
                20
   21         cx       2.84
   22         cx         10
   23         px          0
   24         px          -25   $filter thickness
   99         px         -35
  100         so         50
  101        rpp         -30        -20         -20          20    -20 20
 700         pz        0.5
  800         pz       -0.5
  c
   26         px       -9.5
   27         px       -8.5
   28         px       -7.5
   29         px       -6.5
   30         px       -5.5
   31         px       -4.5
   32         px       -3.5
   33         px       -2.5
   34         px       -1.5
   35         px       -0.5
   36         px        0.5
   37         px        1.5
   38         px        2.5
   39         px        3.5
   40         px        4.5
   41         px        5.5
   42         px        6.5
   43         px        7.5
   44         px        8.5
   45         px        9.5
c
   46         py       -8.5
   47         py       -7.5
   48         py       -6.5
   49         py       -5.5
   50         py       -4.5
   51         py       -3.5
   52         py       -2.5
   53         py       -1.5
   54         py       -0.5
   55         py        0.5
   56         py        1.5
   57         py        2.5
   58         py        3.5
   59         py        4.5
   60         py        5.5
   61         py        6.5
   62         py        7.5
   63         py        8.5

mode n p
imp:n 1 11r 0      1    259r         $ 1, 360
imp:p 1 11r 0      1    259r         $ 1, 360
m1    8016.24c              1 $Water
      1001.24c              2
m2    7014.24c        -0.7552 $ air (chilton)
      8016.24c        -0.2319 18000.42c          -0.0129
m3    74182.24c        0.2631 $W
      74183.24c        0.1428 74184.24c        0.3064
m4    6000.24c              1 $Graphite
```

```
mt4   grph.65t
m5                $ 1010-1020 steel
      26054.24c  0.0581
      26056.24c   0.9175
      26057.24c  0.0215
m100  5010.50c              1 $B-10
c
sdef   pos=-35 0 0 sur=99 x=-35  y=d1 z=d2 vec=1 0 0 dir=1  erg=d3 par=1
       wgt=400
si1  -10 10
sp1  0 1
si2  -10 10
sp2  0 1
# si3     sp3
1.00e-10  0.0
4.14e-07  1.82E-02
1.12e-06  1.18E-03
2.38e-06  7.90E-04
5.04e-06  8.85E-04
1.07e-05  8.28E-04
2.26e-05  6.19E-04
1.01e-04  9.65E-04
4.54e-04  1.06E-03
1.58e-03  8.63E-04
3.35e-03  6.38E-04
7.10e-03  7.93E-04
1.50e-02  1.02E-03
3.18e-02  1.37E-03
8.65e-02  3.49E-03
0.15      4.35E-03
0.22      4.39E-03
0.33      1.15E-02
0.49      1.73E-02
0.74      3.75E-02
0.90      2.73E-02
1.11      1.37E-02
1.35      1.83E-02
1.65      2.02E-02
2.02      2.03E-02
2.46      1.78E-02
3.01      1.70E-02
3.68      1.35E-02
4.49      2.38E-02
5.49      2.12E-02
6.70      1.74E-02
8.19      2.99E-02
10.0      3.17E-02
12.2      2.36E-02
13.5      1.12E-02
14.9      1.20E-02
17.5      4.80E-02
19.6      4.64E-02
22.5      6.57E-02
25        4.51E-02
27.5      4.51E-02
30        4.23E-02
35        7.21E-02
40        6.06E-02
45        5.07E-02
50        2.70E-02
55        2.43E-02
60        2.22E-02
65        2.00E-02
```

```
66        3.76E-03
c
vol 30j 1.623 1 1 1 1.623 1.356 1 6r 1.356 1 214r  1.356 1 6r 1.356
        1.623 1 1 1 1.623
c
 f4:n    118 119 120 121 122 123 124 125 126 127 128 129 130 131 132 133
          134 135 136 137 138 139 140 141 142 143 144 145 146 147 148 149
          150 151 152 153 154 155 156 157 158 159 160 161 162 163 164 165
          166 167 168 169 170 171 172 173 174 175 176 177 178 179 180 181
          182 183 184 185 186 187 188 189 190 191 192 193 194 195 196 197
          198 199 200 201 202 203 204 205 206 207 208 209 210 211 212 213
          214 215 216 217 218 219 220 221 222 223 224 225 226 227 228 229
          230 231 232 233 234 235 236 237 238 239 240 241 242 243 244 245
          246 247 248 249 250 251 252 253 254 255 256 257 258 259 260 261
          262 263 264 265 266 267 268 269 270 271 272 273 274 275 276 277
          278 279 280 281 282 283 284 285 286 287 288 289 290 291 292 293
          294 295 296 297 298 299 300 301 302 303 304 305 306 307 308 309
          310 311 312 313 314 315 316 317 318 319 320 321 322 323 324 325
          326 327 328 329 330 331 332 333 334 335 336 337 338 339 340 341
          342 343 344 345 346 347 348 349 350 351 352 353 354 355 356 357
          358 359 360
 fm4   1.4091e-7  100 207
c  per ppm B-10 using 2.34 MeV per capture
 f6:n,p   118 119 120 121 122 123 124 125 126 127 128 129 130 131 132 133
          134 135 136 137 138 139 140 141 142 143 144 145 146 147 148 149
          150 151 152 153 154 155 156 157 158 159 160 161 162 163 164 165
          166 167 168 169 170 171 172 173 174 175 176 177 178 179 180 181
          182 183 184 185 186 187 188 189 190 191 192 193 194 195 196 197
          198 199 200 201 202 203 204 205 206 207 208 209 210 211 212 213
          214 215 216 217 218 219 220 221 222 223 224 225 226 227 228 229
          230 231 232 233 234 235 236 237 238 239 240 241 242 243 244 245
          246 247 248 249 250 251 252 253 254 255 256 257 258 259 260 261
          262 263 264 265 266 267 268 269 270 271 272 273 274 275 276 277
          278 279 280 281 282 283 284 285 286 287 288 289 290 291 292 293
          294 295 296 297 298 299 300 301 302 303 304 305 306 307 308 309
          310 311 312 313 314 315 316 317 318 319 320 321 322 323 324 325
          326 327 328 329 330 331 332 333 334 335 336 337 338 339 340 341
          342 343 344 345 346 347 348 349 350 351 352 353 354 355 356 357
          358 359 360
 c  fC24  Boron dose MeV/cc per ppm
  fm24     1.4091e-7  100 207
 fmesh24:n geom=xyz origin=-9.5 -8.5 -0.5
           imesh=9.5 IINTS=19
           jmesh=8.5 JINTS=17
           kmesh=0.5 KINTS=1
           out=col
c  c  fc34  Neutron heating tally  MeV/cc
  fm34 0.10031 1 1 -4
  fmesh34:n geom=xyz origin=-9.5 -8.5 -0.5
            imesh=9.5 IINTS=19
            jmesh=8.5 JINTS=17
            kmesh=0.5 KINTS=1
            out=col
 c fc44  Photon heating tally  MeV/cc
  fm44 0.10031  1 -5 -6
  fmesh44:p geom=xyz origin=-9.5 -8.5 -0.5
            imesh=9.5 IINTS=19
            jmesh=8.5 JINTS=17
            kmesh=0.5 KINTS=1
            out=col
nps  1e7
print
```

D2.2 Activation calculation in the tungsten filter and lead collimator of the simplified BNCEFNT assembly

```
c  Collimator: 10 cm Pb; filter: 5 cm W
   1     1      -1 (-2 3 ):(4 -1 -800 ):(800 -1 -3 )  $head
   2     1      -1 -4 -5 6  $neck
   3     2 -0.001293 ((-3 4 1 ):(3 2 ):(5 -4 6 ):-6 )(64 -65 66 -67 68 -69 )
   4     4   -1.65 64 -65 67 -78 68 -69  $ left face reflector
   5     4   -1.65 64 -65 75 -66 68 -69  $ right face reflector
   6     5   -7.87 64 -65 75 -78 69 -85  $ Fe plate
   7     4   -1.65 64 -65 75 -78 85 -86  $ refelctor on top of head
   8     2 -0.001293 70 -64 73 -74 79 -80  $ 5x5 cm^2 hole
   9     6  -11.35 60 -64 76 -77 81 -82 (-73 :74 :-79 :80 ) $ collimator
  91     6  -11.35 61 -60 76 -77 81 -82 (-73 :74 :-79 :80 ) $ collimator
  92     6  -11.35 62 -61 76 -77 81 -82 (-73 :74 :-79 :80 ) $ collimator
  93     6  -11.35 63 -62 76 -77 81 -82 (-73 :74 :-79 :80 ) $ collimator
  94     6  -11.35 70 -63 76 -77 81 -82 (-73 :74 :-79 :80 ) $ collimator
  10     4   -1.65 70 -64 75 -78 68 -86 (-76 :77 :-81 :82 )
  12     4   -1.65 88 -70 75 -78 68 -86 (91 :-92 :89 :-90 )
  13     2 -0.001293 ((-88 :65 :-75 :78 :-68 :86 )-100 :(88 -87 -91 92 -89 90
            ))#51 #52 #53 #54 #55 #56 #57 #58 #59
  20     3   -19.3 26 -70 90 -89 92 -91  $ filter
  21     3   -19.3 27 -26 90 -89 92 -91  $ filter
  22     3   -19.3 28 -27 90 -89 92 -91  $ filter
  23     3   -19.3 29 -28 90 -89 92 -91  $ filter
  24     3   -19.3 87 -29 90 -89 92 -91  $ filter
  c
   51     2 -0.001293 -51
   52     2 -0.001293 -52
   53     2 -0.001293 -53
   54     2 -0.001293 -54
   55     2 -0.001293 -55
   56     2 -0.001293 -56
   57     2 -0.001293 -57
   58     2 -0.001293 -58
   59     2 -0.001293 -59
  c
  999     0         100

    1        sq 0.0106 0.0133 0.0045 0 0 0 -1 0 0 -1
    2        sq 0.0115 0.0145 0.115 0 0 0 -1 0 0 4.7
    3        pz 5.8
    4        pz -11
    5        sq 0.04 0.029 0 0 0 0 -1 0 0 0
    6        pz -17
    c
   c
  100        so 150
  700        pz 0.5
  800        pz -0.5
  c
   26        px -21
   27        px -22
   28        px -23
   29        px -24
   30        px -5.5
   31        px -4.5
   32        px -3.5
   33        px -2.5
   34        px -1.5
   35        px -0.5
   36        px 0.5
```

```
   37        px 1.5
   38        px 2.5
   39        px 3.5
   40        px 4.5
   41        px 5.5
   42        px 6.5
   43        px 7.5
   44        px 8.5
   45        px 9.5
c
   46       rpp -0.5 0.5 -0.5 0.5 -0.5 0.5
   47        py -7.5
   48        py -6.5
   49        py -5.5
c
   51        sx -80 10  $back middle
   52         s -70 0 35 10  $ back top
   53         s -80 0 -25 10  $Back bottom
c
   54        sx 63 10  $front middle
   55         s 53 0 35 10  $front top
   56         s 63 0 -25 10  $front bottom
c
   57         s 0 70 0 10  $side middle
   58         s 0 65 35 10  $side top
   59         s 0 70 -25 10  $ side bottom
c
   60        px -12
   61        px -14
   62        px -16
   63        px -18
   64        px -10
   65        px 14
   66        py -11
   67        py 11
   68        pz -18
   69        pz 9
   c
   70        px -20
   71        py -20
   72        py 20
   73        py -2.5
   74        py 2.5
   75        py -21
   76        py -12.5
   77        py 12.5
  c
   78        py 21
   79        pz -2.5
   80        pz 2.5
   81        pz -12.5
   82        pz 12.5
   c
   85        pz 9.5
   86        pz 19.5
   87        px -25
   88        px -30
   89        py 10
   90        py -10
   91        pz 10
   92        pz -10

mode  n p
```

```
c
m1    8016.24c              1 $Water
      1001.24c              2
m2    7014.24c        -0.7552 $ air (chilton)
      8016.24c        -0.2319 18000.42c       -0.0129
m3    74000.21c         1 $natural W
m30   74180.30y         1
m32   74182.30y         1
m33   74183.30y         1
m34   74184.30y         1
m36   74186.30y         1
m4    6000.24c              1 $Graphite
m5    26054.24c       -0.0552 $ 1010-1020 steel
      26056.24c         -0.904 26057.24c       -0.0216 6000.24c       -0.00298
      24052.24c       -0.0018 24053.24c     -0.000208
m100  5010.50c              1 $B-10
m6    82206.24c         0.241 $MAT
      82207.24c         0.221
      82208.25c         0.524
m64   82204.30y  1
m66   82206.30y  1
m67   82207.30y  1
m68   82208.30y  1
c
m166   82206.24c  1
m167   82207.24c  1
m168   82208.25c  1
imp:n  1           29r         0            $ 1, 999
imp:p  1           29r         0            $ 1, 999
mt4   grph.65t
c
sdef   pos=-30 0 0 sur=88 x=-30  y=d1 z=d2 vec=1 0 0 dir=1  erg=d3 par=1
       wgt=400
si1  -10 10
sp1  0 1
si2  -10 10
sp2  0 1
# si3     sp3
1.00e-10  0.0
4.14e-07  1.82E-02
1.12e-06  1.18E-03
2.38e-06  7.90E-04
5.04e-06  8.85E-04
1.07e-05  8.28E-04
2.26e-05  6.19E-04
1.01e-04  9.65E-04
4.54e-04  1.06E-03
1.58e-03  8.63E-04
3.35e-03  6.38E-04
7.10e-03  7.93E-04
1.50e-02  1.02E-03
3.18e-02  1.37E-03
8.65e-02  3.49E-03
0.15      4.35E-03
0.22      4.39E-03
0.33      1.15E-02
0.49      1.73E-02
0.74      3.75E-02
0.90      2.73E-02
1.11      1.37E-02
1.35      1.83E-02
1.65      2.02E-02
2.02      2.03E-02
```

```
2.46      1.78E-02
3.01      1.70E-02
3.68      1.35E-02
4.49      2.38E-02
5.49      2.12E-02
6.70      1.74E-02
8.19      2.99E-02
10.0      3.17E-02
12.2      2.36E-02
13.5      1.12E-02
14.9      1.20E-02
17.5      4.80E-02
19.6      4.64E-02
22.5      6.57E-02
25        4.51E-02
27.5      4.51E-02
30        4.23E-02
35        7.21E-02
40        6.06E-02
45        5.07E-02
50        2.70E-02
55        2.43E-02
60        2.22E-02
65        2.00E-02
66        3.76E-03
c
c
 fC4  Boron dose MeV/cc per ppm
  fm4     1.4091e-7  100 207
 fmesh4:n geom=xyz origin=-9.5 -8.5 -0.5
          imesh=9.5 IINTS=19
          jmesh=8.5 JINTS=17
          kmesh=0.5 KINTS=1
          out=col
  fc14  Neutron heating tally  MeV/cc
  fm14 0.10031 1 1 -4
  fmesh14:n geom=xyz origin=-9.5 -8.5 -0.5
           imesh=9.5 IINTS=19
           jmesh=8.5 JINTS=17
           kmesh=0.5 KINTS=1
           out=col
  fc24  Photon heating tally  MeV/cc
  fm24 0.10031  1 -5 -6
  fmesh24:p geom=xyz origin=-9.5 -8.5 -0.5
           imesh=9.5 IINTS=19
           jmesh=8.5 JINTS=17
           kmesh=0.5 KINTS=1
           out=col
c
c
c
fc34 absorption (n,gamm+p+a...) caused by W per gram of tungsten
f34:n   20 21 22 23 24
fm34   (3.9308e-6 30 101)(8.6805e-4 32 101)(4.6875E-4 33 101)
       (1.0037e-3 34 101) (9.3127E-4 36 101)
       (3.9308e-6 30 101)(8.6805e-4 132 101)(4.6875E-4 133 101)
       (1.0037e-3 134 101) (9.3127E-4 136 101)
fq34  f  m
c
fc234 (n,2n) caused by W per gram of tungsten
f234:n   20 21 22 23 24
fm234   (3.9308e-6 30 16)(8.6805e-4 32 16)(4.6875E-4 33 16)
       (1.0037e-3 34 16) (9.3127E-4 36 16)
```

```
c
fc334 (n,3n) caused by W per gram of tungsten
f334:n   20 21 22 23 24
fm334   (3.9308e-6 30 17)(8.6805e-4 32 17)(4.6875E-4 33 17)
       (1.0037e-3 34 17) (9.3127E-4 36 17)
c
c
fc44 # of W-181 produced per g of W per uint flux
f44:n 20 21 22 23 24
fm44  (3.9308E-6 30 102)(8.6805E-4 32 16)(4.6875E-4 33 17)
      (8.6805E-4 132 16)(4.6875E-4 133 17)
fq44  f m
c
fc54 # of W-179 produced per g of W per uint flux
f54:n 20 21 22 23 24
fm54  (3.9308E-6 30 16)
fq54  f m
c
fc64 # of W-178 produced per g of W per uint flux
f64:n 20 21 22 23 24
fm64  (3.9308E-6 30 17)
fq64  f m
c
fc74 # of W-185 produced per g of W per uint flux
f74:n 20 21 22 23 24
fm74  (1.0037E-3 34 102)(9.3127E-4 36 16)
      (1.0037E-3 134 102)(9.3127E-4 136 16)
fq74  f  m
c
fc84 # of W-187 produced per g of W per uint flux
f84:n 20 21 22 23 24
fm84  (9.3127E-4 36 102)(9.3127E-4 136 102)
fq84  f m
c
fc94 # of Ta-179 produced per g of W per uint flux
f94:n 20 21 22 23 24
fm94  3.9308E-6 30 (28:104)
fq94  f m
c
fc104 # of Ta-180 produced per g of W per uint flux
f104:n 20 21 22 23 24
fm104  3.9308E-6 30 103
fq104  f  m
c
fc114 # of Ta-182 produced per g of W per uint flux
f114:n 20 21 22 23 24
fm114  (8.6805E-4 32 103)(4.6875E-4 33 (28:104))
       (8.6805E-4 132 103)(4.6875E-4 133 (28:104))
fq114  f m
c
fc124 # of Ta-183 produced per g of W per uint flux
f124:n 20 21 22 23 24
fm124  (1.0037E-3 34 (104:28))(4.6875E-4 33 103)
       (1.0037E-3 134 (104:28))(4.6875E-4 133 103)
fq124  f  m
c
fc134 # of Ta-184 produced per g of W per uint flux
f134:n 20 21 22 23 24
fm134  (1.0037E-3 34 103) (1.0037E-3 134 103)
fq134  f m
c
c
fc144 # of Ta-185 produced per g of W per uint flux
```

```
f144:n 20 21 22 23 24
fm144  (9.3127E-4 36 (28:104))(9.3127E-4 136 (28:104))
fq144  f m
c
fc154 # of Ta-186 produced per g of W per uint flux
f154:n 20 21 22 23 24
fm154  (1.0037E-3 36 103)(1.0037E-3 136 103)
fq154  f m
c
fc164 # of Hf-178m produced per g of W per uint flux
f164:n 20 21 22 23 24
fm164  (8.6805E-4 32 22) (8.6805E-4 132 22)
fq164  f m
c
fc174 # of Hf-179m produced per g of W per uint flux
f174:n 20 21 22 23 24
fm174  (4.6875E-4 33 22)(4.6875E-4 133 22)
fq174  f m
c
fc184 # of Hf-181 produced per g of W per uint flux
f184:n 20 21 22 23 24
fm184  (1.0037E-3 34 107)(1.0037E-3 134 107)
fq184  f m
c
fc194 # of Hf-182/183 produced per g of W per uint flux
f194:n 20 21 22 23 24
fm194  (9.3127E-4 36 (22) (107))(9.3127E-4 136 (22) (107))
fq194  f m
c
fc404 absorption (n,gamm+p+a...) caused by Pb per gram of tungsten
f404:n   9 91 92 93 94
fm404   (4.0689e-5 64 -2)(7.0044e-4 66 -2)(6.4231E-4 67 -2)
       (1.5229e-3 68 -2)(7.0044e-4 166 -2)(6.4231E-4 167 -2)
       (1.5229e-3 168 -2)
fq404  f m
c
fc414 (n,2n) caused by Pb per gram of tungsten
f414:n   9 91 92 93 94
fm414   (4.0689e-5 64 16)(7.0044e-4 66 16)(6.4231E-4 67 16)
       (1.5229e-3 68 16)(7.0044e-4 166 16)(6.4231E-4 167 16)
       (1.5229e-3 168 16)
fq414  f m
c
fc424 (n,3n) caused by Pb per gram of tungsten
f424:n   9 91 92 93 94
fm424   (4.0689e-5 64 17)(7.0044e-4 66 17)(6.4231E-4 67 17)
       (1.5229e-3 68 17)(7.0044e-4 166 17)(6.4231E-4 167 17)
       (1.5229e-3 168 17)
fq424  f m
c
fc434   # of Pb-202 produced per g of Pb per uint flux
f434:n  9 91 92 93 94
fm434    4.0689e-5 64 17
fq434  f m
c
fc444   # of Pb-203 produced per g of Pb per uint flux
f444:n  9 91 92 93 94
fm444    (4.0689e-5 64 16)
fq444  f m
c
fc454   # of Pb-204m produced per g of Pb per uint flux
f454:n  9 91 92 93 94
fm454    4.0689e-5 64 4
```

```
fq454  f m
c
fc464   # of Pb-205 produced per g of Pb per uint flux
f464:n  9 91 92 93 94
fm464    (4.0689e-5 64 102)(7.0044E-4 66 16) (6.4231E-4 67 17)
         (7.0044E-4 166 16) (6.4231E-4 167 17)
fq464  f m
c
fc474   # of Pb-209 produced per g of Pb per uint flux
f474:n  9 91 92 93 94
fm474    (1.5229e-3 68 102)(1.5229e-3 168 102)
fq474  f m
c
fc484   # of Tl-202 produced per g of Pb per uint flux
f484:n  9 91 92 93 94
fm484    4.0689e-5 64 105
fq484  f m
c
fc494   # of Tl-204 produced per g of Pb per uint flux
f494:n  9 91 92 93 94
fm494    (4.0689e-5 64 103)(7.0044E-4 66 105)(7.0044E-4 166 105)
fq494  f m
c
fc504   # of Tl-206 produced per g of Pb per uint flux
f504:n  9 91 92 93 94
fm504    (7.0044E-4 66 103) (6.4231E-4 67 28)
         (7.0044E-4 166 103) (6.4231E-4 167 28)
fq504  f m
c
fc514   # of Tl-207 produced per g of Pb per uint flux
f514:n  9 91 92 93 94
fm514    (1.5229E-3 68 28) (6.4231E-4 67 103)
          (1.5229E-3 168 28) (6.4231E-4 167 103)
fq514  f m
c
fc524   # of Tl-208 produced per g of Pb per uint flux
f524:n  9 91 92 93 94
fm524    (1.5229E-3 68 103)(1.5229E-3 168 103)
fq524  f m
c
fc534   # of Hg-203 produced per g of Pb per uint flux
f534:n  9 91 92 93 94
fm534    (7.0044E-4 66 107) (6.4231E-4 67 22)
         (7.0044E-4 166 107) (6.4231E-4 167 22)
fq534  f m
c
fc544   # of Hg-205 produced per g of Pb per uint flux
f544:n  9 91 92 93 94
fm544    (1.5229E-3 68 107)(1.5229E-3 168 107)
fq544  f m
nps  1e7
print
```

D2.3 Calculation of dose rate due to 1Bq of activation products (^{187}W) in the filter

```
c  Collimator: 10 cm Pb; filter: 5-cm thick 20x20 cm^2 W
c   Dose rate due to 1 Bq of W-187 distributed in tungsten filter
    1     1      -1 (-2 3 ):(4 -1 -800 ):(800 -1 -3 )  $head
    2     1      -1 -4 -5 6  $neck
    3     2 -0.001293 ((-3 4 1 ):(3 2 ):(5 -4 6 ):-6 )(64 -65 66 -67 68 -69 )
    4     4   -1.65 64 -65 67 -78 68 -69  $ left face reflector
    5     4   -1.65 64 -65 75 -66 68 -69  $ right face reflector
    6     5   -7.87 64 -65 75 -78 69 -85  $ Fe plate
    7     4   -1.65 64 -65 75 -78 85 -86  $ refelctor on top of head
    8     2 -0.001293 70 -64 73 -74 79 -80  $ 5x5 cm^2 hole
    9     6  -11.35 60 -64 76 -77 81 -82 (-73 :74 :-79 :80 ) $ collimator
   91     6  -11.35 61 -60 76 -77 81 -82 (-73 :74 :-79 :80 ) $ collimator
   92     6  -11.35 62 -61 76 -77 81 -82 (-73 :74 :-79 :80 ) $ collimator
   93     6  -11.35 63 -62 76 -77 81 -82 (-73 :74 :-79 :80 ) $ collimator
   94     6  -11.35 70 -63 76 -77 81 -82 (-73 :74 :-79 :80 ) $ collimator
   10     4   -1.65 70 -64 75 -78 68 -86 (-76 :77 :-81 :82 )
   12     4   -1.65 88 -70 75 -78 68 -86 (91 :-92 :89 :-90 )
   13     2 -0.001293 (-88 :65 :-75 :78 :-68 :86 )-93:(88 -87 -91 92 -89 90)
 c
   20     3   -19.3 26 -70 90 -89 92 -91  $ filter
   21     3   -19.3 27 -26 90 -89 92 -91  $ filter
   22     3   -19.3 28 -27 90 -89 92 -91  $ filter
   23     3   -19.3 29 -28 90 -89 92 -91  $ filter
   24     3   -19.3 87 -29 90 -89 92 -91  $ filter
  c
   51     2 -0.001293 -51
   52     2 -0.001293 -52
   53     2 -0.001293 -53
   54     2 -0.001293 -54
   55     2 -0.001293 -55
   56     2 -0.001293 -56
   57     2 -0.001293 -57
   58     2 -0.001293 -58
   59     2 -0.001293 -59
   60     6  -11.35  93 -94  $ 1/4'' lead sheet cover
   61     2 -0.001293 (94 -100) #51 #52 #53 #54 #55 #56 #57 #58 #59
  c
  999     0         100

    1        sq 0.0106 0.0133 0.0045 0 0 0 -1 0 0 -1
    2        sq 0.0115 0.0145 0.115 0 0 0 -1 0 0 4.7
    3        pz 5.8
    4        pz -11
    5        sq 0.04 0.029 0 0 0 0 -1 0 0 0
    6        pz -17
    c
   c
  100        so 150
  700        pz 0.5
  800        pz -0.5
  c
   26        px -21
   27        px -22
   28        px -23
   29        px -24
   30        px -5.5
   31        px -4.5
   32        px -3.5
   33        px -2.5
   34        px -1.5
```

```
   35        px -0.5
   36        px 0.5
   37        px 1.5
   38        px 2.5
   39        px 3.5
   40        px 4.5
   41        px 5.5
   42        px 6.5
   43        px 7.5
   44        px 8.5
   45        px 9.5
c
   46       rpp -0.5 0.5 -0.5 0.5 -0.5 0.5
   47        py -7.5
   48        py -6.5
   49        py -5.5
c
   51        sx -80 10  $back middle
   52         s -70 0 35 10  $ back top
   53         s -80 0 -25 10  $Back bottom
c
   54        sx 63 10  $front middle
   55         s 53 0 35 10  $front top
   56         s 63 0 -25 10  $front bottom
c
   57         s 0 70 0 10  $side middle
   58         s 0 65 35 10  $side top
   59         s 0 70 -25 10  $ side bottom
c
   60        px -12
   61        px -14
   62        px -16
   63        px -18
   64        px -10
   65        px 14
   66        py -11
   67        py 11
   68        pz -18
   69        pz 9
   c
   70        px -20
   71        py -20
   72        py 20
   73        py -2.5
   74        py 2.5
   75        py -21
   76        py -12.5
   77        py 12.5
  c
   78        py 21
   79        pz -2.5
   80        pz 2.5
   81        pz -12.5
   82        pz 12.5
   c
   85        pz 9.5
   86        pz 19.5
   87        px -25
   88        px -30
   89        py 10
   90        py -10
   91        pz 10
   92        pz -10
```

```
   93  rpp -30.5 14.5 -21.5 21.5 -18.5 20.5
   94  rpp -31.135 15.135 -22.135  22.135 -18.5 21.135

mode  p
c
m1    8016.24c              1  $Water
      1001.24c              2
m2    7014.24c        -0.7552  $ air (chilton)
      8016.24c        -0.2319 18000.42c       -0.0129
m3    74000.21c             1  $natural W
m4    6000.24c              1  $Graphite
m5    26054.24c       -0.0552  $ 1010-1020 steel
      26056.24c        -0.904 26057.24c       -0.0216 6000.24c       -0.00298
      24050.24c    -9.35e-005 24052.24c       -0.0018 24053.24c     -0.000208
      24054.24c    -5.09e-005 25055.42c       -0.0075
c   Activiation using LA150N libtary
m54   26054.24c             1  $MAT
m56   26056.24c             1  $MAT
m57   26057.24c             1  $MAT
m58   26058.62c             1  $MAT
m50   24050.24c             1  $MAT
m52   24052.24c             1  $MAT
m53   24053.24c             1  $MAT
m55   25055.42c             1  $MAT
m59   24054.24c             1  $MAT
c    Using ACTL library
m155  25055.30y             1  $MAT
m158  26058.30y             1  $MAT
m154  26054.30y             1  $MAT
m156  26056.30y             1  $MAT
m157  26057.30y             1  $MAT
m152  24052.30y             1  $MAT
m153  24053.30y             1  $MAT
m150  24050.30y             1  $MAT
m159  24054.30y             1  $MAT
c
m100  5010.50c              1  $B-10
m6    82206.24c         0.241  $MAT
      82207.24c         0.221 82208.25c         0.524
m64   82204.30y             1  $MAT
m66   82206.24c             1  $MAT
m67   82207.24c             1  $MAT
m68   82208.25c             1  $MAT
c cell 1    2    3  4   5   6   7  8  9  91   92     93     94
c      10  12  13  20  21  22  23  24 51  52  53  54  55
c      56  57  58  59 60  61  999
imp:p  0.5  0.5  1  0.5 0.5  1  1  1  1  0.5  0.25  0.125  0.125
       0.5 0.5  1  1   1   1   1   1   1   1   1   1   1
       1   1   1   1   1   1   0  $ 1, 999
imp:e  0.1  0.1 0.1 0.5 0.5  1  1  1  1  0.5  0.2   0.1  0.1
       0.5 0.5  0.5  0.3  0.1   0.1   0.2   0.8   1   1   1   1   1
       1   1   1   1   1  1   0  $ 1, 999
mt4   grph.65t
c
sdef   pos=-22.5 0 0 erg=d1 cel=d2 x=d3  y=d4 z=d5  par=2
       wgt=1.593
c ************ Energy of W-187  ****************************
si1 L 7.15E-03 7.60E-03 8.59E-03 8.65E-03 9.03E-03 9.85E-03 9.91E-03 1.00E-02
      1.02E-02 1.03E-02 1.05E-02 1.17E-02 1.20E-02 1.20E-02 1.21E-02 1.66E-02
      2.92E-02 3.64E-02 4.09E-02 4.37E-02 5.91E-02 5.97E-02 6.11E-02 6.90E-02
      6.93E-02 6.98E-02 7.13E-02 7.21E-02 7.74E-02 9.32E-02 1.00E-01 1.07E-01
      1.14E-01 1.24E-01 1.34E-01 1.39E-01 1.66E-01 1.69E-01 1.74E-01 1.98E-01
      2.06E-01 2.08E-01 2.39E-01 2.46E-01 2.76E-01 3.53E-01 3.74E-01 3.76E-01
```

```
      4.55E-01 4.80E-01 4.84E-01 4.93E-01 5.12E-01 5.52E-01 5.65E-01 5.74E-01
      5.76E-01 5.79E-01 5.89E-01 6.13E-01 6.18E-01 6.26E-01 6.39E-01 6.47E-01
      6.82E-01 6.86E-01 6.93E-01 7.30E-01 7.45E-01 7.67E-01 7.73E-01 8.17E-01
      8.26E-01 8.27E-01 8.45E-01 8.65E-01 8.79E-01 9.60E-01 1.06E+00 1.09E+00
      1.10E+00 1.19E+00 1.22E+00 1.23E+00
sp1 D 2.63E-05 6.28E-03 1.75E-02 1.57E-01 2.77E-03 2.04E-03 2.06E-03 1.31E-01
      2.83E-03 3.62E-02 1.43E-03 2.51E-02 1.56E-03 6.35E-04 9.15E-04 6.48E-05
      4.07E-05 6.70E-05 1.85E-05 1.85E-05 6.17E-05 7.58E-02 1.31E-01 1.49E-02
      2.87E-02 6.87E-04 1.13E-02 1.19E-01 7.41E-05 6.48E-05 9.63E-05 2.73E-04
      8.24E-04 2.78E-05 9.45E-02 4.63E-05 9.26E-06 2.78E-05 4.63E-06 1.85E-05
      1.53E-03 7.41E-06 9.26E-04 1.28E-03 2.22E-05 1.67E-05 2.78E-05 3.70E-05
      3.15E-04 2.34E-01 1.85E-04 2.78E-04 6.92E-03 5.45E-02 1.30E-04 5.56E-06
      7.13E-05 1.02E-05 1.31E-03 2.22E-05 6.73E-02 1.17E-02 3.43E-05 8.33E-06
      7.41E-05 2.93E-01 1.39E-05 1.85E-04 3.19E-03 1.67E-05 4.42E-02 1.06E-04
      2.50E-06 2.50E-06 2.59E-06 3.60E-03 1.52E-03 1.42E-05 2.41E-06 9.26E-07
      7.41E-07 2.32E-06 1.85E-07 1.42E-05
sb1 D 1.00E-06 1.00E-06 1.00E-06 1.00E-06 1.00E-06 1.00E-06 1.00E-06 1.00E-05
      1.00E-05 1.00E-05 1.00E-05 1.00E-05 1.00E-05 1.00E-05 1.00E-05 1.00E-05
      1.00E-04 1.00E-04 1.00E-03 1.00E-03 1.00E-03 1.00E-03 1.00E-03 1.00E-03
      1.00E-03 1.00E-03 1.00E-03 1.00E-03 1.00E-03 1.00E-02 1.00E-02 1.00E-02
      1.00E-01 1.00E-01 1.00E-01 1.00E-01 1.00E-01 1.00E-01 1.00E-01 5.00E-01
      5.00E-01 5.00E-01 5.00E-01 5.00E-01 5.00E-01 5.00E-01 5.00E-01 5.00E-01
      5.00E-01 5.00E-01 5.00E-01 5.00E-01 5.00E-01 5.00E-01 5.00E-01 5.00E-01
      5.00E-01 5.00E-01 5.00E-01 5.00E-01 1.00E+00 1.00E+00 1.00E+00 1.00E+00
      1.00E+00 1.00E+00 1.00E+00 1.00E+00 1.00E+00 1.00E+00 1.00E+00 1.00E+00
      1.00E+00 1.00E+00 1.00E+00 1.00E+00 1.00E+00 1.00E+00 1.00E+00 1.00E+00
      1.00E+00 1.00E+00 1.00E+00 1.00E+00
c  activity fraction in cells
si2 L 20    21    22    23    24
sp2 D 0.249 0.168 0.161 0.181 0.241
c
si3 -25 -20
sp3  0 1
si4 -10 10
sp4  0 1
si5 -10 10
sp5  0 1
c
e4   0.01 0.015 0.02 0.03 0.04 0.05 0.06 0.07 0.08 0.1 0.15 0.2 0.25 0.3 0.35
     0.4 0.45 0.5 0.55 0.6 0.65 0.7 0.8 1.0 1.4 1.8 2.2 2.6 2.8
c
f4:p 51  54  57
fq4 e f
c
fc14  Photon Flux-to-Dose Rate Conversion Factors ANSI/ANS¨C6.1.1¨C1977
f14:p 51  54  57
fq14 f e
c
c  Photon Flux-to-Dose Rate Conversion Factors ANSI/ANS¨C6.1.1¨C1977
c  (rem/hr)/(p/cm^2/s)
 #  DE14   DF14
  1.00E-02   3.96E-06
  3.00E-02   5.82E-07
  5.00E-02   2.90E-07
  7.00E-02   2.58E-07
  1.00E-01   2.83E-07
  1.50E-01   3.79E-07
  2.00E-01   5.01E-07
  2.50E-01   6.31E-07
  3.00E-01   7.59E-07
  3.50E-01   8.78E-07
  4.00E-01   9.85E-07
  4.50E-01   1.08E-06
```

```
  5.00E-01   1.17E-06
  5.50E-01   1.27E-06
  6.00E-01   1.36E-06
  6.50E-01   1.44E-06
  7.00E-01   1.52E-06
  8.00E-01   1.68E-06
  1.00E+00   1.98E-06
  1.40E+00   2.51E-06
  1.80E+00   2.99E-06
  2.20E+00   3.42E-06
  2.60E+00   3.82E-06
  2.80E+00   4.01E-06
  3.25E+00   4.41E-06
  3.75E+00   4.83E-06
  4.25E+00   5.23E-06
  4.75E+00   5.60E-06
  5.00E+00   5.80E-06
  5.25E+00   6.01E-06
  5.75E+00   6.37E-06
  6.25E+00   6.74E-06
c
 fc24  Photon Flux-to-Dose Rate Conversion Factors ANS-6.1.1-1991
 f24:p 51  54  57
 fq24 f e
c  ANS-6.1.1-1991 photon flux-to-dose rate CF (rem/hr)/(p/cm^2/s)
 #  DE24   DF24
 1.00E-02   2.23E-08
 1.50E-02   5.65E-08
 2.00E-02   8.57E-08
 3.00E-02   1.18E-07
 4.00E-02   1.31E-07
 5.00E-02   1.38E-07
 6.00E-02   1.44E-07
 8.00E-02   1.62E-07
 1.00E-01   1.92E-07
 1.50E-01   2.80E-07
 2.00E-01   3.71E-07
 3.00E-01   5.62E-07
 4.00E-01   7.42E-07
 5.00E-01   9.14E-07
 6.00E-01   1.08E-06
 8.00E-01   1.38E-06
 1.00E+00   1.66E-06
 1.50E+00   1.89E-06
 2.00E+00   2.76E-06
 3.00E+00   3.67E-06
 4.00E+00   4.50E-06
 5.00E+00   5.29E-06
 6.00E+00   6.01E-06
 8.00E+00   7.49E-06
 1.00E+01   8.89E-06
 1.20E+01   1.04E-05
c
fc34  Photon Flux-to-Dose Rate Conversion Factors ICRP-21
f34:p 51  54  57
fq34 f e
 c   ICRP-21    photon flux-to-dose rate CF (rem/hr)/(p/cm^2/s)
 #  DE34   DF34
  1.00e-02  2.78E-06
  1.50e-02  1.11E-06
  2.00e-02  5.88E-07
  3.00e-02  2.56E-07
  4.00e-02  1.56E-07
```

```
  5.00e-02  1.20E-07
  6.00e-02  1.11E-07
  8.00e-02  1.20E-07
  1.00e-01  1.47E-07
  1.50e-01  2.38E-07
  2.00e-01  3.45E-07
  3.00e-01  5.56E-07
  4.00e-01  7.69E-07
  5.00e-01  9.09E-07
  6.00e-01  1.14E-06
  8.00e-01  1.47E-06
  1.00e+00  1.79E-06
  1.50e+00  2.44E-06
  2.00e+00  3.03E-06
  3.00e+00  4.00E-06
  4.00e+00  4.76E-06
  5.00e+00  5.56E-06
  6.00e+00  6.25E-06
  8.00e+00  7.69E-06
  1.00e+01  9.09E-06
c
fc44  Photon Flux-to-Dose Rate Conversion Factors ICRP-21 rem/hr/Bq
f44:p 51  54  57
fq44 f e
c   ICRP-74    photon flux-to-air Kerma CF (rad/hr)/(p/cm^2/s)
#  DE44    Df44
1.00e-02   2.67E-06
1.50e-02   1.12E-06
2.00e-02   6.05E-07
3.00e-02   2.60E-07
4.00e-02   1.54E-07
5.00e-02   1.16E-07
6.00e-02   1.04E-07
8.00e-02   1.11E-07
1.00e-01   1.34E-07
1.50e-01   2.16E-07
2.00e-01   3.08E-07
3.00e-01   4.97E-07
4.00e-01   6.80E-07
5.00e-01   8.57E-07
6.00e-01   1.02E-06
8.00e-01   1.33E-06
1.00e+00   1.61E-06
1.50e+00   2.21E-06
2.00e+00   2.72E-06
3.00e+00   3.59E-06
4.00e+00   4.36E-06
5.00e+00   5.08E-06
6.00e+00   5.80E-06
8.00e+00   7.24E-06
1.00e+01   8.64E-06
c
fc6 photon heating tally in air (rad/hr/Bq)
f6:p 51  54  57
fm6  5.7672e-5
fq6  f e
c
rand   GEN=2 STRIDE=301111  seed=11992299211777
ctme 300
```

D2.4 HPGe detector (GEM-15190-P) efficiency calculation

```
c     This file models the GEM-15190-P HPGe detector (SN: 33-TP30846)
c    The dead layer on top of the crystal is much thicker than specified in the
c     manual, the distance between the crystal and Al can is also adjusted
       1     1   -5.23 6 5 -3 -7 -4 9       $ Ge layer top
    2     0         -8 -7 5 6 4
    3     1   -5.23 (1 -8 -7 )#1 #2 #8   $ detector
    4     1   -5.23 (-2 7 -5 ):(5 7 -4 ) $ Ge dead layer
    5     1   -5.23 1 -3 8 -6            $ Ge dead layer around side
    6     2    -2.7 1 -10 3 -2
    7     0         (-3 8 4 6 5 -2 ):(7 -8 -2 4 6 5 )
    8     0         ((-12 -11 13 )):(-12 -13 1 )  $ certral hole
    9     2    -2.7 -15 14
   10     0         ((-14 10 ):(-14 2 ))#14
   11     2    -2.7   -17                $ Al foil
c  11     4    -8.92  -18                $ Cu foil
   12     3 -0.001293 (-16 15 )#11       $ air around detector
c  12     3 -0.001293 (-16 15 )          $ air for point source
   13     0         16
   14     2  -0.534 -20 2 -5             $ Mylar

    1        pz 0
    2        pz 6.40
    3        cz 2.355
    4        tz 0 0 5.88 1.72 0.65 0.65
    5        cz 2.12
    6        pz 5.99
    7        pz 6.243
    8        cz 2.275
    9        tz 0 0 5.88 1.72 0.56 0.56
   10        cz 2.431
   11        sz 4.5 0.52
   12        cz 0.432
   13        pz 4.5
   14       rcc 0 0 0 0 0 7.00 2.931
   15       rcc 0 0 0 0 0 7.13 3.061
   16       rcc 0 0 0 0 0 20 4
   17       rcc 0 0 7.20 0 0 0.05 0.84667  $ Al foil
c  18       rcc 0 0 7.20 0 0 0.01 0.84667  $ Cu foil
   20        pz 6.455

mode  p
m1    32000.                1  $Ge
m2    13000.                1  $Al
m3    7014.        -0.7653795  $air
      8016.        -0.2346205
m4    29000.                1  $Cu
m5    5000.                 1  $
m6    79000.                1  $Au
c
c  for point source
c  imp:p             1 10r      0  1     $ 1, 14
c  imp:e             1 10r      0  1     $ 1, 14
c  sdef erg=1.836 pos=0 0 7.20
c
c  For disc source
imp:p   1    11r   0  1     $ 1, 14
imp:e   1    11r   0  1     $ 1, 14
sdef erg=1.3685 pos=0 0 7.20 cell=11 rad=d1 ext=d2 axs=0 0 1
si1  0 0.85
si2  0.05                   $ aluminum foil
```

```
c  si2  0.01                $ copper foil
c
e8  0 1999i 2.0
f8:p 3
c ft8 geb 9.374e-4 5.202e-4 0.75967
nps 1e7
```

REFERENCES

[1] J. Bruce, R. C. Anderson, F. T. PharmD, M.J. Kahn, R. McKenna, and .Macdonald, Glioblastoma Multiforme, http://www.emedicine.com/med/topic2692.htm (last visited June 7, 2006)

[2] K.K. Herfarth, S.Gutwein, and Debus J. Postoperative radiotherapy of astrocytomas. *Seminars in Surgical Oncology*, 20:13-23, 2001

[3] M. Catterall, H.J.G. Bloom, D.V. Ash, L. Walsh, A. Richardson, D. Uttley, N. Gowing, P. Lewis, and B. Chaucer, Fast neutrons compared with megavoltage x-rays in the treatment of patients with supratentorial gioblastoma: A controlled pilot study. *Int. J. Radiation Oncology Bio. Phys.,* 6:261-266,1980.

[4] F.M. Waterman,F.T. Kuchnir, L.S. Skaggs, D.K. Bewley, B.C. Page, and F.H. Attix. The use of 10B to enhance the tumor dose in fast-neutron therapy. *Phys. Med. Biol*., 23(4):592-602,1978.

[5] W.H. Sweet. The use of nuclear disintegrations in the diagnosis and treatment of brain tumor. *N. Engl. J. Med.,* 245:875-878, 1951.

[6] L.E.. Farr, W.H. Sweet, J.S. Robertson, C.G. Foster, H.G Locksley, D.L. Sutherland, M.L. Mendelsohn and E.E Stickley, Neutron Capture Therapy with Boron in the Treatment of Globlastoma Multiforme, *AM J. Roentgenol* 71:279-291,1954.

[7] IAEA-TECDOC-1223, Current status of neutron capture therapy, International Atomic Energy Agency, May 2001.

[8] P. M. Busse, O. K. Harling, M. R. Palmer, W.S. Kiger III, J. Kaplan, I. Kaplan, C, F. Chuang, J. T. Goorley, K. J Riley, T. H. Newton, G. A. Santa Cruz, X-Q. Lu and R. G. Zamenhof, "A critical examination of the results from the Harvard-MIT NCT program phase I clinical trial of neutron capture therapy for intracranial disease," *J. Neuro-Oncol* 62 pp. 111-121, 2003.

[9] W. S. Kiger III, X. Q. Lu, O. K. Harling, K. J. Riley, P. J. Binns, J. Kaplan, H. Patel, R. G. Zamenhof, Y. Shibata, I. D. Kaplan, P. M. Busse, M. R. Palmer, "Preliminary treatment planning and dosimetry for a clinical trial of neutron capture therapy using fission converter epithermal neutron beam," *Appl. Radiat. Isot*. 61 pp 1075-1081, 2004.

[10] Y. Nakagawa, K. Pooh, T. Kobayashi and T. Kageji, Clinical review of the Japanese experience with boron neutron capture therapy and a proposed strategy using epithermal neutron beams, *J. Neuro-Oncol*., 62, pp87-99, 2003

[11] T. Yamamoto, A. Matsumura, K. Nakai, Y. Shibata, K. Endo, F. Sakurai, T. Kishi, H. Kumada, K. Yamamoto and Y. Torii, Current clinical results of Tsukuba BNCT trial, *Appl. Rad. Isot*. 61: pp 1089-1093, 2004

[12] IAEA-TECDOC-1223, Current status of neutron capture therapy, International Atomic Energy Agency (IAEA), May 2001.

[13] Chanana, A.D., Capala, J., Chadha, M., Coderre, J.A., Diaz, A.Z., Elowitz, E.H., Iwai, J., Joel, D.D., Liu, H.B., Ma, R., Pendzick, N., Peress, N.S., Shady, M.S., Slatkin, D.N., Tyson, G.W. and Wielopolski, L., Boron neutron capture therapy for glioblastoma multiforme: Interim results from the phase I/II dose-escalation studies. *Neurosurgery* **44**, pp. 1182–1193, 1999.

[14] J.A. Coderre, J.W. Hopewell, J.C. Turcotte, K.J. Riley, P.J. Binns, W.S. Kiger III, and O.K. Harling, Tolerance of normal haman brain to boron neutron capture therapy, *Appl. Rad. Isot*. 61, pp 1083-1087, 2004.

[15] Coderre, J. A., Makar, M.S., Micca, P. L., Nawrocky M.M., Liu, H.B., Joel, D.D., Slatkin, D.N., Amols, H.I., Derivation of relative biological effectiveness for the high-let radiations produced during boron neutron capture irradiations of 9L rat gliosarcomar in vitro and in vivo. *Int. J. Radiat. Oncol. Biol. Phys*. 27: 1121-1129, 1993.

[16] Morris, G.M., et al., Response of the central nervous system to boron neutron capture irradiation: evaluation using rat spinal cord model, Radiother. *Oncl.* 32 (1994), pp.249-255.

[17] Coderre, J.A. and Morris, G.M., 1999. The radiation biology of boron neutron capture therapy. *Radiat. Res.* **151**, pp. 1–18.

[18] Coderre, J.A., Turcotte, J.C., Riley, K.J., Binns, P.J., Harling, O.K. and Kiger III, W.S., 2003. Boron neutron capture therapy: cellular targeting of high linear energy transfer radiation. *Technol. Cancer Res. Treatment* **2**, pp. 355–375.

[19] T. Kageji, S. Nagahiro, Y. Mizobuchi, H. Toi, Y. Nakagawa and H. Kumada, Radiation injury of boron neutron capture therapy using mixed epithermal- and

thermal neutron beams in patients with malignant glioma, *Appl. Rad. Isot*. 61. PP. 1063-1067, 2004.

[20] Palmer, M.R., Goorley, J. T., Kiger, III W. S., Busse, P. M., Riley K. J., Harling, O. K., Zamenhof, R. G., Treatment planning and dosimetry for the Harvard-MIT phase-I clinical trial of cranial neutron capture therapy. *Int. J. Radiat. Oncol. Biol. Phys*. 53: 1361-1379, 2002.

[21] Ono, K. Masunaga, S. Kinashi, Y., Takagaki, M., Kobayashi, T. Imahori Y., Ueda, S., Oda, Y., The dose planning of BNCT for brain tumors. In : Mishima, Y. (ed) *Cancer Neutron Capture Therapy*. Plenum Press, New York, pp 563-569. 1996.

[22] Hideghety, K., Sauerwein, W., deVries, M., Grochulla, F., Goetz, C., Haselsberger, K., Paquis, P., Heimans, J., Wolbers, J., Moss, R., Huiskamp, R., Stecher-Rasmussen, F., Rassow, J., Garbe, S., Frankhauser, H., Gabel, D., Report on the first patient group of the European Phase I trial (EORTC Protocol 11961) at the High Flux Reactor Petten. In: Hawthorn, F.M., Shelley, K., Wiersema, R.J. (eds) *Frontiers in Neutron Capture Therapy*. Kluver Academic/Plenum Publishers, New York, pp 105-111, 2001.

[23] Busse, P.M., Zamenhof, R.G., Harling, O.K., Kaplan, I., Kaplan, J., Chuang, C.F., Goorley, J.T., Kigger III, W.S., Riley, K.J., Tang, L., Solares, G.R., Palmer, M.R., The Harvard-MIT BNCT program: overview of the clinical trials and translational research. In: Hawthorn, F.M., Shelley, K., Wiersema, R.J. (eds) *Frontiers in Neutron Capture Therapy*. Kluver Academic/Plenum Publishers, New York, pp 37-60, 2001.

[24] Busse, P.M., Zamenhof, R.G., Madoc-Jones, H., Solares, G., Kiger III, W.S., Riley K. J., Chuang, C. F., Rogers, G., Harling O.K., Clinical follow-up of patients with melanoma of the etremity treated in a phase I boron neutron capture therapy protocol. In: Larsson, B., Crawford, J. Weinreich, R. (eds) *Advances in Neutron Capture Therapy*. Elsevier, Amsterdam, pp 60-64, 1997.

[25] Chadha, M., Capla, J., Coderre, J. A., Elowitz, E.H., Iwai, J., Joel, D.D., Liu, H.B., Wielopolski, L., Chanana, A. D. Boron neutron capture therapy (BNCT) for glioblastoma multiforme (GBM) using epithermal neutron beam at the Brookhaven National Laboratory. *Int. J. Radiat. Oncol. Boil. Phys*. 40: 829-843, 1998.

[26] Coderre, J.A., Chanana, A.D., Joel, D.D., Elowitz, E.H., Micca, P.L., Nawrocky, M.M., Chadha, M., Gebbers J.O., Shady, M., Peress, N.S., Slatkin, D.N., Biodistribution of boronophenylalanine in patients with glioblastoma multiforme:

boron concentration correlates with tumor cellularity. *Radiat. Res*. 149: 163-170, 1998.

[27] Elowitz, E.H., Bergland, R.M., Coderre, J.A., Joel, D.D., Chadha, M., Chanana, A.D., Biodistribution of p-boronophenylalanine in patients with glioblastoma multiforme for use in boron neutron capture therapy. *Neurosurgery*. 42: 463-469, 1998.

[28] Kiger III, W.S., Palmer, M.R., Riley, K.J., Zamenhof, R.G., and Busse, P. M. A pharmacokinetic model for the concentration of ^{10}B in blood after boronophenylalanine-fructose administration in humans. *Radiat. Res*. 155, 611-618, 2001.

[29] Kiger III, W.S., Palmer, M.R., Riley, K.J., Zamenhof, R.G., and Busse, P. M. Pharmacokinetic modeling for boronophenylalanine-fructose mediated neutron capture therapy: ^{10}B concentration predictions and dosimetric consequences. *J. Neuro-Oncology* 62: 171-186, 2003.

[30] J. Chadwick. Possible existence of a neutron. *Nature*, 129:312, 1932.

[31] J.H. Lawrence, P.C. Abersold, and E.O. Lawrence, Comparative effects of x-rays and neutrons on normal and tumor tissue. *Proc. Natl. Acad. Sci. USA*, 22(9):543-557,1936.

[32] R.S. Stone. Neutron therapy and specific ionization. *Am. J. Roentgenol*, 59:771-785,1948.

[33] D.K. Bewley, J.F. Fowler and R.L. Morgan, et al. Brit. *J. Radiol*. 36:107-15 (1963).

[34] M. Catterall, D. Bewley, Fast neutron in the treatment of Cancer, P. 5. London: Academic Press. PP. 394 (1979).

[35] A. J. Lennox and P.L. Petti, Hadronic Radiotherapy,P. 5-6, Fermilab-pub-94/204, 1994.

[36] Nuclear data for neutron therapy: Status and future needs. Technical Report IAEA-TECDOC-992, International Atomic Energy Agency (IAEA), Vienna, Austria, Decmber 1997.

[37] K.R. Saroja, J. Mansell, F.R. Hendrickson, L. Cohen and A. Lennox, Failure of accelerated neutron therapy to control high grade astrocytomas, *Int. J. Radiation Oncology Biol. Phys*. 27:1295-97, 1989.

[38] Catteral, M., Bloom,H. J. G., Ash, D. V., Walsh, L.,Richardson, A., Uttley, D., Gowing, N. F. C., Lews, P., Chaucer, B., Fast neutrons compared with megavolt X-rays in the treatment of patients with supratentorial glioblastoma: a controlled pilot study, *Int. J. Radiation Oncology Biol. Phys*. Vol. 6, pp. 261-266, 1980.

[39] Buchholz, T.A., Laramore G. E., Stelzer K. J., Risler, R, Wootton, P and Griffin, T.W., Boron neutron capture enhanced radiotherapy for malignant gliomas and other tumors, *J. Neuro-Oncol*., 33:171-178, 1997.

[40] Nigg, D.W., Hartwell, J. K., Wemple, C.A.; Risler, R., Hartwell, J.K., Harker, Y.D., Venhuizen, J.R., and Risler. Spectral characterization of the University of Washington fast neutron therapy facility using activation foil technique. *Transactions of the American Nuclear Society,*V77, 1997, P351-2

[41] Nigg, D.W. ,Wemple, C.A.; Risler, R., Hartwell, J.K.; Harker, Y.D.; Laramore, G.E. Modification of the University of Washington Neutron Radiotherapy Facility for optimization of neutron capture enhanced fast-neutron therapy. *Med. Phys*, v 27, n 2, Feb. 2000, p 359-67.

[42] Nigg, D.W., Wemple, C.A.; Risler, R., Hartwell, J.K.; Harker, Y.D.; Laramore, G.E. Improved neutron sources for neutron capture enhanced fast neutron therapy. *Transactions of the American Nuclear Society,* V.82,2000, Pp116-17.

[43] R.L. Maughan, W. E. Powers and H.G. Blosser, A super conducting cyclotron for neutron radiation therapy, *Med. Phys*, v 21, n 6, June. 1994, pp 779-85.

[44] Maughan, R.L., Kota, C., and Yudelev, M. A microdosimetric study of the dose enhancement in a fast neutron beam due to boron neutron capture. *Physics in Medicine and Biology*, v 38, n 12, Dec. 1993, p 1957-61.

[45] C. Kota, R.L. Maughan, J. Burmeister, and J.D. Forman. A modified fast neutron therapy beam for boron neutron capture enhanced fast neutron therapy (BNCEFNT). In Borje Larsson, John Crawford, and Regin Weinreich, editors, *Advances in Neutron Capture Therapy*, Volume I. Elsevier, New York, 1997.

[46] J. Burmeister, M. Yudelev, C. Kota, and R. L. Maughan. Boron neutron capture enhancement of fast neutron radiotherapy utilizing a moderated fast neutron beam. *Med. Phys*, Vol. 32, No. 3, pp. 666–672, March 2005.

[47] J.P. Pignol, P. Cuendet, N. Brassart *et al.*, Combined use of FLUKA and MCNP-4A for the Monte Carlo simulation of the dosimetry of ^{10}Boron neutron capture enhancement of fast neutron. *Med. Phys.* **25** (1998), pp. 885–891.

[48] Jean-Philippe Pignol, Philippe Paquis, Pascal Cuendet, David Gibon, Cheikh M'Bake Diop and Roland Sabattier, Beam collimation and bolusing material optimizations for 10boron neutron capture enhancement of fast neutron (BNCEFN): definition of the optimum irradiation technique, *Int. J. Radiation Oncology Biol. Phys*, Volume 43, Issue 5, 15 March 1999, Pages 1151-1159.

[49] I. Rosenberg and M.Awschalom. Characterization of a p(66)Be(49) neutron therapy beam I: Center axis depth dose and off-axis ratios. *Med. Phys*., 8:105-107,1981.

[50] M.Awschalom and I. Rosenberg, Fermilab Cancer Therapy Facility, Neutron Beam Calibration and Treatment Planning, Fermilab Technical Memo TM-0834, 1978

[51] Katja M. Langen. *Microdosimetric Investigations at Fast Neutron Therapy facility at Fermilab. PhD thesis*, University of Wisconsin-Madison, 1997.

[52] Laurie S. Waters, editor. *MCNPX User's Manual*, Version 2.1.5. Los Alamos National Laboratory, 1999. LA-UR-99-6058.

[53] J. E. Sweezy, *Development of a Boron Neutron Capture Enhanced Fast Neutron Therapy Beam*. PhD. Thesis, Georgia Institute of Technology, 2002.

[54] Standard Imaging, Inc., 7601 Murphy Drive, Middleton, Wisconsin 53562-2532. phone: 800-261-4446, Fax: 608-831-2202, Internet: http://www.standardimaging.com/ (last visited: October, 2005).

[55] AAPM Report No. 7. Protocol for neutron beam dosimetry. Technical report, American Association of Physicists in Medicine, Madison, WI,1980.

[56] G.M. Hale and P.G. Young. ENDF/B-VI version 1, material 525 B-10 (neutron), 1991. 5-B-10 LANL EVAL-NOV89.

[57] J. E. Sweezy, A. Lennox, and N.E. Hertel, Paired Tissue Equivalent Ionization Chambers for Boron Enhancement Fast Neutron Therapy, *10th International Congression Neutron Capture Therapy*, NCT Essen 2002, September 8-11, 2002, Essen, Germany.

[58] J. A. Grundl, D. M. Gilliam, N.D. Dudey, and R.J. Popek, Measurement of absolute fission rates, *Nuclear Technology*, Vol 25, pp.273-257, 1975

[59] V.R. CUPPS, A.J. Elwyn, A. J. Lennox, and T. Kroc, "Fermilab NTF Neutron Beam Energy Spectrum by Foil Activation," Proceedings of the 44th Annual Meeting of the Radiation Research Society, Chicago, April 14-17, p. 114,Radiation Research Society, (1996)

[60] M.A. Ross, P. M. Deluca Jr., D.T. L. Jones, A. Lennox and R. L. Maughan, *Calculated Fluence Spectra At Neutron Therapy Facilities, Radiation Protection Dosimetry*, v 70, n 1-4, 1997, p 481-4

[61] D. T. L. Jones, J. E. Symons, and T. J. Fulcher, Neutron Fluence and Kerma spectra of a p(66)Be(40) Clinical Source, *Med. Phys*. 19 (5), 1285, 1992.

[62] M. B. CHADWICK, P. G YOUNG, et. al., “Cross Section Evaluations to 150 MeV for Accelerator-Driven Systems and Implementation in MCNPX”, *Nucl Sci. Eng*, **131** 3, 293 (1999).

[63] J. K. Tuli, *Nuclear Wallet Cards*, National Nuclear data Center, January, 2000.

[64] D.C. Kocher. *Radioactive Decay Data Tables, A Handbook of Decay Data for Application to Radiation Dosimetry and Radiological Assessments*. Oak Ridge, Tennessee. Oak Ridge National Laboratory Technical Information Center, U.S. Department of Energy. 1981.

[65] Z. Wang, B. Kahn and J. Valentine, “Efficiency calculation and coincidence summing correction of a germanium detector by Monte-Carlo simulation**”,** 2001 IEEE Nuclear Science Symposium Conference Record (Cat. No.01CH37310), 2002, pt. 2, p 1037-41 vol.2

[66] R. B. Firestone, V. S. Shirley, editor, and C. M Baglin, S. Y. Frank Chu, and J. Zipkin, assistant editor, Table of Isotopes, Eighth edition, Vol. 1. P. 52. John Wiley & Sons, Inc., 1996.

[67] M. REGINATTO, The "Few-Channel" Unfolding Programs in the UMG Package: MXD_FC33, GRV_FC33 and IQU_FC33 , UMG package, Version3.3-release

[68] M. Rehinatto and P. Goldhagen, MAXED, A computer Code for the Deconvolution of Multisphere Neutron Spectrometer Data Using the Maximum Entropy Method, Environmental Measurements Laboratory, USDOE Report EML 595 (1998). Available at http://www.eml.doe.gov/publications/reports/(last accessed June, 2006).

[69] M. Rehinatto and P. Goldhagen, MAXED, A computer Code for the Deconvolution of Multisphere Neutron Spectrometer Data Using the Maximum Entropy Method, *Health Phys*. 77, 579 (1999).

[70] M. Rehinatto and P. Goldhagen, and S. Neumann, Spectrum unfolding, sensitivity analysis and propagation of uncertainties with maximum entropy deconvolution code MAXED, *Nucl. Instr. And Meth*. A 476, 242 (2202).

[71] RSVP phantom^{TM} Manual, available on-line (last accessed June,2006) at http://www.phantomlab.com/pdf/RSVP_phantom_manual_1299.pdf

[72] White Rock Science. BodyBuilder, www.whiterockscience.com/wrs.html (Accessed May 18, 2005).

[73] Van Riper, K.A. White Rock Science Tools for Geometry Modeling. *Transactions of the American Nuclear Society*, Volume 91, 2004.

[73] R. C. Little and R. E. Seamon, "Dosimetry/Activation Cross Sections for MCNP,"Los Alamos National Laboratory internal memorandum, March 13, 1984 (available on-line http://www-xdiv.lanl.gov/PROJECTS/DATA/nuclear/pdf/dosimetry.pdf).

[75] Rad toolbox V 1.0.0, available on line at http://ordose.ornl.gov/downloads.html (last visit June 3, 2006).

[76] International Commission on Radiological Protection, ICRP Publication 38: Radionuclide Transformations: Energy and Intensity of Emissions, 1984.

[77] ANS-6.1.1 Working Group, M. E. Battat (Chairman), "American National Standard Neutron and Gamma-Ray Flux-to-Dose Rate Factors," ANSI/ANS-6.1.1-1977 (N666), American Nuclear Society, LaGrange Park, Illinois (1977).

[78] ICRP Committee 3 Task Group, P. Grande and M. C. O'Riordan, chairmen, "Data forProtection Against Ionizing Radiation from External Sources: Supplement to ICRPPublication 15," ICRP-21, International Commission on Radiological Protection, Pergamon Press (April 1971).

[79] ICRP publication 74: Conversion Coefficients for use in Radiological Protection against External Radiation, Annals of the ICRP, Volume 26 No. ¾ (1996) Pergamon.

[80] D. Biswas, " Rad-in Tissue versus Rad-in-Air"- A look at the Difference and its Effect on 12-Rad Zone Analysis, WSRC-MS-2002-00472, Available electronically at http://sti.srs.gov/fulltext/ms2002472/ms2002472.html (last accessed May,2006)